

# Synopsis of Some Recent Tactical Application of Bioisosteres in Drug Design

Nicholas A. Meanwell\*

Department of Medicinal Chemistry, Bristol-Myers Squibb Pharmaceutical Research and Development, 5 Research Parkway, Wallingford, Connecticut 06492, United States

## 1. INTRODUCTION

The concept of isosterism between relatively simple chemical entities was originally contemplated by James Moir in 1909, a notion further refined by H. G. Grimm's hydride displacement law and captured more effectively in the ideas advanced by Irving Langmuir based on experimental observations.<sup>1–3</sup> Langmuir coined the term "isostere" and, 18 years in advance of its actual isolation and characterization, predicted that the physical properties of the then unknown ketene would resemble those of diazomethane.<sup>3</sup> The emergence of bioisosteres as structurally distinct compounds recognized similarly by biological systems has its origins in a series of studies published by Hans Erlenmeyer in the 1930s, who extended earlier work conducted by Karl Landsteiner. Erlenmeyer showed that antibodies were unable to discriminate between phenyl and thienyl rings or O, NH, and CH<sub>2</sub> in the context of artificial antigens derived by reacting diazonium ions with proteins, a process that derivatized the ortho position of tyrosine, as summarized in Figure 1.<sup>1,2,4,5</sup> The term "bioisostere" was introduced by Harris Friedman in 1950 who defined it as compounds eliciting a similar biological effect while recognizing that compounds may be isosteric but not necessarily bioisosteric.<sup>6</sup> This notion anticipates that the application of bioisosterism will depend on context, relying much less on physicochemical properties as the underlying principle for biochemical mimicry. Bioisosteres are typically less than exact structural mimetics and are often more alike in biological rather than physical properties. Thus, an effective bioisostere for one biochemical application may not translate to another setting, necessitating the careful selection and tailoring of an isostere for a specific circumstance. Consequently, the design of bioisosteres frequently introduces structural changes that can be beneficial or deleterious depending on the context, with size, shape, electronic distribution, polarizability, dipole, polarity, lipophilicity, and pK<sub>a</sub> potentially playing key contributing roles in molecular recognition and mimicry. In the contemporary practice of medicinal chemistry, the development and application of bioisosteres have been adopted as a fundamental tactical approach useful to address a number of aspects associated with the design and development of drug candidates.<sup>1,2,7–13</sup> The established utility of bioisosteres is broad in nature, extending to improving potency, enhancing selectivity, altering physical properties, reducing or redirecting metabolism, eliminating or modifying toxicophores, and acquiring novel intellectual property. In this Perspective, some contemporary themes exploring the role of isosteres in drug design are sampled, with an emphasis placed on tactical applications designed to solve the kinds of problems that impinge on compound optimization and the long-term success of drug

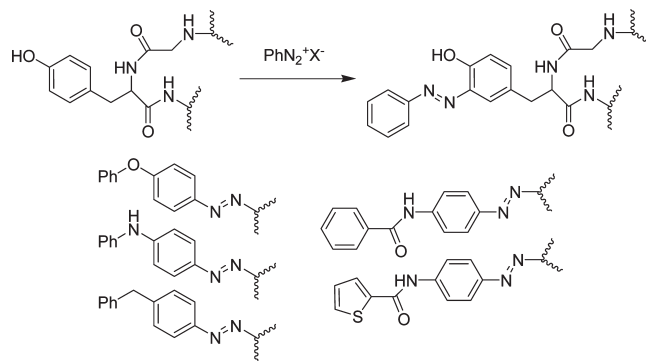


Figure 1

candidates. Interesting concepts that may have been poorly effective in the context examined are captured, since the ideas may have merit in alternative circumstances. A comprehensive cataloging of bioisosteres is beyond the scope of what will be provided, although a synopsis of relevant isosteres of a particular functionality is summarized in a succinct fashion in several sections. Isosterism has also found productive application in the design and optimization of organocatalysts, and there are several examples in which functional mimicry established initially in a medicinal chemistry setting has been adopted by this community.<sup>14</sup>

## 2. CLASSICAL AND NONCLASSICAL BIOISOSTERES

Classical bioisosteres represent the results of an early appreciation of the concept and encompass structurally simple, mono-, di-, and trivalent atoms or groups and ring equivalents that are summarized in the upper half of Table 1.<sup>2</sup> In contrast, nonclassical bioisosteres extend the concept to structural elements that offer a more subtle and sophisticated form of biochemical mimicry, relying upon functionality that can differ quite substantially in electronic, physicochemical, steric, and topological representation from that being emulated.<sup>2</sup>

## 3. RECENT APPLICATIONS OF ISOSTERES IN DRUG DESIGN

**3.1. Isosteres of Hydrogen.** 3.1.1. *Deuterium as an Isostere of Hydrogen.* Substituting a H atom by D represents the most

Received: October 20, 2010

Published: March 17, 2011

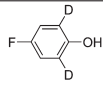
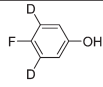
Table 1. Classical and Nonclassical Bioisosteres

| classical bioisosteres  |
|---|
| monovalent bioisosteres   |
| D and H   |
| F and H   |
| NH and OH   |
| RSH and ROH   |
| F, OH, NH <sub>2</sub> and CH <sub>3</sub>  |
| Cl, Br, SH and OH   |
| C and Si  |
| bivalent bioisosteres in which two single bonds are affected  |
| C=C, C=N, C=O, C=S  |
| -CH <sub>2</sub> -, -NH-, -O-, -S-  |
| RCOR', RCONHR', RCOOR', RCOSR'  |
| trivalent bioisosteres in which three bonds are affected  |
| R <sub>3</sub> CH, R <sub>3</sub> N   |
| R <sub>4</sub> C, R <sub>4</sub> Si, R <sub>4</sub> N <sup>+</sup>  |
| alkene, imine   |
| -CH=CH-, -S-  |
| -CH= and -N=C   |
| nonclassical bioisosteres   |
| are structurally distinct, usually comprise different number of atoms and exhibit different steric and electronic properties compared to the functionality being emulated |
| have been divided into two subgroups: <sup>2</sup>  |
| 1. cyclic and noncyclic isosteres   |
| 2. exchangeable group isosterism in which the properties of discrete functional elements are emulated   |

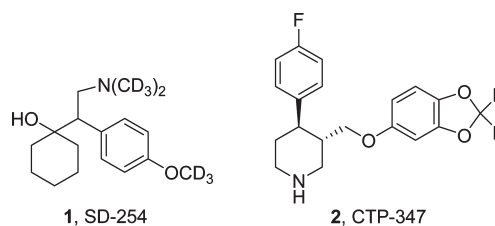
conservative example of bioisosterism given the similarities between the two isotopes, but there are circumstances in drug design where this change can offer a significant advantage. The differences in physical chemical properties between H and D are small but measurable: D is slightly less lipophilic than H,  $\Delta \log P_{oct} = -0.006$ ;<sup>15</sup> the molar volume of D is smaller than H by 0.140 cm<sup>3</sup>/mol per atom; and C–D bonds are shorter than C–H bonds by 0.005 Å. The progressive deuteration of alkanes commensurately reduces lipophilicity, which can be measured by reduced affinity for hydrophobic surfaces,<sup>16</sup> an effect that has been utilized to resolve enantiomers possessing chirality engendered only by virtue of H/D isotopic substitution.<sup>17</sup> Incorporation of a D atom slightly increases the basicity of amines in a nonadditive fashion that shows dependence on stereochemical disposition,<sup>18–20</sup> while the acidity of phenols and carboxylic acids is decreased by up to 0.031 pK units per D atom.<sup>21</sup> Representative data are captured numerically in Table 2.<sup>18–21</sup>

**3.1.2. Deuterium Substitution to Modulate Metabolism.** Intermolecular interactions between drug molecules and proteins are also altered by D/H exchange, although the effect is usually modest and dependent on the site of incorporation, particularly with respect to heteroatoms.<sup>22</sup> Nevertheless, measurable effects have been observed, as exemplified by the deuteration of the cGMP phosphodiesterase V inhibitor sildenafil which affects enzyme inhibitory selectivity by 2- to 5-fold.<sup>23</sup> The primary use of D as an isostere of H in drug discovery has historically focused on taking advantage of the kinetic isotope effect (KIE) to assist in the elucidation of metabolic pathways of drug molecules.<sup>24–26</sup> However, an appreciation of the KIE has led to a heightened awareness that deuteration can be a

Table 2. Representative Examples of the Effect of Deuteration on the Basicity of Amines and on the Acidity of Carboxylic Acids

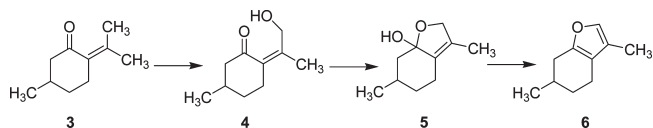
| Amine or acid   | $\Delta pK_a$ relative to the undeuterated analogue |
|---|---|
| CD <sub>2</sub> NH <sub>2</sub>   | +0.017 ± 0.003                                      |
| CD <sub>2</sub> HNH <sub>2</sub>  | +0.034 ± 0.002                                      |
| DCO <sub>2</sub> H  | -0.031 ± 0.0005                                     |
| CD <sub>3</sub> CO <sub>2</sub> H   | -0.013 ± 0.0007                                     |
| CHD <sub>2</sub> (CD <sub>3</sub> ) <sub>2</sub> CO <sub>2</sub> H                  | -0.022 ± 0.0006                                     |
|  | -0.011 ± 0.0005                                     |
|  | -0.0038 ± 0.0007                                    |

useful strategy to improve the pharmacokinetic properties of drug candidates when incorporated at sites relevant to metabolic modification and the first clinical studies with deuterated analogues of known drugs have recently been initiated.<sup>27–29</sup> The KIE for D typically ranges from 1- to 7-fold, depending on the circumstance, although calculations suggest a 7- to 10-fold effect and it can be as high as 16-fold.<sup>30</sup> Consequently, the strategic deployment of D at sites of metabolism where H atom abstraction is the rate determining step can impede metabolism and redirect metabolic pathways, the latter a potentially useful approach to reducing toxicity.<sup>25,26</sup> SD-254 (**1**) is a deuterated form of venlafaxine, the first dual serotonin/norepinephrine reuptake inhibitor to be approved for the treatment of depression, that incorporates deuterium at the primary metabolic sites.<sup>31</sup> Venlafaxine is subject to O-demethylation as the major metabolic pathway, with N-demethylation playing a secondary role, and is a substrate of the polymorphic enzymes CYP 2D6 and 2C19.<sup>31,32</sup> Deuteration reduces the rate of metabolism of **1** in vitro by 50%, and early clinical studies indicate increased exposure of the parent drug, reduced exposure of the O-demethyl metabolite, and less variability in the ratio of the O-demethyl metabolite to parent drug.<sup>33</sup> CTP-347 (**2**), a deuterated version of the antidepressant paroxetine,<sup>34,35</sup> relieves the mechanism-based inhibition of CYP 2D6 in vitro associated with the methylenedioxy moiety<sup>36,37</sup> and preserves enzyme function in normal healthy volunteers following oral dosing.<sup>35</sup>

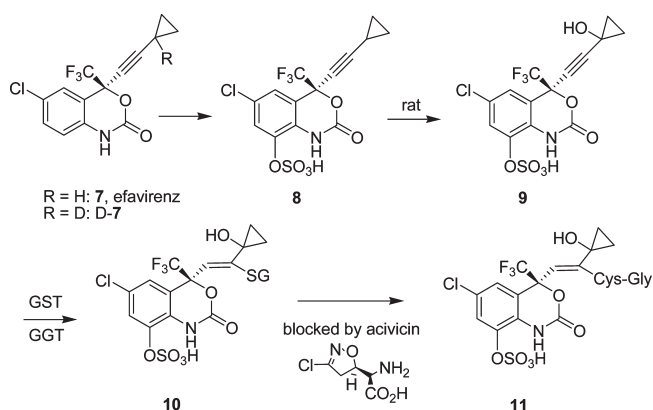


**3.1.3. Deuterium Substitution To Modulate Metabolism and Toxicity.** Perdeuteration of the allylic methyl groups of pulegone (**3**) attenuated the hepatotoxicity seen in mice with the protio analogue, attributed to a reduction in the extent of CYP 450-mediated allylic oxidation to **4**, a precursor to

the furan metabolite **6** that undergoes further metabolic activation to the species that appears to be the ultimate source of hepatotoxicity.<sup>2,5</sup>



The HIV-1 non-nucleoside reverse transcriptase inhibitor (NNRTI) efavirenz (**7**) is subject to a complex and unique metabolic pathway in rats that ultimately affords the nephrotoxic glutathione-derived conjugate **11**. The introduction of deuterium at the labile propargylic site reduced the formation of cyclopropylcarbinol **9** in vivo, reflected in lowered excretion of **11** in urine and a reduction in both the incidence and severity of nephrotoxicity.<sup>38</sup>



**3.1.4. Deuterium to Slow Epimerization.** An interesting application of the deuterium isotope effect has been described for the mechanism-based HCV NS3 protease inhibitor telaprevir (**12**).<sup>39</sup> The (*S*)- $\alpha$ -ketoamide in **12** readily racemizes at higher pH and, most notably, in human plasma to afford the (*R*)-diastereomer, which exhibits 30-fold weaker biological activity (Figure 2). The (*R*)-diastereomer of **12** is the primary metabolite in vivo, accounting for 40% of the drug concentration after oral dosing. Deuteration at the labile center afforded D-**12** which exhibited a  $K_i$  of 20 nM, comparable to that of H-**12**,  $K_i = 44$  nM, and showed increased stability toward racemization in rat, dog, and human plasma compared to the protio form (Table 3). In human plasma, the deuterated analogue of **12** produced only 10% of the epimer over 1 h compared to 35% for the protio version of **12**. In rat plasma, the increase in stability was more modest but the effect translated into a 13% increase in the AUC for the deuterated compound compared to **12** following oral administration to rats and the clearance pathway was not dominated by racemization.<sup>39</sup>

**3.1.5. Fluorine as an Isostere of Hydrogen.** The unique properties of fluorine have led to its widespread application in drug design as an isostere for hydrogen, since incorporation of this halogen can productively modulate a range of properties of interest to medicinal chemists.<sup>40–46</sup> A survey of 293 pairs of molecules in the Roche compound collection that differed only by a F-for-H exchange revealed that the average lipophilicity ( $\log D$ ) increased by 0.25 log units, reflecting the  $\pi$  coefficient of 0.14 measured for F.<sup>41</sup> Perhaps not surprisingly, the histogram of the results exhibited a Gaussian distribution; however, the tail of the plot extended below

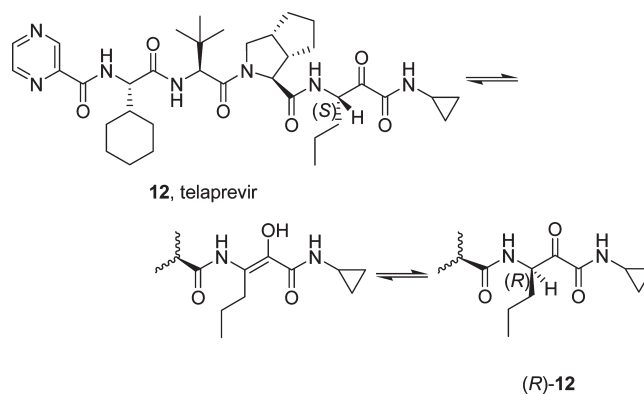


Figure 2

Table 3. Stability of Deuterated **12** toward Racemization in Vitro in Buffer and Plasma

| medium         | initial relative rate of epimerization of H- <b>12</b> | kinetic isotope effect ( $k_H/k_D$ ) |            |
|----------------|--|--------------------------------------|------------|
|                |  | 1 $\mu$ M                            | 10 $\mu$ M |
| buffer, pH 7.4 | 1  | 5                                    | 6          |
| rat plasma     | 1.0–1.5  | 7                                    | 7          |
| dog plasma     | 1.4–3.4  | 4                                    | 6          |
| human plasma   | >8   | >5                                   | >5         |

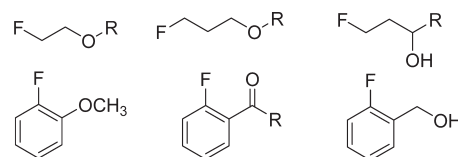


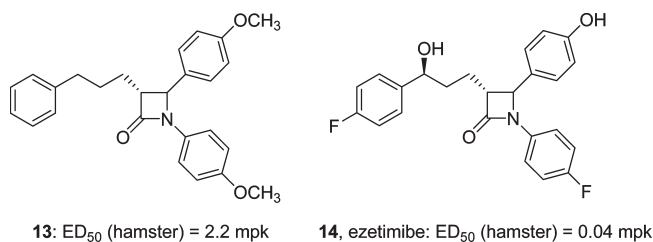
Figure 3. Fluorine-containing fragments associated with increased hydrophilicity compared to the hydrogen-substituted analogues.

zero, indicating that in some structural environments, substitution of H by F reduced the overall lipophilicity of a molecule. A closer inspection of these compounds revealed recurring structural themes, with the observation that in all cases there was a low energy conformation in which the F was proximal to an O atom, with an F to O distance of <3.1 Å. The most prominent structural fragments are summarized in Figure 3. However, the origin of the effect is not understood and has been attributed to either an overall increase in polarity, leading to a gain in solvation energy in polar compared to nonpolar medium, or the F-induced polarization of the proximal O atom, leading to stronger H-bonds in a polar solvent.<sup>41</sup>

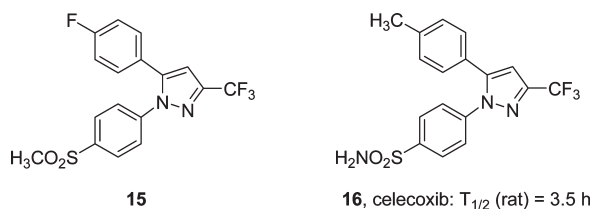
**3.1.6. Fluorine for Hydrogen Exchange To Modulate Metabolism.** Early applications of the exchange of H by F focused on the regiospecific deployment of fluorine to interfere with metabolic processes, a tactic that relies on the powerful electron withdrawing properties of F and the strength of the C–F bond which, at approximately 108 kcal/mol, is the strongest known between C and any other atom.<sup>40–46</sup> This renders the C–F bond chemically inert under most biological conditions, although metabolic activation of fluoroacetic acid<sup>47</sup> and sorivudine (5-fluorouracil)<sup>48</sup> are notable exceptions. Fluorine also increases the strength of adjacent C–F, C–O, and C–C bonds but interestingly

does not exert much influence on the strength of proximal C–H bonds.

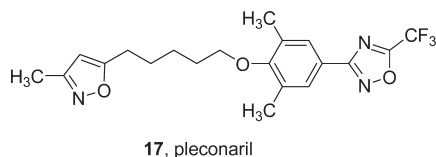
The introduction of two fluorine atoms into the cholesterol absorption inhibitor **13** was a critical step toward increased metabolic stability, ultimately optimized in the context of



ezetimibe (**14**), marketed as Zetia.<sup>41,49</sup> In contrast, the fluorinated cyclooxygenase inhibitor **15** is the close analogue of a compound that exhibited an undesirably long half life of 221 h in vivo in the rat, precipitating examination of the CH<sub>3</sub> moiety as a replacement for the F atom as a means of introducing a metabolic soft spot, a prelude to the identification of celecoxib (**16**).<sup>41,50</sup>



A CF<sub>3</sub> substituent introduced to replace a CH<sub>3</sub> bound at the 5-position of a 1,2,4-oxadiazole ring provided a consistent increase in global metabolic stability in a series of picornavirus entry inhibitors that resulted in the identification of pleconaril (**17**), a compound advanced into clinical evaluation.<sup>51</sup> The origin of this effect is not well understood but has been observed with other molecules,<sup>52–54</sup> although in the case of **17** the effect was not unique to CF<sub>3</sub>, since cyclopropyl, CHF<sub>2</sub>, OEt, and CONH<sub>2</sub> also increased metabolic stability in vitro while interestingly CH<sub>2</sub>CHF<sub>2</sub> and CH<sub>2</sub>CF<sub>3</sub> did not.<sup>51</sup>

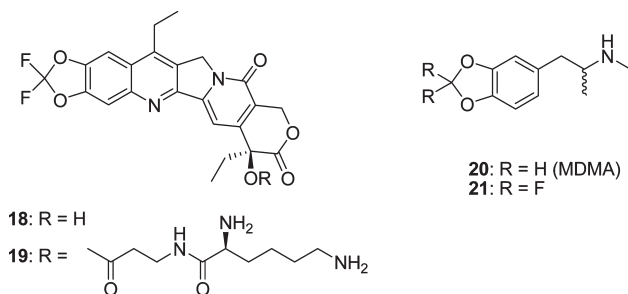


Substituting O–CH<sub>2</sub>–O with O–CF<sub>2</sub>–O in benzo[*d*]-[1,3]dioxole derivatives interferes with cytochrome P-450-mediated metabolic activation of this naturally prevalent moiety to a carbene, a process associated with the formation of problematic CYP 450 metabolic intermediate complexes (MI complexes).<sup>36</sup> A productive example is provided by the favorable in vivo performance of the camptothecin derivative **18** following administration of the prodrug **19**, with the O–CF<sub>2</sub>–O moiety introduced to enhance metabolic stability.<sup>55</sup> A similar tactic has been explored as an approach to reducing metabolism of methylenedioxyamphetamine (**20**, MDMA), better known as ecstasy, a drug of abuse. The difluoro

**Table 4.** Effect of Introduction of Proximal F Atoms on the Basicity of Amines and the Acidity of Carboxylic Acids

| amine   | p <i>K</i> <sub>a</sub> | acid                               | p <i>K</i> <sub>a</sub> |
|---|-------------------------|------------------------------------|-------------------------|
| CH <sub>3</sub> CH <sub>2</sub> NH <sub>3</sub> <sup>+</sup>  | 10.7                    | CH <sub>3</sub> CO <sub>2</sub> H  | 4.76                    |
| CH <sub>2</sub> FCH <sub>2</sub> NH <sub>3</sub> <sup>+</sup> | 9.0                     | CH <sub>2</sub> FCO <sub>2</sub> H | 2.66                    |
| CHF <sub>2</sub> CH <sub>2</sub> NH <sub>3</sub> <sup>+</sup> | 7.3                     | CHF <sub>2</sub> CO <sub>2</sub> H | 1.24                    |
| CF <sub>3</sub> CH <sub>2</sub> NH <sub>3</sub> <sup>+</sup>  | 5.7                     | CF <sub>3</sub> CO <sub>2</sub> H  | 0.23                    |

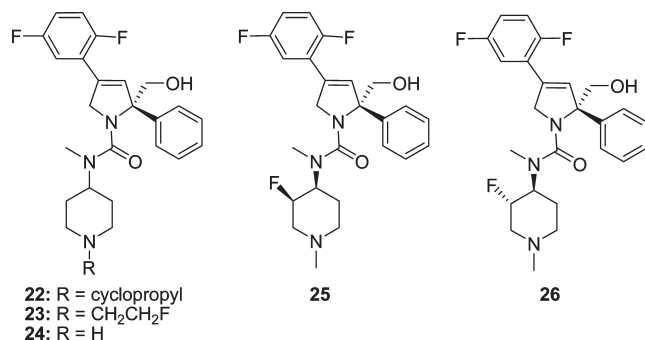
analogue **21** was prepared as a tool to probe the role of metabolism in the psychopharmacology and neurotoxicity associated with the use of **20**, although detailed biological studies that would validate the concept have not been reported.<sup>56</sup>



**3.1.7. Deploying Fluorine To Modulate Basicity in KSP Inhibitors.** The high electronegativity of F reduces the basicity of proximal amines while increasing the acidity of acids (data summarized quantitatively in Table 4).<sup>43</sup> The strategic deployment of a fluorine atom to modulate basicity was probed in the context of inhibitors of kinesin spindle protein (KSP), a family of motor proteins that represents a novel mechanistic target for the treatment of taxane-refractory solid tumors.<sup>57</sup> Optimization of a dihydropyrrole-based series of KSP inhibitors identified **22** as an advanced molecule in which the CH<sub>2</sub>OH moiety was introduced to diminish hERG binding.<sup>57</sup> Variation of the piperidine N-substituent focused on those reducing basicity to a p*K*<sub>a</sub> in the range 6.5–8.0, which had been determined experimentally to reduce PgP efflux in a tumor cell line. The N-cyclopropyl moiety found in **22** aligned basicity in the targeted range but conferred time-dependent CYP P450 inhibition, a phenomenon well-known with cyclopropylamines.<sup>58</sup> A fluoroethyl substituent performed similarly, but **23** was dealkylated in rat liver microsomes (RLM) as the major metabolic pathway to afford **24** and fluoroacetaldehyde, which was oxidized to fluoroacetic acid. The toxicological effects observed in vivo were consistent with release of fluoroacetic acid, a highly toxic substance that enters the tricarboxylic acid cycle and irreversibly inhibits the enzyme aconitase.<sup>47,59</sup> An effective solution was found by deploying the F substituent in the piperidine ring where the effect on p*K*<sub>a</sub> was dependent on stereochemical disposition. In the trans analogue **26**, the F adopts an equatorial position that leads to a 2 log<sub>10</sub> reduction in basicity from p*K*<sub>a</sub> = 8.8 to p*K*<sub>a</sub> = 6.6. In contrast, in the cis isomer **25** the F is disposed axially, expected on the basis of the substituent A values and confirmed by X-ray crystallography, producing a more modest 1.2 log<sub>10</sub> effect on basicity, p*K*<sub>a</sub> = 7.6. This compound, MK-0731 (**25**), was subsequently advanced into clinical trials.<sup>57</sup>

**Table 5. Calculated Conformational Preferences for  $\alpha$ -Fluorocarbonyl Derivatives**

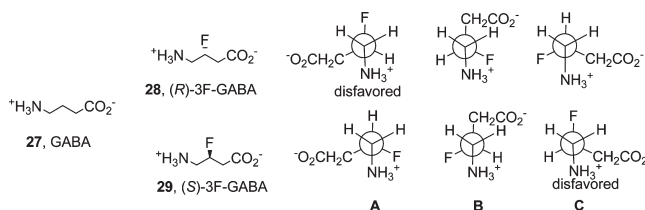
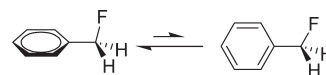
|                  |                             |
|------------------|-----------------------------|
|                  |                             |
| X                | preference for <i>trans</i> |
| NH <sub>2</sub>  | 7.5 kcal mol <sup>-1</sup>  |
| OCH <sub>3</sub> | 4.5 kcal mol <sup>-1</sup>  |
| CH <sub>3</sub>  | 2.2 kcal mol <sup>-1</sup>  |
| H                | 1.68 kcal mol <sup>-1</sup> |



**3.1.8. Substitution of Hydrogen by Fluorine as a Strategy for Influencing Conformation.** As a consequence of the high electronegativity of F, the C–F bond is the most polarized in organic chemistry, producing a large dipole (1.85 D for methyl fluoride) that can influence conformational bias via intramolecular electrostatic interactions with other dipolar bonds, including C=O and C–F moieties.<sup>46</sup> For example,  $\alpha$ -fluorinated carbonyl derivatives favor a conformation in which the C–F and C=O bonds adopt a *trans* orientation to align the dipoles in an antiperiplanar, 180° topology, a preference that correlates with the strength of the carbonyl dipole, as summarized in Table 5.<sup>46,59–62</sup>

**Table 6. Calculated Energy Differences between the *gauche* and *anti* Conformers of F-CH<sub>2</sub>-CH<sub>2</sub>-X**

| X                             | $\Delta$ energy<br><i>gauche</i> – <i>anti</i><br>(kcal/mol) B3LYP | $\Delta$ energy<br><i>gauche</i> – <i>anti</i><br>(kcal/mol) M05-2X | preferred<br>conformer | difference in dipole<br>between the <i>gauche</i> and<br><i>anti</i> conformers (D) | underlying interaction  |
|-------------------------------|--|---|------------------------|---|---|
| –NH <sub>3</sub> <sup>+</sup> | –6.65  | –7.37   | strong <i>gauche</i>   | Not applicable  | electrostatic F $\delta^-$ and NH <sub>3</sub> <sup>+</sup> $\delta^+$                        |
| –O–C=O.H                      | –1.40  | –2.18   | strong <i>gauche</i>   | 4.94  | electrostatic C–F $\delta^-$ and C=O C $\delta^+$   |
| –NO <sub>2</sub>              | –1.22  | –1.12   | strong <i>gauche</i>   | 4.42  | antiparallel $\delta^-$ FC–H and N $\delta^+$ –O $\delta^-$ ; F $\delta^-$ and N              |
| –NHC=O.H                      | –1.00  | –1.12   | strong <i>gauche</i>   | 4.53  | electrostatic C–F $\delta^-$ and N $\delta^+$   |
| –F                            | –0.82  | –0.66   | strong <i>gauche</i>   | 3.02  | $\sigma$ C(F)–H to $\sigma^*$ C–F   |
| –N <sub>3</sub>               | –0.76  | –1.21   | strong <i>gauche</i>   | 3.42  | electrostatic C–F $\delta^-$ and central N $\delta^+$   |
| –N=C=O                        | –0.74  | –1.06   | strong <i>gauche</i>   | 3.97  | electrostatic C–F $\delta^-$ and C=O C $\delta^+$   |
| –CHNH                         | –0.25  | –0.65   | strong <i>gauche</i>   | 3.62  |   |
| –CHCCH <sub>2</sub>           | –0.19  | –0.34   | weak <i>gauche</i>     | 2.00  |   |
| –CH <sub>3</sub>              | –0.18  | –0.35   | weak <i>gauche</i>     | 2.11  |   |
| –CHCH <sub>2</sub>            | –0.01  | –0.17   | weak <i>gauche</i>     | 1.95  |   |
| –C $\equiv$ N                 | 0.64   | –0.64   | strong <i>anti</i>     | 4.68  | p orbital repulsion   |
| –CHO                          | 0.84   | –1.20   | strong <i>anti</i>     | 3.82  | p orbital repulsion and antiparallel dipole:<br>C=O $\delta^- \cdots \delta^+$ HCF $\delta^-$ |
| –C $\equiv$ CH                | 0.98   | –1.03   | strong <i>anti</i>     | 2.18  | p orbital repulsion   |


**Figure 4. Coformal preferences for 28 and 29.**

**Figure 5. Preferred conformation of benzyl fluoride.**

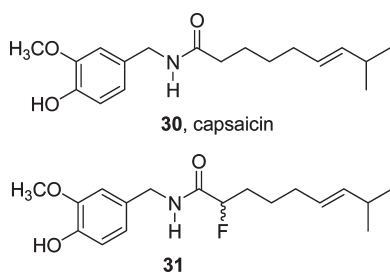
The energetics of interaction of a wide range of substituents common in drug design with the C–F moiety in 2-substituted fluoroethane have been calculated using density functional theory (DFT) in order to quantitatively assess the influence of this *gauche* effect on conformational preferences.<sup>46,63–66</sup> The data are summarized in Table 6, which includes the authors' comments attributing the underlying source of the interaction, a function of either positive electrostatic interactions between F and X, a productive hyperconjugation between the  $\sigma^*$  of the C–F or C–X bond and the C–H bond on the adjacent atom, or a repulsion between the electronegative F and X substituents.<sup>63</sup> For NH<sub>3</sub><sup>+</sup>, OCHO, NO<sub>2</sub>, NHCHO, F, N<sub>3</sub>, and N=C=O, polarization leads to a productive  $\sigma$ (C–H)  $\rightarrow$   $\sigma^*$ (C–X) interaction that further stabilizes the *gauche* conformation.<sup>63</sup>

This preference of a fluorine atom to favor a *gauche* conformation with an adjacent substituent has been exploited in drug design in a striking example that illuminated aspects of biological recognition in the context of the neurotransmitter  $\gamma$ -aminobutyric acid (27, GABA).<sup>67</sup> The two enantiomers of 3-fluoro-GABA, (R)-3-F-GABA (28) and (S)-3-F-GABA (29), were synthesized, an isosteric substitution that reduced the basicity of the amine while increasing the acidity of the acid, as would be anticipated ( $pK_a$ 's of 28 and 29 = 8.95 and 3.30;  $pK_a$ 's of 27 = 10.35 and 4.05) (Figure 4). However, fluorine substitution preserved the zwitterionic nature of the molecule at neutral pH and an extended conformation was found to predominate in solution by <sup>1</sup>H NMR analysis, favored by the *gauche* interaction

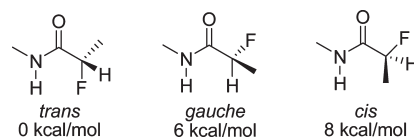
between F and  $\text{NH}_3^+$  (Figure 4).<sup>67</sup> Each enantiomer interacted similarly with the  $\text{GABA}_A$  receptor, but the (*S*)-isomer **29** exhibited higher affinity for GABA transaminase than the (*R*)-isomer **28**. This led to the conclusion that the extended conformer **B** in Figure 4 is recognized by the  $\text{GABA}_A$  receptor but conformer **A**, in which the  $\text{NH}_3^+$  and acid are in a *gauche* relationship and which is disfavored in the (*R*)-isomer **28**, is recognized by the transaminase.<sup>67</sup>

An additional consequence of the highly polarized C–F bond is a low lying  $\sigma^*_{\text{C-F}}$  antibonding orbital that is available for hyperconjugative interactions and that can also influence conformational preferences.<sup>46,63,68</sup> This orbital is available to stereoelectronically aligned donor orbitals, including C–H and  $\pi$  bonds as well as O and N lone pairs, all of which have been shown to contribute to the stabilization of select conformations.<sup>46,63</sup> For example, the modestly preferred ( $\sim 0.4 \text{ kcal mol}^{-1}$ ) conformation of benzyl fluoride projects the C–F bond orthogonal to the aryl ring, stabilized by donation of electron density from the aryl  $\pi$ -orbital into the  $\sigma^*_{\text{C-F}}$  antibonding orbital, as depicted in Figure 5.<sup>69</sup> The conformational preferences of vicinal fluoroalkanes provides another interesting opportunity to exploit the effects of replacing H by F, taking advantage of the preference for fluorines on adjacent carbons to adopt a *gauche* relationship. This approach to conformational bias is based on stabilization by a combination of favorable dipole–dipole, electrostatic, steric, and hyperconjugative interactions (Table 6).

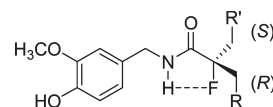
The replacement of a hydrogen atom that is in proximity to an amide NH with a fluorine has been shown to result in interesting effects on biological properties in several systems. In these examples, the preference for an antiperiplanar alignment of dipoles is augmented by a productive interaction between the NH and F atoms, a relationship that has been described as electrostatic in nature rather than a true H-bond. An appreciation of this effect formed the basis of an attempt to elucidate the conformational preferences of capsaicin (**30**) when bound to the transient receptor potential vanilloid 1 (TRPV1) receptor.<sup>73</sup> The enantiomers of  $\alpha$ -fluorocapsaicin (**31**) were synthesized in optically pure form, with the *trans* conformation depicted in Figure 6 calculated to be favored by  $6 \text{ kcal mol}^{-1}$  over the *gauche* conformation and by  $8 \text{ kcal mol}^{-1}$  over the *cis* conformation, stabilized by the C–F/C=O dipole and an electrostatic interaction between  $\text{F}(\delta^-)$  and  $\text{NH}(\delta^+)$ . This preference would influence the topographical projection of the alkylene side chain of the individual enantiomers, providing a potential opportunity to assess any subtleties with respect to the preferred conformation of **30** at the receptor, as depicted in Figure 7. However, the study was not definitive, since both enantiomers of **31** performed similarly as agonists at the TRPV1 receptor, suggesting that the bound conformation is an extended form readily accessible to both enantiomers.<sup>73</sup>



**3.1.8. Fluorine/Hydrogen Exchange To Modulate Potency.** It is well-documented that the judicious substitution of H by F can exert substantial effects on potency.<sup>40,74–76</sup> In the quinolone series of antibacterial gyrase inhibitors represented by **32**, a F substituent at



**Figure 6.** Conformational preferences of 2-fluoro-*N*-methylpropanamide.



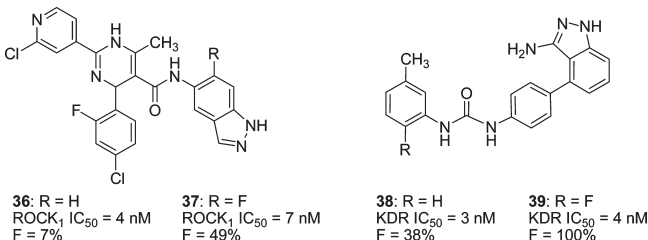
**Figure 7.** Preferred conformation of **31** and the implication for side chain projection in the two enantiomers.

C-6 improves potency by 2- to 7-fold, measured as binding to the enzyme, increases cell penetration up to 70-fold, reduces plasma protein binding, and improves the pharmacokinetic profile.<sup>40,74</sup> In the oxazolidinone antibacterial class, a strategically deployed F atom increases potency and efficacy *in vivo* and is incorporated into the marketed compound linezolid (**33**).<sup>40,75</sup> For inhibitors of HIV-1 attachment, compounds that interfere with the interaction between viral gp120 and host cell CD4, the 4-fluoroindole **35** exhibits a more than 50-fold increased potency compared to the unsubstituted **34**, although in this particular example Cl and Br also led to improved potency.<sup>78</sup>



**3.1.9. Fluorine/Hydrogen Exchange To Influence Membrane Permeability.** In two structurally related series of anilide-based factor Xa inhibitors, a F for H exchange ortho to the NH improves Caco-2 cell permeability (data compiled in Table 7).<sup>77,78</sup> This effect may be due to an electrostatic interaction between the  $\text{C-F}\delta^-$  and  $\text{N-H}\delta^+$  that effectively masks the H-bond, a contention supported by the inability of the linear nitrile to exert a similar effect in the aminobenzisoxazole series.

A fluorine atom proximal to an amide N–H is a motif found in a number of kinase inhibitors where a similar effect may be operative, since oral exposure is often improved, although without the appropriate data it cannot be concluded that this is simply a function of improved membrane penetration. Two examples culled from the literature include the matched pair of  $\rho$ -associated kinase inhibitors **36** and **37**<sup>79</sup> and the multitargeted kinase inhibitors **38** and **39**.<sup>80</sup>



In addition to the anilide motif presented in Table 7 and depicted as motif **A** in Figure 8, a fluorine atom ortho to a benzamide (Figure 8, motif **B**) is a commonly occurring structural element, offering a potentially similar electrostatic interactive effect. Although this might be anticipated to be a somewhat weaker interaction, it may nevertheless be sufficient to mask the NH and improve membrane

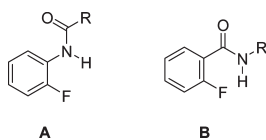
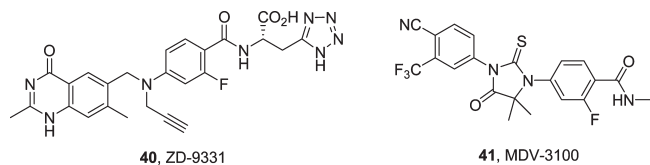


Figure 8. Fluorinated acetanilide and benzamide motifs.

Table 7. Caco-2 Permeability for Two Related Series of Factor Xa Inhibitors

|                 |                              |                              |
|-----------------|------------------------------|------------------------------|
|                 |                              |                              |
| R               | R'                           | Caco-2 permeability          |
| CH <sub>3</sub> | H                            | 1.20 × 10 <sup>-6</sup> cm/s |
| CH <sub>3</sub> | F                            | 3.14 × 10 <sup>-6</sup> cm/s |
| CF <sub>3</sub> | H                            | 3.38 × 10 <sup>-6</sup> cm/s |
| CF <sub>3</sub> | F                            | 4.86 × 10 <sup>-6</sup> cm/s |
|                 |                              |                              |
| R               | Caco-2 permeability          |                              |
| CN              | <0.1 × 10 <sup>-6</sup> cm/s |                              |
| H               | 0.82 × 10 <sup>-6</sup> cm/s |                              |
| F               | 7.41 × 10 <sup>-6</sup> cm/s |                              |

permeability, and this constellation of functionality is represented in several clinically advanced molecules. Prominent examples include ZD-9331 (**40**), a fluorinated analogue of methotrexate that shows activity toward ovarian cancer cells resistant to classical thymidylate synthase inhibitors,<sup>81</sup> and the antiandrogen MDV-3100 (**41**), currently in phase 3 clinical trials for the treatment of castration-resistant prostate cancer.<sup>82,83</sup> The latter exhibits excellent PK, with the implication that the F has a positive impact, although there are no specific data on the PK properties of the protio analogue presented that would allow direct comparison.

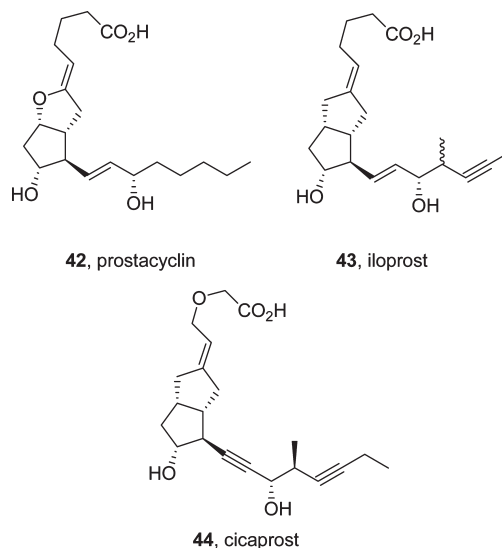


**3.2. Isosteres of Carbon and Alkyl Moieties.** **3.2.1. CH<sub>2</sub>, O, and S Isosterism.** The comparative properties of the classical bivalent isosteres CH<sub>2</sub>, O, and S are summarized in Table 8, which reveals both notable similarities and some marked differences that have the potential to be influential in exercises in drug design.

Table 8. Comparison of the Physical Properties of O, CH<sub>2</sub>, and S

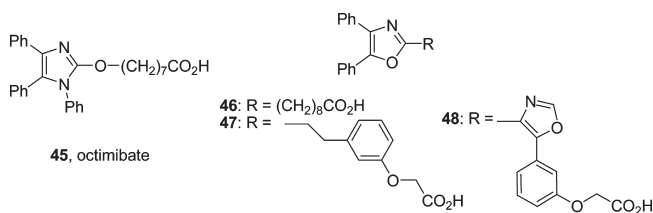
| Property  | RCH <sub>2</sub> -X-CH <sub>2</sub> -R |       |       |
|---|--|-------|-------|
|   | X = CH <sub>2</sub>                    | X = O | X = S |
| C-X bond length (Å)   | 1.54                                   | 1.43  | 1.81  |
| CXC bond angle (°)  | 109.5                                  | 111   | 99    |
|   |  |       |       |
| C...C distance (Å)  | 2.51                                   | 2.37  | 2.87  |
| van der Waals radius of X (Å)                               | 2.0                                    | 1.40  | 1.85  |
| logP  | 3.39                                   | 0.77  | 1.95  |
| Electronegativity   | 2.27                                   | 3.51  | 2.32  |
| Contribution to van der Waals volume (cm <sup>3</sup> /mol) | 10.2                                   | 3.7   | 10.8  |

**3.2.2. CH<sub>2</sub>/O Isosterism in PGI<sub>2</sub> Mimetics.** Prostacyclin (**42**, PGI<sub>2</sub>) is a naturally occurring arachidonic acid metabolite that is both a potent inhibitor of blood platelet aggregation and vasodilator but that is chemically unstable as a result of the hydrolytically sensitive enol ether moiety. Replacing the ether O atom of **42** with CH<sub>2</sub> resolved the hydrolytic lability while modifying the β-side chain restored potency, affording iloprost (**43**) as a PGI<sub>2</sub> mimetic with a profile similar to that of the natural compound.<sup>84</sup> Compound **43** is orally bioavailable in humans but has a biological T<sub>1/2</sub> of only 20–30 min, with β-oxidation of the carboxylic acid moiety identified as the primary metabolic pathway. This process proceeds through the CoA ester which is dehydrogenated prior to the Michael addition of water, a reaction pathway that can be interrupted by several tactical structural modifications including α- and/or β-disubstitution or the introduction of a heteroatom to replace the β-carbon.<sup>85</sup> The latter approach, in conjunction with further manipulation of the β-side chain, was pursued to realize cicaprost (**44**), a molecule that demonstrated hypotensive activity in rats lasting 2–3 times longer than **43**.<sup>84</sup>



**3.2.3. CH<sub>2</sub>/O Isosterism in Non-Prostaonid PGI<sub>2</sub> Mimetics.** An interesting effect of CH<sub>2</sub>/O isosterism was reported in a series of lipophilic carboxylic acid derivatives that function as partial agonists at the PGI<sub>2</sub> receptor and that are effective inhibitors of blood platelet aggregation in vitro in platelet-rich plasma.<sup>86,87</sup> The series originated with the discovery that octimibate (**45**) is a PGI<sub>2</sub> receptor partial agonist, a molecule optimized to afford BMY-45778 (**48**) via the

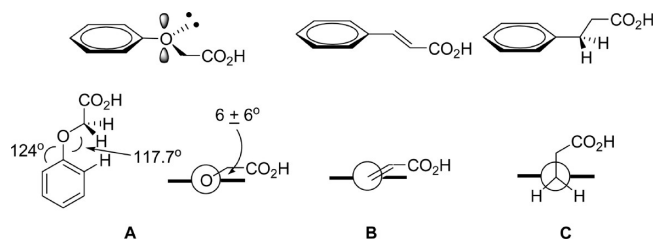
intermediacy of the simpler diphenyloxazoles **46** and BMY-42393 (**47**), part of a progression leading to the elucidation of pharmacophore topography.<sup>86</sup> A systematic survey of the effects of interchanging CH<sub>2</sub> and O in both two-atom linker elements of **47**, summarized in Table 9, revealed that a OCH<sub>2</sub>CO<sub>2</sub>H terminus was >10-fold superior to the analogous CH<sub>2</sub>CH<sub>2</sub>CO<sub>2</sub>H (compare **47** with **49** and **51** with **52**), while the *trans* acrylic acid moiety found in **50** and **53** exhibited equivalent-fold-to-10-fold inferior potency to the OCH<sub>2</sub>CO<sub>2</sub>H analogues **47** and **51**.<sup>87</sup> Thus, the presence of atoms able to interact with the  $\pi$  system improves potency over the simple CH<sub>2</sub>CH<sub>2</sub> linker element. This result may be understood in the context of the preferred conformations adopted by these moieties, summarized in Figure 9, that directs some caution when contemplating the introduction of heteroatoms as CH<sub>2</sub> isosteres when these are directly attached to  $\pi$  systems.<sup>87–91</sup>



Both the OCH<sub>2</sub>CO<sub>2</sub>H (Figure 9A) and *trans* CH=CH–CO<sub>2</sub>H (Figure 9B) moieties preferentially adopt a coplanar arrangement with the phenyl ring, a consequence of interaction between the lone pair on oxygen and the  $\pi$ -system of the aromatic ring or the  $\pi$ -system of the olefin and the phenyl ring, sufficient to surmount A<sup>1,3</sup> strain in the latter.<sup>88–93</sup> In examples in the Cambridge Structural Database (CSD), Ar–O–CH<sub>2</sub> angles are distorted just 2–20° from the plane of the aromatic ring and 30/32 anisole derivatives in the CSD exhibit a dihedral angle of 6 ± 6° and a C–C–O angle of 124°, indicative of significant rehybridization to accommodate the lone pair– $\pi$  interactions.<sup>89</sup> In contrast, the CH<sub>2</sub>CH<sub>2</sub>CO<sub>2</sub>H moiety preferentially adopts a projection orthogonal to the Ph ring in order to avoid A<sup>1,3</sup> strain with the ortho hydrogen atoms (Figure 9C).<sup>93</sup> Interestingly, in this PGI<sub>2</sub> mimetic series the effect of exchange of CH<sub>2</sub> and O at the oxazole–CH<sub>2</sub>–CH<sub>2</sub>–Ar juncture is muted, perhaps because this is sufficiently remote from the carboxylic acid terminus and in a region where structural variation may be more readily accommodated (Table 9).<sup>87</sup>

**Table 9. Structure–Activity Relationships for Blood Platelet Aggregation Inhibition in Platelet-Rich Plasma by a Series of Non-Prostanoid PGI<sub>2</sub> Mimetics**

| Compound  | X               | Y                  | Z               | Inhibition of Blood Platelet Aggregation EC <sub>50</sub> ( $\mu$ M) |
|-----------|-----------------|--------------------|-----------------|--|
| <b>47</b> | CH <sub>2</sub> | O                  | CH <sub>2</sub> | 1.2  |
| <b>49</b> | CH <sub>2</sub> | CH <sub>2</sub>    | CH <sub>2</sub> | 16   |
| <b>50</b> | CH <sub>2</sub> | <i>trans</i> CH=CH |                 | 0.66   |
| <b>51</b> | O               | O                  | CH <sub>2</sub> | 1.2  |
| <b>52</b> | O               | CH <sub>2</sub>    | CH <sub>2</sub> | >80  |
| <b>53</b> | O               | <i>trans</i> CH=CH |                 | 14   |



**Figure 9.** Preferred conformations of phenoxyacetic, cinnamic, and  $\beta$ -phenylpropionic acid derivatives.

**Table 10. Structure–Activity Relationships for a Series EP<sub>3</sub> Receptor Antagonists**

| Compound  | X                | K <sub>i</sub> at EP <sub>3</sub> (nM) | K <sub>i</sub> at EP <sub>3</sub> + 0.005% HSA (nM) |
|-----------|------------------|--|---|
| <b>54</b> | CH <sub>2</sub>  | 1.1                                    | 263   |
| <b>55</b> | O                | 153                                    | 1500  |
| <b>56</b> | S                | 6.7                                    | 356   |
| <b>57</b> | SO               | 17                                     | 200   |
| <b>58</b> | SO <sub>2</sub>  | 2.1                                    | 41  |
| <b>59</b> | OCH <sub>2</sub> | 9.9                                    | 1794  |

An example in which CH<sub>2</sub>/O exchange had an opposing effect on potency occurred in the series of EP<sub>3</sub> receptor antagonists **54–59** compiled in Table 10.<sup>94</sup> PGE<sub>2</sub> acts through several GPCRs, and the EP<sub>3</sub> receptor subtype is of importance in the regulation of ion transport, GI smooth muscle contraction, acid secretion, uterine contraction during fertilization and implantation, fever generation, and PGE<sub>2</sub>-mediated hyperalgesia. In the selective EP<sub>3</sub> receptor antagonists **54–59**, potency was highly sensitive to the identity of the linker atom between the naphthalene and phenyl rings, with CH<sub>2</sub> (**54**) optimal and both S (**56**) and SO<sub>2</sub> (**58**) acting as useful surrogates. However, an oxygen atom linker (**55**) led to an almost 150-fold erosion in potency, attributed to conformational effects that restrict the optimal topographical deployment of the naphthalene ring.<sup>94</sup> Interestingly, the marked serum effect noted was subsequently reduced by modification of the substitution pattern of the thiophene ring.

### 3.2.4. Silicon as an Isostere of Carbon

**A Comparison of the Properties of Silicon and Carbon.** Silicon has been probed as an isostere of carbon in the context of a number of bioactive molecules, and several compounds have been advanced into clinical studies, while the antifungal flusilazole (**60**) and pyrethroid insecticide silafluofen (**61**) are silicon-containing molecules with broad commercial application in agriculture.<sup>95–99</sup> The use of silicon as an isostere of carbon ranges from the simple, structurally benign replacement of an alkyl moiety by trialkylsilyl to the more sophisticated design of silanediol (Si(OH)<sub>2</sub>) as a transition state mimetic in protease inhibitors and the application of Si–OH as a replacement for C–OH in circumstances where this may offer a specific advantage. The metabolism of silicon-containing molecules appears to follow predictable pathways, with the susceptibility of Si dealkylation similar to that of more conventional heteroatoms, and no unusual Si-related toxicities have been identified to date.

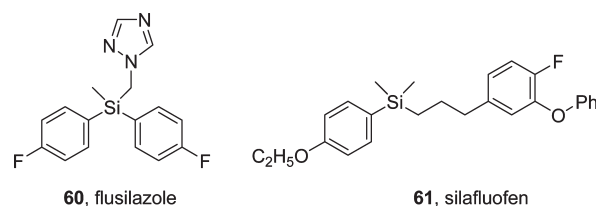


Table 11. Comparison of Key Physical Parameters Associated with Carbon and Silicon

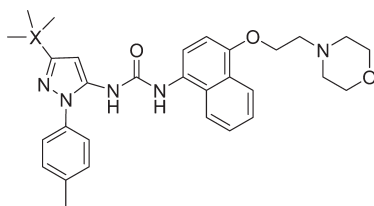
|                   | carbon  | silicon   |
|-------------------|---|---|
| covalent radius   | 77 pm   | 117 pm  |
| bond length       | C–C is 1.54 Å   | Si–C is 1.87 Å  |
| electronegativity | 2.50  | 1.74, more electropositive than C, N, O   |
| lipophilicity     | Ph- <i>t</i> -Bu: cLogP = 3.97  | Ph-Si(CH <sub>3</sub> ) <sub>3</sub> : cLogP = 4.72   |
| bond stability    | C–H stable<br>C–O–C stable<br>C–OH stable<br>C–N stable<br>C=C and C≡C stable | Si–H labile particularly under basic conditions<br>Si–O–C hydrolytically sensitive<br>Si–OH stable but liable to condensation; usually more acidic than C–OH<br>Si–N hydrolyses under acidic conditions<br>Si=Si and Si≡Si are unstable |

Table 12. Comparative in Vitro Data for the p38 $\alpha$  Mitogen-Activated Protein (MAP) Kinase Inhibitor **62** and the Silicon Analogue **63**

|                               | <b>62</b> | <b>63</b> |
|-------------------------------|-----------|-----------|
| pK <sub>a</sub>               | 1.9, 6.4  | 2.3, 6.3  |
| log <i>P</i>                  | 5.2       | 4.7       |
| log <i>D</i> (pH 7.4)         | 5.1       | 4.7       |
| IC <sub>50</sub> (nM)         | 55        | 64        |
| HLM (% turnover after 40 min) | 79        | 62        |

The properties of Si and C are compared in Table 11 where the most notable differences are the increased covalent radius of Si, 50% larger than for C, the 20% longer C–Si bond length, and the higher lipophilicity of Si derivatives. The two atoms also demonstrate some complementarity in both physical properties and chemical stability when bound to heteroatoms, properties that can be exploited in drug design, as illustrated below with select examples from the literature.

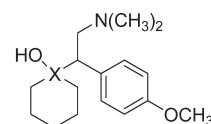
**3.2.5. Silicon in p38 $\alpha$  MAP Kinase Inhibitors.** The substitution of a *tert*-butyl moiety in the p38 $\alpha$  mitogen-activated protein (MAP) kinase inhibitor doramapimod (**62**, BIRB-796) by a trimethylsilane is an effective example of a straightforward bioisosteric substitution of a silicon for a carbon atom.<sup>99</sup> The Si-for-C switch slightly increased the pK<sub>a</sub> of the morpholine N atom, atypically reduced overall lipophilicity, and had no significant effect on metabolic stability (data summarized in Table 12). In a mouse model of LPS-induced TNF $\alpha$  release, sila-BIRB-796 (**63**) exhibited efficacy comparable to that of the progenitor following an oral dose of 10 mpk.<sup>99</sup>



**62:** X = C, BIRB-796  
**63:** X = Si, sila-BIRB-796

**3.2.6. Silicon as a Carbon Isostere in Biogenic Amine Reuptake Inhibitors.** The dual serotonin and noradrenaline reuptake inhibitor venlafaxine (**64**), marketed as the racemic mixture (Effexor) for the treatment of depression, provided an interesting opportunity to deploy Si as a C isostere in a more strategic fashion designed to influence biological and physical properties.<sup>100–102</sup> The essential properties of racemic sila-venlafaxine (**65**) and the resolved enantiomers are compared with the analogous carbon compounds in Table 13, data that reveal some marked differences.

Although log *P*, log *D*, and the pK<sub>a</sub> of **64** and **65** are similar, racemic **64** is a potent inhibitor of SERT/NET, (*S*)-**64** is 100-fold selective for SERT over NET, whereas (*R*)-**64** is a more balanced SERT and NET inhibitor.<sup>100–102</sup> Compound **65** retains NET and DAT but sacrifices SERT, while (*R*)-**65** is much less potent, with no selectivity for SERT and DAT but 10-fold selective for NET. Thus, the in vitro profiles of the individual forms of **65** are quite different from the carbon analogues. (*R*)-**65** expresses antiemetic activity in rats following oral dosing of 5 mpk.



**64:** X = C, venlafaxine  
**65:** X = Si, sila-venlafaxine

**3.2.7. Silicon as a Carbon Isostere in Haloperidol.** The tertiary alcohol of the dopamine D<sub>2</sub> antagonist haloperidol (**66**, Table 14), a clinically useful antipsychotic agent, is associated with a problematic metabolic pathway that was recognized as an opportunity to demonstrate the potential of the analogous silanol **67** to mitigate a potential toxicity issue.<sup>103</sup> Compound **67** is slightly more basic than **66** and exhibits modest changes in receptor affinity that amplify the dopamine D<sub>2</sub> selectivity (data compiled in Table 14). The other properties reported for the two molecules are very similar with the exception that **67** is a 3-fold more potent inhibitor of CYP 3A4 than **66**.

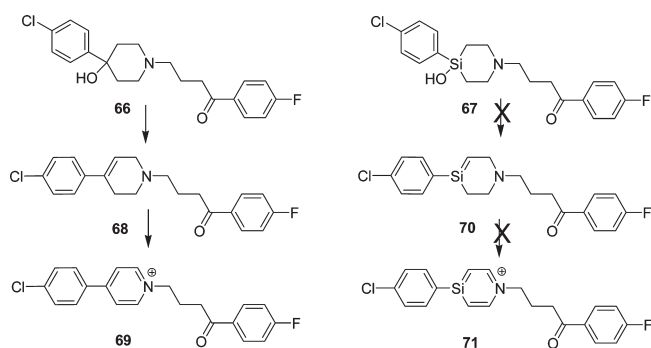
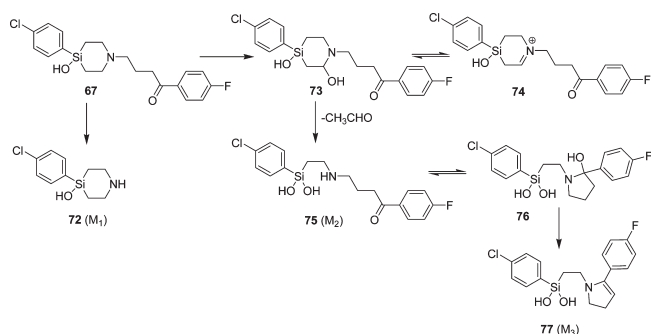
Compound **66** is metabolized in part by dehydration of the tertiary alcohol to afford **68** which is readily oxidized to the pyridinium **69**, a neurotoxin related to the pyridinium derived from 1-methyl-4-phenyl-1,2,3,6-tetrahydropyridine (MPTP) that is suspected as a source of parkinsonism in the clinic (Figure 10).<sup>104</sup> It was anticipated that **67** would not be subject to an analogous metabolic pathway to produce **70** and **71** because C=Si bonds are inherently unstable.<sup>103</sup> Indeed, the metabolism of **67** in HLM, elucidated by MS, is quite different from haloperidol, with no dehydration of the silanol moiety observed, as predicted (Figure 11).<sup>103,105</sup> The major metabolic pathways for **67** involve hydroxylative ring-opening of the sila-piperidine ring, a pathway not observed with **66**, in addition to N-dealkylation. Interestingly, the silanol moiety was not subject to glucuronidation, a significant metabolic pathway for **66**, leading to the suggestion that the silanol functionality may offer an opportunity to introduce a hydrophilic element resistant to this phase II metabolic modification.<sup>105</sup> More recently, the sila analogue **79** of the related dopamine D<sub>2</sub>

**Table 13. Comparison of the Properties of Racemic 65 and the Resolved Enantiomers with the Analogous Carbon Compounds**

|                            | rac-venlafaxine (64) | (R)-venlafaxine | (S)-venlafaxine | rac-sila-venlafaxine (65) | (R)-sila-venlafaxine | (S)-sila-venlafaxine |
|----------------------------|----------------------|-----------------|-----------------|---------------------------|----------------------|----------------------|
| SERT IC <sub>50</sub> (μM) | 0.020                | 0.030           | 0.007           | 1.063                     | 3.168                | 0.791                |
| NET IC <sub>50</sub> (μM)  | 0.149                | 0.061           | 0.754           | 0.109                     | 0.251                | 4.715                |
| DAT IC <sub>50</sub> (μM)  | 4.430                | 19.600          | 6.670           | 2.630                     | 5.270                | 36.35                |
| pK <sub>a</sub>            | 9.7                  |                 |                 | 9.7                       |                      |                      |
| log P                      | 3.13                 |                 |                 | 3.21                      |                      |                      |
| log D (pH 7.4)             | 0.88                 |                 |                 | 0.92                      |                      |                      |

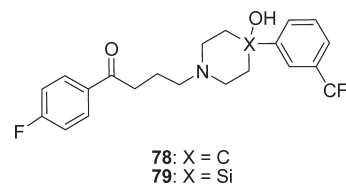
**Table 14. Comparative in Vitro Data for 66 and 67**

|                              | 66: X = C                    | 67: X = Si                   |
|------------------------------|------------------------------|------------------------------|
| logD (pH = 7.4)              | 2.42                         | 2.77                         |
| pK <sub>a</sub>              | 9.07                         | 9.27                         |
| Solubility (μM)              | 90                           | 78                           |
| Caco Papp                    | 18.9 x 10 <sup>-6</sup> cm/s | 19.8 x 10 <sup>-6</sup> cm/s |
| Ki hD <sub>1</sub> (nM)      | 107                          | 162                          |
| Ki hD <sub>2</sub> (nM)      | 2.84                         | 0.55                         |
| Ki hD <sub>3</sub> (nM)      | 10.4                         | 4.73                         |
| Ki hD <sub>4</sub> (nM)      | 7.94                         | 14.1                         |
| Ki hD <sub>5</sub> (nM)      | 38.0                         | 16.6                         |
| Ki σ <sub>1</sub> (nM)       | 1.9                          | 3.4                          |
| Ki σ <sub>2</sub> (nM)       | 78.1                         | 309                          |
| Cl/T <sub>1/2</sub> (rat LM) | 21 mL/min/mg//65 min         | 78 mL/min/mg//18 min         |
| Cl/T <sub>1/2</sub> (HLM)    | 20 mL/min/mg//51 min         | 21 mL/min/mg//65 min         |
| CYP 3A4 inhibition (μM)      | 26.2                         | 9.6                          |

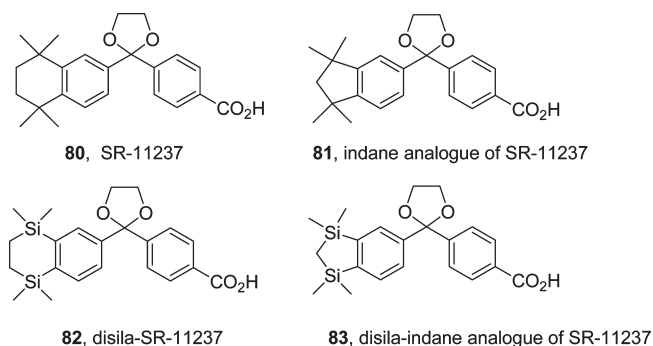
**Figure 10. Metabolism of 66 compared with the analogous sila analogue 67.****Figure 11. Metabolism of 67 in human liver microsomes (HLM).**

antagonist trifluoperidol (78) has been profiled to show that the silicon switch reduced affinity for D2 receptors by 10-fold with

minimal effect on D1 binding, reducing the D2/D1 selectivity of 79 to 3-fold.<sup>106</sup>



**3.2.8. Silicon/Carbon Isosterism in Retinoids.** The silicon analogues of two retinoid X receptor (RXR) activators, SR-11237 (80) and its indane-based homologue 81, were compared with the corresponding disila derivatives 82 and 83, respectively.<sup>107,108</sup> In this study, the two ring sizes were probed based on an appreciation of the increased C–Si bond lengths compared to C–C. While the disilane 82 exhibited a slight advantage over the carbon analogue 80, the disila-indane analogue 83 was found to be a 10-fold more potent RXR activator than the carbon analogue 81, providing the first demonstration of increased potency for a silicon switch. An X-ray cocrystal structure revealed additional interactions between 83 and helices 7 and 11 in the RXR protein, providing a potential explanation for the observed potency differences.<sup>107,108</sup>

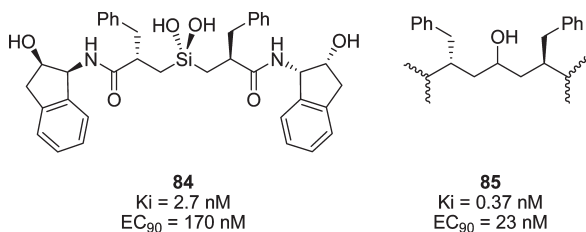


**3.2.9. Silicon/Carbon Exchange in Protease Inhibitors.** Sieburth has pioneered the exploration and application of silane diols as potentially chemically stable transition state mimetics of a hydrated carbonyl moiety in protease inhibitor design.<sup>109</sup> Carbonyl hydration is typically disfavored in the absence of activation by powerful electron withdrawing groups, whereas the silanediol moiety offers diametrically complementary properties, since it will dehydrate only under forcing conditions (Figure 12). Synthetic access to target molecules had to be developed in order to probe these transition state mimetics, and there was concern a priori that the target molecules may be chemically unstable because the simple homologue MeSi(OH)<sub>2</sub>Me readily polymerizes into siloxane, a process known to decrease in rate as the size of the organic group increases.<sup>109</sup>

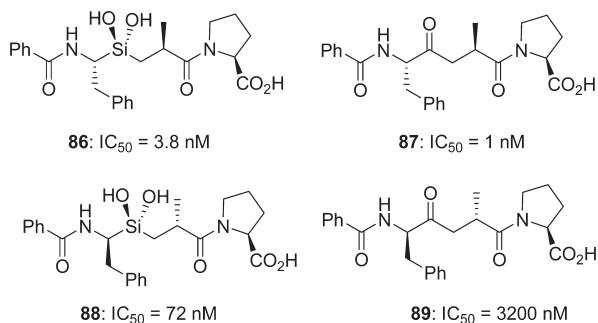


**Figure 12.** Comparison of the hydration equilibrium for the carbonyl and silanone moieties.

**3.2.10. Silanediols as HIV-1 Protease Inhibitors.** Inhibition of HIV-1 protease was examined initially because it offered a well-established class of enzyme inhibitor with extensive existing SAR that would facilitate the appropriate comparisons. The silanediol **84** inhibited HIV-1 protease with  $K_i = 2.7$  nM, which compared favorably to the more conventional secondary alcohol **85**,  $K_i = 0.37$  nM, with the modest 7-fold reduction in potency attributed to the increased size of Si and the attendant longer C–Si bonds.<sup>109,110</sup> In cell culture, the silanediol **84** exhibited antiviral activity commensurate with enzyme inhibitory activity that was not significantly affected by the presence of human serum.<sup>109,110</sup>

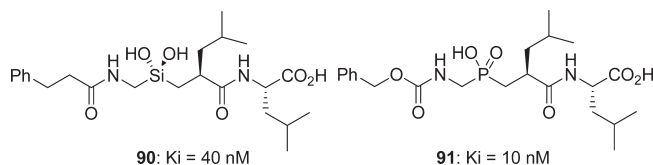


**3.2.11. Silanediols in Angiotensin Converting Enzyme Inhibitors.** Angiotensin converting enzyme (ACE) is a  $Zn^{2+}$ -dependent metalloprotease that is the biochemical target of captopril, the first clinically effective inhibitor of ACE to be marketed. The inhibitory activity of the silanediol-based **86** is just 4-fold weaker than the carbon analogue, ketone **87**. However, inverting the two chiral centers adjacent to the  $Zn^{2+}$ -binding element revealed significant differences in potency between the silicon and carbon homologues, with the Si-based **88** more effectively preserving activity than **89**, hypothesized to be a function of conformational differences between the two molecules.<sup>109,111</sup>



**3.2.12. Silicon in Thermolysin Inhibitors.** Application of the silane diol transition state mimetic was extended to the related  $Zn^{2+}$ -dependent metalloprotease thermolysin for which potent inhibitors are typically based on phosphinic acids. Silicon and phosphorus are second row elements with similar atomic radii, 1.10 and 1.05 Å, respectively, but they are very different electronically. Moreover, their physical properties differ markedly, with phosphinic acids anionic and acidic while silanediols are neutral species at physiological pH. Nevertheless, the silanediol **90** inhibited thermolysin with potency similar to that of the phosphinic acid prototype **91**. Determination of the solid state structure of a silanediol/thermolysin cocrystal revealed a similar

bound conformation to the analogous phosphinic acid, with a single oxygen atom of the silanediol within bonding distance of the active site zinc.<sup>109,112,113</sup>



**3.2.13. Cyclopropyl Rings as Alkyl Isosteres.** Cyclopropyl moieties have been examined as isosteres of alkyl groups based on their size similarity and typically improved metabolic stability. However, prudence is advisable when strategically deploying cyclopropyl moieties because the inherent ring strain can be a source of metabolic activation, well documented in the context of cyclopropyl amines.<sup>58</sup> In the series of respiratory syncytial virus (RSV) fusion inhibitors **92–96** compiled in Table 15, the *N*-isopropenyl (**92**), *N*-isopropyl (**93**), *N*-*tert*-butyl (**94**), and *N*-cyclobutyl (**96**) derivatives were characterized as potent antiviral agents but each exhibited poor metabolic stability in human liver microsomes (HLM).<sup>114,115</sup> The *N*-cyclopropyl analogue **95** provided a satisfactory solution, maintaining antiviral activity while uniquely improving metabolic stability. Notably, although the cyclopropyl moiety reduced cLogP by 0.5 compared to isopropyl, Caco-2 cell permeability was maintained and this element was subsequently incorporated into a molecule closely related to **95** that was identified with the potential for clinical evaluation.<sup>114,115</sup>

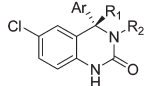
**3.2.14. Cyclopropyl in T-Type  $Ca^{2+}$  Channel Antagonists.** In a potent series of quinazoline-based T-type  $Ca^{2+}$  channel antagonists, a cyclopropyl moiety was introduced to replace the *N*-ethyl substituent in lead **97** in an effort to reduce *N*-dealkylation and improve oral bioavailability (Table 16).<sup>116</sup> Although compound **98** successfully addressed the primary deficiency, time-dependent CYP inhibition was introduced as an unacceptable liability, necessitating further optimization. In this setting, the *N*- $CH_2CF_3$  analogues **99** and **100** provided the sought after compromise in properties.

**3.2.15. Cyclopropyl in CRF-1 Antagonists.** The pyrazolo[3,4-*d*]pyrimidine derivative **101** is a potent corticotropin releasing factor-1 (CRF-1) receptor antagonist that demonstrates poor metabolic stability in HLM, attributed to the high cLogP (Table 17).<sup>117</sup> In an effort to address this problem, the introduction of polarity in the *N*-1 and *C*-4 substituents and at other sites of the molecule was examined. This exercise produced **102**, a compound that reflected a trend of improved metabolic stability broadly correlating with reduced lipophilicity.<sup>117</sup> However, since

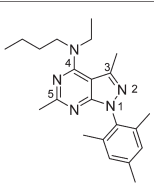
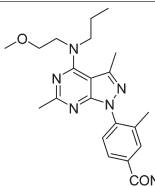
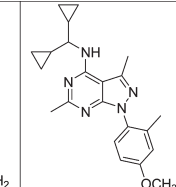
**Table 15. Effect of N-Substituent Variation on the in Vitro Properties of a Series of RSV Inhibitors**

| Compd     | R                  | EC <sub>50</sub> (μM) | HLM T <sub>1/2</sub> (min) | Caco-2 (nm/s) | cLogP |
|-----------|--------------------|-----------------------|----------------------------|---------------|-------|
| <b>92</b> | <i>i</i> -propenyl | 0.003                 | 11                         | 230           | 2.02  |
| <b>93</b> | <i>i</i> -Pr       | 0.004                 | 7.4                        | 169           | 2.21  |
| <b>94</b> | <i>t</i> -Bu       | 0.003                 | 4.0                        | 214           | 2.61  |
| <b>95</b> | <i>c</i> -Pr       | 0.010                 | 39                         | 181           | 1.72  |
| <b>96</b> | <i>c</i> -Bu       | 0.016                 | 4.6                        | 168           | 2.28  |

**Table 16. Effect of N-Substituent Variation on the Biochemical Profile of a Series of T-Type Ca<sup>2+</sup> Channel Antagonists**

| Compd #  |  |                                |                                   |                                    |
|--|---|--------------------------------|-----------------------------------|------------------------------------|
|  | 97  | 98                             | 99                                | 100                                |
| Ar   | C <sub>6</sub> H <sub>5</sub>   | C <sub>6</sub> H <sub>5</sub>  | 4-F-C <sub>6</sub> H <sub>4</sub> | 4-CN-C <sub>6</sub> H <sub>4</sub> |
| R <sup>1</sup>   | C <sub>2</sub> H <sub>5</sub>   | C <sub>2</sub> H <sub>5</sub>  | C <sub>2</sub> H <sub>5</sub>     | cC <sub>3</sub> H <sub>5</sub>     |
| R <sup>2</sup>   | C <sub>2</sub> H <sub>5</sub>   | cC <sub>3</sub> H <sub>5</sub> | CH <sub>2</sub> CF <sub>3</sub>   | CH <sub>2</sub> CF <sub>3</sub>    |
| T-Type Ca <sup>2+</sup> channel antagonist activity - FLIPR depolarized (nM) | 17  | 71                             | 61                                | 14                                 |
| TDI of CYP (% CYP 3A4 activity remaining)                                    | NT  | 15%                            | 74%                               | Weak inhibition                    |
| PXR (% rifampicin @ 10 μM)   | NT  | 17%                            | 63%                               | 66%                                |
| % oral bioavailability in the rat  | 0%  | 44%                            | 100%                              | 49%                                |

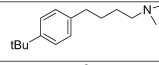
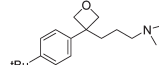
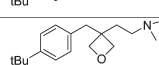
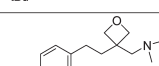
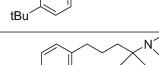
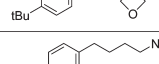
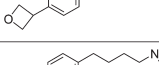
**Table 17. Structure–Activity Relationships Associated with a Series of Corticotropin Releasing Factor-1 (CRF-1) Receptor Antagonists**

| Compound #            |  |  |  |
|-----------------------|---|---|---|
| Ki for CRF1           | 9 nM  | 275 nM  | 32 nM   |
| cLogP                 | 6.75  | 3.5   | 5.0   |
| HLM Cl <sub>int</sub> | >320 mL/min/mg  | 17 mL/min/mg  | <11 mL/min/mg   |

CRF-1 receptor affinity was markedly reduced by the introduction of polar elements, the authors returned to an NCH(cPr)<sub>2</sub> moiety at C-4 that had been explored earlier but that had exhibited instability under acidic conditions. However, in this circumstance **103** emerged as an acid-stable CRF-1 antagonist with an acceptable combination of biological properties.<sup>117</sup>

**3.2.16. Oxetanes as Mimetics of Alkyl Moieties.** The properties of oxetanes have recently been examined in a systematic fashion and shown to productively influence several properties of interest in drug design, including a role as isosteres of alkyl substituents.<sup>118–120</sup> The *gem*-dimethyl moiety is typically introduced as a conformational constraint, taking advantage of the Thorpe–Ingold effect, or as a strategy to block a site of metabolism. However, a *gem*-dimethyl substituent typically increases lipophilicity by ~1 log<sub>10</sub> unit compared to the methylene precursor, frequently leading to the adoption of the cyclopropyl element as an isostere that more modestly alters lipophilicity. The oxetane moiety offers an alternative that is essentially liponeutral, affording no net increase in lipophilicity compared to a dihydrogen progenitor that, more importantly, occupies almost the same van der Waals volume as a *gem*-dimethyl group.<sup>118–121</sup> A systematic analysis of the effect of introducing an oxetane ring into a druglike molecule was explored in the context of the phenylbutylamine **104**, a prototypical amphiphilic compound poorly soluble in water in the neutral form (Table 18).<sup>118–120</sup> The properties of **104** were such that it was a significant inhibitor of the hERG ion channel, IC<sub>50</sub> = 7.5 μM, and expressed properties predictive of the potential to cause phospholipidosis. In the homologous series of oxetane derivatives **105–111** summarized in Table 18, the basicity of the amine element was

**Table 18. Physical Properties Associated with a Series of Oxetane Derivatives Derived from the Phenylbutylamine 104**

| Compound # | Structure  | pKa of N | Solubility (μg/mL) | Cl <sub>int</sub> (HLM) (μL/min/mg) <sup>a</sup> | Cl <sub>int</sub> (MLM) (μL/min/mg) <sup>b</sup> | LogD <sup>c</sup> (LogP) <sup>d</sup> |
|------------|--|----------|--------------------|--|--|---------------------------------------|
| 104        |  | 9.9      | <1                 | 16   | 417  | 1.8 (4.3)                             |
| 105        |  | 9.6      | 270                | 0  | 147  | 1.7 (3.9)                             |
| 106        |  | 9.2      | 4100               | 6  | 13   | 1.7 (3.5)                             |
| 107        |  | 8.0      | 25                 | 42   | 383  | 3.3 (4.0)                             |
| 108        |  | 7.2      | 57                 | 13   | 580  | 3.3 (3.6)                             |
| 109        |  | 9.9      | 4000               | 2  | 27   | -0.1 (2.4)                            |
| 110        |  | 9.9      | 4400               | 0  | 43   | 0.8 (3.3)                             |

<sup>a</sup> HLM = human liver microsomes. <sup>b</sup> MLM = mouse liver microsomes. <sup>c</sup> Logarithm of octanol/water distribution coefficient at pH 7.4. <sup>d</sup> Lipophilicity of the neutral base defined by log P = log D<sup>pH</sup> + log(1 + 10<sup>(pK<sub>a</sub> - pH)</sup>).

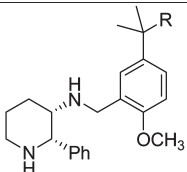
reduced, dependent on proximity to the oxetane ring, while solubility increased in a fashion independent of the site of deployment of the oxetane ring. Moreover, several of these molecules demonstrated increased metabolic stability in human and mouse liver microsomes while compound **110** exhibited diminished hERG inhibition (hERG IC<sub>50</sub> = 35 μM) compared to **104** and a reduced theoretical potential to cause phospholipidosis.<sup>118,119</sup>

**3.2.17. CF<sub>3</sub> as a Substitute for Methyl in a *tert*-Butyl Moiety.** The CF<sub>3</sub> moiety has been explored as a substitute for a CH<sub>3</sub> in *tert*-butyl-substituted antagonists of the neurokinin 1 (NK1) receptor recognized by substance P, agents potentially useful in the treatment of depression and for inducing analgesia, and in antagonists of the TRPV1 receptor, a nonselective cation channel found on peripheral sensory neurons.<sup>122</sup> In both cases, the *tert*-butyl-substituted lead compounds demonstrated poor metabolic stability in vitro with the *t*-Bu group shown to be susceptible to oxidation. CF<sub>3</sub>-substituted NK1 homologues retained intrinsic potency and showed reduced clearance in HLM (Table 19) while in TRPV1 antagonists, a simple CF<sub>3</sub> substitution led to increased HLM stability but poor biological activity, attributed to the electron withdrawing properties of the CF<sub>3</sub> moiety (Table 20).<sup>122</sup>

A key question with respect to the role of the CF<sub>3</sub> moiety as an alkyl isostere is its size relative to the groups that it is replacing. The CF<sub>3</sub> moiety is frequently considered to be isosteric with an isopropyl group, but Taft's Es values suggest that CF<sub>3</sub> is larger than *i*-Pr although smaller than *t*-Bu while the van der Waals volume indicates that CF<sub>3</sub> is similar in size to CH<sub>3</sub>CH<sub>2</sub> and smaller than *i*-Pr (Table 21). In an attempt to resolve this discrepancy, the rotational barriers in ortho-substituted biphenyls have been determined, with the result that in this setting the CF<sub>3</sub> substituent is bulkier than a CH<sub>3</sub> moiety, comparable to isopropyl and actually larger than (CH<sub>3</sub>)<sub>3</sub>Si.<sup>42,123</sup>

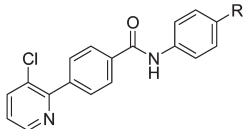
However, the CF<sub>3</sub> moiety clearly has a very different topographical shape to an isopropyl group and a recent investigation

**Table 19.** Comparison of the Effects of Substituting a CH<sub>3</sub> by CF<sub>3</sub> in NK1 Antagonists



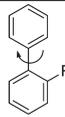
|                                   | R = CH <sub>3</sub> | R = CF <sub>3</sub> |
|-----------------------------------|---------------------|---------------------|
| NK1 binding IC <sub>50</sub> (nM) | 0.6                 | 0.3                 |
| HLM Cl <sub>int</sub> (μL/min/mg) | 87.9                | 44.7                |

**Table 20.** Comparison of the Effects of Introducing a CF<sub>3</sub> Moiety in TRPV1 Antagonists



| R  | tBu | C(CH <sub>3</sub> ) <sub>2</sub> CF <sub>3</sub> | CF <sub>3</sub> |
|--|-----|--|-----------------|
| TRPV1 functional activity hIC <sub>50</sub> (nM) | 37  | 42   | 200             |
| HLM Cl <sub>int</sub> (mL/min/kg)                | 168 | 46   | <10.5           |

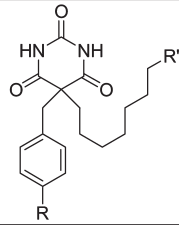
**Table 21.** Comparison of the Steric Size of Alkyl, CF<sub>3</sub>, and Silyl Moieties Using Different Methods of Analysis

| Moiety                             | Taft's Es value | A Values (kcal/mol) | van der Waals volume (Å) | Interference values (kcal/mol) |  |
|------------------------------------|-----------------|---------------------|--------------------------|--------------------------------|---|
| H                                  | 0               |                     | 1.20                     |                                |   |
| CH <sub>3</sub>                    | -1.24           | 1.70                | 21.6                     | 9.7                            |   |
| CH <sub>3</sub> CH <sub>2</sub>    | -1.31           | 1.70                | 38.9                     |                                |   |
| iPr                                | -1.71           | 2.15                | 56.2                     | 12.6                           |   |
| CF <sub>3</sub>                    | -2.40           | 2.10                | 39.8                     | 12.1                           |   |
| tBu                                | -2.78           | >4.50               |                          | 18.3                           |   |
| CH <sub>3</sub> S                  |                 |                     |                          | 9.9                            |   |
| (CH <sub>3</sub> ) <sub>2</sub> Si |                 |                     |                          | 11.3                           |   |
| Br                                 |                 |                     |                          | 10.2                           |   |
| I                                  |                 |                     |                          | 10.9                           |   |

has explored the size of the CF<sub>3</sub> group in the context of inhibitors of matrix metalloprotease-9 (MMP-9).<sup>124</sup> MMP-9 was considered a useful probe of this concept based on the shallow, tunnel-like S1' pocket projecting into a well-defined lipophilic pocket that was viewed as a sensitive probe with which to explore steric effects associated with the side chain terminus of barbiturate-based inhibitors. As summarized in Table 22, a methyl and ethyl terminus afforded potent MMP-9 inhibitors but a terminal isopropyl group reduced potency by 1000-fold while a CF<sub>3</sub> moiety retained activity, leading to the conclusion that CF<sub>3</sub> more closely resembled CH<sub>3</sub>CH<sub>2</sub> rather than *i*-Pr.<sup>124</sup>

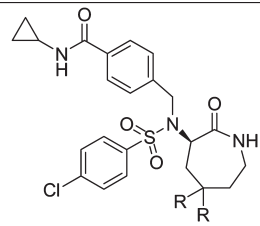
3.2.18. CF<sub>2</sub> as an Isostere of C(CH<sub>3</sub>)<sub>2</sub>. An interesting example of the potential of CF<sub>2</sub> to function as an isostere of C(CH<sub>3</sub>)<sub>2</sub> has been described in a series of  $\gamma$ -secretase inhibitors that demonstrated a potent A $\beta$ -lowering effect in a cell-based assay.<sup>125</sup> As compiled in Table 23, the potency of the prototype **111** was improved 10-fold by *gem*-dimethyl substitution of the azepinone ring (**112**), but metabolic stability in human and mouse

**Table 22.** Structure–Activity Relationships Associated with Variation of the Alkyl Side Chain Terminus in a Series of MMP-9 Inhibitors



| MMP-9 inhibition: IC <sub>50</sub> (nM) |       |                      |
|---|-------|----------------------|
| R'                                      | R = H | R = OCH <sub>3</sub> |
| CH <sub>3</sub>                         | 1     | 10                   |
| Et                                      | 2     | 27                   |
| <i>i</i> Pr                             | 1800  | 4500                 |
| CF <sub>3</sub>                         | 87    | 22                   |

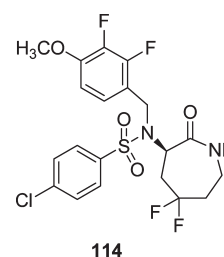
**Table 23.** In Vitro A $\beta$ -Reducing Potency and Metabolic Stability of a Series of 2-Oxoazepane-Based  $\gamma$ -Secretase Inhibitors



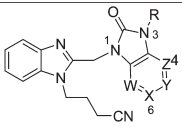
| Compd #    | R               | A $\beta$ reduction: IC <sub>50</sub> (μM) | Cl (μL/min/mg) |          |
|------------|-----------------|--|----------------|----------|
|            |                 |  | HLM            | Mouse LM |
| <b>111</b> | H*              | 0.17                                       | -              | -        |
| <b>112</b> | CH <sub>3</sub> | 0.015                                      | 36             | 655      |
| <b>113</b> | F               | 0.004                                      | 1.9            | 2.2      |

\* tested as a racemic mixture at C-2 of the 2-oxoazepane

liver microsomal preparations was poor. The *gem*-difluoro analogue **113** exhibited improved potency and metabolic stability but was poorly active in a transgenic mouse model of  $\gamma$ -secretase activity, attributed to the two amide functionalities reducing CNS penetration. Optimization to address this issue produced the anisole derivative **114** which retained potency and metabolic stability in HLM and was active in the mouse model at a dose of 20 mpk.<sup>125</sup>



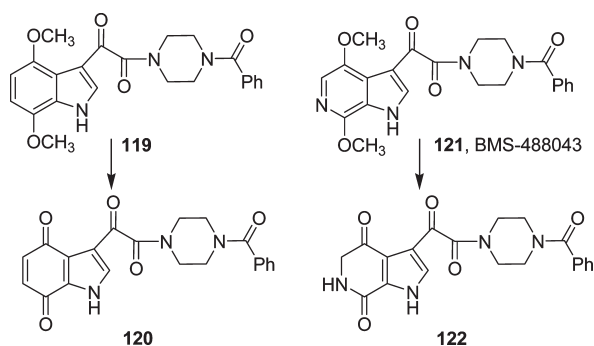
3.3. N Substitution for CH in Benzene Rings. Several examples in the recent literature demonstrate advantage with this classical isosteric substitution.<sup>115,126–132</sup> In the series of potent RSV fusion inhibitors captured in Table 24, the introduction of a pyridine ring was probed systematically with the objective of reducing the hydroxylation of the phenyl ring seen with the parent benzimidazol-2-one **115**.<sup>114,115</sup> Antiviral activity

**Table 24. Structure–Activity Relationships Associated with a Series of RSV Fusion Inhibitors**


| Compd # | W  | X  | Y  | Z  | R   | Inhibition of RSV replication EC <sub>50</sub> (nM) | Cytotoxicity CC <sub>50</sub> (μM) |
|---------|----|----|----|----|---|---|------------------------------------|
| 115     | CH | CH | CH | CH |  | 5   | 13                                 |
| 116     | N  | CH | CH | CH |   | 3   | >216                               |
| 92      | CH | N  | CH | CH |   | 7   | 236                                |
| 117     | CH | CH | CH | N  |   | 200   | 150                                |
| 118     | CH | CH | N  | CH | H   | 5700  | 264                                |

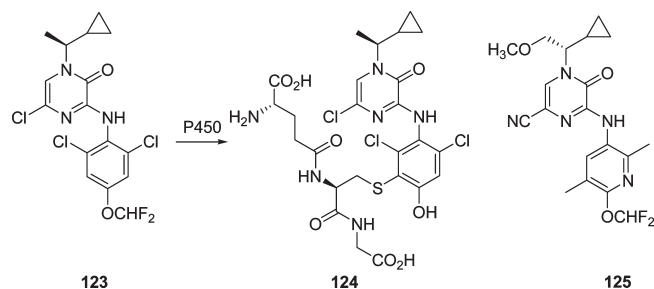
was clearly sensitive to the topological location of the N atom, and preferred compounds demonstrated improved metabolic stability and increased solubility without introducing the burden of CYP 450 inhibition, a potential problem with pyridine derivatives. The 6-aza-benzimidazol-2-one discovered with **92** was ultimately incorporated into the clinical candidate that emerged from these studies.<sup>114,115</sup>

In a series of HIV-1 attachment inhibitors, the 4,7-dimethoxy-substituted indole **119** is a highly potent antiviral agent that is metabolized in HLM by O-demethylation, leading to the potential for quinone formation (**120**), a known toxicophore.<sup>126</sup> A systematic survey that replaced CH with N at each of the aromatic sites of the indole ring revealed that the 6-aza analogue **121** (BMS-488043) offered improved aqueous solubility and abrogated the potential for reactive quinone formation should demethylation occur, which in this series would afford the amide **122**.<sup>126</sup> Compound **121** was advanced into clinical trials where it provided proof-of-concept for inhibition of HIV attachment as an approach to reducing HIV-1 replication in infected subjects.<sup>126</sup>

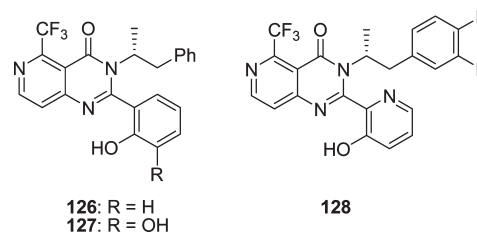


**3.3.1. N for CH in Phenyl Rings in CRF-1 Antagonists.** The pyrazinone **123** is representative of a series of potent CRF-1 receptor antagonists, but 60% of the dose administered to rats appeared as oxidized metabolites in bile, with 25% of the dose excreted as GSH adducts.<sup>127–129</sup> The phenyl ring was identified as the site of metabolic activation, producing the GSH adduct **124**, which led to a focus on pyridine analogues. An initial survey indicated substantially reduced levels of bioactivation with the pyridine heterocycle series, and this element was ultimately incorporated into molecules selected for further development. However, the isolated olefin of the pyrazinone heterocycle was

also subject to oxidative bioactivation, a problem resolved by replacing the Cl atom with an electron withdrawing nitrile. In addition, the introduction of an O-methyl ether in the side chain successfully provided a metabolic soft spot to redirect metabolism, realizing **125** as a compound with an acceptable profile.<sup>127–129</sup>

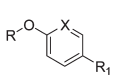


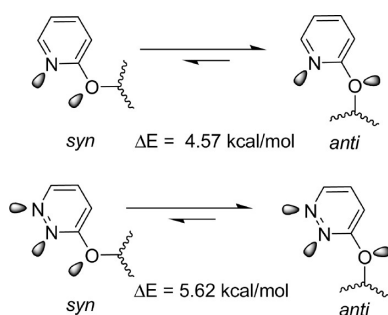
**3.3.2. N for CH in Phenyl Rings in Calcium Sensing Receptor Antagonists.** In a series of short-acting calcium sensing receptor antagonists with potential for the treatment of osteoporosis, CYP 3A4-mediated oxidation of the phenol of **126** to the catechol **127** and then to the ortho quinone was identified as the source of GSH adducts in human and rat liver microsomes.<sup>130,131</sup> The introduction of a nitrogen atom to the phenol ring (**128**) reduced the metabolic activation rate and markedly diminished the formation of GSH adducts by over 50-fold. This observation was supported by quantum chemistry calculations which indicated that oxidation of the aza-catechol derived from **128** to the quinone is energetically less favorable than for the benzene analogue **127**.



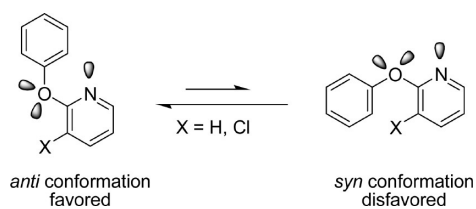
A similarly successful tactic has been described for the partially disclosed phenol ether chemotype **129** presented in Table 25 where tritiated derivatives were used to assess protein covalent binding (PCB) to human and rat liver microsomal proteins in the absence and presence of GSH.<sup>132</sup> Iterative design optimization focused on the simple pyridine analogue **130**, since 3,4-difluoro substitution of the phenyl ring of **129**

**Table 25. In Vitro Protein Covalent Binding for the Phenol Ether 129 and Two Pyridine Analogues**

| Compd # |  | Covalent binding of tritiated compound to liver microsomal protein (pmol equiv. mg <sup>-1</sup> protein after a 1 hour incubation) |               |        |               |
|---------|--|---|---------------|--------|---------------|
|         |  | Human   |               | Rat    |               |
|         |  | No GSH  | With 5 mM GSH | No GSH | With 5 mM GSH |
| 129     | X = CH; R <sub>1</sub> = H   | 3870  | 647           | 1490   | 325           |
| 130     | X = N; R <sub>1</sub> = H  | 911   | 294           | 535    | 139           |
| 131     | X = N; R <sub>1</sub> = CF <sub>3</sub>  | 88  | 27            | 111    | 24            |



**Figure 13.** Calculated energies of *syn* and *anti* 2-methoxypyridine and 3-methoxypyridazine conformers.

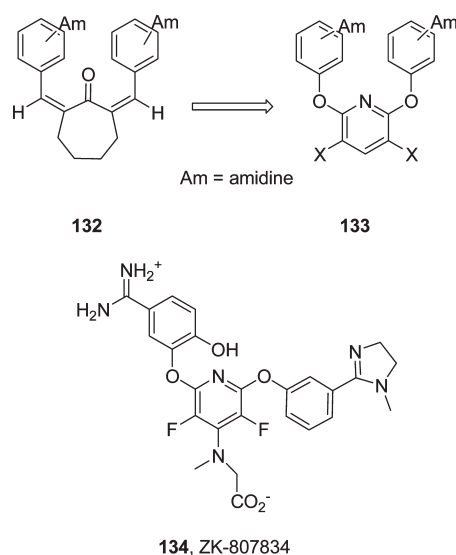


**Figure 14.** Conformational preference in 2-phenoxy pyridines.

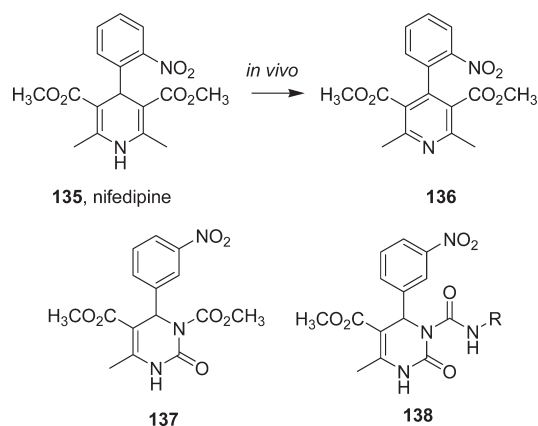
reduced PCB by only 2-fold. Pyridine **130** exhibited 2- to 4-fold reduced PCB that was further refined by the introduction of a  $\text{CF}_3$  substituent to the heterocyclic ring to afford **131**, which diminished microsomal protein binding to acceptable levels.

In the example described above, the nitrogen atom replaces a carbon atom adjacent to the oxygen of an aryl ether to afford a 2-alkoxypyridine, an isosteric conversion that introduces implications with respect to conformational bias and which extends to other heterocyclic ring systems. As a consequence of the preferred orientation of in-plane lone pairs, the *anti* relationship between the lone pairs of the hetero atoms is strongly preferred based on calculated energies.<sup>91,133</sup> This orientation is commonly observed in X-ray crystal structures, leading to an influence on substituent topology, an effect that extends to a range of nitrogen-containing heterocycles.<sup>91,133</sup> Figure 13 illustrates the calculated energetic preferences for 2-methoxypyridine and 3-methoxypyridazine.<sup>133</sup>

The design of a series of factor Xa inhibitors based on the 2,7-dibenzylidencycloheptanone **132** took advantage of this phenomenon to productively influence conformation.<sup>134–136</sup> The substituted phenoxy moiety in **133** was anticipated to act as a partial olefin isostere, presenting the aryl rings in a topology controlled by nonbonded interactions between the ether oxygen atom and pyridine nitrogen lone pairs. This concept is captured schematically in Figure 14, where *syn* and *anti* refer to the relationship between the lone pairs on the heteroatoms.<sup>134–136</sup> These insights were incorporated into the design of ZK-807834 (**134**) in which the predicted topology of the amidine-substituted phenoxy moiety was observed in the X-ray of this compound complexed with factor Xa.<sup>136</sup> Interestingly, however, the other phenoxy moiety adopted the alternative conformation reflected in the topology depicted in **134**.

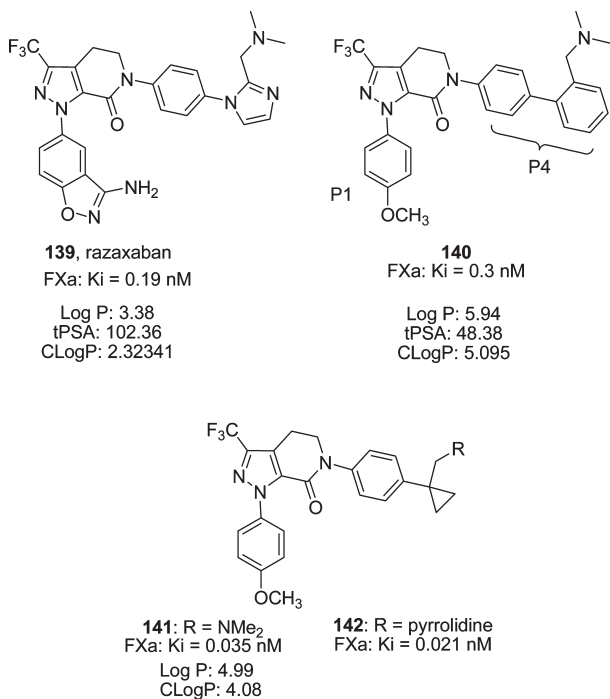


**3.3.3. N for C Substitution in Dihydropyridine Derivatives.** In a strategy seeking to interfere with metabolic deactivation of an active drug, a nitrogen-for-carbon switch was examined in a series of dihydropyridine (DHP)-based  $\text{Ca}^{2+}$ -channel blockers.<sup>137–140</sup> Nifedipine (**135**) is a potent  $\text{Ca}^{2+}$ -channel blocker used as a coronary vasodilator that is subject to a facile first-pass oxidation in vivo to the inactive pyridine **136**. The dihydropyrimidinone heterocycle was established as an effective isosteric pharmacophore that preserves the critical DHP NH as a H-bond donor based on the presence of either a carbonyl or thiocarbonyl at C-2. Acylation of the C-3 nitrogen (**137**) improved mimicry of the DHP ring system with ureido compounds **138** found to be more stable toward deacylation in vivo while favoring a topology analogous to that expressed in the DHPs based on dipole–dipole interactions and intramolecular H-bonding.<sup>137–140</sup> Most importantly, the dihydropyrimidinone ring is resistant to oxidation, and this tactical application of bioisosterism was subsequently adopted to optimize a series of  $\alpha_{1a}$ -adrenergic antagonists based on a DHP core.<sup>141,142</sup>

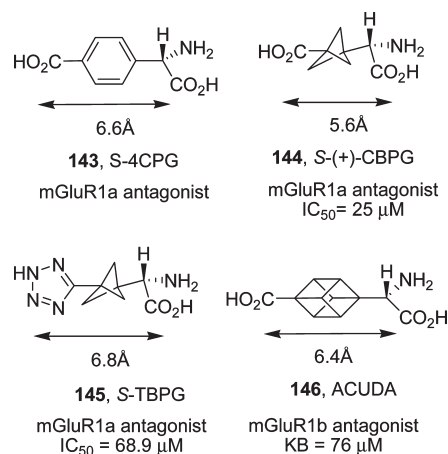


**3.4. Biphenyl and Phenyl Mimetics.** **3.4.1. Biphenyl Mimetics in Factor Xa Inhibitors.** In a series of potent factor Xa inhibitors related to razaxaban (**139**), the methoxyphenyl ring of **140** occupies the S1 pocket while the biphenyl moiety projects into the S4 pocket.<sup>143</sup> Phenylcyclopropanes were explored

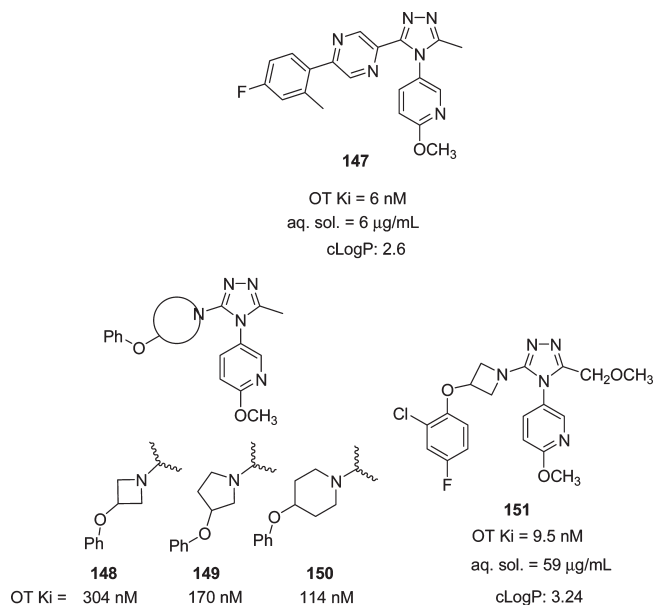
as mimetics of the imidazole-phenyl and biphenyl elements of **139** and **140**, respectively, in an effort to identify compounds with reduced molecular weight and a lower cLogP. With no benzylic ( $\alpha$ -) substituent, the cyclopropane moiety of cyclopropylbenzene preferentially adopts a bisected conformation in which the C–H bond is coplanar with the phenyl ring, since this allows overlap of the cyclopropane orbitals with the  $\pi$  system.<sup>143</sup> However, the introduction of a substituent at the  $\alpha$ -position favors the perpendicular conformation, preferred by 0.7 kcal/mol when the substituent is CH<sub>3</sub>. These insights led to the design of **141** in which the Me<sub>2</sub>N moiety is preferentially projected with a similar vector to that of the biphenyl, confirmed by an X-ray cocrystal of pyrrolidine **142** with factor Xa.<sup>143</sup> Compounds **141** and **142** demonstrated markedly improved potency, a general phenomenon observed across several paired analogues that appears to be a function of optimized hydrophobic interactions with S4 and slightly reduced strain in the bound geometry. The cyclopropylmethyl moiety exhibits lower lipophilicity compared to the biphenyl **140**, with both log P and clog P reduced by  $\sim 1$  log<sub>10</sub>.<sup>143</sup>



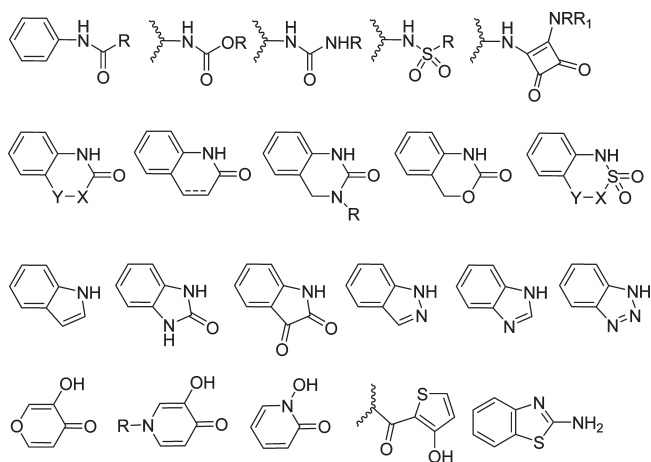
**3.4.2. Phenyl Mimetics in Glutamate Analogues.** S-4CPG (**143**) is a mGluR1 receptor antagonist in which activity is sensitive to both the distance between the CO<sub>2</sub>H and  $\alpha$ -amino acid moieties and the linear topological relationship. The propellane **144** was explored as an isostere of the benzene ring in **143** and exhibited antagonist activity at mGluR1a.<sup>144–146</sup> However, it was recognized that the distance between the CO<sub>2</sub>H functionalities in **144** is shorter than in **143**, leading to the synthesis of the tetrazole **145** as a compound designed to address this deficiency. Although a logical design concept, this compound failed to demonstrate the anticipated improved antagonist potency at mGluR1a.<sup>146</sup> The cubane analogue **146** was also prepared and found to be a modestly active antagonist of mGluR1b.<sup>145</sup>



**3.4.3. Phenyl Mimetics in Oxytocin Antagonists.** The poor aqueous solubility associated with a series of oxytocin antagonists represented by **147** precipitated a strategy designed to explore modification of the biaryl moiety, with a focus on saturated compounds that typically exhibit enhanced solubility.<sup>147,148</sup> The azetidione (**148**), pyrrolidone (**149**), and piperidone (**150**) ethers were evaluated computationally and shown to exhibit good structural overlap with acceptable potency achieved experimentally with the azetidione **148**. Optimization led to the identification of **151** in which the favorable cLogP of the prototype was maintained while aqueous solubility was improved by 10-fold.<sup>147</sup>



**3.5. Phenol, Alcohol, and Thiol Isosteres.** **3.5.1. Phenol and Catechol Isosteres.** There has been a considerable investment in the identification of phenol and catechol isosteres in the medicinal chemistry literature, catalyzed largely by the development of agonists and antagonists of the biogenic amines adrenaline, dopamine, and serotonin, with the result that a range of useful surrogates are well-established, captured synoptically in Figure 15. The structural diversity, electronic properties, lipophilicity, and size of these functionalities varies widely, providing ample flexibility to customize for a

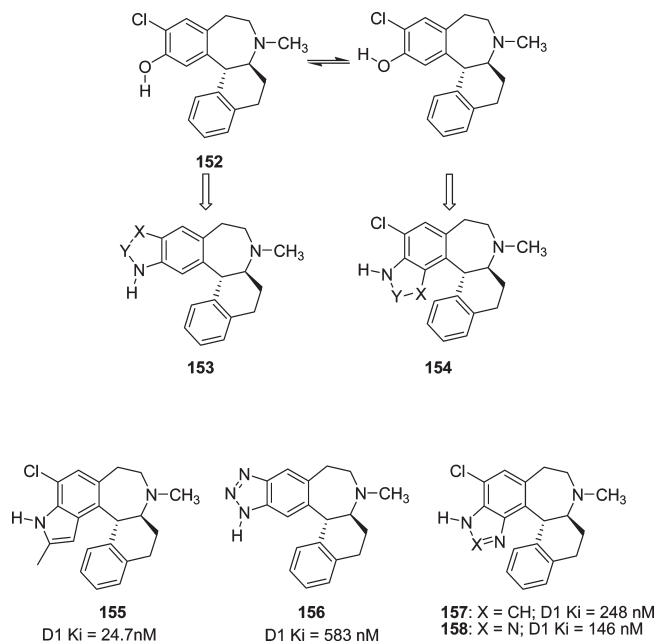


**Figure 15.** Synopsis of phenol and catechol isosteres.

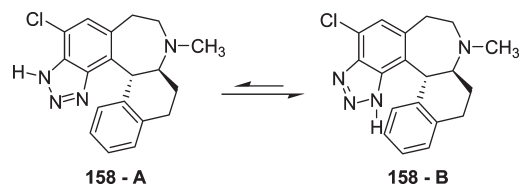
specific application. These isosteres were typically designed to overcome pharmacokinetic and toxicological limitations associated with phenols, which can be glucuronidated as a prelude to excretion, while catechols are substrates for catechol *O*-methyl transferase (COMT). Phenols can also be hydroxylated at the ortho- or para-positions, affording catechols and 1,4-dihydroxybenzenes which can be further oxidized by CYP 450 enzymes to ortho- and para-quinones, chemically reactive metabolites with the potential to bind irreversibly to proteins, a possible source of toxicity.

**3.5.2. Phenol Isosteres in Dopamine D1/D5 Antagonists.** An interesting recent example that probed a series of phenol-containing dopamine dual D1/D5 antagonists highlights the need for careful analysis and consideration in the design and deployment of phenol isosteres.<sup>149</sup> The phenol **152** (D1  $K_i = 1.2$  nM, D5  $K_i = 2.0$  nM) was advanced into clinical trials where it exhibited poor oral bioavailability due to first-pass metabolism (Figure 16). This prompted an examination of heterocycle mimetics designed to address the poor pharmacokinetic properties, with the recognition that this initiative also offered an opportunity to precisely map the topological vector associated with the phenolic H-bond donor based on the localization afforded by the complementary fused heterocyclic rings in **153** and **154** (Figure 16). Initial positive results with the indole **155** compared to the benzotriazole **156** indicated that the preferred topology of the H-bond donor is that in which the vector is projected parallel to the adjacent C–Cl bond, as depicted by **154** in Figure 16, rather than the alternative projection represented by **153**.<sup>149</sup>

However, the benzimidazole **157** and benzotriazole **158** were found to be surprisingly poor mimetics despite projecting the H-bond along the appropriate vector. A closer analysis provided an explanation, with two observations germane to understanding the observed phenomenon: first, the azole heterocycles of both **157** and **158** can exist in two tautomeric forms, and second, the phenyl element of the tetrahydronaphthalene ring adopts a conformation in which it is orthogonal to the plane of the chlorophenyl ring. In the tautomeric form depicted by **158-A** in Figure 17, the nitrogen lone pair and phenyl  $\pi$  cloud experience a repulsive interaction while in tautomer **158-B**, the N–H and aryl  $\pi$  interact productively, engaging in  $\pi$  facial H-bonding. As a consequence, tautomer **158-B** is more stable, providing a basis for the lower activity since the H atom is not available for interaction with the receptor. The relevance of tautomer **158-B** was confirmed by analysis of the <sup>1</sup>H NMR spectrum of the benzimidazole derivative where the NH was observed to resonate at  $\delta$  6.88,

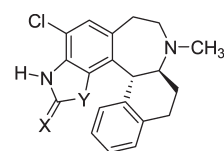


**Figure 16.** Considerations in the design of phenol mimetics in dual dopamine D1/D5 antagonists.



**Figure 17.** Benzotriazole tautomerism in dual dopamine D1/D5 antagonists.

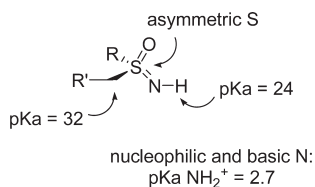
shielded by the  $\pi$  cloud, which compares with a  $\delta$  8.2 for the NH of benzimidazole. These insights predicted that the benzimidazol-2-one **159** and its thione analogue **160** with two H-bond donors should be active, a hypothesis confirmed experimentally. In the <sup>1</sup>H NMR spectra of **159** and **160**, the chemical shift of the NHs indicated that one was shielded by the aryl ring. The benzimidazol-2-one **159** is a highly potent D1/D5 dual ligand, and activity was preserved by the benzothiazolone analogue **161**, with both chemotypes demonstrating improved PK properties in rats compared to the phenol progenitor **152**.<sup>149</sup>



**159**: X = O, Y = NH; D1  $K_i = 7$  nM  
 $\delta$  NH = 10.4 & 5.4  
**160**: X = S, Y = NH; D1  $K_i = 40$  nM  
**161**: X = O, Y = S; D1  $K_i = 2.1$  nM

### 3.5.3. Alcohol and Thiol Mimetics

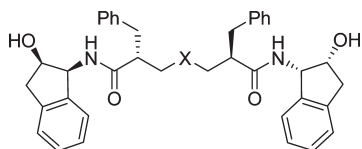
**3.5.3.1. Sulfoximine Moiety As an Alcohol Isostere.** Sulfoximines are the aza analogues of sulfones, and the introduction of the mildly basic nitrogen atom ( $pK_a$  of the protonated form is 2.7) creates asymmetry at sulfur, with the enantiomers



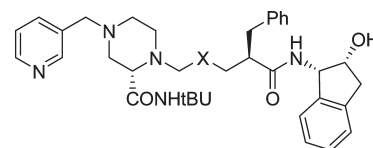
**Figure 18.** Physical properties of the sulfoximine moiety.

readily resolved and configurationally stable, fundamental properties summarized in Figure 18.<sup>150</sup> Although isosteric with sulfones, sulfoximines offer an additional substituent vector capable of projecting a range of functionality. N-Unsubstituted sulfoximines are also capable of being phosphorylated *in vivo*, biochemical pharmacology that was instrumental in the original discovery of the sulfoximine functionality in methionine sulfoximine, a proconvulsant produced in a chemical process used to bleach flour.<sup>151</sup> Phosphorylation of methionine sulfoximine afforded a mimetic of glutamate that inhibited both glutamine and  $\gamma$ -glutamylcysteine synthetases, the former leading to increased levels of glutamate in the brain, the ultimate cause of the observed convulsions.<sup>151</sup>

The unique properties of sulfoximines periodically attract the attention of medicinal chemists, and applications of this functionality have been examined in a variety of settings.<sup>150,152</sup> On the basis of its tetrahedral topography, H-bond accepting properties, and the acidity of the NH,  $pK_a = 24$ , which compares favorably with that of an alcohol ( $pK_a$  of MeOH is 29;  $pK_a$  of *i*-PrOH is 30.2;  $pK_a$  of *t*-BuOH is 33; all measured in DMSO), the sulfoximine moiety has been explored with some success as an alcohol isostere in inhibitors of HIV-1 protease.<sup>153–155</sup>

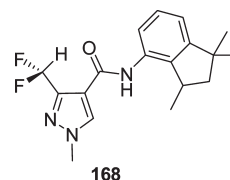


The racemic sulfoximine analogue **163** of the potent HIV-1 protease inhibitor L-700417 (**162**) was synthesized and shown to be only 4-fold less potent than the progenitor *in vitro* and active as an antiviral in cell culture,  $EC_{50} = 408$  nM, without overt cytotoxicity,  $CC_{50} > 10$   $\mu$ M.<sup>153,154</sup> The sulfoxide **164** also demonstrated biological activity,  $IC_{50} = 21.1$  nM, but the sulfone **165** was poorly active, suggestive of a role for the sulfoximine NH in alcohol mimicry.



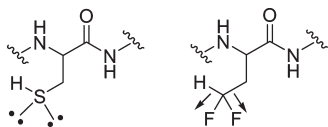
However, an attempt to extend the sulfoximine-alcohol bioisosterism to the HIV-1 protease inhibitor indinavir (**166**) by preparing the sulfoximine analogue **167** revealed surprisingly poor inhibitory activity with an  $IC_{50}$  that was determined to be 250000-fold higher than that of the alcohol **166**.<sup>155</sup> Although no structural data were obtained, docking studies suggested that the result may be a function of the limited conformational flexibility associated with this particular peptidic template that interferes with the ability of **167** to adopt an optimal binding orientation.

**3.5.3.2. RCHF<sub>2</sub> as an Isostere of ROH.** The difluoromethyl ethers CF<sub>3</sub>OCHF<sub>2</sub> and CHF<sub>2</sub>OCHF<sub>2</sub> have been shown to donate a H-bond to a variety of bases, while the CHF<sub>2</sub> moiety engages in intramolecular H-bonding with a proximal carbonyl moiety, studied in the context of the pyrazole fungicide **168** for which the CF<sub>3</sub> analogue exhibited weaker biological activity.<sup>156</sup> Both the IR and <sup>1</sup>H NMR spectral data for **168** were consistent with an intramolecular H-bond estimated to be about 1.0 kcal/mol, a weak H-bond donor compared to more traditional interactions which typically range from 2 to 15 kcal/mol. However, the CF<sub>2</sub>H is a more lipophilic H-bond donor than either OH or NH, offering the potential for improved membrane permeability.<sup>157</sup>

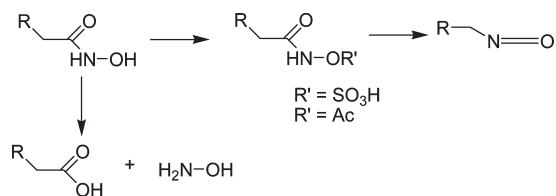


**3.5.3.3. RCHF<sub>2</sub> as a Thiol Mimetic in HCV NS3 Protease Inhibitors.** Although the CF<sub>2</sub>H moiety has not been widely exploited by medicinal chemists, it is beginning to attract attention and several interesting applications have recently been examined. In one of the most successful demonstrations of utility, the RCHF<sub>2</sub> moiety was recognized as a potential isostere of a thiol in the context of inhibitors of HCV NS3 protease, an important antiviral target that cleaves substrates at the carboxy terminal of cysteine. Difluoro-Abu was designed as a potential isostere of the cysteine CH<sub>2</sub>SH P1 element in peptide-based inhibitors following a careful analysis of properties that indicated substantial structural similarity.<sup>158</sup> The van der Waals surfaces of the two elements are similar (HCF<sub>2</sub>CH<sub>3</sub>, 46.7 Å; HSCH<sub>3</sub>, 47.1 Å), while electrostatic potential maps indicated surface similarities between the negative potential around the sulfur lone pairs and the two fluorine atoms and the positive potential around the CF<sub>2</sub>H and SH hydrogen atoms, captured in a simplistic fashion in Figure 19.

The difluoro-Abu analogue **171** of the hexapeptide NS3 inhibitor **169** proved to be equipotent and 20-fold more potent than the simple Abu derivative **170**. An X-ray cocrystal of a related inhibitor revealed the key ligand–protein interactions,

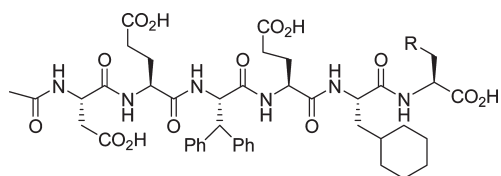


**Figure 19.** Similarity of the electronic and steric properties of cysteine and difluoro-Abu.



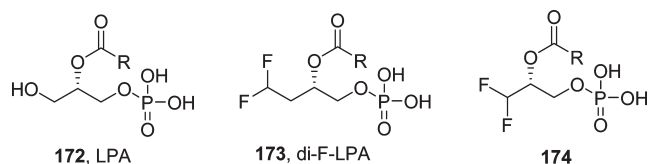
**Figure 20.** Metabolic pathways associated with hydroxamic acids.

with the  $\text{CF}_2\text{H}$  moiety donating a H bond to the  $\text{C}=\text{O}$  of  $\text{Lys}_{136}$  and one fluorine close to the C-4-hydrogen atom of  $\text{Phe}_{154}$ , suggestive of a weak C–H to F hydrogen-bond.<sup>158</sup>



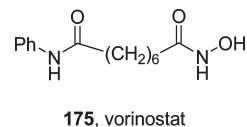
**169:** R = SH;  $K_i$  = 40 nM  
**170:** R =  $\text{CH}_3$ ;  $K_i$  = 700 nM  
**171:** R =  $\text{CHF}_2$ ;  $K_i$  = 30 nM

**3.5.3.4. Application of  $\text{RCHF}_2$  as an Alcohol Isostere in Lysophosphatidic Acid.** Lysophosphatidic acid (**172**, LPA) interacts with G-protein-coupled receptors (GPCRs) that have been classified into four subtypes, designated LPA1–4, and also acts as an agonist for the nuclear hormone receptor  $\text{PPAR}\gamma$ . Acting on its cognate GPCRs, compound **172** mediates cell proliferation, migration, and survival, providing an opportunity for antagonists to exhibit potential utility in oncological applications. The  $\text{CF}_2\text{H}$ -containing analogues diF-LPA (**173**) and its homologue **174**, were designed as isosteres of **172** in which troublesome migration of the acyl moiety is prevented.<sup>159,160</sup> Compound **173** was found to stimulate luciferase production in CV-1 cells transfected with luciferase under control of a  $\text{PPAR}\gamma$ -responsive element. However, neither **173** nor **174** interacted appreciably with LPA receptors 1–3, either as agonists or antagonists, providing an interesting example of an isostere enhancing specificity.<sup>159</sup>



**3.6. Hydroxamic Acid Isosteres.** **3.6.1. Application of  $\text{RCHF}_2$  to Hydroxamic Acid Isosteres.** Hydroxamic acids are excellent ligands for metals, particularly zinc, and are a key pharmacophoric element for both matrix metalloprotease and histone deacetylase (HDAC) inhibitors.<sup>161</sup> However, hydroxamic acids can express toxicity based on metabolic activation, which manifests either as a Lossen rearrangement to the corresponding isocyanate or as hydrolytic degradation to release a carboxylic acid and hydroxylamine, with the latter a cause of methemoglobinemia,

reaction pathways summarized in Figure 20.<sup>162</sup> Metabolism and toxicity are dependent on structure, and several hydroxamic acid-containing drugs have successfully reached the market, the most recent being the HDAC inhibitor vorinostat (**175**) launched in 2006 as a treatment for cutaneous T-cell lymphoma (CTCL).<sup>163</sup>



The potential of a  $\text{CHF}_2$  moiety to act as an isostere of the hydroxyl of hydroxamic acids has been evaluated in a series of dual inhibitors of cyclooxygenase-2 (COX-2) and 5-lipoxygenase (5-LOX), molecules designed to prevent arachidonic acid metabolism being directed to the alternative pathway by single enzyme inhibition as a means of reducing the potential for side effects.<sup>164</sup> Hydroxamic acids are well-established inhibitors of 5-LOX, binding to the active site iron, and substitution of the toluene ring of **16** with a cyclic hydroxamic acid affords the dual inhibitor **176** (Table 26). The  $\text{NCHF}_2$  analogue **177** was explored as a non-hydroxamic acid isostere and appeared to be an effective mimetic, although the mechanism of action of this compound has not been fully clarified. Nevertheless, **177** shows protective activity in the rat carrageenan foot paw edema model following oral administration.<sup>164</sup>

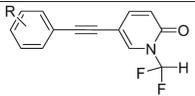
In the alternative series of alkyne-based cyclooxygenase inhibitors **178–180** where the cyclic hydroxamic acid effectively introduced 5-LOX inhibition (Table 27), a difluoromethylpyridone isostere provided consistent 5-LOX inhibition across the series of analogues **181–184** (Table 28).<sup>165</sup> These compounds appear to offer improved activity in the carrageenan-induced rat paw edema model of inflammation following oral dosing, with activity in vivo attributed to 5-LOX rather than COX inhibition because of the weaker in vitro COX-1 and COX-2 inhibitory activity associated with these compounds.<sup>165</sup> This hydroxamic acid isostere has subsequently been explored as a means of introducing LOX inhibition to a range of cyclooxygenase-inhibiting chemotypes.<sup>166–170</sup>

**Table 26. Cyclooxygenase and Lipoxygenase Inhibition Associated with a Series of Pyrazole-Based Inhibitors**

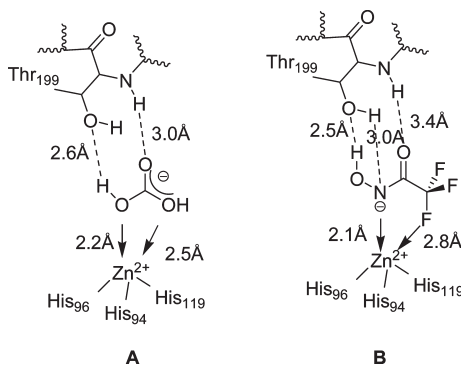
| Compound                                 | R         |            |            |
|--|-----------|------------|------------|
|  |           |            |            |
| Compound                                 | <b>16</b> | <b>176</b> | <b>177</b> |
| $\text{IC}_{50}$ COX-1 ( $\mu\text{M}$ ) | 7.7       | 10.2       | 13.1       |
| $\text{IC}_{50}$ COX-2 ( $\mu\text{M}$ ) | 0.12      | 7.5        | 0.69       |
| $\text{IC}_{50}$ 5-LOX ( $\mu\text{M}$ ) | inactive  | 4.9        | 5.0        |
| $\text{ED}_{50}$ (mpk)                   | 10.8      | 99.8       | 27.7       |

**Table 27. 5-Lipoxygenase Inhibition by a Series of Alkyne-Based Hydroxamic Acid Derivatives**

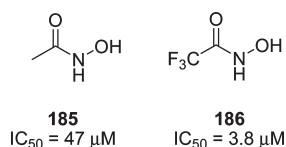
| Compound # | R                           |  |                                    |
|------------|-----------------------------|--|------------------------------------|
|            |                             | 5-LOX $\text{IC}_{50}$ ( $\mu\text{M}$ ) | AI Activity $\text{ED}_{50}$ (mpk) |
| <b>178</b> | 2- $\text{SO}_2\text{NH}_2$ | 10                                       | 86.0                               |
| <b>179</b> | 3- $\text{SO}_2\text{NH}_2$ | 15                                       | inactive                           |
| <b>180</b> | 4- $\text{SO}_2\text{NH}_2$ | 68                                       | inactive                           |

**Table 28.** Cyclooxygenase and 5-Lipoxygenase Inhibition by a Series of Alkyne-Based N-Difluoromethylpyridone Derivatives


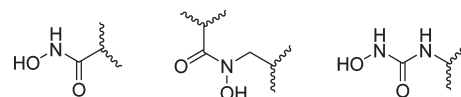
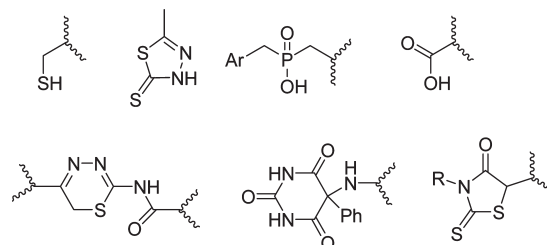
| Compd #    | R                                 | COX-1 IC <sub>50</sub> (μM) | COX-2 IC <sub>50</sub> (μM) | 5-LOX IC <sub>50</sub> (μM) | AI Activity ED <sub>50</sub> (mpk) |
|------------|-----------------------------------|-----------------------------|-----------------------------|-----------------------------|------------------------------------|
| <b>181</b> | 2-SO <sub>2</sub> CH <sub>3</sub> | >100                        | 9.4                         | 3.4                         | >100                               |
| <b>182</b> | 3-SO <sub>2</sub> CH <sub>3</sub> | 32.4                        | 3.7                         | 3.2                         | 66.1                               |
| <b>183</b> | 4-SO <sub>2</sub> CH <sub>3</sub> | 14.1                        | 5.1                         | 3.3                         | 68.5                               |
| <b>184</b> | 4-SO <sub>2</sub> NH <sub>2</sub> | 5.2                         | 6.0                         | 3.5                         | 86.5                               |
| <b>16</b>  | celecoxib                         | 7.7                         | 0.12                        | IA                          | 10.8                               |

**Figure 21.** Binding of substrate (A) and the inhibitor **186** (B) to carbonic anhydrase II.

**3.6.2. Hydroxamic Acids in Carbonic Anhydrase II Inhibitors.** In a somewhat unusual example of intrinsic bioisosterism that relies upon the potential for ambidentate binding modes, the hydroxamic acid derivatives **185** and **186** were found to bind in an unanticipated fashion to carbonic anhydrase II, a 260 amino acid enzyme in which a Zn<sup>2+</sup> atom catalyzes the addition of H<sub>2</sub>O to CO<sub>2</sub> (Figure 21A).<sup>171</sup> In this enzyme, Thr<sub>199</sub> accepts a H-bond from Zn<sup>2+</sup>-bound hydroxide and donates to Glu<sub>106</sub> as part of the catalytic mechanism and simple hydroxamic acids were probed as inhibitors based on the known propensity of this functionality to bind to Zn<sup>2+</sup> via a five-membered chelate involving the two oxygen atoms. Both compounds inhibit enzyme function with IC<sub>50</sub>s in the micromolar range, but an X-ray cocrystal revealed that both inhibitors bound in a similarly unusual mode in which the nitrogen atom is ionized and coordinates to the Zn<sup>2+</sup>, a binding orientation stabilized by a H-bond donated from Thr<sub>199</sub> to the hydroxamate carbonyl (Figure 21B). In the case of **186**, an additional, weakly polar C–F→Zn<sup>2+</sup> appears to add to the stability of the complex.<sup>171</sup>



**3.6.3. Hydroxamic Acid Mimetics in TNFα-Converting Enzyme (TACE) Inhibitors.** The bidentate interaction of hydroxamic acids with the metal of Zn<sup>2+</sup> metalloproteases offers increased potency compared to monodentate ligands like the thiol found in captopril or the carboxylic acid of lisinopril, both potent ACE inhibitors. However, hydroxamic acids typically bind more tightly to Fe(III) and often exhibit poor pharmacokinetic properties due, in part, to hydrolytic cleavage of the hydroxamate and release of

**Figure 22.** Hydroxamic acid motifs explored as the key Zn<sup>2+</sup>-binding pharmacophore in metalloprotease inhibitors.**Figure 23.** Isosteres of the hydroxamic acid moiety explored in the context of tumor necrosis factor-α-converting enzyme (TACE) inhibitors.

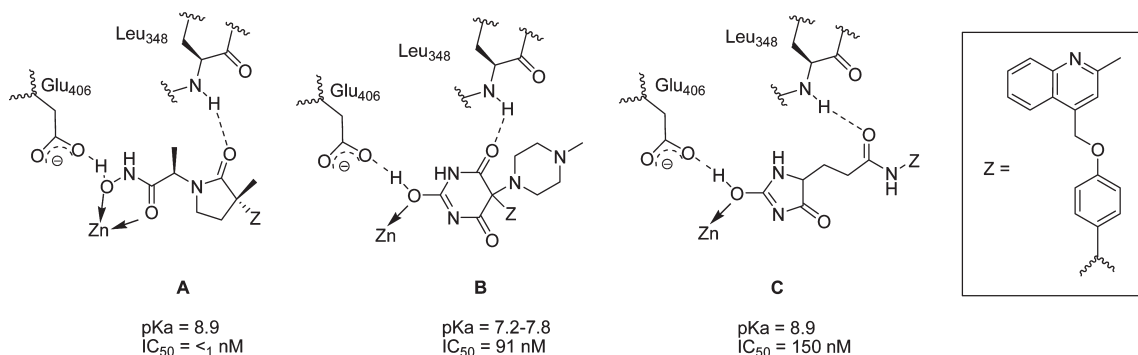
NH<sub>2</sub>OH, although the alternative hydroxamic acid structures presented in Figure 22 may abrogate this pathway. These limitations have stimulated the identification of useful hydroxamic acid surrogates with improved properties, with the more common isosteres probed in the context of tumor necrosis factor-α-converting enzyme (TACE) inhibitors summarized in Figure 23.

Unlike hydroxamic acids, which bind as depicted in Figure 24A, many of these isosteres are thought to coordinate Zn<sup>2+</sup> in a monodentate fashion that requires additional enzyme–inhibitor interactions for optimal potency and selectivity (Figure 24, B and C).<sup>161,172</sup> Imides were proposed to enolize and displace the nucleophilic H<sub>2</sub>O that is activated by Glu<sub>406</sub>, providing an explanation for the pK<sub>a</sub> of 7–9 that is required for these chemotypes to be effective inhibitors.<sup>161,172</sup> An X-ray cocrystallographic analysis of a structurally simple hydantoin-based TACE inhibitor has recently elucidated the binding mode in the enzyme active site, confirming the monodentate interaction with Zn<sup>2+</sup> in the S1 subsite but also revealing the presence of a second molecule in the S1' subsite.<sup>173</sup>

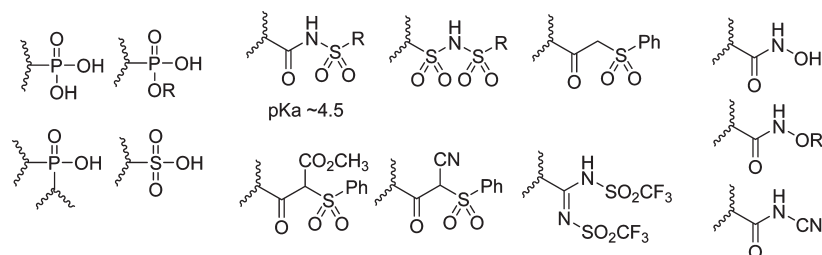
**3.7. Carboxylic Acid Isosteres.** Isosteres of carboxylic acid have been studied extensively, driven in part by interest in inhibitors of the arachidonic acid pathway and excitatory amino acids receptors and by the development of angiotensin II receptor antagonists. These studies have typically focused on enhancing potency, reducing polarity, and increasing lipophilicity in order to improve membrane permeability, enhancing pharmacokinetic properties in vivo and reducing the potential for toxicity. The latter is based on the potentially problematic rearrangement of acyl glucuronides formed in vivo that can lead to chemically reactive species, while CoA esters, another potential metabolite, are electrophilic and have been implicated as a source of toxicity.<sup>174</sup> A synopsis of the more common carboxylic acid isosteres is presented in Figure 25.

The use of heterocycles, either those with intrinsic acidity or those in which substituents are used to modulate pK<sub>a</sub>, not only broadens the palette of carboxylic acid isosteres but offers considerable additional structural variation with which to enhance complementarity to a target protein or nucleic acid. A synopsis of acidic heterocycles that have been explored as acid isosteres is provided in Figure 26 where patterns of substitution and the potential for charge delocalization by enolization offer additional flexibility to modulate vectorial projection and reach while providing for a wide-ranging structural diversity.

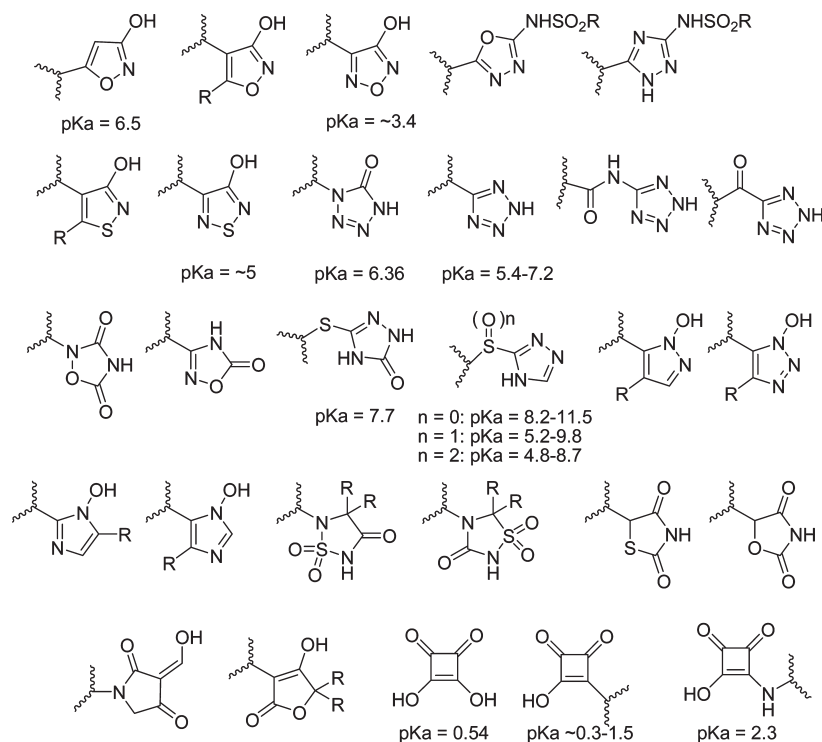
**3.7.1. Carboxylic Acid Isosteres in Angiotensin II Receptor Antagonists.** Angiotensin II receptor antagonists provide



**Figure 24.** Proposed binding mode of hydroxamic acid and nonhydroxamic acid tumor necrosis factor- $\alpha$ -converting enzyme (TACE) inhibitors.



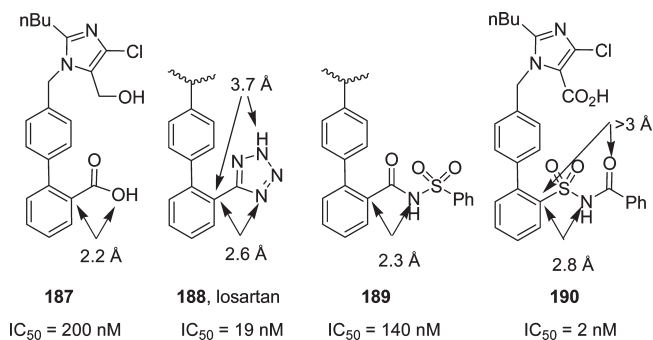
**Figure 25.** Synopsis of the more common carboxylic acid isosteres.



**Figure 26.** Synopsis of heterocycle-based carboxylic acid isosteres.

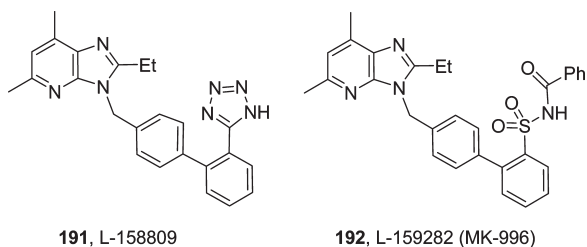
instructive insight into carboxylic acid isostere design, since binding affinity to the receptor in a series of biphenyl acids is quite sensitive to the identity of the acidic element.<sup>175,176</sup> The tetrazole moiety in losartan (**188**) confers a 10-fold increase in potency compared to the carboxylic acid analogue **187**, a result explored through geometrical analysis that indicated that the tetrazole projects the acidic NH 1.5 Å further from the aryl ring than a CO<sub>2</sub>H (data summarized in Figure 27). The CON-

HSO<sub>2</sub>Ph moiety incorporated into **189** exhibits a similar geometrical topology to CO<sub>2</sub>H and offers comparable potency. However, the reverse acylsulfonamide, SO<sub>2</sub>NHCOPh, found in **190** with its longer aryl ring-S bond length projects the charge further away from the biphenyl core, more effectively approximating the Ar to distal NH distance in the more potent tetrazole, particularly if the negative charge resides on the carbonyl oxygen, as might be anticipated.<sup>175,176</sup>



**Figure 27.** Geometrical arrangements associated with the carboxylic acid moiety and tetrazole and acylsulfonamide isosteres in angiotensin II antagonists.

In a second example from the angiotensin antagonist field, L-158809 (**191**) was identified as a potent and selective  $AT_1$  antagonist,  $IC_{50} = 0.3$  nM, that shows prolonged antihypertensive activity in rats that lasted for more than 6 h after iv or po dosing.<sup>177</sup> However, the duration was shorter in dog and rhesus monkey following iv dosing, attributed to rapid clearance by glucuronidation of the tetrazole moiety. Replacing the tetrazole of **191** with an acylsulfonamide, as exemplified by **192**, preserved potency ( $IC_{50} = 0.2$  nM) and extended the hypotensive effect in rats to over 6 h following po dosing. A similarly long duration of action was observed in the dog and rhesus monkey, results attributed to the resistance of the acylsulfonamide toward glucuronidation.<sup>177</sup>



**3.7.2. Acylsulfonamide in HCV NS3 Protease Inhibitors.** The potency of the tripeptidic acid-based inhibitor of HCV NS3 protease **193** can be improved by occupying the well-defined  $PI'$  pocket that is ignored by the carboxylate.<sup>178</sup> The  $PI'$  pocket is readily and uniquely accessed by an acylsulfonamide moiety that preserves acidity while establishing H-bonding interactions between the protease active site and both oxygen atoms of the sulfone (Table 29).<sup>178</sup> A cyclopropylacylsulfonamide (**194**) is optimal based on comparison with the homologues **195–197** and typically confers a significant potency advantage to the extent that this moiety has been widely adopted by the industry.<sup>179</sup>

**3.7.3. Acylsulfonamide in  $EP_3$  Antagonists.** The potent carboxylic acid-based  $EP_3$  antagonist **198** shows modest functional activity in blocking  $PGE_2$ -induced  $Ca^{2+}$  release in cells in culture, but modification to the *N*-phenylacylsulfonamide **200** afforded a compound with 40-fold increased binding affinity, attributed to the contribution of productive interactions between the larger inhibitor and the receptor (Table 30).<sup>180</sup> However, functional activity remained poor, considered to be due to high compound binding to the 1% BSA protein present in the medium. Substitution of the phenyl ring improved potency and efficacy, with the 3,4-difluoro analogue **201** being 256- and 480-fold more potent in the binding and functional assays, respectively.<sup>180</sup>

**3.7.4. Acylsulfonamides in Bcl-2 Inhibitors.** An acylsulfonamide moiety proved to be a critical element in a series of inhibitors of

**Table 29.** Structure–Activity Relationships Associated with the Acylsulfonamide Moiety of a Series of Tripeptidic Inhibitors of HCV NS3 Protease

| Compd #    | R              | $IC_{50}$ (nM) |
|------------|----------------|----------------|
| <b>193</b> | OH             | 54             |
| <b>194</b> | $NHSO_2C_3H_5$ | 1              |
| <b>195</b> | $NHSO_2iPr$    | 19             |
| <b>196</b> | $NHSO_2C_4H_7$ | 4              |
| <b>197</b> | $NHSO_2C_5H_9$ | 71             |

**Table 30.** Structure–Activity Relationships Associated with a Series of  $EP_3$  Antagonists

| Compd #    | R                       | $K_i$ binding | $IC_{50}$ in a functional assay |
|------------|-------------------------|---------------|---------------------------------|
| <b>198</b> | OH                      | 21 nM         | 580 nM                          |
| <b>199</b> | $NHSO_2CH_3$            | 22 nM         | > 10 $\mu$ m                    |
| <b>200</b> | $NHSO_2Ph$              | 0.5 nM        | 140 nM                          |
| <b>201</b> | $NHSO_2-3,4-dif-C_6H_3$ | 0.086 nM      | 1.2 nM                          |
| <b>202</b> | $NHSO_2-3-CN-C_6H_4$    | 0.065 nM      | 18 nM                           |

the antiapoptotic protein Bcl-2 that have application in oncology therapy. NMR screening (SAR by NMR) identified two structural fragments, the biphenylcarboxylic acid **203** and the phenol **204**, that bound weakly to Bcl-2, confirmed using a fluorescence polarization assay (FPA) (Figure 28).<sup>181,182</sup> However, attempts to link the 2 fragments via the ortho position of the benzoic acid fragment, as depicted by **205**, failed to identify molecules with increased binding affinity. The acylsulfonamide **206** provided a more effective vector to access the Ile<sub>85</sub> pocket occupied by the phenol **204** while preserving the acidic functionality that interacts with Arg<sub>139</sub> of the Bcl-2 protein.<sup>181,182</sup> ABT-263 (**207**) ultimately emerged from this work as a clinical candidate that is orally bioavailable despite a molecular weight of 974.

Acylsulfonamides and several other carboxylic acid isosteres developed originally for medicinal chemistry applications have found utility in proline-based organocatalyst design as a means of modulating physical properties to overcome limitations associated with proline.<sup>183,184</sup>

**3.7.5. 2,6-Difluorophenol as a  $CO_2H$  Mimetic.** The introduction of fluorine atoms at the 2- and 6-positions of phenol increases the acidity from a  $pK_a$  of 9.81 for phenol to a  $pK_a$  of 7.12 for 2,6-difluorophenol, prompting the hypothesis that this functionality may function as a lipophilic carboxylic acid mimetic.<sup>185</sup> The concept of an isosteric relationship was based on a combination of the acidity of the

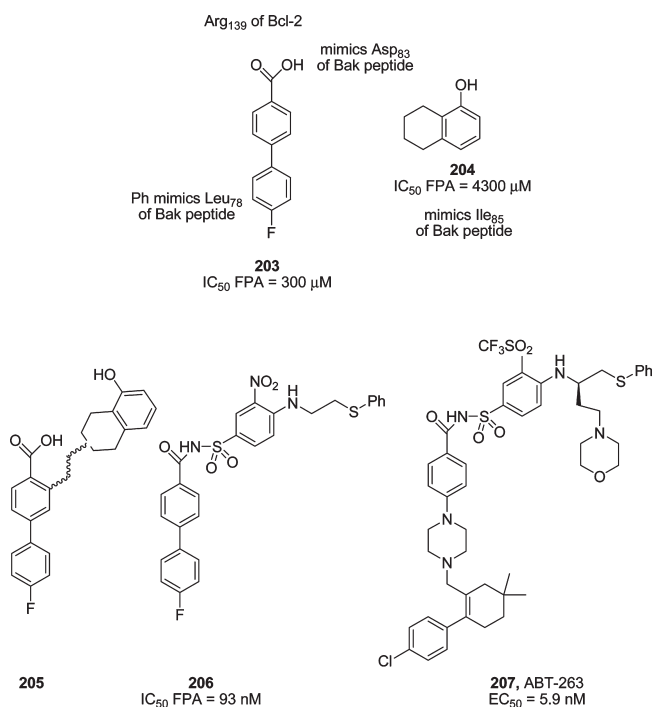
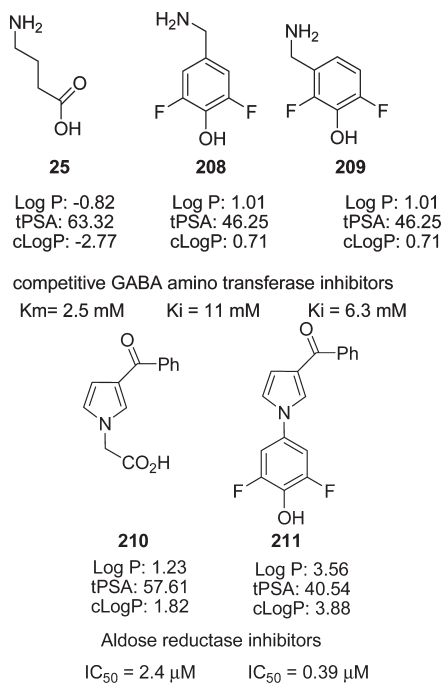


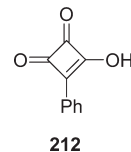
Figure 28. Fragments binding to Bcl-2 identified by NMR studies.

OH and the potential for fluorine to mimic the carboxylic acid C=O by acting as a H-bond acceptor. With a view to improving the poor CNS penetration of **25**, the more lipophilic<sup>186</sup> 2,6-difluorophenol derivatives **208** and **209** were synthesized and found to be competitive inhibitors of GABA amino transferase, although neither acted as a substrate.<sup>185</sup> The 2,6-difluorophenol moiety was also examined as an isostere of the carboxylic acid in the aldose reductase inhibitor **210** with the result that **211** offered 6-fold increased potency.<sup>187</sup>



3.7.6. Squaric Acid Derivatives as CO<sub>2</sub>H Mimetics. Cyclobutenediones, more commonly referred to as squaric acids, are

useful isosteres of carboxylic acids and tetrazoles in the context of angiotensin II antagonists based on their high intrinsic acidity; the pK<sub>a</sub> of 3-hydroxy-4-phenylcyclobut-3-ene-1,2-dione (**212**), for example, is 0.37.<sup>188</sup>



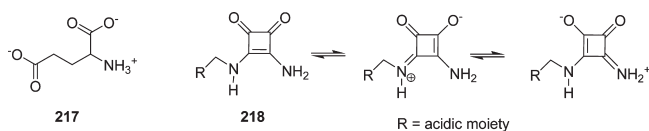
The affinity of the squaric acid derivative **213** for the angiotensin II receptor was within 10-fold of that measured for the tetrazole **214** and superior to both the carboxylic acid **215** and sulfonamide **216**.<sup>175,188</sup> This was attributed to the increased size of the cyclobutenedione moiety and its ability to project acidic functionality an optimal distance from the biphenyl core (Table 31).<sup>175,188</sup> Squarate **213** reduced blood pressure in Goldblatt hypertensive rats following oral administration with a long lasting effect, although efficacy was lower than the analogous tetrazole.<sup>188</sup>

3.7.7. Aminosquarate Derivatives as Amino Acid Mimetics. In an elegant example of isostere design, diaminosquaric acid derivatives **218** were conceived as achiral mimetics of glutamic acid (**217**) based on structural homology, the inherent strong dipole, and electron density residing on the oxygen atoms that is supported by the NH moieties, depicted by the tautomers in Figure 29.<sup>189</sup> Several of these molecules, in which the amine is non-nucleophilic and neither basic nor acidic at neutral pH, exhibited modest affinity for the *N*-methyl-D-aspartate (NMDA) glutamate receptor but showed no activity at  $\alpha$ -amino-3-hydroxy-5-methyl-4-isoxazolepropionic acid (AMPA) or kainate receptors (data summarized in Table 32). The phosphonate derivative was a somewhat more potent NMDA ligand, although all showed markedly lower affinity than glutamic acid, IC<sub>50</sub> = 70 nM.<sup>189</sup>

3.7.8. Heterocycles as Amino Acid Mimetics. Amino acid isosterism that exhibits some analogy to the amino squarate chemotype has been recognized in the series of heterocycles summarized in Figure 30, explored as antagonists of the AMPA receptor subtype that recognizes glutamate and the glycine site associated with the NMDA receptor. For the quinoxaline diones, effective mimicry of glycine is thought to rely on the tautomeric isomerism highlighted in the bolded enol form depicted in Figure 30 that overlays the corresponding elements of glycine with good topological similarity.<sup>190</sup> Isosterism with AMPA was

Table 31. Structure–Activity Relationships Associated with Isosteres of a Carboxylic Acid in a Series of Angiotensin II Receptor Antagonists

| Compound # | R                                 | Angiotensin II receptor binding IC <sub>50</sub> (nM) |
|------------|-----------------------------------|---|
| <b>213</b> | squarate                          | 25  |
| <b>214</b> | tetrazole                         | 3   |
| <b>215</b> | CO <sub>2</sub> H                 | 275   |
| <b>216</b> | NHSO <sub>2</sub> CF <sub>3</sub> | 100   |



**Figure 29.** Structures of glutamic acid, a diaminosquaric acid derivative, and its tautomers.

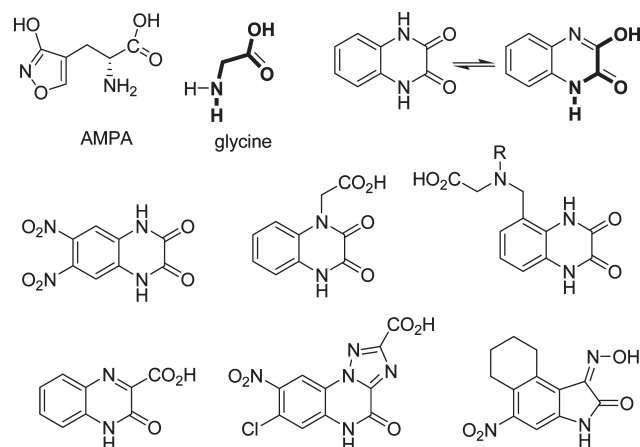
**Table 32. Binding Affinity for a Series of Diaminosquaric Acid-Based NMDA Antagonists**

| R   | IC <sub>50</sub> for NMDA receptor binding (μM) |
|---|---|
| CO <sub>2</sub> H                                     | 2.3   |
| CH <sub>2</sub> CO <sub>2</sub> H                     | 1.6   |
| CH <sub>2</sub> CH <sub>2</sub> CO <sub>2</sub> H     | 10.0  |
| CH <sub>2</sub> CH <sub>2</sub> P(O)(OH) <sub>2</sub> | 0.47  |

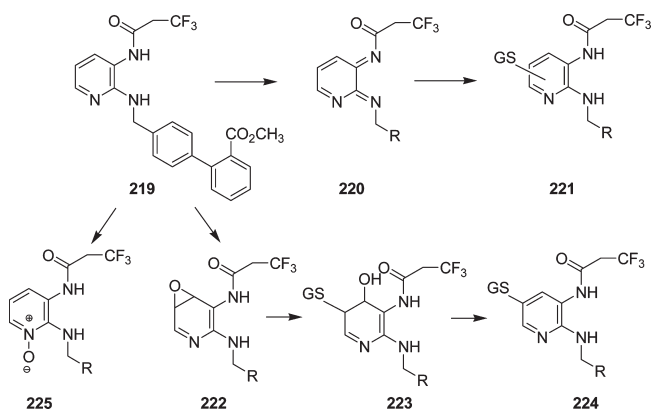
established by incorporating an additional acidic moiety, although the enol form of the quinoxaline dione appears to be of lesser importance in this context.<sup>190</sup> Potency and selectivity can be further modulated by varying the nature and pattern of substitution of the heterocycle N atom and the fused benzene ring that allows control of vector presentation.

**3.8. Isosteres of Heterocycles.** *3.8.1. Avoiding Quinonedimine Formation in Bradykinin B<sub>1</sub> Antagonists.* The 2,3-diaminopyridine **219** is a potent bradykinin B<sub>1</sub> antagonist, K<sub>i</sub> = 11.8 nM, that was being evaluated as a potential treatment for the relief of pain (Figure 31).<sup>191</sup> However, the diaminopyridine moiety is susceptible to metabolic activation by both rat and human liver microsomes, forming glutathione (GSH) adducts **221** that were observed in rat bile following oral administration of **219**.<sup>191,192</sup> The metabolic activation pathway was considered to be via formation of either the diiminoquinone **220** or the generation of a pyridine epoxide **222**, both of which are anticipated to be electrophilic toward GSH, with the latter specifically producing **224**, as summarized in Figure 31. Oxidation of **219** to the N-oxide **225** was also observed, although GSH addition to this metabolite appeared to be a minor pathway.<sup>191,192</sup>

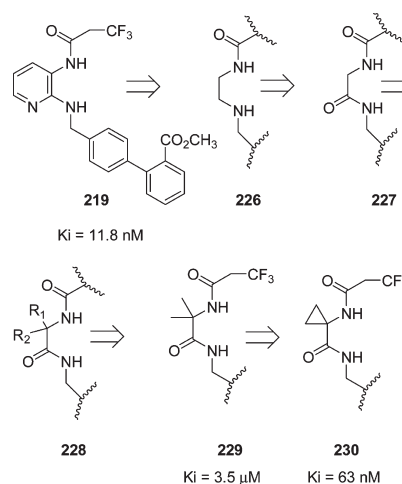
The design strategy to identify a suitable replacement for the 2,3-diaminopyridine scaffold of **219** relied upon the premise that both NHs were important, allowing simplification to an ethylene diamine **226** as the fundamental linker element, as depicted in Figure 32.<sup>193</sup> An acyl moiety was introduced in a fashion that allowed the C=O element to mimic the pyridine nitrogen atom while simultaneously acidifying the pendent NH, thereby modifying the linker to that of an α-amino acid **227**. In order to favor the topology of the substituents presented by the pyridine scaffold, the final design consideration sought to exploit the Thorpe–Ingold effect<sup>194</sup> represented generically by **228**. However, the dimethylglycine analogue **229** exhibited only modest affinity for the B<sub>1</sub> receptor but potency was improved substantially by optimization to the cyclopropyl analogue **230**. This result was attributed to the effect of π–π hyperconjugation between the cyclopropyl C–C bonds and the amide C=O exerting a conformational bias based on the in-



**Figure 30.** Synopsis of heterocycle-based isosteres of glycine and α-amino-3-hydroxy-5-methyl-4-isoxazolepropionic acid (AMPA).

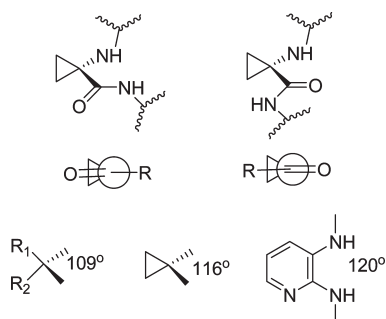


**Figure 31.** Metabolic pathways associated with the bradykinin B<sub>1</sub> receptor antagonist **219**.



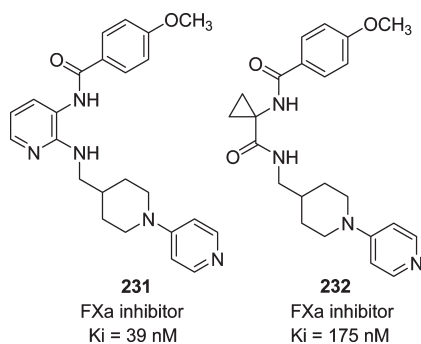
**Figure 32.** Principles underlying the design of a 2,3-diaminopyridine isostere in the context of the bradykinin B<sub>1</sub> receptor antagonist **219**.

creased π character of cyclopropyl C–C bonds which can optimally interact with the amide C=O moiety at 0° and 180° (summarized in Figure 33). Moreover, the 116° bond angle enforced by the cyclopropyl ring is closer to the 120° vector inherent to the pyridine

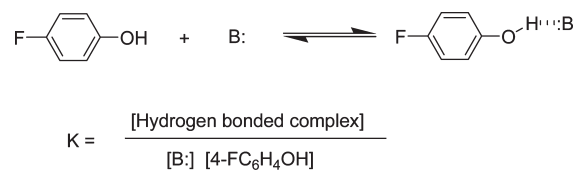


**Figure 33.** Conformation and topology of cyclopropyl amino acid amides as 2,3-diaminopyridine mimetics.

core (Figure 33). This isostere was also applied with some success to the factor Xa inhibitor **231**, with **232** showing only a 4-fold loss in potency.<sup>193</sup>



**3.8.2. Isosterism between Heterocycles in Drug Design.** Five- and six-membered heterocycles play a prominent role in drug design, ubiquitous in their application as drug scaffolds or important structural elements. The versatility of heterocycles is based on their size and shape, which allows substituent projection along a range of vectors, while inherent electronic and physical properties are of importance in mediating drug–target interactions. By judicious selection and deployment of substituents, electronic and physical properties and acidity and basicity can readily be modulated in an incrementally graded fashion, particularly for unsaturated heterocycles. The most important properties in drug design and biofunctional mimicry are H-bond donor (N–H, O–H, C–H) or acceptor properties, electron withdrawing or donating effects, and the potential to engage in  $\pi$ – $\pi$  interactions. In addition, tautomerism offers additional opportunities to optimize both the topographical presentation of substituents and drug–target interactions while heterocycles incorporating a bivalent sulfur atom provide unique opportunities for inter- and intramolecular interactions that have demonstrated relevance in drug design. Although the silhouettes of unsaturated heterocyclic rings within a homologous five- or six-membered series are similar, their inherent physical and electronic properties frequently lead to significant discrimination of their capacity to function as isosteres of each other in biological systems. There are many situations where the careful selection of a heterocycle has been a critical element in successfully addressing a specific problem encountered in drug design or introducing targeted activity. Consequently, a detailed understanding of the fundamental properties of individual heterocycles is



$$pK_{\text{BHX}} = -\log_{10} K_{\text{BHX}} = +\log_{10} K \quad X = 4\text{-FC}_6\text{H}_4\text{O}$$

**Figure 34.** Equilibrium of complex formation used to establish hydrogen bonding potential  $pK_{\text{BHX}}$  of acceptors.

**Table 33.**  $pK_{\text{BHX}}$  Values for Common Functional Groups Arranged in Order of Descending Hydrogen-Bond Basicity

| functionality   | $pK_{\text{BHX}}$ |
|---|-------------------|
| Me <sub>3</sub> P=O                                     | 3.53              |
| pyrrolidine   | 2.59              |
| MeSO.Me   | 2.54              |
| (Me) <sub>2</sub> NCON(Me) <sub>2</sub>                 | 2.44              |
| N-Me-pyrrolidone  | 2.38              |
| <i>n</i> -PrCO.N(Me) <sub>2</sub>                       | 2.36              |
| Et <sub>2</sub> NH                                      | 2.25              |
| N-Me-pyrrolidine  | 2.19              |
| EtNH <sub>2</sub>                                       | 2.17              |
| Me <sub>2</sub> NCHO                                    | 2.10              |
| Et <sub>3</sub> N                                       | 1.98              |
| morpholine  | 1.78              |
| <i>c</i> -C <sub>3</sub> H <sub>5</sub> NH <sub>2</sub> | 1.72              |
| $\delta$ -valerolactone                                 | 1.57              |
| cyclohexanone   | 1.39              |
| oxetane   | 1.36              |
| MeSO <sub>2</sub> N(Me) <sub>2</sub>                    | 1.30              |
| THF   | 1.28              |
| acetone   | 1.18              |
| MeSO <sub>2</sub> Me                                    | 1.10              |
| EtOAc   | 1.07              |
| EtOH  | 1.02              |
| EtOEt   | 1.01              |
| CH <sub>3</sub> CN                                      | 0.91              |

of paramount importance if they are to be deployed effectively in a fashion that takes advantage of properties that can be uniquely dependent on context.

**3.8.3. Heterocycles as Hydrogen Bond Acceptors:  $pK_{\text{BHX}}$  Scale of H-Bonding Basicity.** The  $pK_{\text{BHX}}$  (previously  $pK_{\text{BH}}$ ) scale of hydrogen bond basicity has been developed based on the formation of a complex between the acceptor and 4-FC<sub>6</sub>H<sub>4</sub>OH in CCl<sub>4</sub> at 298 K, monitored by Fourier transform infrared techniques as a shift in the frequency of the OH stretching vibration.<sup>195–198</sup> In this experiment, a strong H-bond acceptor forms a complex with 4-FC<sub>6</sub>H<sub>4</sub>OH that exhibits a large association constant ( $K$ ) and low dissociation constant ( $1/K$ ), the position of equilibrium defining the strength of the H-bond (Figure 34). Thus, a strong acceptor has a higher  $pK_{\text{BHX}}$ . H-Bonding strength has been found to depend on multiple factors including the position of the acceptor atom in the periodic table, polarizability, field/inductive and resonance effects of substituents around the acceptor atom, proximity effects, steric hindrance surrounding

**Table 34. Comparison of  $pK_{\text{BHx}}$  and  $pK_{\text{BH}^+}$  ( $pK_{\text{a}}$ ) Values for Common Five- and Six-Membered Ring Heterocycles**

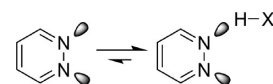
| heterocycle       | $pK_{\text{BHx}}$ | $pK_{\text{BH}^+}$ ( $pK_{\text{a}}$ ) |
|-------------------|-------------------|--|
| 1-methylimidazole | 2.72              | 7.12                                   |
| imidazole         | 2.42              | 6.95                                   |
| 1-methylpyrazole  | 1.84              | 2.06                                   |
| thiazole          | 1.37              | 2.52                                   |
| oxazole           | 1.30              | 0.8                                    |
| isoxazole         | 0.81              | 1.3                                    |
| furan             | -0.40             |  |
| pyridazine        | 1.65              | 2.00                                   |
| pyridine          | 1.86              | 5.20                                   |
| pyrimidine        | 1.07              | 0.93                                   |
| pyrazine          | 0.92              | 0.37                                   |
| triazine          | 0.88              |  |

the acceptor site, the potential for intramolecular H-bonding, and lone pair–lone pair interactions.<sup>195–198</sup>

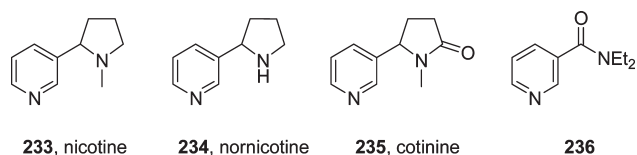
**3.8.4. H-Bonding Capacity of Common Functional Groups.** The  $pK_{\text{BHx}}$  scale provides an excellent index of H-bonding basicity, and experimentally determined data are available for many of the functional groups commonly encountered in medicinal chemistry. As summarized in Table 33, the H-bonding capacity of esters, ethers, and ketones falls in the range of  $pK_{\text{BHx}} = 1.00–1.50$  while amides, carbamates, and ureas act as stronger acceptors,  $pK_{\text{BHx}} \approx 2.00–2.55$ .<sup>196</sup> Sulfoxides are good H-bond acceptors,  $pK_{\text{BHx}} = 1.70–2.50$ , with sulfones and sulfonamides somewhat weaker, with  $pK_{\text{BHx}}$  values ranging from 1.10 to 1.40. Although these functional groups present a good dynamic range and are commonly deployed in drug design, they frequently offer only limited potential for subtle and graded optimization of electronic properties or modulation of vector projection topology that is frequently of importance in the optimization of drug–target interactions. In addition, many of these functional groups can present problems based on pharmacokinetic or toxicological considerations. Heterocycles offer several advantages in this context, providing a broad range of H-bond acceptor properties and often improved metabolic stability compared to, for example, esters, amides, ketones, and aldehydes.<sup>196–198</sup>

**3.8.5. Heterocycles and H-Bonds: Filling the Gaps.** The H-bond-accepting capacity of a series of simple five- and six-membered heterocycles that are widely used in drug design is compiled in Table 34 along with proton basicity measurements  $pK_{\text{BH}^+}$ . These data demonstrate the potential of heterocycles to offer graded variation in H-bonding capacity, and this property can be refined further in a subtly graded fashion by the careful selection and deployment of substituents. Moreover, selection between heterocycles facilitates optimization of shape, size, and vector presentation to effectively complement a specific drug target.<sup>196–198</sup>

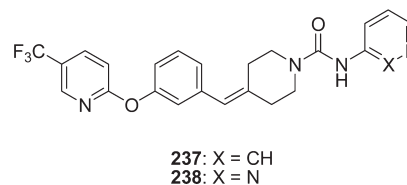
**3.8.6. H-Bonding and Brønsted Basicity Differences.** It is important to recognize that the Brønsted proton basicity ( $pK_{\text{BH}^+}$ ) and H-bonding basicity, as determined by  $pK_{\text{BHx}}$  measurement for acceptors, shows a poor quantitative correlation across functional groups, although correlations do typically exist within homologous series (Table 34).<sup>196</sup> As an illustrative example, the pyrrolidine N atoms of nicotine (**233**) and nornicotine (**234**) are the first sites of protonation in water but 90% of the H-bonding

**Figure 35.** H-bonding associated with the pyridazine heterocycle.

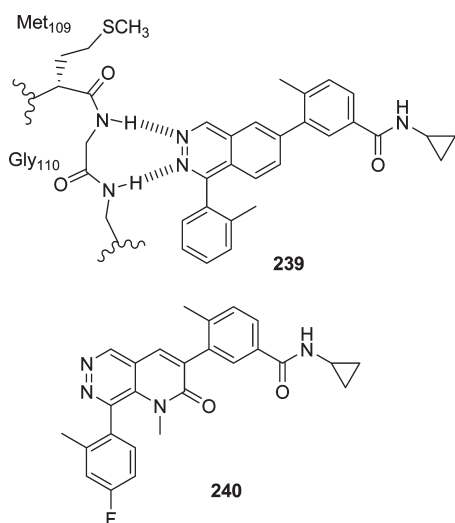
interaction between 4-fluorophenol and **233** occurs at the pyridine nitrogen while for **234** the figure is 80%.<sup>199</sup> This observation has been attributed to the electron withdrawing and steric effects associated with the pyridine ring interfering with access to the pyrrolidine nitrogen atom. Cotinine (**235**) is also a bifunctional H-bond acceptor, and in this case the amide carbonyl has been determined to be the major site of H-bonding in all solvents.<sup>199–205</sup> The H-bond basicity of the amide moiety of **235** is 1.6 units higher than that of the pyridine nitrogen atom despite the fact that pyridine, with  $pK_{\text{BH}^+} = 5.20$ , is more basic than the amide carbonyl,  $pK_{\text{BH}^+} = -0.71$ . Similarly, *N,N*-diethylnicotinamide (**236**) protonates on the pyridine nitrogen atom but the amide is a markedly stronger H-bond acceptor.<sup>199–205</sup>



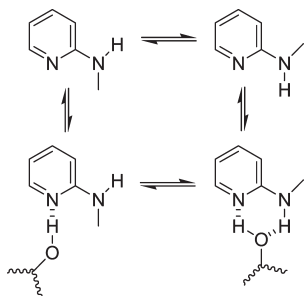
Within the homologous series of six-membered heterocycles, pyridazine is an outlier from the correlation between Brønsted basicity ( $pK_{\text{BH}^+}$ ) and  $pK_{\text{BHx}}$ , providing an interesting exception that can be exploited in drug design (Table 34). The H-bond acceptor properties of pyridazine approaches those of pyridine, but it is much less basic while it is both a better H-bond acceptor and more basic than pyrazine and pyrimidine.<sup>196,197,206</sup> The higher than expected H-bond accepting strength of pyridazine has been attributed to the  $\alpha$ -effect which reflects unfavorable electrostatic lone pair–lone pair interactions that are relieved by accepting a H-bond from a donor (Figure 35). Interestingly, pyridazines do not appear to be overtly associated with CYP P450 inhibition, suggesting that this ring system may be a useful isostere in situations where H-bonding is important but pyridine may cause problems. As an illustrative example, the mechanism-based fatty acid amide hydrolase (FAAH) inhibitor **237** inhibited CYP 2D6 with an  $\text{IC}_{50}$  of 1.4  $\mu\text{M}$  and CYP 3A4 with an  $\text{IC}_{50}$  of 0.8–4.3  $\mu\text{M}$  depending on the substrate.<sup>207</sup> However, the pyridazine analogue **238** exhibited a 2-fold improvement in FAAH inactivation kinetics that was associated with a 10-fold reduction in CYP 2D6 inhibition while CYP 3A4 was weakly inhibited,  $\text{IC}_{50}$  of 30  $\mu\text{M}$ , regardless of the substrate used.<sup>207</sup>



**3.8.7. Pyridazine H-Bonding in p38 $\alpha$  MAP Kinase Inhibitors.** A series of p38 $\alpha$  mitogen-activated protein (MAP) kinase inhibitors that bind to the ATP site of the enzyme provides an interesting illustration of the unique H-bond accepting properties of the pyridazine heterocycle.<sup>208</sup> The phthalazine **239** resulted from careful optimization as a potent p38 MAP kinase



**Figure 36.** Key binding interactions between the p38 $\alpha$  MAP kinase inhibitor **239** and the enzyme and the structure of an optimized analogue **240**.

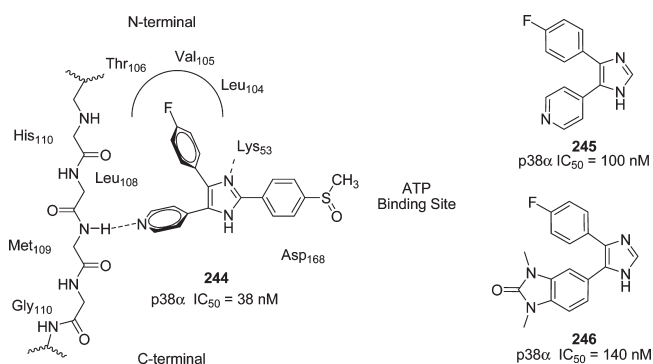


**Figure 37.** Topology of H-bonding interactions between 2-methylaminopyridine and a phenol.

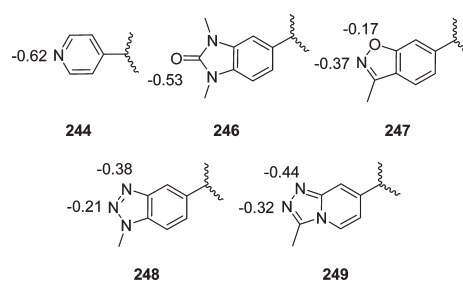
**Table 35.** H-Bonding Basicity ( $pK_{\text{BHX}}$ ) Associated with Derivatives of 2-Aminopyridine

| Compd #    |   | $pK_{\text{BHX}}$ |
|------------|---|-------------------|
| <b>241</b> | R = R <sub>1</sub> = CH <sub>3</sub>    | 1.61              |
| <b>242</b> | R = H; R <sub>1</sub> = CH <sub>3</sub> | 2.11              |
| <b>243</b> | R = R <sub>1</sub> = H                  | 2.12              |

inhibitor,  $IC_{50} = 0.8$  nM, with excellent selectivity over the related enzymes Kdr, Lck, CKII, JNK1, JNK2, and JNK3. An X-ray cocrystal of **239** with p38 $\alpha$  kinase revealed that the pyridazine element established H-bonds with the NHs of both Met<sub>109</sub> and Gly<sub>110</sub>, with the latter flipping to project its amide hydrogen into the ATP binding pocket, a conformational change that accounted for the high enzyme specificity (Figure 36).<sup>208</sup> This phthalazine chemotype formed the basis for further optimization focused on improving pharmacokinetic properties with the pyrido[2,3-*d*]pyridazine derivative **240**, a refined compound that reduced paw swelling in a rat collagen-induced model of arthritis.<sup>209,210</sup>



**Figure 38.** Interactions between the imidazole-based p38 $\alpha$  MAP kinase inhibitor **244** and the enzyme and the structure of two analogous inhibitors **245** and **246**.

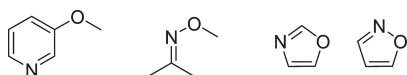


**Figure 39.** Electrostatic potential of heterocycles designed to interact with Met<sub>109</sub> in the hinge region of p38 $\alpha$  MAP kinase.

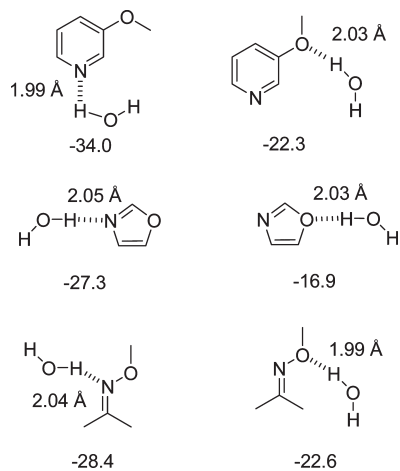
**3.8.8. Heterocycle Substituents and H-Bonding.** 2-Dimethylaminopyridine (**241**) exhibits reduced H-bond basicity compared to 2-methylaminopyridine (**242**) and 2-aminopyridine (**243**) (data compiled in Table 35).<sup>211</sup> This effect is not considered to be steric in origin based on analogy to 2-picoline and 2-isopropylpyridine where there is only a 0.27 difference in  $pK_{\text{BHX}}$ . Rather, this observation has been attributed to an artifact of the method of measuring H-bonding potential. In this case, an additional H-bond forms between the NH and the oxygen atom of the phenol used to assess H-bonding in **242** and **243** that is unavailable to **241**, as summarized in Figure 37.<sup>211</sup>

**3.8.9. Heterocycle Isosteres in p38 $\alpha$  MAP Kinase Inhibitors.** The H-bond between the NH of Met<sub>109</sub> in the hinge region of p38 $\alpha$  MAP kinase and inhibitors is a critical drug–target interaction in a series of 4,5-disubstituted imidazole derivatives that were established as effective inhibitors, exemplified by SB-203580 (**244**) (Figure 38).<sup>212,213</sup> In smaller inhibitors, the benzimidazol-2-one **246** was established as an effective isostere for the pyridine, a source of CYP 450 inhibition, in **245** since both compounds inhibited p38 $\alpha$  MAP kinase with similar potencies. However, an attempt to replace the pyridine of **244** with a benzimidazol-2-one was not successful, attributed to the larger heterocycle altering the bound conformation such that the introduction of an aryl substituent at C-2 of the imidazole ring projected this moiety beyond the boundaries of the ATP binding site. As a consequence, potency was decreased by over 40-fold and smaller H-bond acceptors to replace the benzimidazol-2-one moiety were sought.

Compound design focused on benzo-fused, diheteroatomic systems, since saturated single heteroatom systems would possess hydrogen atoms or lone pairs projecting orthogonally

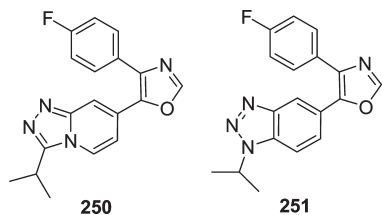


**Figure 40.** Examples of functionality with two potential H-bond acceptors.

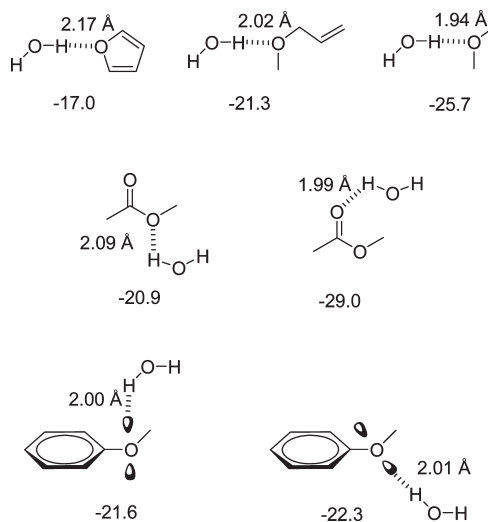


**Figure 41.** Comparison of the calculated energetics (kJ/mol) of the interaction of H<sub>2</sub>O with N and O atoms in molecules incorporating both elements.

to the ring plane. Molecular electrostatic potential maps were generated for the series of truncated heterocycles captured in Figure 39 which revealed that the benzimidazol-2-one moiety was closest to pyridine, but hydrophobicity,  $\pi$ - $\pi$  stacking interactions, and dipoles were also considered in the analysis.<sup>212,213</sup> However, the predictions were associated with sufficient ambiguity to necessitate experimental evaluation and an X-ray cocrystal of the triazolopyridine **250** revealed two H-bonding interactions between the kinase and the inhibitor, one from Met<sub>109</sub> NH to N3 and a second from Gly<sub>110</sub> NH to N2. However, the benzo-1,2,3-triazole derivative **248** was 5-fold more potent in the context of **251**, an observation attributed to hydrophobic and  $\pi$ - $\pi$  interactions in addition to desolvation effects. The free energy of binding divided by the number of heavy atoms, a measure of ligand efficiency, indicated that the benzimidazol-2-one moiety was the least efficient of these ligands.<sup>212,213</sup>



**3.8.10. Heteroatoms as H-Bond Acceptors.** Two approaches have been taken to address the question of which atom, O or N, engages a H-bond donor in a competitive situation where both are available as acceptors as in, for example, alkoxy pyridines, alloximes, oxazoles, and isoxazoles (Figure 40). An ab initio study of functional groups complexed with water provided theoretical insight, while an analysis of H-bonding interactions in molecules presenting both opportunities in the CSD catalogued practical examples.<sup>214</sup>



**Figure 42.** Energetics (kJ/mol) of the interaction of H<sub>2</sub>O with O atoms in common functional groups.

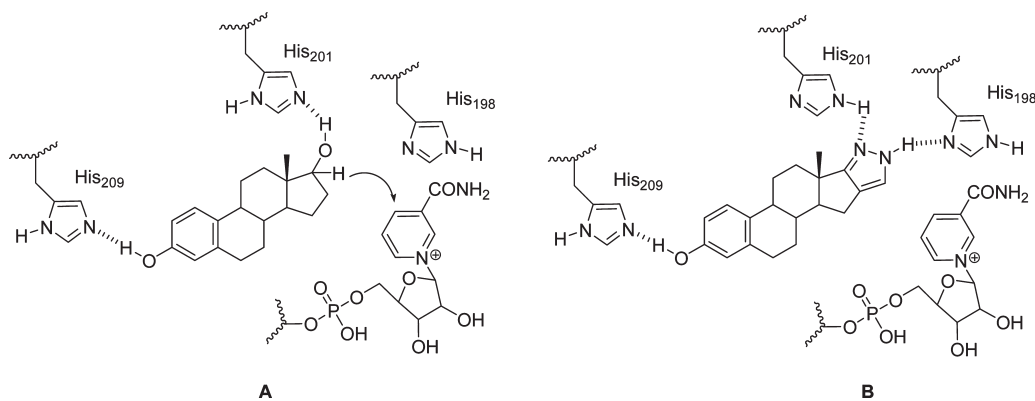
**Table 36. Statistics Associated with the Presence and Number of H-Bonds to N and O in Functional Groups in the Cambridge Structural Database<sup>214</sup>**

|                | no. of fragments | no. H bonds to N | no. H bonds to O |
|----------------|------------------|------------------|------------------|
| oxazole        | 36               | 17               | 1                |
| isoxazole      | 75               | 25               | 0                |
| 3-MeO-pyridine | 12               | 7                | 0                |
| oxime ether    | 136              | 4                | 0                |

The ab initio studies calculated H-bond lengths and interaction energies (kJ/mol), with the data indicating that N is a much stronger H-bond acceptor than O when integral to or conjugated with an sp<sup>2</sup>  $\pi$ -system (Figure 41). For oxazole and methoxypyridine, the difference in energy between N and O acting as acceptors is more than 10 kJ/mol, supported by the prevalence of N acting as the H-bond acceptor in the CSD, summarized by the frequencies presented in Table 36.<sup>214</sup>

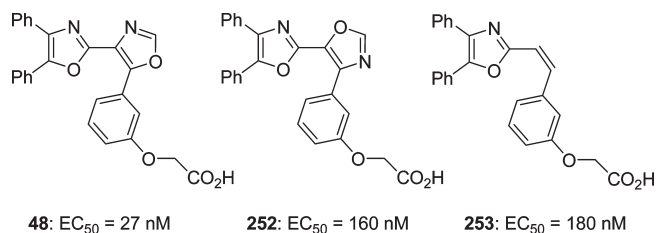
**3.8.11. Oxygen Atoms and H-Bonding.** These results were reinforced by calculated H-bond lengths and interaction energies (kJ/mol) between an oxygen atom bound to sp<sup>2</sup> sites of unsaturation and H<sub>2</sub>O that showed reduced potential for O to function as an acceptor (summarized in Figure 42). For example, in esters the carbonyl oxygen always acts as the acceptor with the lone pair *syn* to the OR moiety, a slightly stronger acceptor.<sup>214</sup>

**3.8.12. Isosterism between Heterocycles in Non-Prostanoid PGI<sub>2</sub> Mimetics.** A practical example of the effect of the difference in H-bonding associated with oxazole rings is provided by the series non-prostanoid PGI<sub>2</sub> mimetics **48**, **252**, and **253** that inhibit ADP- and collagen-induced blood platelet aggregation in platelet-rich plasma *in vitro*.<sup>86,87,215,216</sup> Potency is sensitive to the topology of the central oxazole ring with a 5-fold difference in the EC<sub>50</sub> between the isomers **48** and **252**. The weaker inhibitor **252** is comparable to the simple *cis*-olefin **253**, suggesting that in this orientation the oxazole acts simply as a scaffolding element providing the optimal geometry to complement the PGI<sub>2</sub> receptor. Data from a related series had formulated the hypothesis that the PGI<sub>2</sub> receptor projects a



**Figure 43.** Interactions between estradiol 17 $\beta$ -dehydrogenase and its substrate (A) and the inhibitor **256** (B).

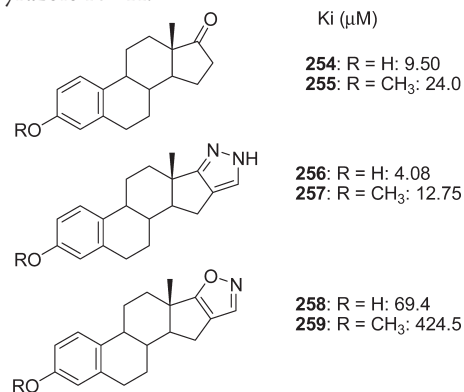
H-bond donor in the vicinity of the central oxazole ring. Consequently, the oxazole nitrogen atom was deduced to be acting as the acceptor in **48**, a concept reflected in the intermolecular interactions observed in the single crystal X-ray structures of the oxazoles **48** and **252**.<sup>215,216</sup> In the solid state, the N atom of the central oxazole ring in both compounds engages in an intermolecular H-bond interaction with the carboxylic acid hydrogen of another molecule, leading to markedly different packing in the unit cell. However, the shape adopted by each individual molecule is essentially identical, providing an interesting example of exact isosterism, defined as “two molecules with close atom-for-atom correspondence with regard to both internal coordinates and van der Waals radii”.<sup>217</sup>



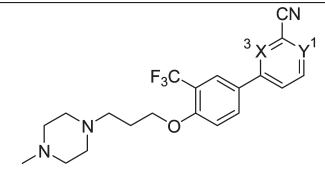
**3.8.13. Isosterism between Heterocycles in Estradiol 17 $\beta$ -Dehydrogenase Inhibitors.** Another example where the subtle effect of H-bonding topology appears to affect potency is in a series of human estradiol 17 $\beta$ -dehydrogenase inhibitors where H-bonds between estradiol or estrone and the catalytically active histidines His<sub>198</sub> and His<sub>201</sub> were hypothesized to stabilize substrate complexes, as depicted in Figure 43A.<sup>218</sup>

In order to explore this concept, pyrazoles **256** and **257** and isoxazoles **258** and **259** were prepared as analogues of the ketones **254** and **255** and shown to be competitive inhibitors of estradiol 17 $\beta$ -dehydrogenase, with potency consistent with the postulated H-bond acceptor and donor patterns at both the A and D rings. For the A ring, the 2.5- to 6-fold difference in potency in favor of the OH compared to the OCH<sub>3</sub> substituent supported the importance of a substrate H-bond donor interaction to the enzyme. For the D ring interactions, a potency difference of 1.9- to 7.3-fold was viewed as being consistent with the D ring functionality accepting a H-bond from the enzyme that could be reinforced by a D ring H-bond donor, realized only by the pyrazoles **256** and **257**.<sup>218</sup> The latter was interpreted as the pyrazole N-H donating a H-bond to His<sub>198</sub>, with His<sub>201</sub> adopting a tautomeric config-

uration in order to donate a H-bond to the pyrazole nitrogen atom. These SAR data are consistent with the C3-OH functioning as a H-bond donor to His<sub>209</sub> and a C17 H-bond acceptor from His<sub>201</sub> to either the ketone C=O of estrone or the pyrazole or isoxazole sp<sup>2</sup> N atoms of the inhibitors, depicted in Figure 43B.<sup>218</sup> Unfortunately, the isoxazoles isomeric with **258** and **259**, which would have been an excellent test of the concept, were not synthesized. The potency difference between estrone and the pyrazole analogue was attributed to an additional H-bond donor interaction to His<sub>198</sub> by the pyrazole N-H.



**3.8.14. Role of Pyrimidine Nitrogen Atoms in Cathepsin S Inhibitors.** An interesting example of the importance of the correct topology of a heteroatom for biological activity that illustrates the limits of the potential for isosterism between heterocycles is provided by a series of nonpeptidic heteroaryl nitriles that have been developed as inhibitors of cathepsins K and S.<sup>219</sup> In these compounds, the nitrile moiety acts as an electrophile toward the catalytic cysteine thiol of the enzyme, reversibly forming a stable, covalent complex. Incorporation of the nitrile moiety at the 2-position of a pyrimidine provided the potent and effective inhibitor **260** (Table 37). However, this arrangement results in an overactivation of the electrophilicity of the nitrile, leading to indiscriminate reactions with microsomal proteins. As part of the optimization process, a series of pyridines were examined in a systematic fashion with the anticipation of moderating nitrile electrophilicity, an exercise that provided fundamental insights into parameters associated with biological activity. Concordant with the underlying hypothesis, replacing the pyrimidine N-1 atom with a CH afforded the pyridine **261**, a compound that exhibited 44-fold reduced potency toward

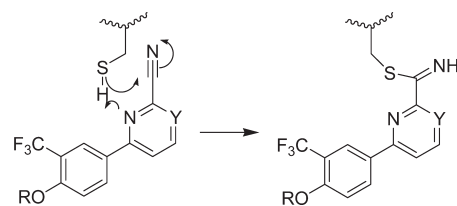
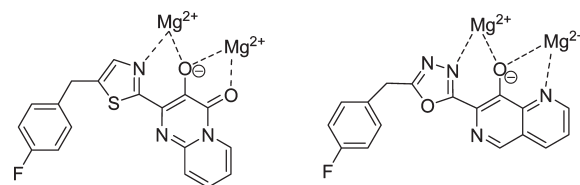
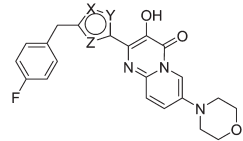
**Table 37. SAR Associated with a Series of Inhibitors Cathepsins S and K**


| Compd #    | X  | Y  | IC <sub>50</sub> (nM) |             |
|------------|----|----|-----------------------|-------------|
|            |    |    | cathepsin S           | cathepsin K |
| <b>260</b> | N  | N  | 1.3                   | 13          |
| <b>261</b> | N  | CH | 58                    | 1660        |
| <b>262</b> | CH | N  | inactive              | inactive    |

cathepsin S and 127-fold lower inhibition of cathepsin K. However, the isomeric pyridine **262** was inactive toward both cysteine proteases, leading to the conclusion that the pyrimidine N-3 interacts with the H of the cysteine thiol, facilitating addition to the nitrile moiety as depicted in Figure 44. When the pyrimidine N-3 atom is replaced with a C–H to afford the pyridine **262**, not only is this function lost but a negative steric interaction between the ring CH and the SH is introduced.<sup>219</sup>

**3.8.15. Heterocycles and Metal Coordination.** An assessment of isosterism within a series of azoles designed to function as amide surrogates has been explored in the context of inhibitors of HIV-1 integrase in which biological activity is a function of the ability of the heterocycle to coordinate with one of the two Mg<sup>2+</sup> atoms involved in catalysis.<sup>220–224</sup> Azoles were selected over six-membered heterocycles based on their ability to more readily adopt a coplanar arrangement with the additional metal chelating elements presented by a series of pyrido[1,2-*a*]pyrimidine and 1,6-naphthyridine-based integrase inhibitors. The selection of azoles introduced topological asymmetry that facilitated a precise analysis of the capacity of heteroatoms to engage Mg<sup>2+</sup> based on the distinct topological preference for the presentation of the fluorobenzyl moiety relative to the pyrimidine ring (Figure 45). Enzyme inhibitory data for representatives of the pyrido[1,2-*a*]pyrimidine series are summarized in Table 38 which reveals the importance of presenting an azole nitrogen atom for coordination with Mg<sup>2+</sup>, most evident in the comparison between the 1,2,4-oxadiazoles **267** and **268**, an observation mirrored by the 1,6-naphthyridine series.<sup>221,223</sup> In the pyrido[1,2-*a*]pyrimidine series, the thiazole series represented by **264** was selected for further optimization<sup>222</sup> while the 1,3,4-oxadiazole ring (**266**) that performs modestly in this series was the most effective amide surrogate studied in the 1,6-naphthyridine series, reflecting subtle differences between the two chemotypes.<sup>223,224</sup>

**3.8.16. Heterocycles and C–H Bonding.** Hydrogen atoms bound to the sp<sup>2</sup> carbon atoms of aromatic and heterocyclic rings have been established as weak C–H bond donors in small molecule X-ray crystallographic studies, an observation beginning to attract attention as direct and indirect mediators of ligand–target interactions in drug design.<sup>225,226</sup> The observation of both inter- and intramolecular variants of this kind of H-bonding interaction in protein kinase inhibitors prompted *ab initio* calculations to evaluate the strength of C–H to water bonds, performed in conjunction with an analysis of the protein data bank (PDB), in order to understand the scope of the effect.<sup>226</sup> The latter provided broader evidence for the existence of C–H H-bond interactions between ligands and proteins.

**Figure 44.** Interaction between pyrimidine-based cathepsin inhibitors and the catalytic cysteine thiol that facilitates addition of the thiol to the activated nitrile.**Figure 45.** Interactions between azole-substituted pyrido[1,2-*a*]pyrimidines and 1,6-naphthyridines and the catalytic Mg<sup>2+</sup> atoms of HIV-1 integrase.**Table 38. Structure–Activity Relationships for a Series of Azole-Substituted Pyrido[1,2-*a*]pyrimidine-Based Inhibitors of HIV-1 Integrase**


| Compd #    | Heterocycle  | IC <sub>50</sub> (nM) | Compd #    | Heterocycle   | IC <sub>50</sub> (nM) |
|------------|--|-----------------------|------------|---|-----------------------|
| <b>263</b> |  | 59                    | <b>267</b> |  | 450                   |
| <b>264</b> |  | 20                    | <b>268</b> |  | >10,000               |
| <b>265</b> |  | 45                    | <b>269</b> |  | -                     |
| <b>266</b> |  | 310                   | <b>270</b> |  | 225                   |

The results of the *ab initio* studies for a series of ring systems prevalent in drug design are compiled in Table 39, with the energy of the C–H H-bond donor activity indexed to H<sub>2</sub>O and CH<sub>4</sub> as the two bookends. Not surprisingly, these hydrogen atoms are weaker H-bond donors than H<sub>2</sub>O but stronger than CH<sub>4</sub>, and heterocycles offer advantage over a phenyl ring, with strength dependent on the regiochemical relationship of the C–H to the heteroatoms. While unlikely to dominate a small molecule–protein interaction, these weak interactions would be anticipated to play an augmenting role and examples are beginning to be documented.

**3.8.17. Heterocycle C–H Bond Donors in GSK3 Inhibitors.** The serine/threonine kinase glycogen synthase kinase 3 (GSK3) is known to be involved in several cellular signaling pathways and represents a potential molecular target for type 2 diabetes and Alzheimer's disease, where GSK3 levels have been shown to be elevated. GSK3 also has proapoptotic activity and may be involved in neuronal cell death, while inhibitors may mimic the action of mood stabilizers such as lithium and valproic acid, suggesting potential for

Table 39. Calculated H-Bond Donor Interaction Energies between a C–H and H<sub>2</sub>O Compared to H<sub>2</sub>O and CH<sub>4</sub><sup>226</sup>

| Structure   | H-bond donor interaction energy with H <sub>2</sub> O (kcal/mol) |
|---|--|
| HO-H  | -5.51  |
| CH <sub>3</sub> -H  | -0.87  |
| Benzene   | -1.47  |
|    | -1.77  |
|    | -2.71  |
|    | -2.23  |
|    | -11.6  |
|    | -2.90  |
|    | -3.06  |
|   | -3.48  |
|  | -3.04  |
|  | -2.91  |
|  | -2.08  |
|  | -6.37  |
|  | -2.22  |
|  | -2.24  |
|  | -2.41  |
|  | -2.71  |
|  | -3.21  |
|  | -2.16  |
|  | -2.71  |

the treatment of bipolar mood disorders. An X-ray crystal structure of the enzyme was solved in 2001, facilitating structure-based design and

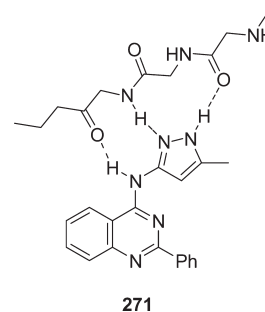
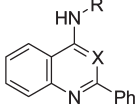
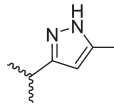
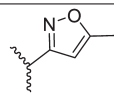
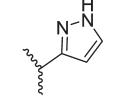
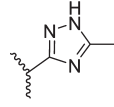
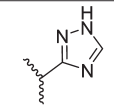
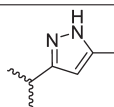


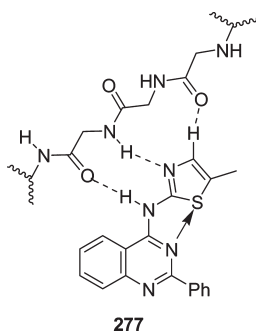
Figure 46. Key H-bonding interactions between 271 and glycogen synthase kinase 3.

Table 40. SAR Associated with a Series of Glycogen Synthase Kinase 3 Inhibitors

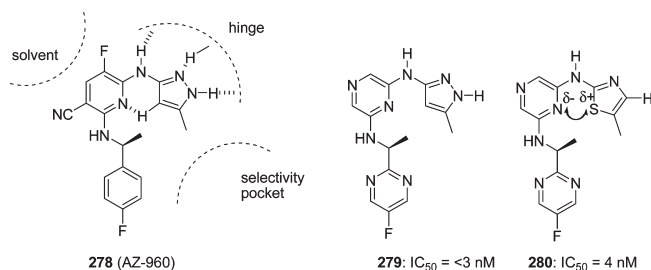
|  |    |   |                          |
|---|----|---|--------------------------|
| Compd #   | X  | R   | GSK3 K <sub>i</sub> (μM) |
| 271   | N  |    | 0.024                    |
| 272   | N  |   | >2.0                     |
| 273   | N  |  | 0.11                     |
| 274   | N  |  | 23                       |
| 275   | N  |  | 0.25                     |
| 276   | CH |  | 2.5                      |

leading to the development of a seam of biological activity associated with structurally diverse inhibitors. The 4-aminoquinazoline derivative 271 was a potent early lead, K<sub>i</sub> = 24 nM, that exhibited inhibition kinetics consistent with the compound acting as a competitive inhibitor of ATP binding (Table 40).<sup>227</sup> An X-ray cocrystal structure confirmed the mode of inhibition and revealed three H-bonding interactions between the enzyme and 271, which adopted an overall planar topography in the active site, as depicted in Figure 46.

However, much of the fundamental SAR associated with 271 appeared to be cryptic in nature. The poor activity of the isoxazole 272 was explained by the loss of a H-bond donor moiety, while the 4-fold reduced activity of pyrazole 273 was attributed to the loss of an important hydrophobic interaction associated with the CH<sub>3</sub> moiety



**Figure 47.** Drug–target interactions between the thiazole **277** and glycogen synthase kinase 3.



**Figure 48.** Binding interactions between Janus kinase 2 and the inhibitor **278** and the structure of two analogues **279** and **280**.

of **271** (data summarized in Table 40).<sup>227</sup> However, replacing the pyrazole ring of **271** by a triazole (**274**), which preserves the H-bond donor capability, resulted in 1000-fold reduction in potency while removing the CH<sub>3</sub> group, to afford **275**, restored potency by 100-fold, a result that contrasts markedly with the data for the related pyrazoles **271** and **273**. Adding to the enigma, the quinoline **276** was found to be 100-fold less active than **271**, with a *K<sub>i</sub>* of 2.5 μM.<sup>227</sup>

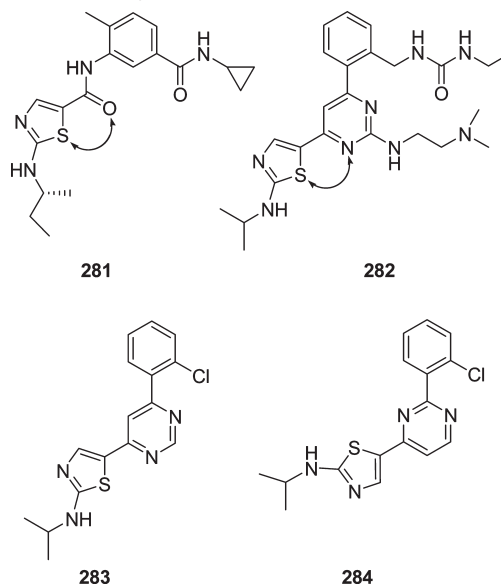
A careful analysis of this series based on an assessment of the preferred conformations of the azole moieties in relation to the quinazoline or quinoline heterocycle and an appreciation of H-bonding patterns, including C–H H-bond donors, provided a coherent explanation for the data that are summarized in Table 41.

**3.8.18. Evolution of GSK3 Inhibitors.** Taking advantage of these observations and seeking new active inhibitors of GSK3, the thiazole **277** was designed based on modeling that revealed a planar conformation preferred by 9 kcal/mol, attributed to a productive N to S  $\sigma^*$  stabilizing interaction that is a function of a partial positive charge on S (+0.35) and a partial negative charge on N (−0.65) (Figure 47).<sup>227</sup> A heteroaryl C–H H-bond donor interaction to an enzyme backbone carbonyl oxygen atom was also invoked, optimal when the H-bond donor is bound to a carbon adjacent to a heteroatom (Figure 47). This compound was synthesized and tested, displaying a *K<sub>i</sub>* of 150 nM, just 6-fold weaker than the pyrazole **271**, an observation attributed to the weaker C–H H-bond donor in **277** compared to the pyrazole NH. An X-ray cocrystal structure confirmed the predicted interactions, providing the first example where CH $\cdots$ X H bonds play an important role in drug–target binding.<sup>227</sup>

**3.8.19. Janus Kinase 2 (JAK2) Inhibitors.** AZ-960 (**278**) is a potent JAK2 inhibitor, *IC*<sub>50</sub> ≤ 3 nM, that acts as a competitive inhibitor of ATP, with the orientation in the binding site depicted in

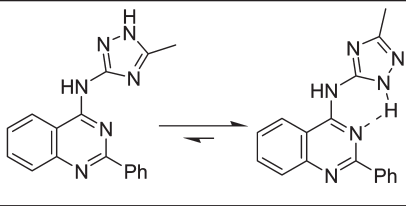
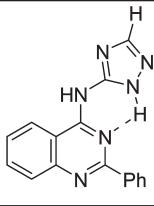
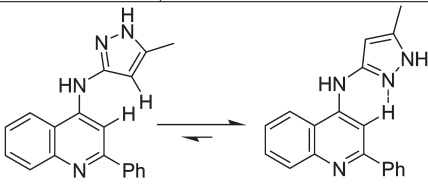
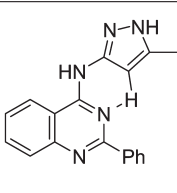
Figure 48.<sup>228,229</sup> In this series, a pyrazine was shown to be an effective isostere of the pyridine while a thiazole was examined as a pyrazole replacement, pursuing a hypothesis based on the proposed binding mode and concepts developed from the earlier observations described above for GSK3 inhibitors. In the event, pyrazole **279** and thiazole **280** showed comparable potency attributed to a productive N–S interaction to replace the C–H H-bond donor interaction between the pyrazole and pyrazine in **278** and **279**.<sup>228,229</sup>

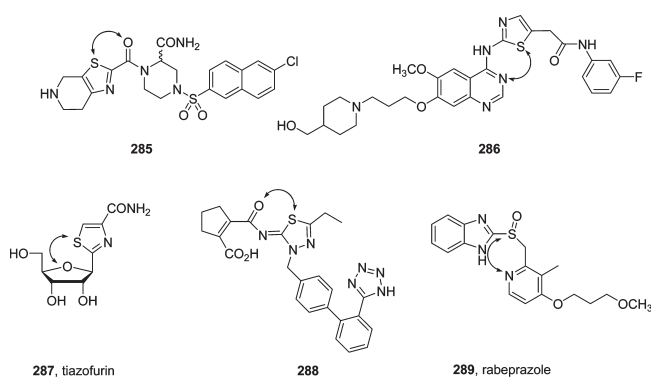
The unique properties of sulfur in heterocyclic ring systems have been appreciated more broadly as a means of influencing conformational preferences. A recent example took advantage of establishing a  $n_o \rightarrow \sigma^*$  interaction between a pyrimidine nitrogen and a thiazole sulfur atom to bias conformational constraint in a series of p38 $\alpha$  MAP kinase inhibitors.<sup>230,231</sup> In a successful attempt to optimize the thiazole **281**, for which the X-ray cocrystal with the enzyme suggested an interaction between the thiazole S atom and the proximal amide carbonyl lone pair,<sup>231</sup> the pyrimidine **282** emerged as a potent p38 $\alpha$  MAP kinase inhibitor, *IC*<sub>50</sub> = 7 nM. An X-ray cocrystal of **282** bound to the enzyme revealed coplanarity between the thiazole and pyrimidine rings, consistent with the proposed  $n_o \rightarrow \sigma^*$  interaction. Confirmation was obtained from single crystal X-ray structures of **283** and **284** in which the more potent **283** (*IC*<sub>50</sub> = 46 nM) adopted a conformation with a short (2.90 Å) contact distance while the less potent **284** (*IC*<sub>50</sub> = 223 nM) crystallized with the topology shown, also stabilized by a  $n_o \rightarrow \sigma^*$  interaction that favors the alternative conformation that is not complementary to the topology of the enzyme active site.<sup>231</sup>



This kind of  $n \rightarrow \sigma^*$  donation to sulfur that creates close contacts between the atoms has been analyzed theoretically for S $\cdots$ O interactions<sup>232</sup> and recognized as contributing to conformational preorganization and, hence, biological activity in the factor Xa inhibitor **285**,<sup>233</sup> the Aurora A and B kinase inhibitor **286**,<sup>234</sup> the nucleoside analogue tiazofurin (**287**) and related compounds,<sup>235–238</sup> the angiotensin II receptor antagonist **288**,<sup>239</sup> and the proton pump inhibitor rabeprazole (**289**).<sup>240</sup> In the case of **286**, **287**, and **288**, the corresponding oxygen analogues have been shown to be markedly less potent, demonstrating the importance of selecting the correct azole moiety and defining the limits of isosteric replacement between heterocycles.

Table 41. Factors Underlying the Conformational Preferences of a Family of Glycogen Synthase Kinase 3 Inhibitors

|  |  |   |
|--|--|---|
|   | <p>This is the bound form in the X-ray co-crystal with the enzyme but this conformation establishes an unfavorable dipole-dipole interaction between the triazole and quinazoline N atoms and sacrifices the intramolecular H-bond available to the alternate conformer.</p>   |  |
| <p>This conformer is favored by 10.1 Kcal/mole with the planar topography stabilized by the triazole NH to quinazoline N to H-bond. This arrangement preserves 1 H-bond donor and 1 acceptor interaction with the enzyme but the CH<sub>3</sub> group presents unfavorable steric interactions with the protein.</p> | <p>Removing the CH<sub>3</sub> relieves the unfavorable steric interactions and the intramolecular H bond stabilizes the planar conformation. A C-H H-bond donor from the triazole to the enzyme is weaker than the N-H of the pyrazole but this arrangement preserves the full array of 3 H bonds seen in lead compound <b>271</b>.</p> |   |
|   | <p>A planar topography is disfavored by allylic 1,3 strain between the pyrazole and quinoline H atoms increasing the energy of this conformation.</p>  |  |
| <p>This conformer is favored by 1.9 Kcal/mole, stabilized by an N to aryl CH H-bond that favors a planar topography. However, the CH<sub>3</sub> group presents an unfavorable steric interaction with the enzyme which is dependent on only 1 H-bond donor and no acceptor.</p>                                     | <p>The N-heteroaryl to CH H-bond favors a planar topography, the CH<sub>3</sub> moiety is optimally displayed and the full complement of H-bond donors to the enzyme is preserved. This conformer is 0.4 Kcal/mole lower in energy than the alternate topology.</p>  |   |



### 3.8.20. Electron Demand of Heterocycles and Applications.

The electron withdrawing properties of heterocycles, which are dependent on the identity of the heterocycle, the site of attachment, and the nature and position of substituents, have been exploited extensively in drug design. Two of the most prominent applications include the activation of carbonyl moieties to electrophilic species that readily react with the catalytic serine of serine proteases and related serine hydrolases to afford mechanism-based inhibitors and the acidification of amine or amide moieties to improve H-bond donor properties, culminating in carboxylic acid isosterism in the case of sulfonamide-based antibacterial agents. In an effort to quantify electron withdrawal, the concept of charge demand has been formulated, defined as the fraction of  $\pi$ -charge transferred from a negatively charged trigonal carbon atom to the adjacent X group, as depicted in

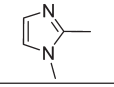
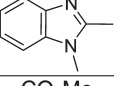
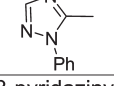
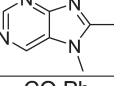


**Figure 49.** Charge demand is defined as the fraction of  $\pi$ -charge transferred from a negatively charged trigonal carbon atom to the adjacent X group.

Figure 49.<sup>241–244</sup> A ranking of resonance electron withdrawing capacity of a range of functional groups and heterocycles of interest to medicinal chemists, measured by <sup>13</sup>C NMR chemical shifts of trigonal benzylic carbanions, is compiled in Table 42.

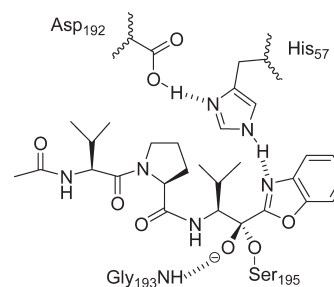
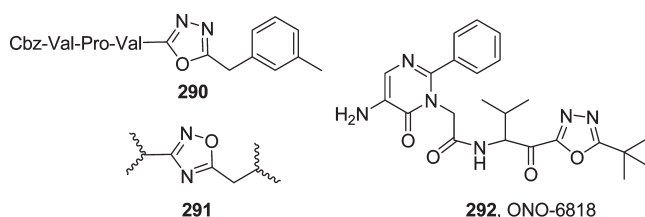
3.8.21. *Heterocycles and Activation of a C=O in Serine Protease Inhibitors.* One aspect of the design of serine protease inhibitors has focused on presenting the enzyme with a substrate mimetic in which the scissile amide bond is replaced with an electrophilic carbonyl element to which the catalytic serine hydroxyl reacts to form a stable but unproductive tetrahedral intermediate. The equilibrium in favor of the adduct is a function of the electrophilicity of the C=O moiety, and peptidic aldehydes were adopted as the vehicle for the initial examination of this concept.<sup>245</sup> Subsequent refinement probed trifluoromethyl ketones and pyruvate derivatives, the latter providing an opportunity for the incorporation of structural elements designed to interact more extensively and productively with the S' pockets. Further evolution along this path of inquiry focused on a series of tripeptidic, mechanism-based inhibitors of human neutrophil elastase (HNE) that incorporated heterocycles as the carbonyl activating element.<sup>246–252</sup>  $\alpha$ -Ketoamides were included in

**Table 42. Charge Demand Associated with Functional Groups and Heterocycles Arranged in Order of Increasing Electron Withdrawal**

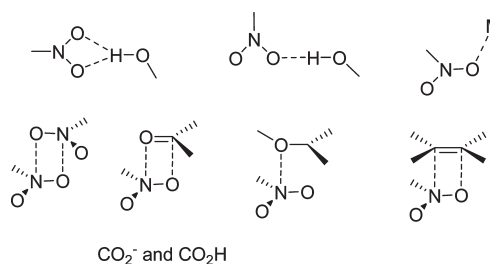
| Substituent   | Charge Demand $c_X^{\text{Ph}}$ |
|---|---------------------------------|
| $\text{P(O)(OEt)}_2$  | 0.26                            |
| SO.Ph   | 0.26                            |
| SO <sub>2</sub> Ph  | 0.28                            |
| CN  | 0.28                            |
|    | 0.283                           |
| Ph  | 0.29                            |
| 2-oxazolyl  | 0.346                           |
| 2-thiazolyl   | 0.380-0.413                     |
|    | 0.382                           |
| CO <sub>2</sub> Me  | 0.40                            |
| 4-pyridyl   | 0.408                           |
| 2-pyridyl   | 0.411                           |
|    | 0.411                           |
| 3-pyridazinyl   | 0.417                           |
| CONMe <sub>2</sub>  | 0.42                            |
| 2-benzoxazolyl  | 0.424-0.436                     |
| 2-pyrimidinyl   | 0.430                           |
| pyrazinyl   | 0.446                           |
| 2-benzothiazolyl  | 0.457-0.471                     |
| 4-pyrimidinyl   | 0.501                           |
| CO.Me   | 0.51                            |
|  | 0.536                           |
| CO.Ph   | 0.56                            |

this study as comparators, and inhibitory potency was found to correlate with the electrophilicity of the carbonyl moiety (results summarized in Table 43).<sup>247</sup> These heterocyclic carbonyl-activating moieties were considered to offer several advantageous opportunities for drug design, including the potential for unique interactions with enzyme and the ability to probe interactions with *S'* sites, while the size of the heterocycle was considered to offer potential to sterically interfere with metabolism of the carbonyl moiety.<sup>246–248,252</sup>

Subsequent studies examining an oxadiazole activating element found that activity was quite sensitive to the identity of the heterocycle with the 1,3,4-oxadiazole **290**, a highly potent inhibitor of HNE,  $K_i = 0.025$  nM, but the isomeric 1,2,4-oxadiazole **291** was 20-fold weaker,  $K_i = 0.49$  nM.<sup>249</sup> The 1,3,4-oxadiazole was subsequently incorporated into ONO-6818 (**292**), an orally bioavailable, nonpeptidic inhibitor of HNE advanced into clinical trials.<sup>250</sup>



**Figure 50.** Key interactions between a tripeptidic ketobenzoxazole derivative and HNE.

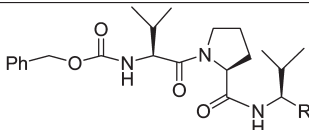


**Figure 51.** Contact interactions between nitro and functional groups abstracted from the Cambridge Structural Database.<sup>256</sup>

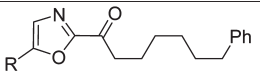
An X-ray cocrystal structure of a benzoxazole derivative bound to HNE revealed the key enzyme–inhibitor interactions, confirming the addition of the catalytic serine hydroxyl to the activated carbonyl moiety and revealing the development of a productive H-bonding interaction between the benzoxazole N atom and the NH of the imidazole of the catalytic histidine (Figure 50).<sup>246</sup>

Fatty acid amide hydrolase (FAAH) is a serine hydrolase responsible for degrading endogenous lipid amides, including anandamide and related fatty acid amides that have been identified as neuronal modulators. Heterocycles have been productively examined as activators of carbonyl moieties in mechanism-based inhibitor design<sup>252</sup> with the focus directed toward a series of 2-ketooxazole derivatives.<sup>253,254</sup> In these studies, the electronic properties of the oxazole moiety were modulated by the introduction of substituents capable of indirectly influencing carbonyl electrophilicity, with the structure–activity relationships captured in Table 44 demonstrating the effects on potency. FAAH inhibitory activity correlated nicely with the Hammett  $\sigma$  constant for substituents, a fundamental structure–activity relationship that allowed both deduction and prediction of the physicochemical nature of the oxazole substituent. For example, the 5-CO<sub>2</sub>H derivative was deduced to bind as CO<sub>2</sub><sup>-</sup> under the assay conditions based on the  $\sigma_p$  of 0.11 for the charged species versus a  $\sigma_p$  of 0.44 for CO<sub>2</sub>H.<sup>253,254</sup> Similarly, it was concluded that the 5-CHO and 5-COCF<sub>3</sub> analogues bind as the hydrates, observed as the species in solution by <sup>1</sup>H and <sup>13</sup>C NMR, providing the first estimates of  $\sigma_p$  for these substituents (0.26 for CH(OH)<sub>2</sub> and 0.33 for C(OH)<sub>2</sub>CF<sub>3</sub>).<sup>253,254</sup>

**3.9. Isosteres of the Nitro Group.** The nitro moiety is a small, moderately polar substituent<sup>255</sup> capable of H-bonding, with several such contacts observed in structures in the CSD, as summarized in Figure 51.<sup>256</sup> Most typically, the nitro group is encountered as a substituent on aryl or heteroaryl rings where it polarizes the

**Table 43. Structure–Activity Relationships Associated with a Series of Tripeptidic Mechanism-Based Inhibitors of HNE**


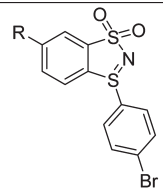
| R                         | HNE $K_i$ (nM) |
|---------------------------|----------------|
| CO.CH <sub>3</sub>        | 8,000          |
| CHO                       | 41             |
| CO.CF <sub>3</sub>        | 1.6            |
| CO.Ph                     | 16,000         |
| CO-2-thienyl              | 4,300          |
| CO-2-benzoxazole          | 3              |
| CH(OH)-2-benzoxazole      | 21,000         |
| CO-2-oxazole              | 28             |
| CO-2-oxazolidine          | 0.6            |
| CO-2-benzothiazole        | 25             |
| CO-2-thiazole             | 270            |
| CO-2-(1-Me)-imidazole     | 80,000         |
| CO-2-(1-Me)-benzimidazole | 12,000         |
| CO-2-benzimidazole        | 5,600          |
| CO-2-pyridine             | 22,000         |
| CO-2-benzofuran           | 3,400          |

**Table 44. Structure–Activity Relationships Associated with a Series of Ketoazole-Based Inhibitors of Fatty Acid Amide Hydrolase (FAAH)**


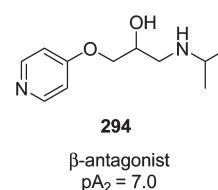
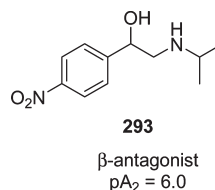
| R                                  | FAAH $K_i$ (nM) |
|------------------------------------|-----------------|
| H                                  | 48              |
| CO <sub>2</sub> H                  | 30              |
| CO <sub>2</sub> CH <sub>3</sub>    | 0.9             |
| CONH <sub>2</sub>                  | 5               |
| CON(CH <sub>3</sub> ) <sub>2</sub> | 2               |
| CO.CH <sub>3</sub>                 | 2               |
| CHO                                | 6               |
| CO.CF <sub>3</sub>                 | 3.5             |
| CN                                 | 0.4             |
| CH <sub>3</sub>                    | 80              |
| CF <sub>3</sub>                    | 0.8             |
| I                                  | 3               |
| Br                                 | 3               |
| Cl                                 | 5               |
| F                                  | 30              |
| SCH <sub>3</sub>                   | 25              |

$\pi$ -system, and a number of protein–ligand interactions involve the  $\pi$ -system of aromatic rings. However, nitro-substituted benzene derivatives are associated with toxicity as a function of partial reduction to the hydroxylamine which can undergo metabolic activation to an electrophilic nitroso species. Identifying suitable replacements for nitro-substituted aryl or heteroaryl rings has proven to be challenging, with pyridine the most common isostere, although a carboxylate has been shown to function as a nitro isostere in an inhibitor of ribonucleotide carboxylase.<sup>257</sup>

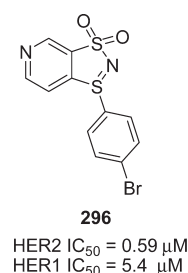
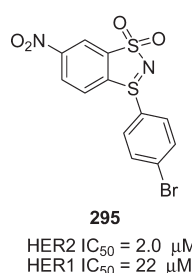
In an early study of nitro isosteres, pyridine was probed as a replacement for a nitrophenyl in the context of the  $\beta$ -adrenergic antagonist **293** with the 4-pyridyl analogue **294** 10-fold more potent.<sup>258</sup>

**Table 45. SAR Associated with a Series of Human Epidermal Growth Factor Receptor Kinase Inhibitors**


| R                                 | HER2 IC <sub>50</sub> ( $\mu$ M) | HER1 IC <sub>50</sub> ( $\mu$ M) |
|-----------------------------------|----------------------------------|----------------------------------|
| F                                 | >40                              | >40                              |
| CONH <sub>2</sub>                 | >40                              | >40                              |
| CO <sub>2</sub> CH <sub>3</sub>   | 1                                | 1                                |
| CF <sub>3</sub>                   | >40                              | >40                              |
| CN                                | 3.0                              | >40                              |
| NHSO <sub>2</sub> CH <sub>3</sub> | >40                              | >40                              |
| NHSO <sub>2</sub> Ph              | >40                              | >40                              |



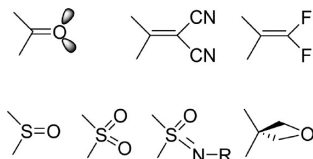
A successful and more recent example of the replacement of a nitrophenyl moiety by a pyridine is provided by a series of human epidermal growth factor receptor kinase inhibitors for which the lead molecule **295** contained a nitrophenyl moiety.<sup>259</sup> In these inhibitors, SAR suggested a role for the nitro group as a H-bond acceptor that was nicely mimicked by the pyridine **296** while attempts to replace the NO<sub>2</sub> group with alternative substituents were much less successful (data summarized in Table 45).<sup>259</sup>



Nimesulide (**297**) is a COX-2-inhibiting NSAID first prepared in 1974 but never marketed in the U.K., U.S., and Canada because of a poor safety profile (Table 46).<sup>260</sup> The drug was subsequently withdrawn in Spain and Finland in 2002–2003 because of idiosyncratic cases of hepatotoxicity which occurred at the rate of 9.4 cases per million patients treated, and marketing authorization was suspended in Ireland in 2007 because of six cases of liver transplant following the use of nimesulide-containing products. Both nimesulide and its amine metabolite cause mitochondrial toxicity to isolated rat hepatocytes, attributed to oxidation of the 1,4-diaminobenzene metabolite to an electrophilic diiminouinone.<sup>260</sup> In an attempt to identify safer analogues,

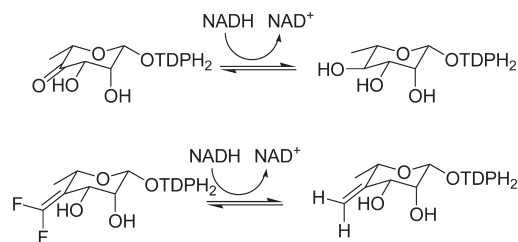
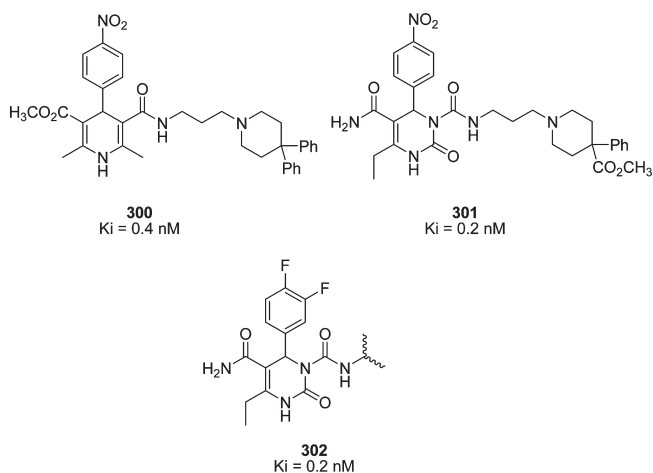
**Table 46. Structure–Activity Relationships Associated with 297 and Analogues**

| Compound                    |               |               |      |
|-----------------------------|---------------|---------------|------|
| IC <sub>50</sub> COX-1 (μM) | 3.76          | 0.14          | 0.91 |
| IC <sub>50</sub> COX-2 (μM) | 0.70          | 0.62          | 0.12 |
| pKa                         | 6.56          | <1/6.1        |      |
| Rat paw edema               | 58.0 @ 10 mpk | 54.1 @ 30 mpk |      |

**Figure 52.** Synopsis of carbonyl isosteres.

the pyridine **298** was synthesized and found to retain intrinsic potency while preventing metabolic activation, and this compound was active in an animal model of inflammation (Table 46).<sup>261,262</sup> Further optimization explored substitution of the ether oxygen atom by NH and adding a Br substituent to the phenyl ring to afford **299**. However, it is noted that this molecule contains an embedded 1,2-phenylenediamine element that has the potential to undergo oxidation to the alternative ortho diiminoquinone to that observed with the metabolite of **297**.

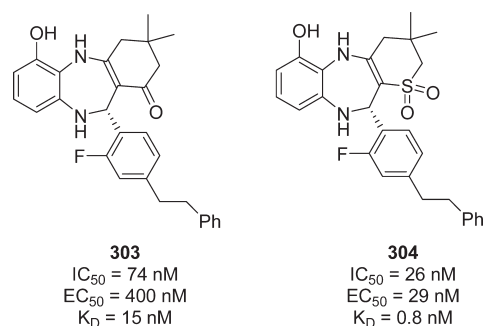
**3.9.1. Nitro Isosteres in  $\alpha_{1a}$  Adrenoreceptor Antagonists.** Isosteres of a nitro substituent were sought in a series of selective  $\alpha_{1a}$  adrenoreceptor antagonists targeted for the treatment of benign prostatic hyperplasia, a urological disorder, based on the observation that the  $\alpha_{1a}$  adrenoreceptor mediates contraction of lower urinary tract and prostate smooth muscle.<sup>141,142,263,264</sup> Although the lead dihydropyridines, represented by **300**, were related to niguldipine, they showed no Ca<sup>2+</sup>-channel blockade but exhibited poor oral bioavailability due to oxidation to the pyridine, leading to the adoption of a dihydropyrimidin-2-one as the core scaffold. Nitrophenyl mimetics were sought in the context of **301** in order to remove an additional metabolic liability, an exercise that identified the 3,4-difluorophenyl moiety found in **302** as a suitable and effective surrogate.<sup>141,142,263,264</sup>

**Figure 53.** TDP-L-rhamnose synthase-mediated reduction of a ketone and a structurally analogous difluoroethylene derivative.

### 3.10. Isosteres of Carbonyl Moieties. 3.10.1. Ketone Isosteres.

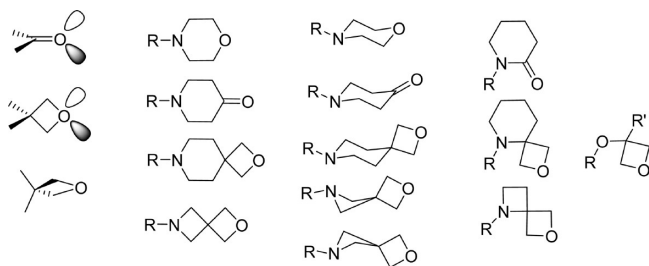
Simple ketones and aldehydes typically have a low prevalence in drugs and candidates because of their potential chemical reactivity and susceptibility to engaging in a reduction/oxidation pathway *in vivo*. Some of the more prominent ketone isosteres are captured in Figure S2, including substituted ethylenes in which the electronegative substituents are designed to replace the oxygen atom lone pairs. Both F and CN preserve the geometry and electronics of a C=O moiety, but both motifs present potential issues associated with inherent chemical reactivity, exemplified by the TDP-L-rhamnose synthase-mediated reduction of a difluoroethylene moiety, as summarized in Figure 53.<sup>265</sup>

Sulfoxide, sulfone, sulfoximine, and oxetane moieties have been probed as ketone isosteres, with the tetrahedral geometry of the former three of potential advantage dependent upon context. The sulfone moiety functioned as an effective ketone isostere in a series of HCV NSSB polymerase inhibitors that bind near the interface of the palm and thumb subdomains of the enzyme and proximal to the nucleotide binding site, referred to as the primer grip.<sup>266</sup> An X-ray cocrystal revealed that the C=O moiety of **303** engaged the NH of Tyr<sub>448</sub>, leading to an examination of the effect of probing a sulfone as an isostere, with recognition a priori of the potential of this moiety to establish a second H-bond with the NH of Gly<sub>449</sub>. In the event, the sulfone analogue **304** demonstrated improved binding affinity for the enzyme with a 19-fold shift in the K<sub>D</sub> and a 14-fold improvement in potency in a cell-based replicon assay.<sup>266</sup>

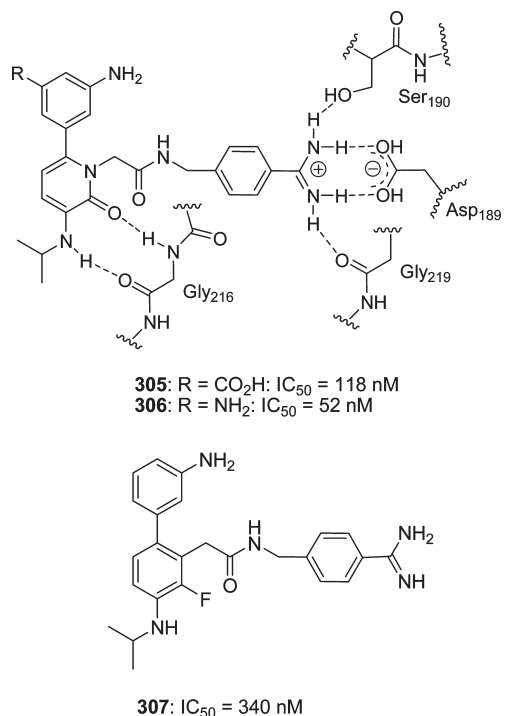


**3.10.2. Oxetane as a C=O Isostere.** A series of oxetane derivatives were prepared as part of a broader effort to explore their inherent physical and conformational properties, with a focus on establishing isosterism with the carbonyl moiety based on the nonpuckered shape of the oxetane ring (Figure S4).<sup>118–120,267</sup>

All of the compounds examined were stable over the pH range 1–10, including the azetidines. In addition, the oxetane oxygen atom expresses a similar capacity to the C=O moiety to accept a H-bond: the pK<sub>HB</sub> for oxetane is 1.36 which is comparable to a pK<sub>HB</sub> for cyclopentanone of 1.27.<sup>268,269</sup> However, oxetanes are more lipophilic than their analogous C=O derivatives and differentially affect electronic properties, exemplified by the 2-oxa-6-azaspiro[3.3]heptane ring



**Figure 54.** Isosteric relationships between carbonyl-containing functionality and oxetanes.



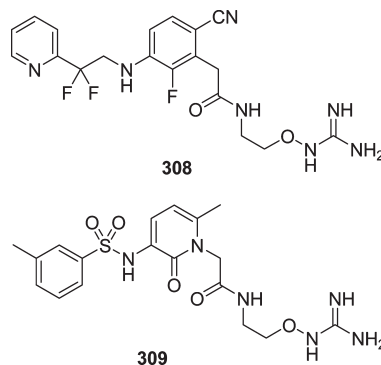
**Figure 55.** Binding interactions between factor VIIa and inhibitors **305** and **306** and the structure of a fluorobenzene-based analogue **307**.

system, a potential morpholine isostere, which is physically more slender and more basic,  $pK_a = 8$ , than morpholine,  $pK_a = 7$ .<sup>118–120,267</sup>

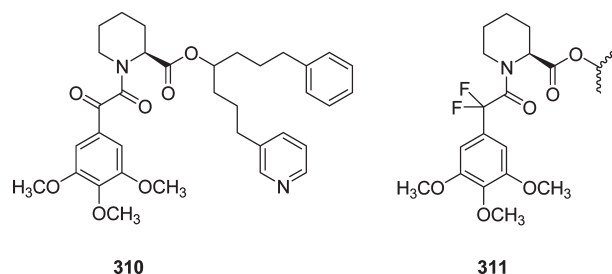
**3.10.3. Fluorine as a C=O Isostere in Factor VIIa and Thrombin Inhibitors.** A C–F moiety has been examined as a potential C=O isostere in the context of the pyridone-based factor VIIa inhibitors **305** and **306** in which the amide C=O and proximal NH engage in complementary H-bonding interactions with Gly<sub>216</sub> of the enzyme, as summarized in Figure 55.<sup>270,271</sup> Although replacement of the pyridone with a fluorobenzene ring modestly compromised potency, an X-ray cocrystal structure of **307** bound to factor VIIa at 3.4 Å resolution revealed a close contact between the F atom and the NH of Gly<sub>216</sub>, interpreted as a H-bond that was anticipated during the design phase.<sup>270,271</sup>

This motif performed with similar effectiveness in a series of thrombin inhibitors with **308**,  $K_i = 1.2$  nM, a potent analogue derived from the pyridone **309**,  $K_i = 4$  nM, that demonstrated

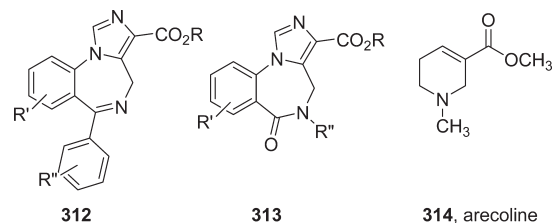
good oral bioavailability in the dog, an advance on **309** which was poorly bioavailable.<sup>272,273</sup>



**3.10.4. Fluorine as a C=O Isostere in FKBP12 Mimetics.** V-10367 (**310**) and related compounds mimic the FKBP12-binding portion of FK506 and were examined as potential neurotrophins, an activity observed for FK506 in vitro and in vivo. Replacement of the keto carbonyl with a *gem*-difluoro moiety afforded **311** which displayed  $K_i = 19$  nM as an inhibitor of FKBP12 rotamase activity, with potency comparable to that of **310**.<sup>274</sup> Analysis of an X-ray cocrystal structure revealed that one fluorine atom is close (3.18 Å) to the phenolic OH of Tyr<sub>26</sub> of FKBP12 that forms a H-bond with the ketone C=O of **310** while the second fluorine interacts with a hydrogen atom of the aryl ring of Phe<sub>36</sub>, 3.02 Å away.<sup>274</sup>



**3.10.5. Amide and Ester Isosteres.** Amide and ester isosteres have been extensively studied, with a focus on amides in the context of peptidomimetics, while seminal studies of ester isosteres examined with the benzodiazepines **312** and **313** were subsequently extended into muscarinic agonists based on arecoline (**314**), probed as potential agents for the treatment of Alzheimer's disease.<sup>275,276</sup> Amide isosteres have typically been of interest as a means of modulating polarity and bioavailability, while ester isosteres have frequently been developed to address metabolism issues since esters can be rapidly cleaved in vivo.



A synopsis of the amide and esters isosteres is presented in Figure 56 which exemplifies azole heterocycles among the most common and prominent replacements, although more recent design efforts have focused on mimetics that offer greater conformational flexibility.

**3.10.6. Trifluoroethylamines as Amide Isosteres.** The trifluoroethylamine moiety, CF<sub>3</sub>CH(R)NHR', was studied initially as an amide isostere in the context of peptide-based enzyme inhibitors

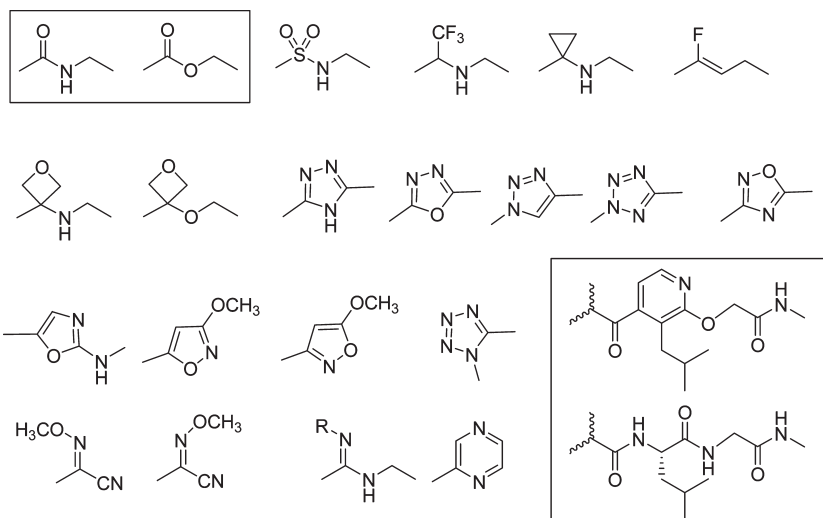


Figure 56. Synopsis of amide and ester isosteres.

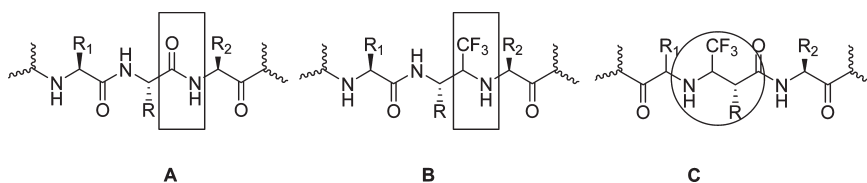


Figure 57. Comparison of two potential motifs by which the trifluoroethylamine moiety can act as an isostere of an amide moiety in peptide-based molecules. In part B the trifluoroethylamine is introduced in register directly mimicking the amide moiety in part A, while in part C the trifluoroethylamine is incorporated with partial retroinversion of the reading frame.

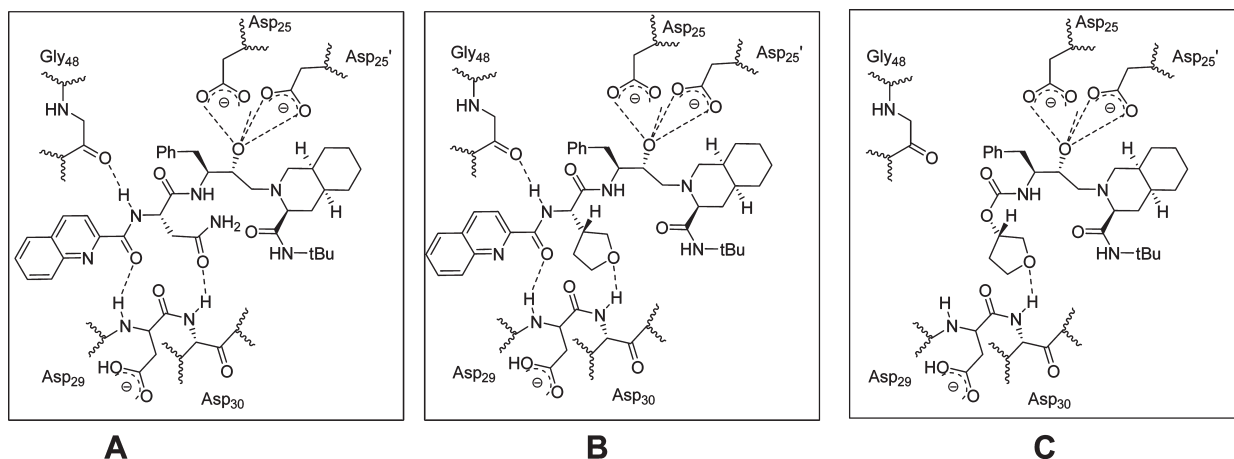


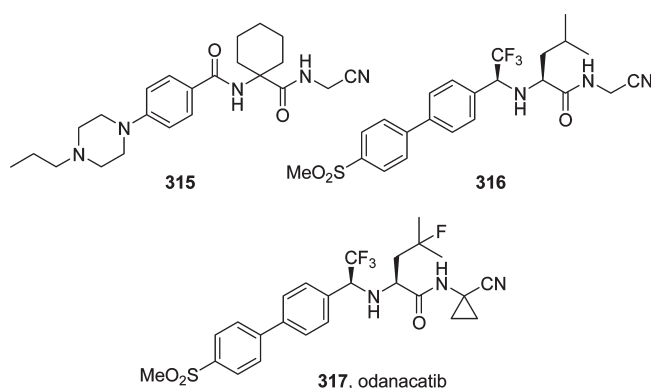
Figure 58. Binding interactions between HIV-1 protease and inhibitors.

(Figure 57A) where it can be incorporated in register (Figure 57B) or with partial retroinversion of the reading frame (Figure 57C).<sup>277–283</sup> In this context, the trifluoroethylamine can be considered to be structurally similar to the tetrahedral intermediate associated with peptide proteolysis. More recently, the trifluoroethylamine element has been adopted as an effective amide isostere in drug discovery campaigns, with compounds incorporating this functionality now entering clinical trials.<sup>284,285</sup> Functional mimicry is based on the trifluoromethyl moiety reducing the basicity of the amine without compromising the ability of the NH to function as a H-bond donor. In addition, the  $\text{CF}_3\text{CH(R)NHR}'$  bond is close to the  $120^\circ$  observed with an amide, and the  $\text{C}-\text{CF}_3$  bond is isopolar with a  $\text{C}=\text{O}$ .<sup>277–283</sup> Of potential

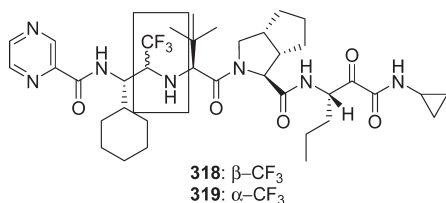
advantage depending on context, the trifluoromethylethylamine moiety confers conformational flexibility that may improve complementarity with a target protein although at the expense of introducing a stereogenic center. The pentafluoroethylamine moiety,  $\text{CF}_3\text{CF}_2\text{CH(R)NHR}'$ , performs in a functionally similar fashion.<sup>284,285</sup>

**3.10.7. Trifluoroethylamines as Amide Isosteres in Cathepsin K Inhibitors.** Cathepsin K is a lysosomal cysteine protease in osteoclasts responsible for bone degradation during remodeling, with inhibitors preventing bone resorption and offering potential in the treatment of osteoporosis.<sup>284,285</sup> The cathepsin K inhibitor L-006235 (**315**) presents a nitrile functionality to the enzyme that reacts reversibly with the catalytic

cysteine that, although exhibiting good pharmacokinetic properties, was poorly selective for cathepsin K compared to the related enzymes cathepsins B, L, and S. This profile was attributed to the lysosomotropic nature of **315** which is both basic and lipophilic. Optimization led to the identification of L-873724 (**316**), a compound in which the amide moiety of **315** was replaced by a trifluoroethylamine element, resulting in improved selectivity but poorer pharmacokinetic properties. Odanacatib (**317**) was the product of further refinement that solved both problems, with the fluorinated valine blocking hydroxylation and the quaternary cyclopropyl moiety at P1 reducing the propensity for amide hydrolysis.<sup>284,285</sup> Compound **317** is currently in phase 3 clinical trials.

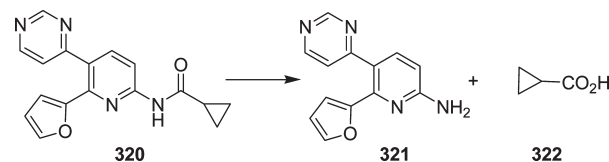


**3.10.8. Trifluoroethylamine as an Amide Replacement in the HCV NS3 Inhibitor Telaprevir.** An interesting example where examination of the trifluoroethylamine moiety as an amide isostere markedly affected target specificity and selectivity is provided by the tetrapeptidic, mechanism-based inhibitor of HCV NS3 protease, **12**.<sup>286</sup> Compound **12** inhibits HCV NS3 with an  $IC_{50}$  of 70 nM and is an effective antiviral agent,  $EC_{50}$  = 210 nM in the replicon.<sup>39</sup> However, telaprevir also inhibits cysteine proteases, including cathepsin B with an  $IC_{50}$  of ~210 nM. Although cathepsin S inhibition data have not been reported for **12**, replacing the P4 amide with a trifluoroethylamine moiety produced the potent cathepsin S inhibitors **318** ( $IC_{50}$  = 2 nM) and **319** ( $IC_{50}$  = 0.6 nM) in which activity is largely insensitive to the absolute configuration.<sup>286</sup> Most interestingly given that the structural changes are remote from the active site of HCV NS3, both compounds are much less active in the HCV replicon with only 34% and 29% inhibition observed at 25  $\mu$ M for **318** and **319**, respectively. Cathepsin S activity has been implicated as an underlying cause of aspects of allergic disorders and both Alzheimer's and autoimmune diseases.



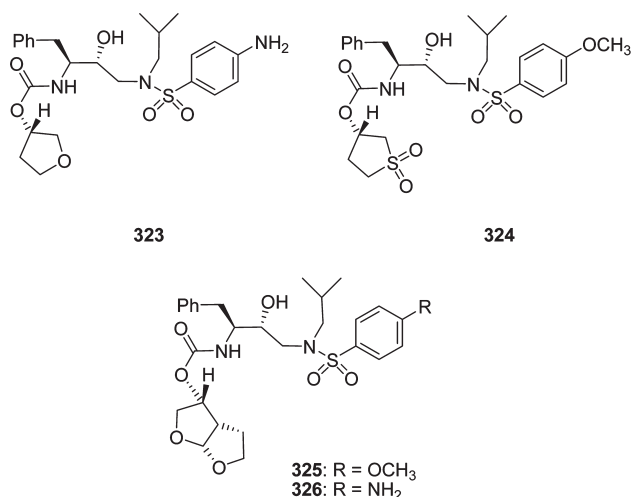
**3.10.9. Amide Isosteres in Adenosine<sub>2B</sub> Antagonists.** The amide **320** is a potent adenosine<sub>2B</sub> antagonist,  $K_i$  = 4 nM, explored for its potential to prevent adenosine-mediated inflammation in asthma.<sup>287</sup> However, simple amides were cleaved

in liver microsomes *in vitro* by a nonoxidative pathway releasing, in the case of **320**, the 2-aminopyridine **321** and cyclopropanecarboxylic acid **322**, a simple molecule associated with toxicity *in vivo*.<sup>288</sup> A range of effective isosteres were developed that offered improved metabolic stability *in vitro*, as summarized in Table 47.<sup>287</sup>



### 3.11. Ether/Sulfone and Glyoxamide/Sulfone Isosterism.

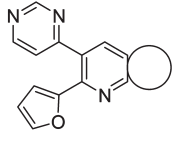
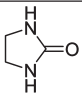
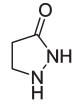
**3.11.1. Ether/Sulfone Isosterism in HIV-1 Protease Inhibitors.** Saquinavir was the first HIV-1 protease inhibitor to be approved, but this compound, although highly potent with  $IC_{50}$  = 0.23 nM, is poorly bioavailable, attributed to the peptidic nature of the molecule and the number of NH bonds (Figure S8A). Replacing the asparagine moiety embedded within saquinavir with a 3(*R*)-tetrahydrofuranyl-glycine moiety improved potency several-fold,  $IC_{50}$  = 0.05 nM (Figure S8B), while removal of the quinoline moiety decreased potency markedly,  $IC_{50}$  = 160 nM (Figure S8C).<sup>289,290</sup> Taking a cue from these data, Ghosh replaced the (*R*)-3-THF moiety found in amprenavir (**323**),  $K_i$  = 0.6 nM, with a cyclic sulfone to afford **324**, a compound that maintained inhibitory potency,  $K_i$  = 1.4 nM. In models of **324** bound to HIV-1 protease, the cyclic sulfone oxygen atoms were proposed to accept H-bonds from both the Asp<sub>29</sub> and Asp<sub>30</sub> NHs, as depicted in Figure S9A. Further optimization took advantage of this observation and led to the design of a bicyclic ether ring system as an effective and more lipophilic sulfone isostere, initially explored in **325** as a prelude to identifying the highly potent HIV-1 protease inhibitor darunavir (**326**), licensed in the United States in June 2006. The design emphasis in arriving at **326** focused on optimizing essential interactions between the inhibitor and the backbone of HIV-1 protease, captured in Figure S9B, with a view to minimizing the potential for resistance.<sup>289,290</sup>



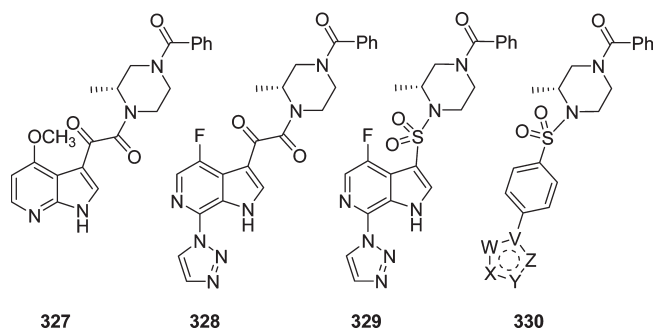
**3.11.2. Sulfone/Glyoxamide Isosterism in HIV Attachment Inhibitors.** The indole glyoxamides **327** and **328** are potent inhibitors of HIV-1 replication in cell culture,  $EC_{50}$  = 7 nM and  $EC_{50}$  < 5 nM, respectively, that act by interfering with the binding of viral gp120

to the host cell CD4 receptor.<sup>291,292</sup> The glyoxamide moiety typically adopts an orthogonal arrangement of the two carbonyl groups in order to minimize nonbonded interactions while deploying the dipoles in the most stable orientation. A sulfone moiety was postulated as an effective mimetic based on 3D structural analysis, and although a potent antiviral,  $EC_{50} = 7$  nM, **329** was less impressive than the structurally analogous glyoxamide **328**,  $EC_{50} < 5$  nM.<sup>292</sup> An attempt to compensate for the topological differences between the two chemotypes examined a series of biaryl derivatives represented

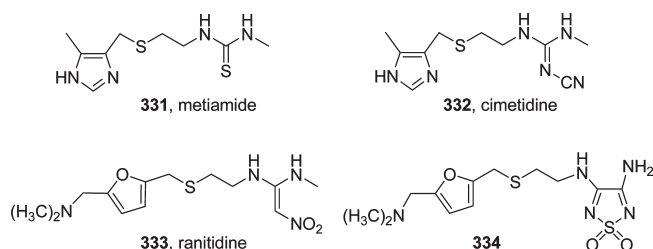
**Table 47. Structure–Activity Relationships Associated with a Series of Adenosine 2B Antagonists**

|    |   |
|---|---|
| Fused ring  | Ki for adenosine <sub>2B</sub> binding (nM) |
|    | 6   |
|    | 3   |
|   | 21  |
|  | 23  |
|  | 13  |
|  | 1   |

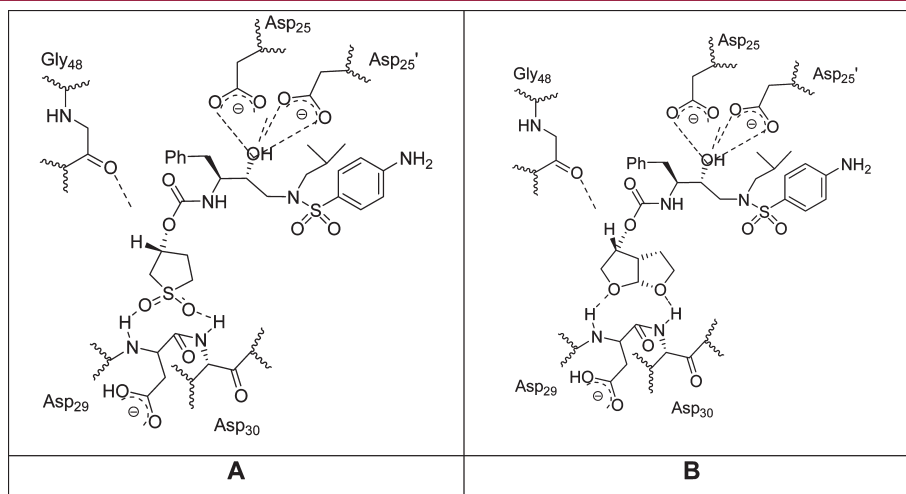
generally by **330** with only limited success, since this series generally exhibited poor antiviral activity.<sup>293</sup>



**3.12. Urea Isosteres.** **3.12.1. Urea Isosteres in Histamine Antagonists.** The development of histamine H<sub>2</sub> antagonists fostered a considerable understanding of the design of isosteres of ureas and thioureas, with classic studies representing an early application of the careful and detailed analysis of physical chemistry properties to drug design.<sup>294</sup> Metiamide (**331**) was used as the lead compound to design cimetidine (**332**) in which the thiourea was replaced by a cyanoguanidine.<sup>294</sup> A 2,2-diamino-1-nitroethene functioned as an effective urea isostere in ranitidine (**333**), while later studies focused on 1,2,5-thiadiazole oxides related to **334** as potent H<sub>2</sub> antagonists.<sup>295,296</sup>

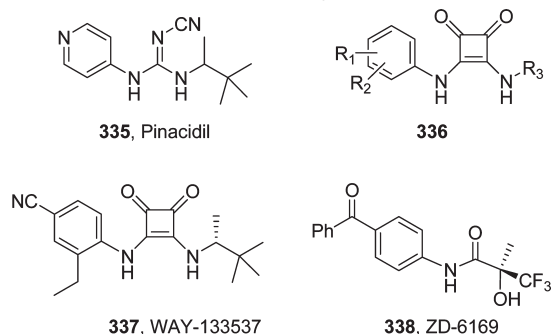


**3.12.2. Urea-Type Isosteres in K<sub>ATP</sub> Openers.** Pinacidil (**335**), a K<sub>ATP</sub> opener studied clinically for the treatment of hypertension, attracted the attention of a group focused on optimizing its bladder smooth muscle relaxant properties as a potential

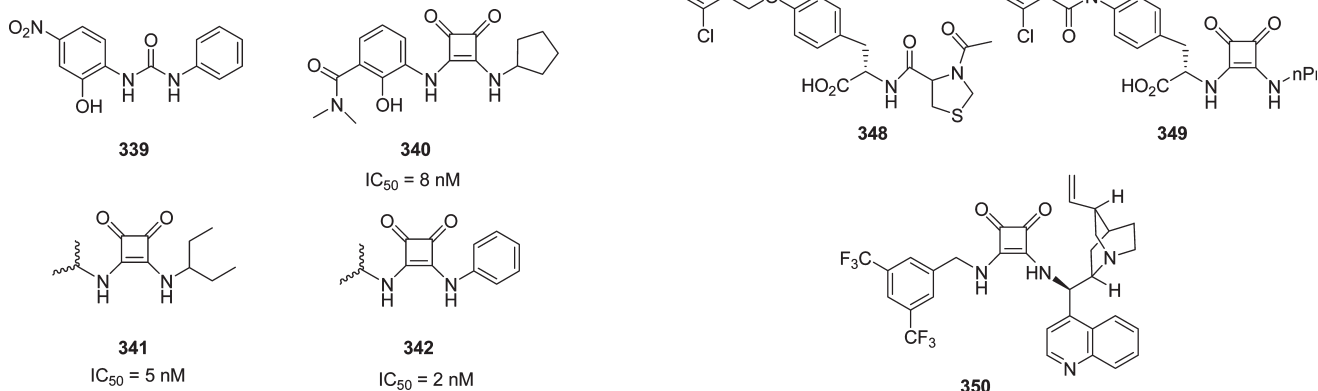


**Figure 59.** Proposed binding interactions between HIV-1 protease and the sulfone-based inhibitor **324** (A) and key binding interactions observed between HIV-1 protease and **326** in the X-ray cocrystal structure (B).

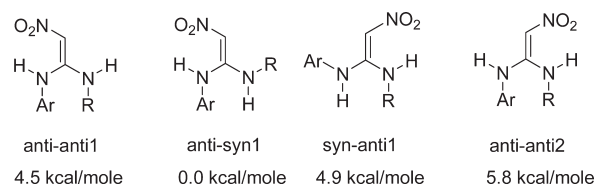
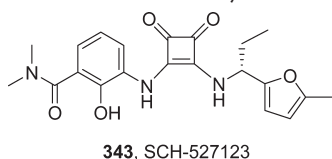
therapy for urge urinary incontinence. A series of diaminosquarate derivatives **336** was developed based on the recognition of an isosteric relationship with the cyanoguanidine moiety of **335**.<sup>297</sup> It was found that a 2-ethyl substituent on the aryl ring of diaminosquarate derivatives enhanced bladder potency by 6-fold, leading to the emergence of WAY-133537 (**337**) as a lead candidate.<sup>297</sup> The squaramide **337** exhibits 70% oral bioavailability in the rat, is clean in an AMES test, and revealed no significant drug-related toxicities in rats at doses up to 200 mpk. In vivo, the compound inhibited spontaneous bladder contractions at doses lower than that at which hypotensive effects were manifest.<sup>297</sup> An alternative urea/cyanoguanidine isostere is found in ZD-6169 (**338**), another bladder-selective  $K_{ATP}$  opener evaluated clinically for urge urinary incontinence.<sup>298</sup>



**3.12.3. Urea Isosteres in CXCR2 Antagonists.** 3,4-Diaminocyclobut-3-ene-1,2-diones were also probed as urea mimetics in the context of the CXCR2 ligand **339**, leading to the identification of the potent CXCR2 antagonists **340–342**.<sup>299</sup> These compounds demonstrated good activity in a chemotaxis assay in vitro with the phenyl derivative **342** identified as the most potent agent. Caco-2 permeability and aqueous solubility were better for the alkylamine analogues **340** and **341** compared to the phenyl derivative **342**, while all demonstrated good metabolic stability in HLM.<sup>299</sup>

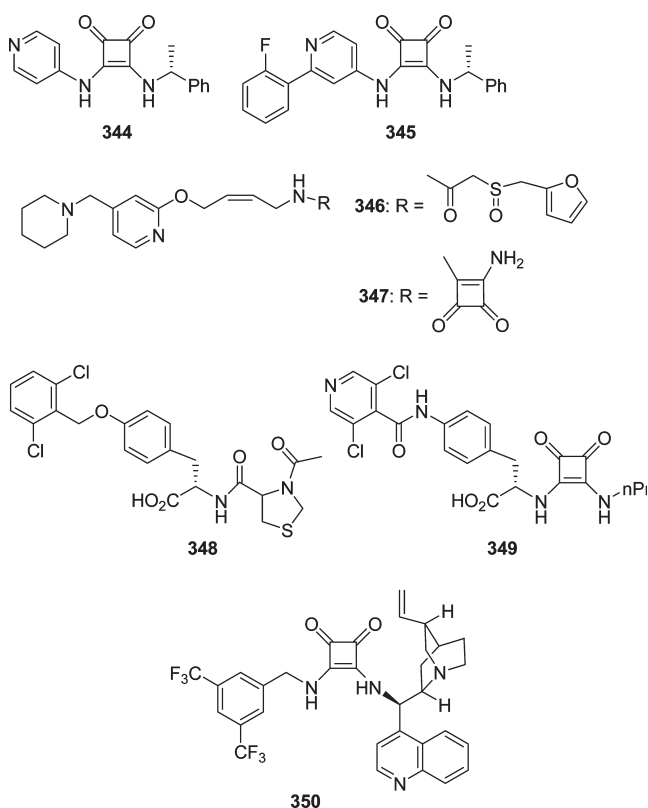


The diaminocyclobut-3-ene-1,2-dione SCH-527123 (**343**) is a dual CXCR2/CXCR1 antagonist (CXCR2  $IC_{50} = 2.6$  nM; CXCR1  $IC_{50} = 36$  nM) that inhibits human neutrophil chemotaxis in vitro induced by CXCL1 or CXCL8 and was viewed as possessing potential for the treatment of inflammatory diseases.<sup>300</sup> Phase IIa trials of **343** for COPD and asthma have been completed, and two 500-patient phase IIb trials were recently initiated.

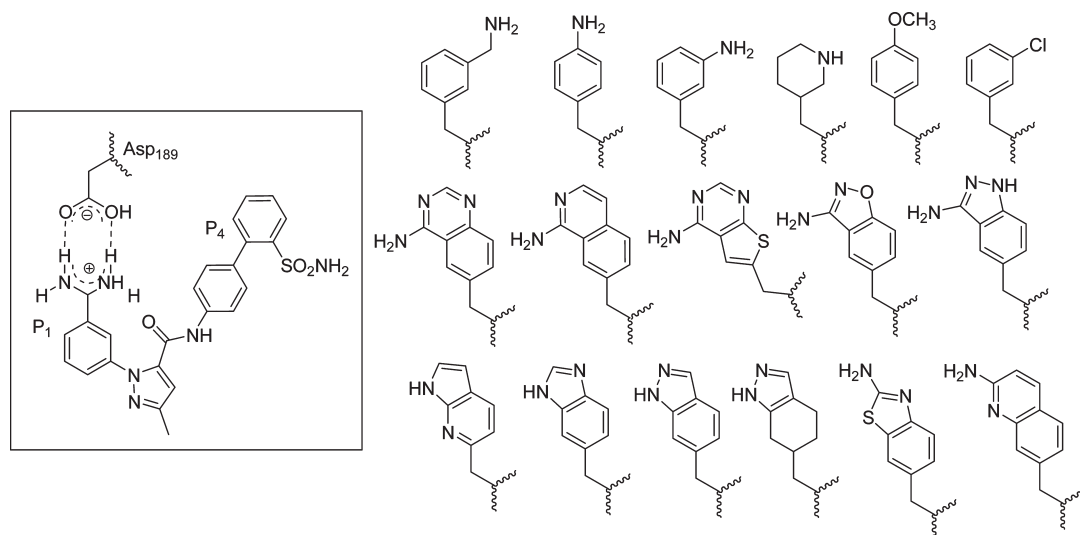


**Figure 60.** Calculated energies associated with the four lowest energy nitroketene amina conformers.

**3.12.4. Additional Squaric Acid Urea Isosteres.** Squaric acid derivatives are well represented in drug design and include the mitogen-activated protein kinase-activated protein kinase 2 inhibitors **344** and **345**,<sup>301</sup> the marketed histamine  $H_2$  antagonist pibutidine (**347**), an isostere of lafutidine (**346**), and **349**, a very late antigen-4 (VLA-4) integrin antagonist designed after **348**.<sup>302</sup> By use of similar fundamental design principles, the chiral squaric diamide **350** is an effective organic catalyst whose design is based after the analogous urea.<sup>303</sup>

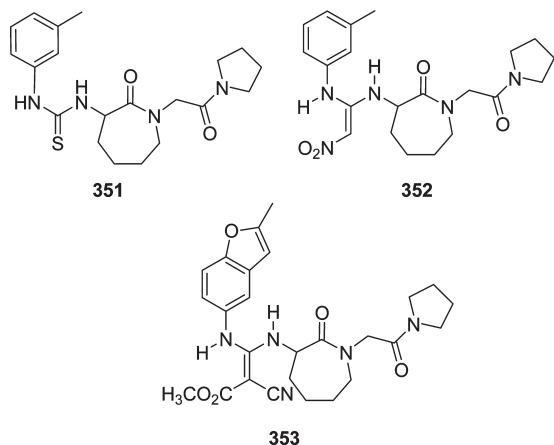


**3.12.5. Urea/Thiourea Isosteres in Factor Xa Inhibitors.** The disubstituted lactam **351** is a potent inhibitor of the serine protease factor Xa,  $IC_{50} = 110$  nM, for which effective replacements of the thiourea were sought in order to avoid the potential for toxicity.<sup>304</sup> A careful analysis of the conformational preferences of the four lowest energy nitroketene amina conformers was conducted (summarized in Figure 60) and compared to thiourea, both of which were found to favor the *anti-syn1* conformation and suggesting the potential for effective isosterism. However, the nitroketene amina **352** was a 60-fold weaker inhibitor of factor Xa,  $IC_{50} = 6400$  nM, necessitating further optimization of both the thiourea mimetic



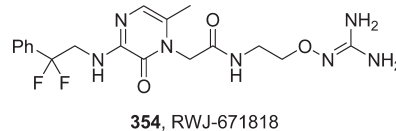
**Figure 61.** Synopsis of guanidine and amidine isosteres examined in the context of P1 elements in factor Xa inhibitors.<sup>313</sup>

and the aniline moiety, an exercise that ultimately afforded the potent factor Xa inhibitor **353**,  $IC_{50} = 20$  nM.<sup>304</sup>

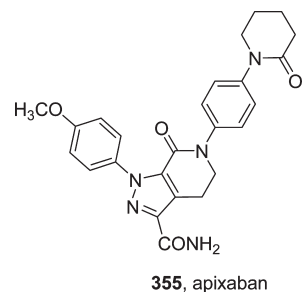


**3.13. Guanidine and Amidine Isosteres.** Interest in identifying isosteres of the amidine and guanidine functionality has largely been driven by attempts to develop inhibitors of the serine proteases that constitute the coagulation cascade and that includes thrombin and factor Xa, both of which recognize an arginine at P1 of substrates.<sup>305,306</sup> Guanidines and amidines are highly basic entities that are protonated at physiological pH, which leads to poor membrane permeability, a significant impediment to developing orally bioavailable compounds. Basicity can be reduced from a  $pK_a$  of 13–14 by replacement of an adjacent  $CH_2$  with either a carbonyl moiety to afford an acylguanidine,  $pK_a \approx 8$ , or an oxygen atom,  $pK_a \approx 7$ –7.5. These modifications, which represent isosteric replacement of a  $CH_2$ , have the potential to significantly compromise potency depending on the application. However, acylguanidines have been successful in developing a family of histamine  $H_2$  agonists<sup>307,308</sup> while oxyguanidines are useful P1 surrogates in thrombin inhibitors, as demonstrated by RWJ-671818 (**354**), a compound advanced into phase 1 clinical studies.<sup>272,273,309–311</sup> Although prodrugs have also been extensively explored and offered a solution for some drug candidates, alternative structural elements designed to mimic aspects of guanidine have been devised with greater overall success. Typically, these inhibitors rely upon

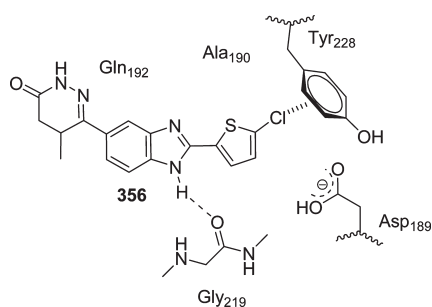
optimized interactions at other subsites of the enzymes in order to fully secure potency and selectivity, with clinically effective, orally bioavailable inhibitors of the coagulation enzymes, particularly factor Xa, in late stage clinical development.<sup>312</sup>



**3.13.1. Arginine Isosteres in Factor Xa Inhibitors.** The wide range of arginine mimetics compiled in Figure 61 were examined in the context of P1 elements in factor Xa inhibitors and provide a synopsis of the more prominently successful arginine isosteres.<sup>313</sup> Of particular interest are the neutral elements, with the 3-chlorophenyl moiety offering potency,  $K_i = 37$  nM, comparable to that of the 3-aminophenyl,  $K_i = 63$  nM, 10-fold weaker than the 3-aminomethyl,  $K_i = 2.7$  nM, although all are markedly less potent than the 3-amidino prototype which displayed  $K_i = 0.013$  nM.<sup>313</sup> The 4-methoxy analogue exhibited good potency,  $K_i = 11$  nM, and this P1 moiety is found in the clinically relevant factor Xa inhibitor apixaban (**355**).<sup>312</sup>

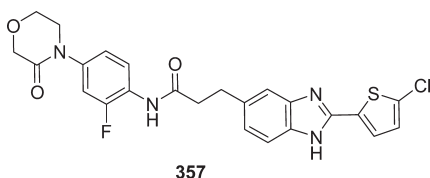


More recently, chlorothiophenes have emerged as useful P1 elements for factor Xa and thrombin inhibitors.<sup>314,315</sup> Pyridazinone **356**, originally prepared as a phosphodiesterase-3 inhibitor with potential as a positive inotropic agent, was identified by screening as a weak factor Xa inhibitor,  $IC_{50} = 1.1$   $\mu$ M (Figure 62).<sup>314</sup> An X-ray cocrystal of **356** with the enzyme established the binding mode with the chlorothiophene establishing a halogen bonding interaction with the  $\pi$ -cloud of Tyr<sub>228</sub>,

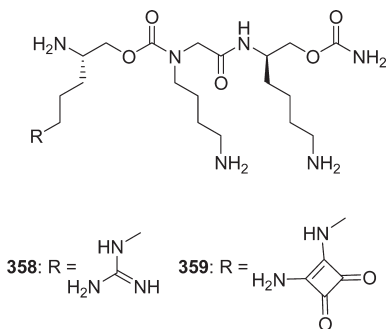


**Figure 62.** Key interactions between factor Xa and the pyridazinone-based inhibitor **356**.

captured in Figure 62.<sup>314</sup> Optimization afforded the more potent inhibitor **357**,  $IC_{50} = 5.9$  nM, and several additional examples have appeared in the literature.<sup>312,315</sup>



The diaminosquarate moiety has been explored successfully as a guanidine mimetic in the context of the arginine-derived peptidomimetic **358**, an inhibitor of the interaction between the HIV-1 transcription regulator Tat and the Tat-responsive RNA element TAR.<sup>316</sup> The guanidine **358** binds to HIV-1 TAR RNA with  $K_d = 1.8$   $\mu$ M, while the squaric acid diamide analogue **359** is a 4-fold weaker ligand,  $K_d = 7.7$   $\mu$ M, providing the first example of this moiety acting as a functional guanidine isostere.<sup>316</sup>



**3.14. Phosphate and Pyrophosphate Isosteres.** One of the most challenging functionalities to mimic in the design of drugs for development has been the phosphate or pyrophosphate functionality.<sup>317</sup> For *in vitro* inhibitors, a phosphonate is a useful and stable phosphate mimetic that can be improved by difluorination of the  $\alpha$ -C atom to increase the acidity to more closely match that of the phosphate moiety.<sup>318</sup> Phosphate isosteres have been explored primarily in the context of nucleotide analogues and phosphatase inhibitors, with a wide range of isosteres that offer less severe acidic functionality explored in an effort to find surrogates compatible with oral absorption. This initiative has enjoyed only limited success, since a general solution has not been identified and solutions to individual problems are rare. Consequently, prodrugs have been the usual resort in situations where phosphates or phosphonates are an absolute requirement

**Table 48.** Acidity of a Series of Diphosphonates Compared to Diphosphate

| X                  | pKa2 | pKa3 | pKa4  |
|--------------------|------|------|-------|
| CH <sub>2</sub>    | 2.87 | 7.45 | 10.96 |
| CCl <sub>2</sub>   |      | 6.11 | 9.78  |
| C(OH) <sub>2</sub> |      | 5.81 | 8.42  |
| CHF                | <2.7 | 6.15 | 9.35  |
| CF <sub>2</sub>    | <2.6 | 5.80 | 8.00  |
| O                  | 2.36 | 5.77 | 8.22  |

**Table 49.** Acidity of Phenyl Phosphate and a Series of Phosphonate Analogues

| compd                                   | pK <sub>a2</sub> |
|---|------------------|
| PhOP(O)(OH) <sub>2</sub>                | 6.22             |
| PhCH <sub>2</sub> P(O)(OH) <sub>2</sub> | 7.72             |
| PhCH(F)P(O)(OH) <sub>2</sub>            | 6.60             |
| PhCF <sub>2</sub> P(O)(OH) <sub>2</sub> | 5.71             |

for drug–target interactions, and there are several examples of clinically useful prodrugs either marketed or in development. Nevertheless, there have been some productive advances, most notably in the context of HIV-1 integrase strand transfer inhibitors, where a wide range of successful mimetics of the transition state in phosphate hydrolysis have been identified. Of particular interest are a series of hydroxylated pyrimidinones that, when appropriately configured, extend isosterism to that of the pyrophosphate moiety.

**3.14.1. Phosphate and Pyrophosphate Mimetics.** The lower acidity of phosphonates often leads to poor mimicry of phosphates, rectified by judicious substitution with electronegative substituents, with mono- or difluorophosphonates more closely mimicking the pK<sub>a</sub> of phosphate (data compiled in Tables 48 and 49).<sup>318–321</sup> However, the highly acidic nature of fluorophosphonates has limited their application and utility in drug design largely to biochemical evaluation *in vitro*.

**3.14.2. Phosphate Isosteres in PTP-1B.** Protein tyrosine phosphatase-1B (PTP-1B) is a negative regulator of the insulin and leptin signal transduction pathways, and inhibitor design has focused on peptide-based recognition fragments that incorporate mimetics of phosphotyrosine. Compounds presenting dicarboxylic acids, related polyacidic analogues, and polar functionality as well as PhCF<sub>2</sub>P(O)(OH)<sub>2</sub> derivatives are represented among isosteres that have been identified as effective, competitive PTP1B inhibitors *in vitro*, moieties summarized in Figure 63.<sup>322,323</sup> In an interesting example of inhibitor design, an analysis of the overlay of the two inhibitor motifs depicted in Figure 64 led to the proposal of the novel isothiazolidinone-based inhibitor **360**.<sup>322–325</sup> Interestingly, this chemotype was arrived at independently based on X-ray data of the small ligand **361** in which the ortho methoxy substituent increased potency by promoting orthogonality of the heterocycle ring.<sup>326</sup>

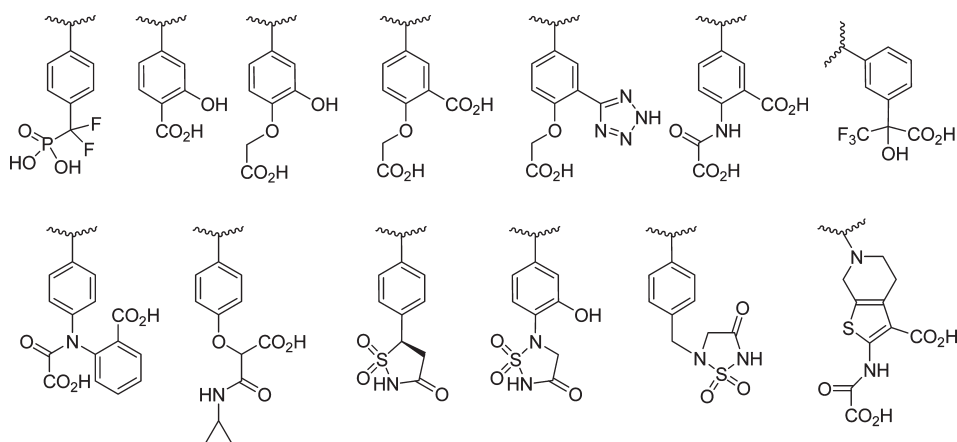
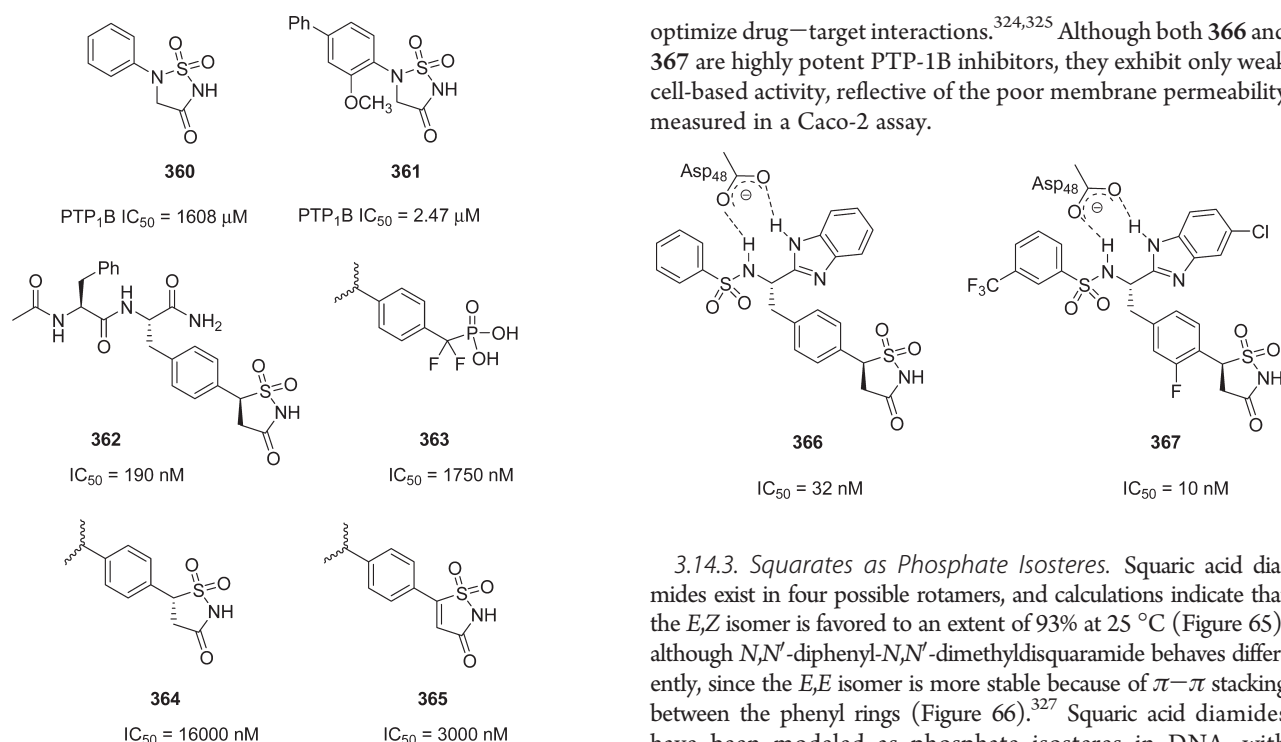
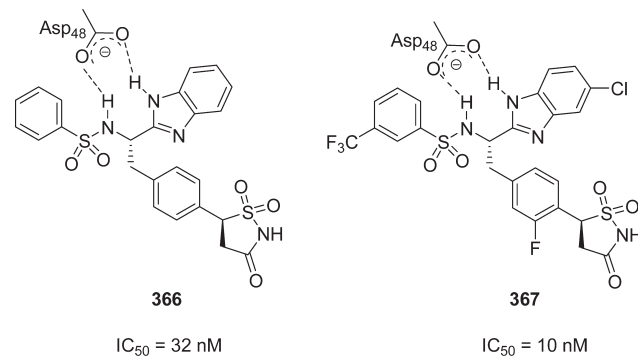


Figure 63. Synopsis of protein tyrosine phosphatase-1B (PTP-1B) inhibitor motifs.

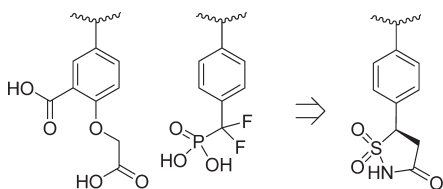


Incorporation of the isothiazolidinone moiety into a peptide fragment providing enzyme recognition afforded **362**, a PTP-1B inhibitor almost 10-fold more potent than the corresponding difluorophosphonate **363**.<sup>324,325</sup> Chirality was found to be critically important, since the enantiomer **364** and the unsaturated analogue **365** were found to be considerably weaker enzyme inhibitors. However, this series of isothiazolidinone-based inhibitors failed to demonstrate activity in cell-based assays, attributed to poor membrane permeability.<sup>322,324,325</sup> Attempts to address this problem by diminishing the peptidic nature of the molecule focused on introducing a benzimidazole moiety as a lipophilic amide isostere designed to maintain an important H-bond with Asp<sub>48</sub>, a tactic exemplified by **366** and **367**.<sup>324,325</sup> The sulfonamide NH of both compounds similarly maintains a H-bond to the other oxygen atom of Asp<sub>48</sub>, and the phenyl ring is important for activity because the methyl analogue is 18-fold less potent. The ortho-F atom in **367** promotes an orthogonal topography for the isothiazolidinone element designed to

optimize drug–target interactions.<sup>324,325</sup> Although both **366** and **367** are highly potent PTP-1B inhibitors, they exhibit only weak cell-based activity, reflective of the poor membrane permeability measured in a Caco-2 assay.

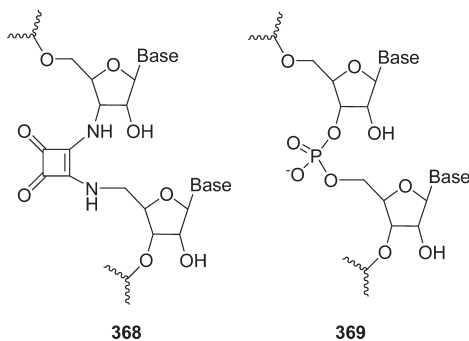


3.14.3. *Squarates as Phosphate Isosteres.* Squaric acid diamides exist in four possible rotamers, and calculations indicate that the *E,Z* isomer is favored to an extent of 93% at 25 °C (Figure 65), although *N,N'*-diphenyl-*N,N'*-dimethyldisquaramide behaves differently, since the *E,E* isomer is more stable because of  $\pi$ – $\pi$  stacking between the phenyl rings (Figure 66).<sup>327</sup> Squaric acid diamides have been modeled as phosphate isosteres in DNA, with electrostatic potential maps indicative of reasonable phosphate mimicry based on significant charge residing on the key oxygen atoms. Squarate oxygen atoms carry charges of  $-0.47$  and  $-0.51$ , compared to a charge of  $-0.84$  on each phosphate oxygen atom.<sup>328</sup> This analysis provided confidence to prepare a series of thymidine dimers based on the squaryldiamide **368** designed to mimic the natural dinucleotide **369** for incorporation into oligonucleotides.<sup>328</sup> By use of thymidine as the base, the squaryldiamide, designated TsqT, was shown to possess a similar structure by CD and UV analysis to the natural analogue, designated TpT. TsqT was shown to bind Mg<sup>2+</sup> by <sup>1</sup>H NMR and further examined in the context of the hybridization of the oligonucleotide 5'-d(CGCATsqTAGCC)-3' to its complementary natural sequence 5'-(DGGCTAATGCG)-3'. The base pairing ability of the TsqT-containing oligonucleotide was preserved, but the DNA duplex was distorted by the TsqT moiety, detected in the melting temperature  $T_m$  of 30.4 °C compared to a  $T_m$  of 41.7 °C for the unmodified duplex. Notably, 5'-d(CGCATsqTAGCC)-3'

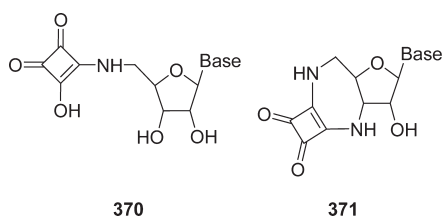


**Figure 64.** Design of isothiazolidinone-based inhibitors of protein tyrosine phosphatase-1B (PTP-1B) based on topological overlay of two structurally different chemotypes.

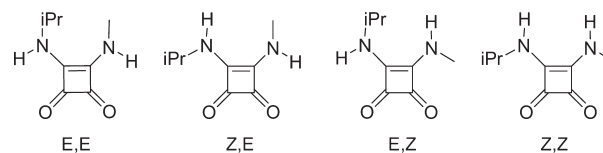
was stable toward both snake venom phosphodiesterase and alkaline phosphatase.<sup>328</sup>



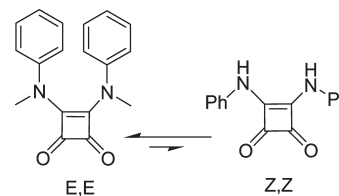
The squaric acid monoamide moiety was evaluated as a phosphate isostere in the context of nucleotides **370** and their cyclic analogues **371** based on the acidity of this element,  $pK_a = 2.3$ . The cyclic analogue **371** showed ribose puckering in the N conformation similar to cGMP, and although derivatives were probed as antiviral agents, the results were not disclosed.<sup>329</sup>



A recent attempt to refine phosphate isosterism by this motif probed the introduction of an additional metal coordinating element to a squaric diamide, examined in a molecule designed to mimic the sugar-nucleotide GDP-mannose (**372**), a central mediator of prokaryotic and eukaryotic carbohydrate and glycoconjugate biosynthesis, metabolism, and cell signaling.<sup>330</sup> The squaric diamide **373** was designed as a potential inhibitor of the GDP-mannose-dependent mannosyl transferase dolichol phosphate mannose synthase (DPMS) from *Trypanosoma brucei*, a validated antitrypanosomal target. It was anticipated that the squaric diamide moiety would coordinate to the catalytic metal in the active site of DPMS while allowing the introduction of an additional proximal polar element capable of coordinating to the metal, explored with a nitro or carboxylic acid substituent, the latter exemplified by **373**. However, despite modeling studies supporting the potential for these molecules to bind to the DPMS active

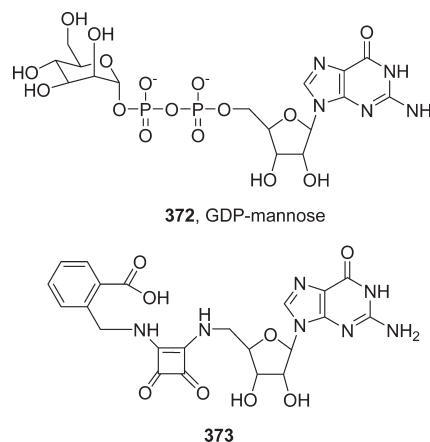


**Figure 65.** Conformational isomers of squaric acid diamides.



**Figure 66.** Preferred conformation of *N,N'*-diphenyl-*N,N'*-dimethyl-disquaramide.

site and  $^1\text{H}$  NMR data indicative of association of the squaric diamide moiety with  $\text{Mg}^{2+}$ , **373** demonstrated only modest inhibition, with residual enzyme activity measured as 64% at 1 mM drug concentration compared to 8.5% for the natural feedback inhibitor GDP at the same concentration. The poor activity was rationalized by considering the two major rotamers associated with the squaric diamide moiety, both stabilized by intramolecular H-bonds, with one failing to adequately represent the extended conformation frequently adopted by sugar nucleotides.<sup>330</sup>



**3.14.4. HIV-1 Integrase Inhibitors and Phosphate Isosterism.** HIV-1 integrase catalyzes the cleavage of the 5' terminal GT dinucleotide from the newly reverse-transcribed viral DNA following infection (Figure 67A) and, after translocating to the cell nucleus, the integration of HIV-1 DNA into the host cell chromosome, the so-called strand transfer step depicted in Figure 67B.<sup>331</sup>

Successful inhibitors of integrase specifically target the strand transfer step, binding to the active site  $\text{Mg}^{2+}$  ions in conjunction with viral DNA and acting as mimics of the transition state intermediate.<sup>332</sup> A synopsis of some of the more successful motifs that have been designed as part of the search for clinically useful HIV integrase inhibitors is collected in Figure 68.

While a large family of HIV-1 integrase inhibitors have been disclosed that are based on a wide range of scaffolds, the only

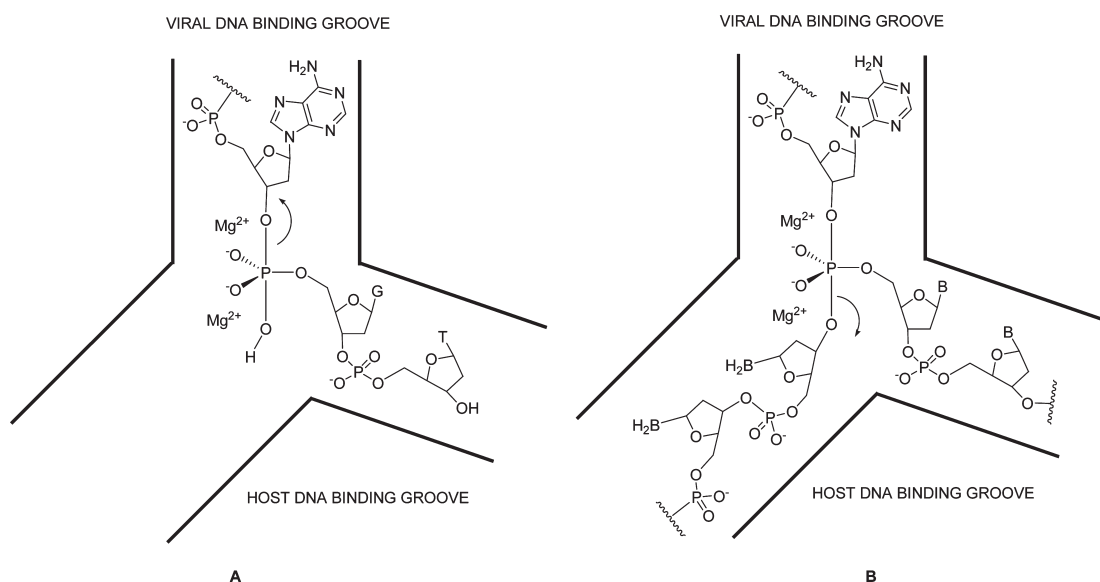


Figure 67. Topology of the HIV-1 integrase enzyme-substrate complex during the cleavage (A) and strand transfer step (B).

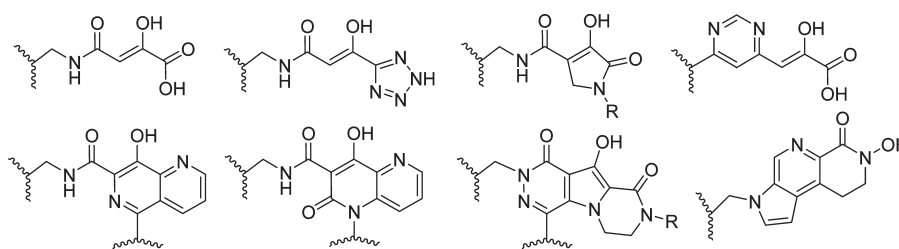


Figure 68. Synopses of HIV-1 integrase-inhibiting motifs.

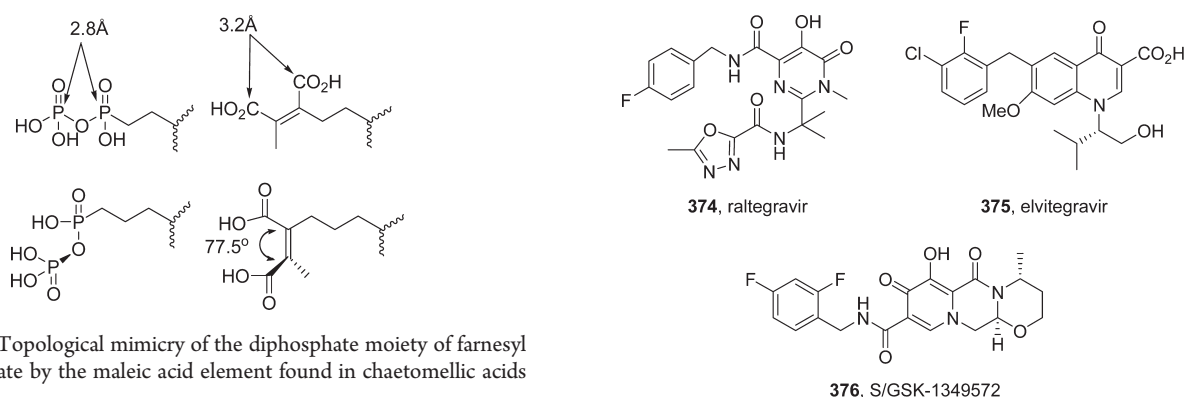


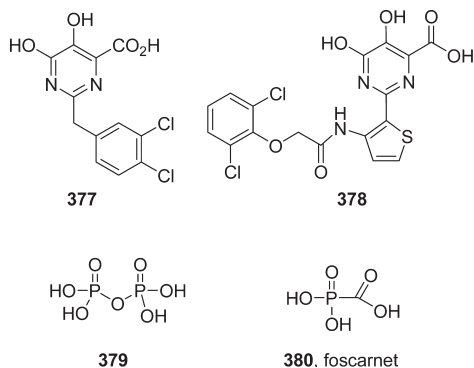
Figure 69. Topological mimicry of the diphosphate moiety of farnesyl pyrophosphate by the maleic acid element found in chaetomelic acids A and B.

clinically relevant compounds to emerge to date are the pyrimidinedione raltegravir (374), licensed in the United States in 2007, the quinoline carboxylic acid elvitegravir (375), currently in phase 3 clinical trials, and the pyrido[1,2-*a*]pyrazine S/GSK-1349572 (376) which has recently completed phase 2 studies. These three compounds represent interesting and distinct variants on phosphate transition state mimicry. Most interestingly, 375 is being developed as part of the so-called “quad pill” in which it is coformulated with the nucleoside analogue emtricitabine, the nucleotide analogue tenofovir, and the cytochrome P450 inhibitor cobicistat, the last included to inhibit metabolism of the integrase inhibitor.

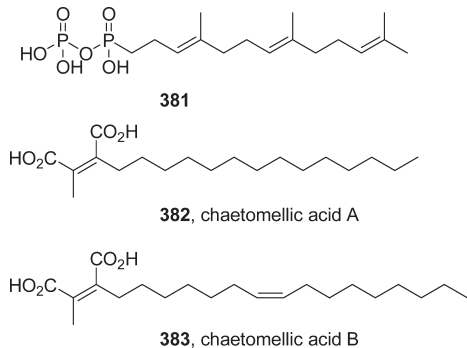
3.14.5. Phosphate Isosteres in HIV-1 RNase H and HCV NSSB Inhibitors. The dihydroxypyrimidine 377 is an inhibitor of the RNase H activity associated with HIV-1 reverse transcriptase, with X-ray crystallographic analysis indicating that 377 chelates to the active site metals, presumably acting as a mimic of elements of the transition state during phosphate hydrolysis.<sup>333</sup>

The dihydroxypyrimidine 378 inhibits HCV NSSB RNA-dependent RNA polymerase activity with  $IC_{50} = 0.73 \mu M$  by a mechanism involving competition with nucleotide incorporation.<sup>334</sup> In addition, 378 inhibits pyrophosphate-mediated excision, which is the reverse reaction and is a mechanism by which a nucleotide can be removed from an oligonucleotide. The compound was thus concluded to act as a mimic of

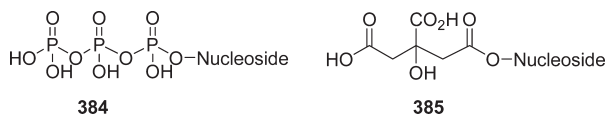
pyrophosphate (379), a mechanism analogous to that attributed to foscarnet (380), a simple pyrophosphate analogue marketed for the treatment of several viral infections.



**3.14.6. Pyrophosphate Isosteres in Ras Inhibitors.** Ras proteins are membrane-bound GTP-binding proteins involved in signal transduction, and farnesylation of cysteine in a CAAX motif in Ras initiates a sequence of post-translational modifications that ultimately leads to membrane association and activation of the mitotic signaling activity.<sup>335</sup> Inhibitors of Ras farnesylation have potential applications in oncology, and several classes of inhibitor have been explored. Chaetomelic acids A (382) and B (383) rely upon structural mimicry of farnesyl pyrophosphate (381) to compete with the natural substrate.<sup>336</sup> These compounds inhibit human FTPase with IC<sub>50</sub>S of 55 and 185 nM, respectively, with the maleic acid element hypothesized to function as a pyrophosphate isostere based on the topological mimicry captured in Figure 69.

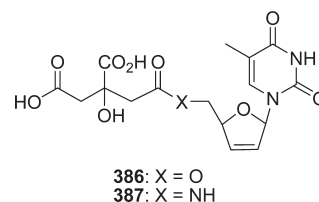


A molecular modeling exercise established good structural and charge correspondence between a triphosphate moiety 384 and the citrate derivative 385 when configured in the extended conformation, suggesting the potential for isosterism.<sup>337,338</sup> The concept was explored in the context of the HIV-1 nucleoside inhibitor d4T with the ester 386 and amide 387 linkers used to connect citrate to the sugar. Ester 386 demonstrated HIV-1 inhibition in cell culture with potency 10-fold weaker than that of d4T and showed weaker activity in thymidine kinase-deficient cells, while the amide 387 was inactive. However, neither compound inhibited HIV-1 reverse transcriptase in a biochemical assay, leading to the conclusion that the ester 386 was cleaved in cell culture to liberate d4T which was phosphorylated by thymidine kinase.<sup>337,338</sup>



**Table 50. Pyrophosphate Mimics Explored in the Context of a Series of Nucleoside Triphosphate Analogues Presented to HIV-1 Reverse Transcriptase as Potential Substrates**

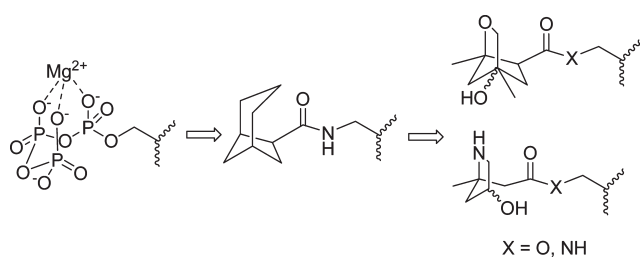
| Cpmd # | B | X   | R |
|--------|---|---|---|
| 388    | A | NH  |   |
| 389    | G |   |   |
| 390    | T |   |   |
| 391    | C |   |   |
| 392    | A | NH  |   |
| 393    | A | O   |   |
| 394    | C | NH  |   |
| 395    | A | N(CH <sub>2</sub> CO <sub>2</sub> H) <sub>2</sub> | - |
| 396    | A | NH  |   |
| 397    | G |   |   |
| 398    | T |   |   |
| 399    | C |   |   |
| 400    | A | NH  |   |
| 401    | A | NH  |   |
| 402    | A | NH  |   |
| 403    | A | O   |   |
| 404    | A | O   |   |



**3.14.7. Phosphate Isosteres in HIV-1 Reverse Transcriptase Substrates.** The series of pyrophosphate isosteres summarized in Table 50 has been examined in the context of modified nucleotides probed as substrates of HIV-1 reverse transcriptase (RT).<sup>339–347</sup> Initial studies focused on phosphoramidates prepared from adenine monophosphate and the natural amino acids aspartate, glutamate, histidine, and proline.<sup>340,341</sup> While the glutamate and proline derivatives were found to be poor substrates of HIV-1 RT, the L-Asp (388) and L-His (392) derivatives

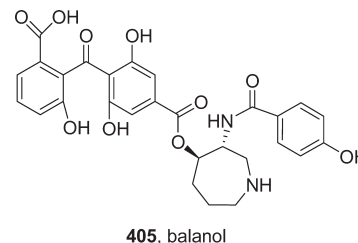
**Table 51. Steady State Kinetics for Incorporation of a Series of Natural and Modified Nucleotides by HIV-1 Reverse Transcriptase**

| substrate      | $V_{\max}$<br>(pmol/(min U)) | $K_m$ ( $\mu$ M) | $V_{\max}/K_m$<br>( $\times 10^6 \text{ min}^{-1}$ ) |
|----------------|------------------------------|------------------|--|
| dATP           | 8.39                         | 0.46             | 18.1   |
| Asp-dAMP (388) | 2.63                         | 185.3            | 0.014  |
| dGTP           | 28.81                        | 0.54             | 53.4   |
| Asp-dGMP (389) | 2.14                         | 168.8            | 0.013  |
| dTTP           | 30.82                        | 0.53             | 58.2   |
| Asp-dTMP (390) | 2.33                         | 288.2            | 0.008  |
| dCTP           | 5.62                         | 3.74             | 1.5  |
| Asp-dCMP (391) | 0.59                         | 130.8            | 0.005  |
| His-dAMP (392) | 0.33                         | 505.0            | 0.0007   |
| ILA-dAMP (393) | 2.75                         | 204.7            | 0.013  |

**Figure 70.** Shape mimetics of the  $\text{Mg}^{2+}$ -bound triphosphate moiety.

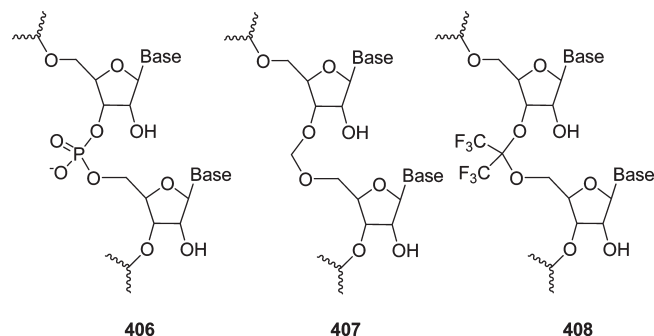
were processed by the enzyme with the  $V_{\max}$  for Asp just 3-fold lower than that of the natural substrate (data compiled in Table 51). However, the  $K_m$  value for 388 is substantially higher than that of the natural substrate, reflecting a scenario in which this modified triphosphate is an efficient substrate for the enzyme but possesses only low affinity for the substrate binding site. Extending the Asp-based phosphoramidate concept to the bases guanine, cytosine, and thymine produced substrates with  $K_m$  values 10- to 15-fold lower than those of the natural triphosphate counterparts, quite remarkable given the significant structural differences.<sup>341,342</sup> These results prompted a broader probe of modified substrates from which the cytidine-based malonate derivative 394 was found to be incorporated 1.5-fold more slowly than L-Asp-dAMP while the iminodiacetic acid derivative 395 is a superior substrate with a  $V_{\max}/K_m$  just 15-fold lower than that of dATP.<sup>343,345</sup> Modification of the amino leaving group of the L-His derivative 392 to an oxygen atom afforded ILA-dAMP (393) for which the  $V_{\max}$  improved almost 10-fold, while the  $K_m$  was lowered by 2-fold.<sup>344</sup> The phosphate 396, an analogue of 388, is an improved substrate with a  $K_m$  78-fold higher than that of dATP and a  $V_{\max}$  1.3-fold slower, affording a  $V_{\max}/K_m$  ratio that differs by only 99-fold.<sup>346</sup> The guanosine (397), thymine (398), and cytosine (399) analogues of 396 were also probed as bases, with 399 being a poorer substrate than either 397 or 398, while the sulfonic acid analogue 400 was also a poor substrate.<sup>346</sup> More radical structural changes to the amino acid moiety have been examined recently, including the isophthalic acid 403, which is incorporated to an extent that is 88% of L-Asp-dAMP, and the aniline analogue 402, which is a poorer substrate.<sup>347</sup> Demonstrating the importance of the topological presentation of the two carboxylic acid moieties to the enzyme within this series, the phthalic acid derivative 404 was not recognized by HIV-1 RT as a substrate.<sup>347</sup>

3.14.8. *Phosphate Isosterism in Balanol.* Balanol (405) is a fungal metabolite that inhibits both protein kinase C,  $\text{IC}_{50} = 4 \text{ nM}$ , and cAMP-dependent protein kinase,  $\text{IC}_{50} = 4 \text{ nM}$ .<sup>348–350</sup> In both cases, 405 is competitive with ATP and an X-ray cocrystal structure with cAMP-dependent protein kinase revealed that balanol occupies the ATP binding site. The benzophenone moiety occupies the triphosphate site, presenting a constellation of polar elements that function as a triphosphate mimetic. However, the benzophenone moiety of 405 is not a precise triphosphate isostere, since the molecule binds in a distinct fashion to the ATP site with the benzamide mimicking adenine and the azepine ring mimicking the ribose moiety of ATP.<sup>348–350</sup>

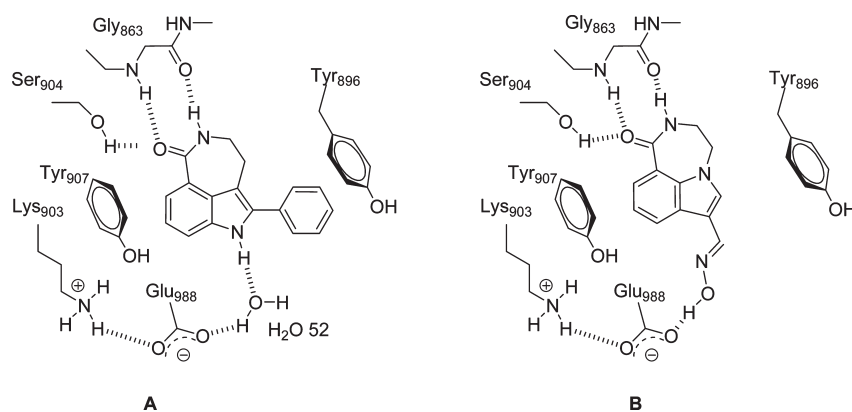


405, balanol

3.14.9. *Phosphate Shape Mimetics.* Shape mimetics of phosphate have been probed for their potential to function as isosteres in a nucleotide sequence where the phosphate moiety was replaced with a less polar isostere.<sup>351–353</sup> A simple acetal linkage 407 was examined as a noncharged mimetic of the natural phosphate 406 by incorporation of two of these elements into a 15mer oligonucleotide, both as the 3',5'-linkage shown and as the 2',5'-linked isomer.<sup>351</sup> The melting temperature,  $T_m$ , of hybrids with natural cDNA and RNA sequences was found to vary, with the RNA hybrids more stable than the DNA hybrids. For the 2',5'-linked topology, the  $T_m$  decreased approximately 0.5 °C per linkage for RNA. The hexafluoroacetone ketal 408 was subsequently conceived based on the notion of optimizing the steric similarity with phosphate, and two of these dinucleotide elements were also incorporated into a 15mer for hybrid stability analysis.<sup>352</sup> In this example, the  $T_m$  of the hybrid with both RNA and DNA oligonucleotides decreased by 2–2.5 °C compared to the natural oligonucleotides, with the modest level of bioisosterism attributed to reduced hydration of the  $\text{CF}_3$  group when compared to oxygen.<sup>352</sup>

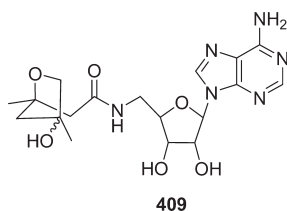


Mimetics designed to recapitulate the shape of a nucleoside triphosphate bound to  $\text{Mg}^{2+}$  observed in X-ray structures have been probed based on the structural analogy summarized in Figure 70. However, compounds based on this concept, including the adenine triphosphate analogue 409, demonstrated no significant biological activity and the modest



**Figure 71.** Binding interactions between inhibitors of poly(ADP-ribose) polymerase-1 and the chicken PARP enzyme.

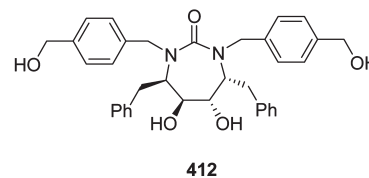
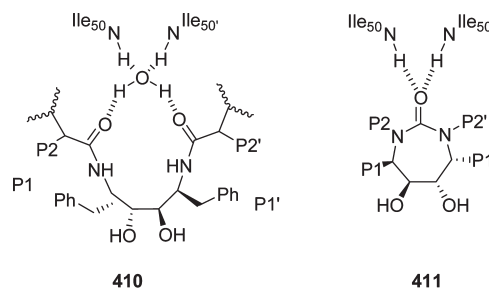
HIV-1 inhibition observed in cell culture with esters derived from d4T and AZT was attributed to hydrolysis to the parent nucleoside.<sup>354–356</sup>



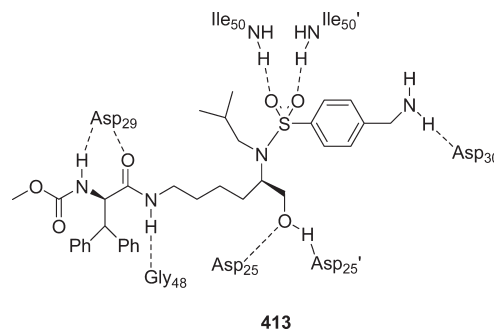
**3.15. Isosteres of Ligand–Water Complexes.** Ligand–protein complexes may contain water as a mediator of the interface, and there is potential affinity gain based on an increase in entropy by releasing a bound water molecule.<sup>357,358</sup> The strategy of introducing functionality to protein ligands in a fashion designed to displace an interfacial water molecule, in essence creating an isostere of the molecular combination, has been successfully exploited as a means of increasing potency in several drug–target interactions. However, this tactic has not always been effective and the examples described to date suggest that the success of this approach is dependent upon the context, both of the ligand and the protein.

**3.15.1. Displacing Water from the Binding Site of HIV-1 Protease.** The synthesis of novel HIV-1 protease inhibitors that relied upon replacing the water molecule mediating the interfacial interactions between the flap Ile<sub>50</sub>/Ile<sub>50'</sub> NHs and the P2/P2' carbonyl moieties of linear peptidomimetic inhibitors related to **410** represented a pioneering approach to drug design.<sup>359–361</sup> A series of cyclic ureas, exemplified by **411**, were conceived based on the premise that the urea carbonyl oxygen could effectively replace the water molecule, with additional benefit afforded by conformational preorganization of the inhibitor. Emerging from the early phase of this work, the urea **412** is a potent HIV protease inhibitor,  $K_i = 0.27$  nM, that demonstrates antiviral activity in cell culture,  $EC_{90} = 57$  nM.<sup>359</sup>

Another class of HIV-1 protease inhibitor that displaces the flap water is a series of lysine sulfonamide derivatives that are based on classic peptidomimetic inhibitors but modified by the introduction of an additional methylene between the classic hydroxyl transition state mimetic and the alkylene backbone.<sup>362</sup> Crystallization of the sulfonamide **413**, a potent antiviral in cell culture with an  $EC_{50} = 30$  nM, with HIV-1 protease revealed that the CH<sub>2</sub>OH moiety is within H-bonding distance of both catalytic residues Asp<sub>25</sub> and Asp<sub>25'</sub>, but the



inclusion of the extra CH<sub>2</sub> induces a distortion in the binding mode compared to more conventional peptide-derived inhibitors. As a consequence, the sulfonamide moiety is projected toward the flap residues, displacing the water molecule with both sulfone oxygen atoms accepting H-bonds from the flap Ile<sub>50</sub> and Ile<sub>50'</sub> NHs while the hydroxymethyl moiety is within H-bonding distance of the catalytic aspartate residues.<sup>362</sup>



**3.15.2. Displacing Water in Poly(ADP-ribose) Polymerase-1 (PARP) Inhibitors.** Inhibitors of poly(ADP-ribose) polymerase-1 are of potential utility in preventing DNA repair, thereby prolonging the antitumor activity of certain anticancer therapeutic agents.<sup>363–365</sup> 5-Phenyl-2,3,4,6-tetrahydro-1*H*-azepino[5,4,3-*cd*]indol-1-one is a potent inhibitor of human PARP-1,  $K_i = 6$  nM, that was cocrystallized with chicken PARP to reveal an interfacial water molecule, H<sub>2</sub>O-52, mediating an

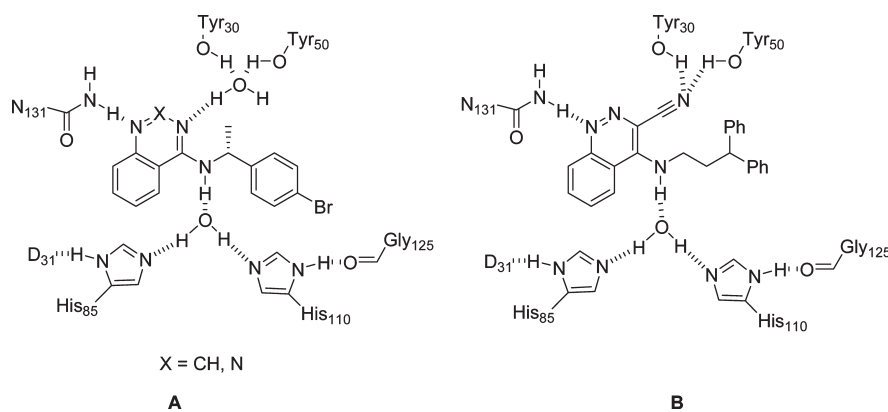


Figure 72. Binding interactions between scytalone dehydratase and inhibitors.

Table 52. Inhibition of Human Poly(ADP-ribose) Polymerase-1 by Substituted 3,4-Dihydro[1,4]diazepino[6,7,1-*hi*]-indol-1(2*H*)-ones

| Cmpd #     |                                    |                                  | Ki vs human PARP (nM) |
|------------|------------------------------------|----------------------------------|-----------------------|
|            | R <sub>1</sub>                     | R <sub>2</sub>                   |                       |
| <b>414</b> | H                                  | H                                | 105                   |
| <b>415</b> | H                                  | CH <sub>2</sub> OH               | 79                    |
| <b>416</b> | H                                  | ( <i>E</i> )-CH=NOH              | 9.4                   |
| <b>417</b> | H                                  | C(CH <sub>3</sub> )=NOH          | 39                    |
| <b>418</b> | H                                  | ( <i>E</i> )-C=NOCH <sub>3</sub> | 809                   |
| <b>419</b> | H                                  | ( <i>Z</i> )-C=NOCH <sub>3</sub> | 121                   |
| <b>420</b> | 4-F-C <sub>6</sub> H <sub>4</sub>  | ( <i>E</i> )-CH=NOH              | 6                     |
| <b>421</b> | 4-Cl-C <sub>6</sub> H <sub>4</sub> | ( <i>E</i> )-CH=NOH              | 7.5                   |
| <b>422</b> | 4-F-C <sub>6</sub> H <sub>4</sub>  | C(CH <sub>3</sub> )=NOH          | 9.1                   |
| <b>423</b> | 4-F-C <sub>6</sub> H <sub>4</sub>  | H                                | 11                    |

interaction between the indole NH and Glu<sub>988</sub>, as summarized in Figure 71A.<sup>363</sup> By inversion of the topology of the indole moiety, a series of 3,4-dihydro[1,4]diazepino[6,7,1-*hi*]indol-1(2*H*)-ones were designed that provided an opportunity to functionalize C-3 with substituents with the potential to engage Glu<sub>988</sub> by displacing H<sub>2</sub>O-52 (Figure 71B).<sup>364</sup> The (*E*)-carboxaldehydeoxime **416** satisfied the design criteria and is a potent human PARP-1 inhibitor,  $K_i = 9.4$  nM, an order of magnitude more potent than the unsubstituted parent **414** and several-fold more potent than the hydroxymethyl derivative **415** (data compiled in Table 52). The structure–activity relationships surrounding C- and O-methylation (**417**–**419**) supported the design hypothesis that the oxime moiety displaced H<sub>2</sub>O-52, confirmed by solving the cocrystal structure with (*E*)-carboxaldehydeoxime **416** which revealed the oxime OH engaging Glu<sub>988</sub> (Figure 72B). However, in the C-6 aryl series **420**–**423**, the effect of introducing the oxime moiety was less visible.

**3.15.3. Displacing Water in Scytalone Dehydratase.** Scytalone dehydratase is an enzyme in the plant fungal pathogen *Magnaporthe grisea* that catalyzes two steps in the melanin

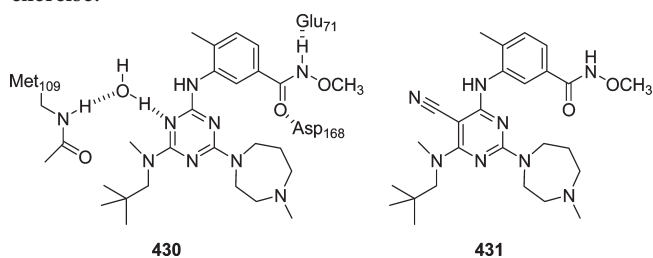
Table 53. Kinetic Constants for Inhibitors of Scytalone Dehydratase

|            |    |      | Ki (nM) |
|------------|----|------|---------|
|            | X  | Y    |         |
| <b>424</b> | CH | N    | 0.15    |
| <b>425</b> | CH | CH   | 200     |
| <b>426</b> | CH | C-CN | 0.0066  |
| <b>427</b> | N  | N    | 0.22    |
| <b>428</b> | N  | CH   | 140     |
| <b>429</b> | N  | C-CN | 0.0077  |

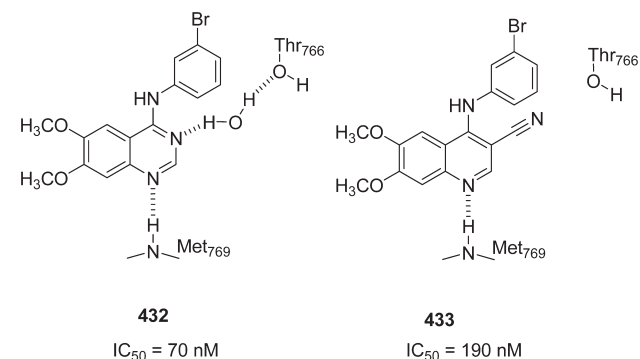
biosynthesis pathway.<sup>366</sup> The quinazoline **424** and benzotriazine **427** are potent inhibitors of scytalone dehydratase that were modeled in the enzyme active site as isosteres of a salicylamide derivative cocrystallized with the enzyme (Figure 72A). This exercise recognized the potential to displace the water molecule interfacing between the inhibitor and Tyr<sub>50</sub> by introducing a H-bond acceptor to the heterocyclic nucleus, realized with the nitriles **426** and **429** (Table 53). Both compounds were markedly more potent inhibitors of the enzyme than the parent molecules and substantially more potent than the C–H analogues **425** and **428**, consistent with the modeling hypothesis. An X-ray cocrystal of **429** with scytalone dehydratase validated the predictions, revealing the interactions depicted in Figure 72B.<sup>366</sup>

**3.15.4. Displacing Water in p38 $\alpha$  MAP Kinase Inhibitors.** The tactic of replacing the nitrogen atom of the triazine-based p38 $\alpha$  MAP kinase inhibitor **430**,  $K_i = 3.7$  nM, with C–CN in order to displace a bound water molecule observed in an X-ray structure led to the design of the cyanopyrimidine **431** which, with measured  $K_i = 0.057$  nM, offered a 60-fold enhancement of potency.<sup>367</sup> X-ray crystallographic data obtained with a closely analogous compound demonstrated that the cyano moiety engaged the NH of Met<sub>109</sub> in a H-bonding interaction, displacing the water molecule interfacing Met<sub>109</sub>

with the triazine N of **430**, as anticipated during the design exercise.



**3.15.5. Displacing Water in Epidermal Growth Factor Receptor Kinase Inhibitors.** An attempt to devise inhibitors of the epidermal growth factor receptor (EGFR) kinase inhibitor that displaced an interfacial water molecule proposed to bridge the prototype **432** to Thr<sub>766</sub> in a homology model of the kinase was, however, not successful.<sup>358,368</sup> Somewhat surprisingly, the C-3 nitrile **433** was found to be almost 3-fold weaker than **432**, and ester, amide, carbinol, and carboxylic acid substituents at C-3 were even poorer inhibitors. While this may be a function of inaccuracies associated with the homology model, a detailed analysis of the energetics of the interaction of a series of quinazolines, quinolines, and quinoline nitriles related to **432** and **433** with the EGFR protein suggested an alternative explanation.<sup>358</sup> In these modeling studies, the water remained strongly stabilized in the active site in the presence of **432** and the corresponding quinoline analogue, while the water molecule was displaced by the nitrile of **433**, as anticipated. A possible explanation recognized the potential for the quinoline analogue of **432** to bind in a fashion that retained the water molecule which was suggested to reorient itself to donate a H-bond to the bromophenyl ring, leading to a preservation of binding energy rather than the anticipated loss in affinity when the H-bonding interaction is lost by exchange of the quinazoline N by a C–H.<sup>358</sup>



#### 4. SUMMARY

This Perspective highlighted a selection of recent approaches to the design of bioisosteres that places an emphasis on practical applications focused on problem solving. The design and application of isosteres have inspired medicinal chemists for almost 80 years, fostering creativity directed toward solving a range of problems in drug design, including understanding and optimizing drug–target interactions and specificity, improving drug permeability, reducing or redirecting metabolism, and avoiding toxicity. As an established and powerful concept in medicinal chemistry, the application of bioisosteres will continue to play an important role in drug discovery, with the anticipation of increased sophistication in the recognition and design of functional mimetics.

#### AUTHOR INFORMATION

##### Corresponding Author

\*Contact information. Phone: 203-677-6679. Fax: 203-677-7884. E-mail: Nicholas.Meanwell@bms.com.

#### BIOGRAPHIES

Nicholas A. Meanwell received his Ph.D. degree from the University of Sheffield, U.K., with Dr. D. Neville Jones and conducted postdoctoral studies at Wayne State University, MI, in collaboration with Professor Carl R. Johnson. He joined Bristol-Myers Squibb in 1982 where he is currently Executive Director of Discovery Chemistry with responsibility for the optimization of new therapies for the treatment of viral diseases. His team has pioneered several areas of antiviral drug discovery, including the identification of inhibitors of respiratory syncytial virus fusion peptide 6-helix bundle function and the development of the cyclopropylacetylsulfonamide moiety that is widely used in HCV NS3 protease inhibitors, inhibitors of HIV attachment, and inhibitors of HCV NS5A, the last two of which have established clinical proof-of-concept for their respective mechanisms.

#### ACKNOWLEDGMENT

This article is based on a short course presented at an ACS ProSpectives conference held in Philadelphia, PA, October 4–6, 2009. I thank Dr. Paul S. Anderson for encouragement to publish this synopsis and my colleagues Drs. Lawrence B. Snyder, John V. Duncia, Dinesh Vyas, Richard A. Hartz, John F. Kadow, Yan Shi, and James E. Shepeck for sharing some of their insights and for stimulating discussions. I also thank Drs. Naidu Narasimhulu and Dinesh Vyas for critical appraisals of the manuscript.

#### ABBREVIATIONS USED

ACE, angiotensin converting enzyme; AMPA,  $\alpha$ -amino-3-hydroxyl-5-methyl-4-isoxazole propionate; BK, bradykinin; CSD, Cambridge Structural Database; COMT, catechol *O*-methyl transferase; COX, cyclooxygenase; CRF, corticotropin-releasing factor; CTCL, cutaneous T-cell lymphoma; CYP 450, cytochrome P450; D, deuterium; DAT, dopamine transporter; DFT, density functional theory; DHP, dihydropyridine; DPMS, GDP-mannose-dependent mannosyl transferase dolichol phosphate mannosyl synthase; EGFR, epidermal growth factor receptor; FAAH, fatty acid amide hydrolase; FPA, fluorescence polarization assay; GABA,  $\gamma$ -aminobutyric acid; GluR, glutamate receptor; GPCR, G-protein-coupled receptor; GSH, glutathione; GSK3, glycogen synthase kinase 3; GST, glutathione transferase; H, hydrogen; HDAC, histone deacetylase; hERG, human ether-a-go-go-related gene; KIE, kinetic isotope effect; KSP, kinesin spindle protein; HCV, hepatitis C virus; HIV, human immunodeficiency virus; HLM, human liver microsomes; HNE, human neutrophil elastase; JAK2, Janus kinase 2; LOX, 5-lipoxygenase; LPA, lysophosphatidic acid; MI, CYP 450 metabolic intermediate; MMP, matrix metalloprotease; MPTP, 1-methyl-4-phenyl-1,2,3,6-tetrahydropyridine; NET, norepinephrine transporter; NMDA, *N*-methyl-D-aspartate; NNRTI, non-nucleoside reverse transcriptase inhibitor; PCB, protein covalent binding; PDB, Protein Data Bank; PK, pharmacokinetic; PGI<sub>2</sub>, prostacyclin; PGE<sub>2</sub>, prostaglandin E<sub>2</sub>; PTB-1B, protein tyrosine phosphatase 1B; RLM, rat liver microsomes; RSV, respiratory syncytial virus; RT, reverse transcriptase; RXR, retinoid X receptor; SAR, structure–activity relationship; SERT, serotonin transporter; TNF $\alpha$ , tumor necrosis factor  $\alpha$ ; TRPV1, transient receptor potential vanilloid 1; TACE,

tumor necrosis factor  $\alpha$ -converting enzyme; VLA-4, very late antigen-4 (CD49d/CD29)

## REFERENCES

- (1) Burger, A. Isosterism and bioisosterism in drug design. *Prog. Drug Res.* **1991**, *37*, 288–362.
- (2) Patani, G. A.; LaVoie, E. J. Bioisosterism: a rational approach in drug design. *Chem. Rev.* **1996**, *96*, 3147–3176.
- (3) Langmuir, I. Isomorphism, isosterism and covalence. *J. Am. Chem. Soc.* **1919**, *41*, 1543–1559.
- (4) Erlenmeyer, H.; Berger, E. Studies on the significance of structure of antigens for the production and the specificity of antibodies. *Biochem. Z.* **1932**, *252*, 22–36.
- (5) Erlenmeyer, H.; Berger, E.; Leo, M. Relationship between the structure of antigens and the specificity of antibodies. *Helv. Chim. Acta* **1933**, *16*, 733–738.
- (6) Friedman, H. L. Influence of Isosteric Replacements upon Biological Activity. NAS-NRS Publication No. 206; NAS-NRS: Washington, DC, 1951; Vol. 206, pp 295–358.
- (7) Thornber, C. W. Isosterism and molecular modification in drug design. *Chem. Soc. Rev.* **1979**, *8*, 563–580.
- (8) Lipinski, C. A. Bioisosterism in drug design. *Annu. Rep. Med. Chem.* **1986**, *21*, 283–291.
- (9) *The Practice of Medicinal Chemistry*; Wermuth, C. G., Ed.; Academic Press: San Diego, CA, 1996; Chapters 12–16, pp 181–310 (2nd ed., 2003).
- (10) Olsen, P. H. The use of bioisosteric groups in lead optimization. *Curr. Opin. Drug Discovery Dev.* **2001**, *4*, 471–478.
- (11) Sheridan, R. P. The most common chemical replacements in drug-like compounds. *J. Chem. Inf. Comput. Sci.* **2002**, *42*, 103–108.
- (12) Wermuth, C. G. Similarity in drugs: reflections on analogue design. *Drug Discovery Today* **2005**, *11*, 348–354.
- (13) Lima, L. M.; Barriero, E. J. Bioisosterism: a useful strategy for molecular modification in drug design. *Curr. Med. Chem.* **2005**, *12*, 23–49.
- (14) MacMillan, D. W. C. The advent and development of organocatalysis. *Nature* **2008**, *455*, 304–308.
- (15) El Tayar, N.; van de Waterbeemd, H.; Gryllaki, M.; Testa, B.; Trager, W. F. The lipophilicity of deuterium atoms. A comparison of shake-flask and HPLC methods. *Int. J. Pharm.* **1984**, *19*, 271–281.
- (16) Turowski, M.; Yamakawa, N.; Meller, J.; Kimata, K.; Ikegami, T.; Hosoya, K.; Nobuo Tanaka, N.; Thornton, E. R. Deuterium isotope effects on hydrophobic interactions: the importance of dispersion interactions in the hydrophobic phase. *J. Am. Chem. Soc.* **2003**, *125*, 13836–13849.
- (17) Kimata, K.; Hosoya, K.; Araki, T.; Tanaka, N. Direct chromatographic separation of racemates on the basis of isotopic chirality. *Anal. Chem.* **1997**, *69*, 2610–2612.
- (18) Perrin, C. L.; Ohta, B. K.; Kuperman, J.  $\beta$ -Deuterium isotope effects on amine basicity, “inductive” and stereochemical. *J. Am. Chem. Soc.* **2003**, *125*, 15008–15009.
- (19) Perrin, C. L.; Ohta, B. K.; Kuperman, J.; Liberman, J.; Erdélyi, M. Stereochemistry of  $\beta$ -deuterium isotope effects on amine basicity. *J. Am. Chem. Soc.* **2005**, *127*, 9641–9647.
- (20) Perrin, C. L.; Dong, Y. Nonadditivity of secondary deuterium isotope effects on basicity of triethylamine. *J. Am. Chem. Soc.* **2008**, *130*, 11143–11148.
- (21) Perrin, C. L.; Dong, Y. Secondary deuterium isotope effects on the acidity of carboxylic acids and phenols. *J. Am. Chem. Soc.* **2007**, *129*, 4490–4497.
- (22) Wade, D. Deuterium isotope effects on noncovalent interactions between molecules. *Chem.-Biol. Interact.* **1999**, *117*, 191–217.
- (23) Schneider, F.; Mattern-Dogru, E.; Hillgenberg, M.; Alken, R.-G. Changed phosphodiesterase selectivity and enhanced in vitro efficacy by selective deuteration of sildenafil. *Arzneim.-Forsch.* **2007**, *57*, 293–298.
- (24) Blake, M. I.; Crespi, H. I.; Katz, J. J. Studies with deuterated drugs. *J. Pharm. Sci.* **1975**, *64*, 367–391.
- (25) Nelson, S. D.; Trager, W. F. The use of deuterium isotope effects to probe the active site properties, mechanism of cytochrome P450-catalyzed reactions, and mechanisms of metabolically dependent toxicity. *Drug Metab. Dispos.* **2003**, *31*, 1481–1498.
- (26) Mutlib, A. E. Application of stable isotope-labeled compounds in metabolism and in metabolism-mediated toxicity studies. *Chem. Res. Toxicol.* **2008**, *21*, 1672–1689.
- (27) Sanderson, K. Big interest in heavy drugs. *Nature* **2009**, *458*, 269.
- (28) Yarnell, A. T. Heavy-hydrogen drugs turn heads, again. Firms seek to improve drug candidates by selective deuterium substitution. *Chem. Eng. News* **2009**, *87*, 36–39.
- (29) Schneider, F.; Hillgenberg, M.; Koytchev, R.; Alken, R.-G. Enhanced plasma concentration by selective deuteration of rofecoxib in rats. *Arzneim.-Forsch.* **2006**, *56*, 295–300.
- (30) Westheimer, F. H. The magnitude of the primary kinetic isotope effect for compounds of hydrogen and deuterium. *Chem. Rev.* **1961**, *61*, 265–273.
- (31) Gant, T. G.; Sarshar, S. Substituted Phenethylamines with Serotonergic and/or Norepinephrine Activity. U.S. Patent 7,456,317, November 25, 2008.
- (32) Fukuda, T.; Nishida, Y.; Zhou, Q.; Yamamoto, I.; Kondo, S.; Azuma, J. The impact of the CYP2D6 and CYP2C19 genotypes on venlafaxine pharmacokinetics in a Japanese population. *Eur. J. Clin. Pharmacol.* **2000**, *56*, 175–180.
- (33) Auspex Pharmaceuticals. Data release available at [http://www.auspexpharma.com/auspex\\_SD254.html](http://www.auspexpharma.com/auspex_SD254.html).
- (34) Tung, R. Novel Benzo-[d][1,3]-dioxol Derivatives. WO 2007/016431 A2, February 8, 2007.
- (35) Concert Pharmaceuticals. Press release on September 14th, 2009, available at <http://www.concertpharma.com/ACCPPresentation.htm>.
- (36) Murray, M. Mechanisms of inhibitory and regulatory effects of methylenedioxyphenyl compounds on cytochrome P450-dependent drug oxidation. *Curr. Drug Metab.* **2000**, *1*, 67–84.
- (37) Bertelsen, K. M.; Venkatakrishnan, K.; von Moltke, L. L.; Obach, R. S.; Greenblatt, D. J. Apparent mechanism-based inhibition of human CYP 2D6 in vitro by paroxetine: comparison with fluoxetine and quinidine. *Drug Metab. Dispos.* **2003**, *31*, 289–293.
- (38) Mutlib, A. E.; Gerson, R. J.; Meunier, P. C.; Haley, P. J.; Chen, H.; Gan, L. S.; Davies, M. H.; Gemzik, B.; Christ, D. D.; Krahn, D. F.; Markwalder, J. A.; Seitz, S. P.; Robertson, R. T.; Miwa, G. T. The species-dependent metabolism of efavirenz produces a nephrotoxic glutathione conjugate in rats. *Toxicol. Appl. Pharmacol.* **2000**, *169*, 102–113.
- (39) Maltais, F.; Jung, Y. C.; Chen, M.; Tanoury, J.; Perni, R. B.; Mani, N.; Laitinen, L.; Huang, H.; Liao, S.; Gao, H.; Tsao, H.; Block, E.; Ma, C.; Shawgo, R. S.; Town, C.; Brummel, C. L.; Howe, D.; Pazhanisamy, S.; Raybuck, S.; Namchuk, M.; Bennani, Y. L. In vitro and in vivo isotope effects with hepatitis C protease inhibitors: enhanced plasma exposure of deuterated telaprevir versus telaprevir in rats. *J. Med. Chem.* **2009**, *52*, 7993–8001.
- (40) Bégue, J.-P.; Bonnet-Delpon, D. *Bioorganic and Medicinal Chemistry of Fluorine*; John Wiley & Sons: Hoboken, NJ, 2008.
- (41) Böhm, H.-J.; Banner, D.; Bendels, S.; Kansy, M.; Kuhn, B.; Müller, K.; Obst-Sander, U.; Stahl, M. Fluorine in medicinal chemistry. *ChemBioChem* **2004**, *5*, 637–643.
- (42) Müller, K.; Faeh, C.; Diederich, F. Fluorine in pharmaceuticals: looking beyond intuition. *Science* **2007**, *317*, 1881–1886.
- (43) Hagman, W. K. The many roles for fluorine in medicinal chemistry. *J. Med. Chem.* **2008**, *51*, 4359–4369.
- (44) Purser, S.; Moore, P. R.; Swallow, S.; Gouverneur, V. Fluorine in medicinal chemistry. *Chem. Soc. Rev.* **2008**, *37*, 320–330.
- (45) Shah, P.; Westwell, A. D. The role of fluorine in medicinal chemistry. *J. Enzyme Inhib. Med. Chem.* **2007**, *22*, 527–540.
- (46) O’Hagan, D. Understanding organofluorine chemistry. An introduction to the C–F bond. *Chem. Soc. Rev.* **2008**, *37*, 308–319.

- (47) Goncharov, N. V.; Richard O. Jenkins, R. O.; Radilov, A. S. Toxicology of fluoroacetate: a review, with possible directions for therapy research. *J. Appl. Toxicol.* **2006**, *26*, 148–161.
- (48) Okuda, H.; Ogura, K.; Kato, A.; Takubo, H.; Watabe, T. A possible mechanism of eighteen patient deaths caused by interactions of sorivudine, a new antiviral drug, with oral 5-fluorouracil prodrugs. *J. Pharmacol. Exp. Ther.* **1998**, *287*, 791–799.
- (49) Clader, J. W. The discovery of ezetimibe: a view from outside the receptor. *J. Med. Chem.* **2004**, *41*, 1–9.
- (50) Penning, T. D.; Talley, J. J.; Bertenshaw, S. R.; Carter, J. S.; Collins, P. W.; Docter, S.; Graneto, M. J.; Lee, L. F.; Malecha, J. W.; Miyashiro, J. M.; Rogers, R. S.; Rogier, D. J.; Yu, S. S.; Anderson, G. D.; Burton, E. G.; Cogburn, J. N.; Gregory, S. A.; Koboldt, C. M.; Perkins, W. E.; Seibert, K.; Veenhuizen, A. W.; Zhang, Y. Y.; Isakson, P. C. Synthesis and biological evaluation of the 1,5-diarylpyrazole class of cyclooxygenase-2 inhibitors: identification of 4-[5-(4-methylphenyl)-3-(trifluoromethyl)-1H-pyrazol-1-yl]benzenesulfonamide (SC-58635, celecoxib). *J. Med. Chem.* **1997**, *40*, 1347–1365.
- (51) Diana, G. D.; Rudewicz, P.; Pevear, D. C.; Nitz, T. J.; Aldous, S. C.; Aldous, D. J.; Robinson, D. T.; Draper, T.; Dutko, F. J.; Aldi, C.; Gendron, G.; Oglesby, R. C.; Volkots, D. L.; Reurnan, M.; Bailey, T. R.; Czerniak, R.; Block, T.; Roland, R.; Opperman, J. Picornavirus inhibitors: trifluoromethyl substitution provides a global protective effect against hepatic metabolism. *J. Med. Chem.* **1996**, *38* (1355–1371), 1355.
- (52) Park, R.; Kitteringham, N. R. Effects of fluorine substitution on drug metabolism: pharmacological and toxicological implications. *Drug Metab. Rev.* **1994**, *26*, 605–643.
- (53) Swaminathan, S.; Siddiqui, A. U.; Pinkerton, N. G.; Wilson, W. K.; Schroepfer, G. J. Inhibitors of sterol synthesis: 3 $\beta$ -hydroxy-25,26,26,26,27,27-heptafluoro-5 $\alpha$ -cholestan-15-one, an analog of a potent hypocholesterolemic agent in which its major metabolism is blocked. *Biochem. Biophys. Res. Commun.* **1994**, *201*, 168–173.
- (54) Banni, K.; Tom, T.; Oba, T.; Tanaka, T.; Okamura, N.; Watanabe, K.; Hazato, A.; Kurozumi, S. Synthesis of chemically stable prostacyclin analogs. *Tetrahedron* **1983**, *39*, 3807–3819.
- (55) Rose, W. C.; Marathe, P. H.; Jang, G. R.; Monticello, T. M.; Balasubramanian, B. N.; Long, B.; Fairchild, C. R.; Wall, M. E.; Wani, M. C. Novel fluoro-substituted camptothecins: in vivo antitumor activity, reduced gastrointestinal toxicity and pharmacokinetic characterization. *Cancer Chemother. Pharmacol.* **2006**, *58*, 73–85.
- (56) Traschel, D.; Hadorn, M.; Baumberger, F. Synthesis of fluoro analogues of 3,4-(methylenedioxy)amphetamine (MDA) and its derivatives. *Chem. Biodiversity* **2006**, *3*, 326–336.
- (57) Cox, C. D.; Coleman, P. J.; Breslin, M. J.; Whitman, D. B.; Garbaccio, R. M.; Fraley, M. E.; Buser, C. A.; Walsh, E. S.; Hamilton, K.; Schaber, M. D.; Lobell, R. B.; Tao, W.; Davide, J. P.; Diehl, R. E.; Abrams, M. T.; South, V. J.; Huber, H. E.; Torrent, M.; Prueksaritanont, T.; Li, C.; Slaughter, D. E.; Mahan, E.; Fernandez-Metzler, C.; Yan, Y.; Kuo, L. C.; Kohl, N. E.; Hartman, G. D. Kinesin spindle protein (KSP) inhibitors. 9. Discovery of (2S)-4-(2,5-difluorophenyl)-N-[(3R,4S)-3-fluoro-1-methylpiperidin-4-yl]-2-(hydroxymethyl)-N-methyl-2-phenyl-2,5-dihydro-1H-pyrrole-1-carboxamide (MK-0731) for the treatment of taxane-refractory cancer. *J. Med. Chem.* **2008**, *51*, 4239–4252.
- (58) Cerny, M. A.; Hanzlik, R. P. Cyclopropylamine inactivation of cytochromes P450: role of metabolic intermediate complexes. *Arch. Biochem. Biophys.* **2005**, *436*, 265–275.
- (59) O'Hagan, D.; Rzepa, H. S. Some influences of fluorine in bioorganic chemistry. *Chem. Commun.* **1997**, 645–652.
- (60) Briggs, C. R. S.; O'Hagan, D.; Howard, J. A. K.; Yufit, D. S. The C–F bond as a tool in the conformational control of amides. *J. Fluorine Chem.* **2003**, *119*, 9–13.
- (61) Banks, J. W.; Batsanov, A. S.; Howard, J. A. K.; O'Hagan, D.; Rzepa, H. S.; Martin-Santamaria, S. The preferred conformation of  $\alpha$ -fluoroamides. *J. Chem. Soc., Perkin Trans. 2* **1995**, 2409–2411.
- (62) O'Hagan, D.; Bilton, C.; Howard, J. A. K.; Knight, L.; Tozer, D. J. The preferred conformation of *N*- $\beta$ -fluoroethylamides. Observation of the fluorine amide *gauche* effect. *J. Chem. Soc., Perkin Trans. 2* **2001**, 605–607.
- (63) Buissonneaud, D. Y.; van Mourik, T.; O'Hagan, D. A DFT study on the origin of the fluorine *gauche* effect in substituted fluoroethanes. *Tetrahedron* **2010**, *66*, 2196–2202.
- (64) Hyla-Kryspin, I.; Grimme, S.; Hruschka, S.; Haufe, G. Conformational preferences and basicities of monofluorinated cyclopropylamines in comparison to cyclopropylamine and 2-fluoroethylamine. *Org. Biomol. Chem.* **2008**, *6*, 4167–4175.
- (65) Abraham, R. J.; Chambers, E. J.; Thomas, W. A. Conformational analysis. Part 22. An NMR and theoretical investigation of the *gauche* effect in fluoroethanols. *J. Chem. Soc., Perkin Trans. 2* **1994**, 949–955.
- (66) Briggs, C. R. S.; Allen, M. J.; O'Hagan, D.; Tozer, D. J.; Slawin, A. M. Z.; Goeta, A. E.; Howard, J. A. K. The observation of a large *gauche* preference when 2-fluoroethylamine and 2-fluoroethanol become protonated. *Org. Biomol. Chem.* **2004**, *2*, 732–740.
- (67) Deniau, G.; Slawin, A. M. Z.; Lebl, T.; Chorki, F.; Issberner, J. P.; van Mourik, T.; Heygate, J. M.; Lambert, J. J.; Etherington, L.-A.; Sillar, K. T.; O'Hagan, D. Synthesis, conformation, and biological evaluation of the enantiomers of 3-fluoro- $\gamma$ -aminobutyric acid ((*R*)- and (*S*)-3F-GABA): an analogue of the neurotransmitter GABA. *ChemBioChem* **2007**, *8*, 2265–2274.
- (68) Borden, W. T. Effects of electron donation into C–F  $\sigma^*$  orbitals: explanations, predictions and experimental tests. *Chem. Commun.* **1998**, 1919–1925.
- (69) Tozer, D. J. The conformation and internal rotational barrier of benzyl fluoride. *Chem. Phys. Lett.* **1999**, *308*, 160–164.
- (70) Bitencourt, M.; Freitas, M. P.; Rittner, R. Conformational and stereoelectronic investigation in 1,2-difluoropropane: the *gauche* effect. *J. Mol. Struct.* **2007**, *840*, 133–136.
- (71) Schüller, M.; O'Hagan, D.; Slawin, A. M. Z. The vicinal F–C–C–F moiety as a tool for influencing peptide conformation. *Chem. Commun.* **2005**, 4324–4326.
- (72) Hunter, L.; Kirsch, P.; Hamilton, J. T. G.; O'Hagan, D. The multi-vicinal fluoroalkane motif: an examination of 2,3,4,5-tetrafluorohexane stereoisomers. *Org. Biomol. Chem.* **2008**, *6*, 3105–3108.
- (73) Winkler, M.; Moraux, T.; Khairy, H. A.; Scott, R. H.; Slawin, A. M. Z.; O'Hagan, D. Synthesis and vanilloid receptor (TRPV1) activity of the enantiomers of  $\alpha$ -fluorinated capsaicin. *ChemBioChem* **2009**, *10*, 823–828.
- (74) Domagala, J. M.; Hanna, L. D.; Heifetz, C. L.; Hutt, M. P.; Mich, T. F.; Sanchez, J. P.; Solomon, M. New structure–activity relationships of the quinolone antibacterials using the target enzyme. The development and application of a DNA gyrase assay. *J. Med. Chem.* **1986**, *29*, 394–404.
- (75) Barbachyn, M. R.; Ford, C. W. Oxazolidinone structure–activity relationships leading to linezolid. *Angew. Chem., Int. Ed.* **2003**, *42*, 2010–2023.
- (76) Meanwell, N. A.; Wallace, O. B.; Fang, H.; Wang, H.; Deshpande, M.; Wang, T.; Yin, Z.; Zhang, Z.; Pearce, B. C.; James, J.; Yeung, K.-S.; Qiu, Z.; Wright, J. J. K.; Yang, Z.; Zadajura, L.; Tweedie, D. L.; Yeola, S.; Zhao, F.; Ranadive, S.; Robinson, B. A.; Gong, Y.-F.; Wang, H.-G. H.; Blair, W. S.; Shi, P.-Y.; Colonna, R. J.; Lin, P.-f. Inhibitors of HIV-1 attachment. Part 2: An initial survey of indole substitution patterns. *Bioorg. Med. Chem. Lett.* **2009**, *19*, 1977–1981.
- (77) Pinto, D. J. P.; Orwat, M. J.; Wang, S.; Fevig, J. M.; Quan, M. L.; Amparo, E.; Cacciola, J.; Rossi, K. A.; Alexander, R. S.; Smallwood, A. M.; Luetgten, J. M.; Liang, L.; Aungst, B. J.; Wright, M. R.; Knabb, R. M.; Wong, P. C.; Wexler, R. R.; Lam, P. Y. S. Discovery of 1-[3-(aminomethyl)phenyl]-N-[3-fluoro-2'-(methylsulfonyl)-[1,1'-biphenyl]-4-yl]-3-(trifluoromethyl)-1H-pyrazole-5-carboxamide (DPC423), a highly potent, selective, and orally bioavailable inhibitor of blood coagulation factor Xa. *J. Med. Chem.* **2001**, *44*, 566–578.
- (78) Quan, M. L.; Lam, P. Y. S.; Qi Han, Q.; Pinto, D. J. P.; He, M. Y.; Li, R.; Ellis, C. D.; Clark, C. G.; Teleha, C. A.; Sun, J.-H.; Alexander, R. S.; Bai, S.; Luetgten, J. M.; Knabb, R. M.; Wong, P. C.; Wexler, R. R. Discovery of 1-(3'-(aminobenzisoxazol-5'-yl)-3-trifluoromethyl-N-[2-fluoro-4'-(2'-dimethylaminomethyl)imidazol-1-yl]phenyl]-1H-pyrazole-5-carboxamide hydrochloride (razaxaban), a highly potent, selective,

- and orally bioavailable factor Xa inhibitor. *J. Med. Chem.* **2005**, *48*, 1729–1744.
- (79) Sehon, C. A.; Wang, G. Z.; Viet, A. Q.; Goodman, K. B.; Dowdell, S. E.; Elkins, P. A.; Semus, S. F.; Evans, C.; Jolivet, L. J.; Kirkpatrick, R. B.; Dul, E.; Khandekar, S. S.; Yi, T.; Wright, L. L.; Smith, G. K.; Behm, D. J.; Bentley, R.; Doe, C. P.; Hu, E.; Lee, D. Potent, selective and orally bioavailable dihydropyrimidine inhibitors of rho kinase (ROCK1) as potential therapeutic agents for cardiovascular diseases. *J. Med. Chem.* **2008**, *51*, 6631–6634.
- (80) Dai, Y.; Hartandi, K.; Ji, Z.; Ahmed, A. A.; Albert, D. H.; Bauch, J. L.; Bouska, J. J.; Bousquet, P. F.; Cunha, G. A.; Glaser, K. B.; Harris, C. M.; Hickman, D.; Guo, J.; Li, J.; Marcotte, P. A.; Marsh, K. C.; Moskey, M. D.; Martin, R. L.; Olson, A. M.; Osterling, D. J.; Pease, L. L.; Soni, N. B.; Stewart, K. D.; Stoll, V. S.; Tapang, P.; Reuter, D. R.; Davidsen, S. K.; Michaelides, M. R. Discovery of *N*-(4-(3-amino-1*H*-indazol-4-yl)phenyl)-*N'*-(2-fluoro-5-methylphenyl)urea (ABT-869), a 3-aminoinazole-based orally active multitargeted receptor tyrosine kinase inhibitor. *J. Med. Chem.* **2007**, *50*, 1584–1597.
- (81) Marsham, P. R.; Wardleworth, J. M.; Boyle, F. T.; Hennequin, L. F.; Kimbell, R.; Brown, M.; Jackman, A. L. Design and synthesis of potent non-polyglutamatable quinazoline antifolate thymidylate synthase inhibitors. *J. Med. Chem.* **1999**, *42*, 3809–3820.
- (82) Tran, C.; Ouk, S.; Clegg, N. J.; Chen, Y.; Watson, P. A.; Arora, V.; Wongvipat, J.; Smith-Jones, P. M.; Yoo, D.; Kwon, A.; Wasielewska, T.; Welsbie, D.; Chen, C.; Higoan, C. S.; Beer, T. M.; Hung, D. T.; Scher, H. I.; Jung, M. E.; Sawyers, C. L. Development of a second-generation antiandrogen for treatment of advanced prostate cancer. *Science* **2009**, *324*, 787–790.
- (83) Jung, M. E.; Ouk, S.; Yoo, D.; Sawyers, C. L.; Chen, C.; Tran, C.; Wongvipat, J. Structure–activity relationship for thiohydantoin androgen receptor antagonists for castration-resistant prostate cancer (CRPC). *J. Med. Chem.* **2010**, *53*, 2779–2796.
- (84) Skuballa, W.; Schillinger, E.; Stürzebecher, C.-St.; Vorbrüggen, H. Synthesis of a new chemically and metabolically stable prostacyclin analogue with high and long-lasting oral activity. *J. Med. Chem.* **1986**, *29*, 313–315.
- (85) Kim, J.-J. P.; Battaile, K. P. Burning fat: the structural basis of fatty acid  $\beta$ -oxidation. *Curr. Opin. Struct. Biol.* **2002**, *12*, 721–728.
- (86) Meanwell, N. A.; Romine, J. L.; Seiler, S. M. Non-prostanoid prostacyclin mimetics. *Drugs Future* **1994**, *19*, 361–385.
- (87) Meanwell, N. A.; Rosenfeld, M. J.; Trehan, A. K.; Wright, J. J. K.; Brassard, C. L.; Buchanan, J. O.; Federici, M. E.; Fleming, J. S.; Gamberdella, M.; Zavoico, G. B.; Seiler, S. M. Nonprostanoid prostacyclin mimetics. 2. 4,5-Diphenyloxazole derivatives. *J. Med. Chem.* **1992**, *35*, 3483–3497.
- (88) Hehre, W. J.; Radom, L.; Pople, J. A. Molecular orbital theory of the electronic structure of organic compounds. XII. Conformations, stabilities, and charge distributions in monosubstituted benzenes. *J. Am. Chem. Soc.* **1972**, *94*, 1496–1504.
- (89) Anderson, G. M., III; Kollman, P. A.; Domelsmith, L. N.; Houk, K. N. Methoxy group nonplanarity in *o*-dimethoxybenzenes. Simple predictive models for conformations and rotational barriers in alkoxyaromatics. *J. Am. Chem. Soc.* **1979**, *101*, 2344–2352.
- (90) Hummel, W.; Huml, K.; Bürgi, H.-B. Conformational flexibility of the methoxyphenyl group studies by statistical analysis of crystal structure data. *Helv. Chim. Acta* **1988**, *71*, 1291–1302.
- (91) Brameld, K. A.; Kuhn, B.; Reuter, D. C.; Stahl, M. Small molecule conformational preferences derived from crystal structure data. A medicinal chemistry focused analysis. *J. Chem. Inf. Model.* **2008**, *48*, 1–24.
- (92) Bryan, R. F.; Freyberg, D. P. Crystal structures of  $\alpha$ -*trans*- and *p*-methoxy-cinnamic acids and their relation to thermal mesomorphism. *J. Chem. Soc. Perkin Trans. 2* **1975**, 1835–1840.
- (93) Johnson, F. Allylic strain in six-membered rings. *Chem. Rev.* **1968**, *68*, 375–413.
- (94) Juteau, H.; Gareau, Y.; Labelle, M.; Sturino, C. F.; Sawyer, N.; Tremblay, N.; Lamontagne, S.; Carrière, M.-C.; Denis, D.; Metters, K. M. Structure–activity relationship of cinnamic acylsulfonamide analogues on the human EP<sub>3</sub> prostanoid receptor. *Bioorg. Med. Chem.* **2001**, *9*, 1977–1984.
- (95) Bains, W.; Tacke, R. Silicon chemistry as a novel source of chemical diversity in drug design. *Curr. Opin. Drug Discovery Dev.* **2003**, *6*, 526–543.
- (96) Showell, G. A.; Mills, J. S. Chemistry challenges in lead optimization: silicon isosteres in drug discovery. *Drug Discovery Today* **2003**, *8*, 551–556.
- (97) Mills, J. S.; Showell, G. A. Exploitation of silicon medicinal chemistry in drug discovery. *Expert Opin. Invest. Drugs* **2004**, *13*, 1149–1157.
- (98) Franz, A. K. The synthesis of biologically active organosilicon small molecules. *Curr. Opin. Drug Discovery Dev.* **2007**, *10*, 654–671.
- (99) Barnes, M. J.; Conroy, R.; Miller, D. J.; Mills, J. S.; Montana, J. G.; Pooni, P. K.; Showell, G. A.; Walsh, L. M.; Warneck, J. B. H. Trimethylsilylpyrazoles as novel inhibitors of p38 MAP kinase: a new use of silicon bioisosteres in medicinal chemistry. *Bioorg. Med. Chem. Lett.* **2007**, *17*, 354–357.
- (100) Showell, G. A.; Barnes, M. J.; Daiss, J. O.; Mills, J. S.; Montana, J. G.; Tacke, R.; Warneck, J. B. H. (*R*)-Sila-venlafaxine: a selective noradrenaline reuptake inhibitor for the treatment of emesis. *Bioorg. Med. Chem. Lett.* **2006**, *16*, 2555–2558.
- (101) Daiss, J. O.; Burschka, C.; Mills, J. S.; Montana, J. G.; Showell, G. A.; Warneck, J. B. H.; Tacke, R. Sila-venlafaxine, a sila-analogue of the serotonin/noradrenaline reuptake inhibitor venlafaxine: synthesis, crystal structure analysis, and pharmacological characterization. *Organometallics* **2006**, *25*, 1188–1198.
- (102) Daiss, J. O.; Burschka, C.; Mills, J. S.; Montana, J. G.; Showell, G. A.; Warneck, J. B. H.; Tacke, R. Synthesis, crystal structure analysis, and pharmacological characterization of desmethoxy-sila-venlafaxine, a derivative of the serotonin/noradrenaline reuptake inhibitor sila-venlafaxine. *J. Organomet. Chem.* **2006**, *691*, 3589–3595.
- (103) Tacke, R.; Popp, F.; Müller, B.; Theis, B.; Burschka, C.; Hamacher, A.; Kassack, M. U.; Schepmann, D.; Wunsch, B.; Jurva, U.; Wellner, E. Sila-haloperidol, a silicon analogue of the dopamine (D<sub>2</sub>) receptor antagonist haloperidol: synthesis, pharmacological properties, and metabolic fate. *ChemMedChem* **2008**, *3*, 152–164.
- (104) Subramanyam, B.; Woolf, T.; Castagnoli, N., Jr. Studies on the in-vitro conversion of haloperidol to a potentially neurotoxic pyridinium metabolite. *Chem. Res. Toxicol.* **1991**, *4*, 123–128.
- (105) Johansson, T.; Weidolf, L.; Popp, F.; Tacke, R.; Jurva, U. In vitro metabolism of haloperidol and sila-haloperidol: new metabolic pathways resulting from carbon/silicon exchange. *Drug Metab. Dispos.* **2010**, *38*, 73–83.
- (106) Tacke, R.; Nguyen, B.; Burschka, C.; Lippert, W. P.; Hamacher, A.; Urban, C.; Kassack, M. U. Sila-trifluperidol, a silicon analogue of the dopamine (D<sub>2</sub>) receptor antagonist trifluperidol: synthesis and pharmacological characterization. *Organometallics* **2010**, *29*, 1652–1660.
- (107) Lippert, W. P.; Burschka, C.; Götz, K.; Kaupp, M.; Ivanova, D.; Gaudon, C.; Sato, Y.; Antony, P.; Rochel, N.; Moras, D.; Gronemeyer, H.; Tacke, R. Silicon analogues of the RXR-selective retinoid agonist SR11237 (BMS649): chemistry and biology. *ChemMedChem* **2009**, *4*, 1143–1152.
- (108) Tacke, R.; Müller, V.; Büttner, M. W.; Lippert, W. P.; Bertermann, R.; Daiss, J. O.; Khanwalkar, H.; Furst, A.; Gaudon, C.; Gronemeyer, H. Synthesis and pharmacological characterization of disila-AM80 (disilatamibarotene) and disila-AM580, silicon analogues of the RAR $\alpha$ -selective retinoid agonists AM80 (tamibarotene) and AM580. *ChemMedChem* **2009**, *4*, 1797–1802.
- (109) Sieburth, S. McN.; Chen, C.-A. Silanediol protease inhibitors: from conception to validation. *Eur. J. Org. Chem.* **2006**, 311–322.
- (110) Chen, C.-A.; Sieburth, S. McN.; Glekas, A.; Hewitt, G. W.; Trainor, G. L.; Erickson-Viitanen, S.; Garber, S. S.; Cordova, B.; Jeffry, S.; Klabe, R. M. Drug design with a new transition state analog of the hydrated carbonyl: silicon-based inhibitors of the HIV protease. *Chem. Biol.* **2001**, *8*, 1161–1166.
- (111) Kim, J.; Sieburth, S. McN. Silanediol peptidomimetics. Evaluation of four diastereomeric ACE inhibitors. *Bioorg. Med. Chem. Lett.* **2004**, *14*, 2853–2856.

- (112) Kim, J.; Glekas, A.; Sieburth, S. McN. Silanediol-based inhibitor of thermolysin. *Bioorg. Med. Chem. Lett.* **2002**, *12*, 3625–3627.
- (113) Juers, D. H.; Kim, J.; Matthews, B. W.; Sieburth, S. McN. Structural analysis of silanediols as transition-state-analogue inhibitors of the benchmark metalloprotease thermolysin. *Biochemistry* **2005**, *44*, 16524–16528.
- (114) Meanwell, N. A.; Krystal, M. Respiratory syncytial virus: the discovery and optimization of orally bioavailable fusion inhibitors. *Drugs Future* **2007**, *32*, 441–455.
- (115) Yu, K.-L.; Sin, N.; Civiello, R. L.; Wang, X. A.; Combrink, K. D.; Gulgeze, H. B.; Venables, B. L.; Wright, J. J. K.; Dalterio, R. A.; Zadajura, L.; Marino, A.; Dando, S.; D'Arienzo, C.; Kadow, K. F.; Cianci, C. W.; Li, Z.; Clarke, J.; Genovesi, E. V.; Medina, L.; Lamb, L.; Colonna, R. J.; Yang, Z.; Krystal, M.; Meanwell, N.A. Respiratory syncytial virus fusion inhibitors. Part 4: Optimization for oral bioavailability. *Bioorg. Med. Chem. Lett.* **2007**, *17*, 895–901.
- (116) Barrow, J. C.; Rittle, K. E.; Reger, T. S.; Yang, Z.-Q.; Bondiskey, P.; McGaughey, G. B.; Bock, M. G.; Hartman, G. D.; Tang, C.; Ballard, J.; Kuo, Y.; Prueksaritanont, T.; Nuss, C. E.; Doran, S. M.; Fox, S. V.; Garson, S. L.; Kraus, R. L.; Li, Y.; Marino, M. J.; Graufelds, V. K.; Uebele, V. N.; Renger, J. J. Discovery of 4,4-disubstituted quinazolin-2-ones as T-type calcium channel antagonists. *ACS Med. Chem. Lett.* **2010**, *1*, 75–79.
- (117) Miller, D. C.; Klutea, W.; Calabrese, A.; Brown, A. D. Optimising metabolic stability in lipophilic chemical space: the identification of a metabolically stable pyrazolopyrimidine CRF-1 receptor antagonist. *Bioorg. Med. Chem. Lett.* **2009**, *19*, 6144–6147.
- (118) Wuitschik, G.; Rogers-Evans, M.; Müller, K.; Fischer, H.; Wagner, B.; Schuler, F.; Polonchuk, L.; Carreira, E. M. Oxetanes as promising modules in drug discovery. *Angew. Chem., Int. Ed.* **2006**, *45*, 7736–7739.
- (119) Wuitschik, G.; Carreira, E. M.; Wagner, B.; Fischer, H.; Parrilla, I.; Schuler, F.; Rogers-Evans, M.; Müller, K. Oxetanes in drug discovery: structural and synthetic insights. *J. Med. Chem.* **2010**, *53*, 3227–3246.
- (120) Burkhard, J. A.; Wuitschik, G.; Rogers-Evans, M.; Müller, K.; Carreira, E. M. Oxetanes as versatile elements in drug discovery and synthesis. *Angew. Chem., Int. Ed.* **2010**, *49*, 9052–9067.
- (121) For example, cLogP values calculated using the chemical properties function of ChemDraw Ultra, version 9, are as follows: tetrahydro-2H-pyran, 0.96; 4,4-dimethyltetrahydro-2H-pyran, 1.99; 6-oxaspiro[2.5]octane (the cyclopropyl analogue), 1.27; 2,7-dioxaspiro[3.5]nonane (the oxetane homologue), –0.57.
- (122) Tanaka, H.; Shishido, Y. Synthesis of aromatic compounds containing a 1,1-dialkyl-2-trifluoromethyl group, a bioisostere of the *tert*-alkyl moiety. *Bioorg. Med. Chem. Lett.* **2007**, *17*, 6079–6085.
- (123) Leroux, F. Atropisomerism, biphenyls, and fluorine: a comparison of rotational barriers and twist angles. *ChemBioChem* **2004**, *5*, 644–649.
- (124) Jagodzinska, M.; Huguenot, F.; Candiani, G.; Zanda, M. Assessing the bioisosterism of the trifluoromethyl group with a protease probe. *ChemMedChem* **2009**, *4*, 49–51.
- (125) Kitas, E. A.; Galley, G.; Jakob-Roetne, R.; Flohr, A.; Wostl, W.; Mauser, H.; Alker, A. M.; Czeck, C.; Ozmen, L.; David-Pierson, P.; Reinhardt, D.; Jacobsen, H. Substituted 2-oxo-azepane derivatives are potent, orally active  $\gamma$ -secretase inhibitors. *Bioorg. Med. Chem. Lett.* **2008**, *18*, 304–308.
- (126) Wang, T.; Yin, Z.; Zhang, Z.; Bender, J. A.; Yang, Z.; Johnson, G.; Yang, Z.; Zadajura, L. M.; D'Arienzo, C. J.; DiGiugno Parker, D.; Gesenberg, C.; Yamanaka, G. A.; Gong, Y.-F.; Ho, H.-T.; Fang, H.; Zhou, N.; McAuliffe, B. V.; Eggers, B. J.; Fan, L.; Nowicka-Sans, B.; Dicker, I. B.; Gao, Q.; Colonna, R. J.; Lin, P.-F.; Meanwell, N. A.; Kadow, J. F. Inhibitors of human immunodeficiency virus type 1 (HIV-1) attachment. 5. An evolution from indole to azaindoles leading to the discovery of 1-(4-benzoylpiperazin-1-yl)-2-(4,7-dimethoxy-1H-pyrrolo-[2,3-*c*]pyridin-3-yl)ethane-1,2-dione (BMS-488043), a drug candidate that demonstrates antiviral activity in HIV-1-infected subjects. *J. Med. Chem.* **2009**, *52*, 7778–7787.
- (127) Hartz, R. A.; Ahuja, V. T.; Zhuo, X.; Mattson, R. J.; Denhart, D. J.; Deskus, J. A.; Vrudhula, V. M.; Pan, S.; Ditta, J. L.; Shu, Y.-Z.; Grace, J. E.; Lentz, K. A.; Lelas, S.; Li, Y.-W.; Molski, T. F.; Krishnananthan, S.; Wong, H.; Qian-Cutrone, J.; Schartman, R.; Denton, R.; Lodge, N. J.; Zaczek, R.; Macor, J. E.; Bronson, J. J. A strategy to minimize reactive metabolite formation: discovery of (S)-4-(1-cyclopropyl-2-methoxyethyl)-6-[6-(difluoromethoxy)-2,5-dimethylpyridin-3-ylamino]-5-oxo-4,5-dihydropyrazine-2-carbonitrile as a potent, orally bioavailable corticotropin-releasing factor-1 receptor antagonist. *J. Med. Chem.* **2009**, *52*, 7653–7658.
- (128) Hartz, R. A.; Ahuja, V. T.; Schmitz, W. D.; Molski, T. F.; Mattson, G. K.; Lodge, N. J.; Bronson, J. J.; Macor, J. E. Synthesis and structure–activity relationships of  $N^3$ -pyridylpyrazinones as corticotropin-releasing factor-1 (CRF1) receptor antagonists. *Bioorg. Med. Chem. Lett.* **2010**, *20*, 1890–1894.
- (129) Zhuo, X.; Hartz, R. A.; Bronson, J. J.; Wong, H.; Ahuja, V. T.; Vrudhula, V. M.; Leet, J. E.; Huang, S.; Macor, J. E.; Shu, Y.-Z. Comparative biotransformation of pyrazinone-containing corticotropin-releasing factor receptor-1 antagonists: minimizing the reactive metabolite formation. *Drug Metab. Dispos.* **2010**, *38*, 5–15.
- (130) Kalgutkar, A. S.; Griffith, D. A.; Ryder, T.; Sun, H.; Miao, Z.; Bauman, J. N.; Didiuk, M. T.; Frederick, K. S.; Zhao, S. X.; Prakash, C.; Soglia, J. R.; Bagley, S. W.; Bechle, B. M.; Kelley, R. M.; Dirico, K.; Zawistoski, M.; Li, J.; Oliver, R.; Guzman-Perez, A.; Liu, K. K. C.; Walker, D. P.; Benbow, J. W.; Morris, J. Discovery tactics to mitigate toxicity risks due to reactive metabolite formation with 2-(2-hydroxyaryl)-5-(trifluoromethyl)pyrido[4,3-*d*]pyrimidin-4(3H)-one derivatives, potent calcium-sensing receptor antagonists and clinical candidate(s) for the treatment of osteoporosis. *Chem. Res. Toxicol.* **2010**, *23*, 1115–1126.
- (131) Southers, J. A.; Bauman, J. N.; Price, D. A.; Humphries, P. S.; Balan, G.; Sagal, J. F.; Maurer, T. S.; Zhang, Y.; Oliver, R.; Herr, M.; Healy, D. R.; Li, M.; Kapinos, B.; Fate, G. D.; Riccardi, K. A.; Paralkar, V. M.; Brown, T. A.; Kalgutkar, A. S. Metabolism-guided design of short-acting calcium-sensing receptor antagonists. *ACS Med. Chem. Lett.* **2010**, *1*, 219–223.
- (132) Samuel, K.; Yin, W.; Stearns, R. A.; Tang, Y. S.; Chaudhary, A. G.; Jewell, J. P.; Lanza, T., Jr.; Lin, L. S.; Hagmann, W. K.; Evans, D. C.; Kumar, S. Addressing the metabolic activation potential of new leads in drug discovery: a case study using ion trap mass spectrometry and tritium labeling techniques. *J. Mass Spectrom.* **2003**, *38*, 211–221.
- (133) Chien, R. J.; Corey, E. J. Strong conformational preferences of heteroaromatic ethers and electron pair repulsion. *Org. Lett.* **2010**, *12*, 132–135.
- (134) Phillips, G. B.; Buckman, B. O.; Davey, D. D.; Eagen, K. A.; Guilford, W. J.; Hinchman, J.; Ho, E.; Koovakkat, S.; Liang, A.; Light, D. R.; Mohan, R.; Ng, H. P.; Post, J. M.; Shaw, K. J.; Smith, D.; Subramanyam, B.; Sullivan, M. E.; Trinh, L.; Vergona, R.; Walters, J.; White, K.; Whitlow, M.; Wu, S.; Xu, W.; Morrissey, M. M. Discovery of *N*-[2-[5-[amino(imino)methyl]-2-hydroxyphenoxy]-3, 5-difluoro-6-[3-(4,5-dihydro-1-methyl-1H-imidazol-2-yl)phenoxy]pyridin-4-yl]-*N*-methylglycine (ZK-807834): a potent, selective, and orally active inhibitor of the blood coagulation enzyme factor Xa. *J. Med. Chem.* **1998**, *41*, 3557–3562.
- (135) Phillips, G.; Davey, D. D.; Eagen, K. A.; Koovakkat, S. K.; Liang, A.; Ng, H. P.; Pinkerton, M.; Trinh, L.; Whitlow, M.; Beatty, A. M.; Morrissey, M. M. Design, synthesis, and activity of 2,6-diphenoxypyridine-derived factor Xa inhibitors. *J. Med. Chem.* **1999**, *42*, 1749–1756.
- (136) Adler, M.; Davey, D. D.; Phillips, G. B.; Kim, S.-H.; Jancarik, J.; Rumennik, G.; Light, D. R.; Whitlow, M. Preparation, characterization, and the crystal structure of the inhibitor ZK-807834 (CI-1031) complexed with factor Xa. *Biochemistry* **2000**, *39*, 12534–12542.
- (137) Atwal, K. S.; Rovnyak, G. C.; Schwartz, J.; Moreland, S.; Hedberg, A.; Gougoutas, J. Z.; Malley, M. M.; Floyd, D. M. Dihydropyrimidine calcium channel blockers: 2-heterosubstituted 4-aryl-1,4-dihydro-6-methyl-5-pyrimidinecarboxylic acid esters as potent mimics of dihydropyridines. *J. Med. Chem.* **1990**, *33*, 1510–1515.
- (138) Atwal, K. S.; Rovnyak, G. C.; Kimball, S. D.; Floyd, D. M.; Moreland, S.; Swanson, B. N.; Gougoutas, J. Z.; Schwartz, J.; Smillie, K. M.; Malley, M. F. Dihydropyrimidine calcium channel blockers. 2.

3-Substituted-4-aryl-1,4-dihydro-6-methyl-5-pyrimidinecarboxylic acid esters as potent mimics of dihydropyridines. *J. Med. Chem.* **1990**, *33*, 2629–2635.

(139) Atwal, K. S.; Swanson, B. N.; Unger, S. E.; Floyd, D. M.; Moreland, S.; Hedberg, A.; O'Reilly, B. C. Dihydropyrimidine calcium channel blockers. 3. 3-Carbamoyl-4-aryl-1,2,3,4-tetrahydro-6-methyl-5-pyrimidinecarboxylic acid esters as orally effective antihypertensive agents. *J. Med. Chem.* **1991**, *34*, 806–811.

(140) Rovnyak, G. C.; Atwal, K. S.; Hedberg, A.; Kimball, S. D.; Moreland, S.; Gougoutas, J. Z.; O'Reilly, B. C.; Schwartz, J.; Malley, M. F. Dihydropyrimidine calcium channel blockers. 4. Basic 3-substituted-4-aryl-1,4-dihydropyrimidine-5-carboxylic acid esters. Potent antihypertensive agents. *J. Med. Chem.* **1992**, *35*, 3254–3263.

(141) Nagarathnam, D.; Miao, S. W.; Lagu, B.; Chiu, G.; Fang, J.; Dhar, T. G. M.; Zhang, J.; Tyagarajan, S.; Marzabadi, M. R.; Zhang, F.; Wong, W. C.; Sun, W.; Tian, D.; Wetzell, J. M.; Forray, C.; Chang, R. S. L.; Broten, T. P.; Ransom, R. W.; Schorn, T. W.; Chen, T. B.; O'Malley, S.; Kling, P.; Schneck, K.; Bendesky, R.; Harrell, C. M.; Vyas, K. P.; Gluchowski, C. Design and synthesis of novel  $\alpha_{1a}$  adrenoceptor-selective antagonists. 1. Structure–activity relationship in dihydropyrimidinones. *J. Med. Chem.* **1999**, *42*, 4764–4777.

(142) Wong, W. C.; Sun, W.; Lagu, B.; Tian, D.; Marzabadi, M. R.; Zhang, F.; Nagarathnam, D.; Miao, S. W.; Wetzell, J. M.; Peng, J.; Forray, C.; Chang, R. S. L.; Chen, T. B.; Ransom, R.; O'Malley, S.; Broten, T. P.; Kling, P.; Vyas, K. P.; Zhang, K.; Gluchowski, C. Design and synthesis of novel  $\alpha_{1a}$  adrenoceptor-selective antagonists. 4. Structure–activity relationship in the dihydropyrimidine series. *J. Med. Chem.* **1999**, *42*, 4804–4813.

(143) Qiao, J. X.; Cheney, D. L.; Alexander, R. S.; Smallwood, A. M.; King, S. R.; He, K.; Rendina, A. R.; Luettgen, J. M.; Knabb, R. M.; Wexler, R. R.; Lam, P. Y. S. Achieving structural diversity using the perpendicular conformation of alpha-substituted phenylcyclopropanes to mimic the bioactive conformation of ortho-substituted biphenyl P4 moieties: discovery of novel, highly potent inhibitors of factor Xa. *Bioorg. Med. Chem. Lett.* **2008**, *18*, 4118–4123.

(144) Pellicciari, R.; Raimondo, M.; Marinozzi, M.; Natalini, B.; Costantino, G.; Thomsen, C. (S)-(+)-2-(3'-Carboxybicyclo[1.1.1]pentyl)glycine, a structurally new group 1 metabotropic glutamate receptor antagonist. *J. Med. Chem.* **1996**, *39*, 2874–2876.

(145) Pellicciari, R.; Costantino, G.; Giovagnoni, E.; Mattoli, L.; Brabet, I.; Pin, J.-P. Synthesis and preliminary evaluation of (S)-2-(4'-carboxycubyl)glycine, a new selective mGluR1 antagonist. *Bioorg. Med. Chem. Lett.* **1998**, *8*, 1569–1574.

(146) Costantino, G.; Maltoni, K.; Marinozzi, M.; Camaioni, E.; Prezeau, L.; Pin, J.-P.; Pellicciari, R. Synthesis and biological evaluation of 2-(3'-(1H-tetrazol-5-yl)bicyclo[1.1.1]pent-1-yl)glycine (S-TBPG), a novel mGlu1 receptor antagonist. *Bioorg. Med. Chem.* **2001**, *9*, 221–227.

(147) Brown, A.; Brown, T. B.; Calabrese, A.; Ellis, D.; Puhalo, N.; Ralph, M.; Watson, L. Triazole oxytocin antagonists: identification of an aryloxyazetidone replacement for a biaryl substituent. *Bioorg. Med. Chem. Lett.* **2010**, *20*, 516–520.

(148) Lovering, F.; Bikker, J.; Humblet, C. Escape from flatland: increasing saturation as an approach to improving clinical success. *J. Med. Chem.* **2009**, *52*, 6752–6756.

(149) Wu, W.-L.; Burnett, D. A.; Spring, R.; Greenlee, W. J.; Smith, M.; Favreau, L.; Fawzi, A.; Zhang, H.; Lachowicz, J. E. Dopamine D1/D5 receptor antagonists with improved pharmacokinetics: design, synthesis, and biological evaluation of phenol bioisosteric analogues of benzazepine D1/D5 antagonists. *J. Med. Chem.* **2005**, *48*, 680–693.

(150) Reggelin, M.; Zur, C. Sulfoximines. Structures, properties, and synthetic applications. *Synthesis* **2000**, 1–64.

(151) Bentley, H. R.; McDermott, E. E.; Whitehead, J. K. Action of nitrogen trichloride on proteins: synthesis of the toxic factor from methionine. *Nature* **1950**, *165*, 735.

(152) Satzinger, G. Drug discovery and commercial exploitation. *Drug News Perspect.* **2001**, *14*, 197–207.

(153) Lua, D.; Vince, R. Discovery of potent HIV-1 protease inhibitors incorporating sulfoximine functionality. *Bioorg. Med. Chem. Lett.* **2007**, *17*, 5614–5619.

(154) Lu, D.; Sham, Y. Y.; Vince, R. Design, asymmetric synthesis, and evaluation of pseudosymmetric sulfoximine inhibitors against HIV-1 protease. *Bioorg. Med. Chem.* **2010**, *18*, 2037–2048.

(155) Raza, A.; Sham, Y. Y.; Vince, R. Design and synthesis of sulfoximine-based inhibitors for HIV-1 protease. *Bioorg. Med. Chem. Lett.* **2008**, *18*, 5406–5410.

(156) Erickson, J. A.; McLoughlin, J. I. Hydrogen bond donor properties of the difluoromethyl group. *J. Org. Chem.* **1995**, *60*, 1626–1631.

(157) For example, cLogP values calculated using the chemical properties function of ChemDraw Ultra, version 9, are as follows: PhOH, 1.48; PhNH<sub>2</sub>, 0.92; PhCHF<sub>2</sub>, 2.34; PhCH<sub>2</sub>OH, 1.10; PhCH<sub>2</sub>NH<sub>2</sub>, 1.09; PhCH<sub>2</sub>CHF<sub>2</sub>, 2.32.

(158) Narjes, F.; Koehler, K. F.; Koch, U.; Gerlach, B.; Colarusso, S.; Steinkühler, C.; Brunetti, M.; Altamura, S.; De Francesco, R.; Matassa, V. G. A designed P1 cysteine mimetic for covalent and non-covalent inhibitors of HCV NS3 protease. *Bioorg. Med. Chem. Lett.* **2002**, *12*, 701–704.

(159) Xu, Y.; Qian, L.; Pontsler, A. V.; McIntyre, T. M.; Prestwich, G. D. Synthesis of difluoromethyl substituted lysophosphatidic acid analogues. *Tetrahedron* **2004**, *60*, 43–49.

(160) Xu, Y.; Prestwich, G. D. Concise synthesis of acyl migration-blocked 1,1-difluorinated analogues of lysophosphatidic acid. *J. Org. Chem.* **2002**, *67*, 7158–7161.

(161) Sheppeck, J. E., II; Gilmore, J. L.; Yang, A.; Chen, X.-T.; Xue, C.-B.; Roderick, J.; Liu, R.-Q.; Covington, M. B.; Decicco, C. P.; Duan, J.J.-W. Discovery of novel hydantoins as selective non-hydroxamate inhibitors of tumor necrosis factor- $\alpha$  converting enzyme (TACE). *Bioorg. Med. Chem. Lett.* **2007**, *17*, 1413–1417.

(162) Flipo, M.; Charton, J.; Hocine, A.; Dassonneville, S.; Deprez, B.; Deprez-Poulain, R. Hydroxamates: relationships between structure and plasma stability. *J. Med. Chem.* **2009**, *52*, 6790–6802.

(163) Watanabe, T. Investigational histone deacetylase inhibitors for non-Hodgkin lymphomas. *Expert Opin. Invest. Drugs* **2010**, *19*, 1113–1127.

(164) Chowdhury, M. A.; Abdellatif, K. R. A.; Dong, Y.; Das, D.; Suresh, M. R.; Knaus, E. E. Synthesis of celecoxib analogues possessing a N-difluoromethyl-1,2-dihydropyrid-2-one 5-lipoxygenase pharmacophore: biological evaluation as dual inhibitors of cyclooxygenases and 5-lipoxygenase with anti-inflammatory activity. *J. Med. Chem.* **2009**, *52*, 1525–1529.

(165) Chowdhury, M. A.; Chen, H.; Abdellatif, K. R. A.; Dong, Y.; Petruk, K. C.; Knaus, E. E. Synthesis and biological evaluation of 1-(benzenesulfonamido)-2-[5-(N-hydroxypyridin-2(1H)-one)]acetylene regioisomers: a novel class of 5-lipoxygenase inhibitors. *Bioorg. Med. Chem. Lett.* **2008**, *18*, 4195–4198.

(166) Chowdhury, M. A.; Abdellatif, K. R. A.; Dong, Y.; Rahman, M.; Das, D.; Suresh, M. R.; Knaus, E. E. Synthesis of 1-(methanesulfonyl- and aminosulfonylphenyl)acetylenes that possess a 2-(N-difluoromethyl-1,2-dihydropyridin-2-one) pharmacophore: evaluation as dual inhibitors of cyclooxygenases and 5-lipoxygenase with anti-inflammatory activity. *Bioorg. Med. Chem. Lett.* **2009**, *19*, 584–588.

(167) Chowdhury, M. A.; Abdellatif, K. R. A.; Dong, Y.; Das, D.; Yu, G.; Velazquez, C. A.; Suresh, M. R.; Knaus, E. E. Synthesis and biological evaluation of salicylic acid and N-acetyl-2-carboxybenzenesulfonamide regioisomers possessing a N-difluoromethyl-1,2-dihydropyrid-2-one pharmacophore: dual inhibitors of cyclooxygenases and 5-lipoxygenase with anti-inflammatory activity. *Bioorg. Med. Chem. Lett.* **2009**, *19*, 6855–6861.

(168) Yu, G.; Praveen Rao, P. N.; Chowdhury, M. A.; Abdellatif, K. R. A.; Dong, Y.; Das, D.; Velazquez, C. A.; Suresh, M. R.; Knaus, E. E. Synthesis and biological evaluation of N-difluoromethyl-1,2-dihydropyrid-2-one acetic acid regioisomers: dual inhibitors of cyclooxygenases and 5-lipoxygenase. *Bioorg. Med. Chem. Lett.* **2010**, *20*, 2168–2173.

(169) Yu, G.; Chowdhury, M. A.; Abdellatif, K. R. A.; Dong, Y.; Praveen Rao, P. N.; Das, D.; Velazquez, C. A.; Suresh, M. R.; Knaus, E. E. Phenylacetic acid regioisomers possessing a N-difluoromethyl-1,2-dihydropyrid-2-one pharmacophore: evaluation as dual inhibitors of cyclooxygenases and 5-lipoxygenase with anti-inflammatory activity. *Bioorg. Med. Chem. Lett.* **2010**, *20*, 896–902.

- (170) Chowdhury, M. A.; Huang, Z.; Abdellatif, K. R. A.; Dong, Y.; Yu, G.; Velazquez, C. A.; Knaus, E. E. Synthesis and biological evaluation of indomethacin analogs possessing a *N*-difluoromethyl-1,2-dihydropyrid-2-one ring system: a search for novel cyclooxygenase and lipoxygenase inhibitors. *Bioorg. Med. Chem. Lett.* **2010**, *20*, 5776–5780.
- (171) Scolnick, L. R.; Clements, A. M.; Liao, J.; Crenshaw, L.; Hellberg, M.; May, J.; Dean, T. R.; Christianson, D. W. Novel binding mode of hydroxamate inhibitors to human carbonic anhydrase II. *J. Am. Chem. Soc.* **1997**, *119*, 850–851.
- (172) Sheppeck, J. E., II; Tebben, A.; Gilmore, J. L.; Yang, A.; Wasserman, Z. R.; Decicco, C. P.; Duan, J.J.-W. A molecular modeling analysis of novel non-hydroxamate inhibitors of TACE. *Bioorg. Med. Chem. Lett.* **2007**, *17*, 1408–1412.
- (173) Yu, W.; Guo, Z.; Orth, P.; Madison, V.; Chen, L.; Dai, C.; Feltz, R. J.; Girijavallabhan, V. M.; Kim, S. H.; Kozlowski, J. A.; Lavey, B. J.; Li, D.; Lundell, D.; Niu, X.; Piwinski, J. J.; Popovici-Muller, J.; Rizvi, R.; Rosner, K. E.; Shankar, B. B.; Shih, N.-Y.; Siddiqui, M. A.; Sun, J.; Tong, L.; Umland, S.; Wong, M. K. C.; Yang, D.-y.; Zhou, G. Discovery and SAR of hydantoin TACE inhibitors. *Bioorg. Med. Chem. Lett.* **2010**, *20*, 1877–1880.
- (174) Li, C.; Benet, L. Z.; Grillo, M. P. Studies on the chemical reactivity of 2-phenylpropionic acid 1-*O*-acyl glucuronide and S-acyl-CoA thioester metabolites. *Chem. Res. Toxicol.* **2002**, *5*, 1309–1317.
- (175) Carini, D. J.; Christ, D. D.; Duncia, J. V.; Pierce, M. E. The discovery and development of angiotensin II antagonists. *Pharm. Biotechnol.* **1998**, *11*, 29–56.
- (176) Naylor, E. M.; Chakravarty, P. K.; Costello, C. A.; Chang, R. S.; Chen, T.-B.; Faust, K. A.; Lotti, V. J.; Kivlighn, S. D.; Zingaro, G. J.; Siegl, P. K. S.; Wong, P. C.; Carini, D. J.; Wexler, R. R.; Patchett, A. A.; Greenlee, W. J. Potent imidazole angiotensin II antagonists: acyl sulfonamides and acyl sulfamides as tetrazole replacements. *Bioorg. Med. Chem. Lett.* **1993**, *3*, 69–74.
- (177) Chakravarty, P. K.; Naylor, E. M.; Chen, A.; Chang, R. S. L.; Chen, T.-B.; Faust, K. A.; Lotti, V. J.; Kivlighn, S. D.; Gable, R. A.; Zingaro, G. J.; Schorn, T. W.; Schaffer, L. W.; Broten, T. P.; Siegl, P. K. S.; Patchett, A. A.; Greenlee, W. J. A highly potent, orally active imidazo[4,5-*b*]pyridine biphenylacetyl sulfonamide (MK-996; L-159,282): a new AT<sub>1</sub>-selective angiotensin II receptor antagonist. *J. Med. Chem.* **1994**, *37*, 4068–4072.
- (178) Scola, P. M.; Sun, L.-Q.; Chen, J.; Wang, A. X.; Sit, S.-Y.; Chen, Y.; D'Andrea, S. V.; Zheng, Z.; Sin, N.; Venables, B. L.; Cocuzza, A.; Bilder, D.; Carini, D.; Johnson, B.; Good, A. C.; Rajamani, R.; Klei, H. E.; Friberg, J.; Barry, D.; Levine, S.; Chen, C.; Sheaffer, A.; Hernandez, D.; Falk, P.; Yu, F.; Zhai, G.; Knipe, J. O.; Mosure, K.; Shu, Y.-Z.; Phillip, T.; Arora, V. K.; Loy, J.; Adams, S.; Schartman, R.; Browning, M.; Levesque, P. C.; Li, D.; Zhu, J. L.; Sun, H.; Pilcher, G.; Bounous, D.; Lange, R. W.; Pasquinelli, C.; Eley, T.; Colonna, R.; Meanwell, N. A.; McPhee, F. Discovery of BMS-650032, an NS3 Protease Inhibitor for the Treatment of Hepatitis C. Presented at the 239th National Meeting and Exposition of the American Chemical Society, San Francisco, CA, March 21–25, 2010; MEDI-38.
- (179) Chen, K. X.; Njoroge, F. G. A review of HCV protease inhibitors. *Curr. Opin. Invest. Drugs* **2009**, *10*, 821–837.
- (180) Asada, M.; Obitsu, T.; Kinoshita, A.; Nakai, Y.; Nagase, T.; Sugimoto, I.; Tanaka, M.; Takizawa, H.; Yoshikawa, K.; Sato, K.; Narita, M.; Ohuchida, S.; Nakai, H.; Toda, M. Discovery of novel *N*-acylsulfonamide analogs as potent and selective EP3 receptor antagonists. *Bioorg. Med. Chem. Lett.* **2010**, *20*, 2639–2643.
- (181) Wendt, M. D. Discovery of ABT-263, a Bcl-family protein inhibitor: observations on targeting a large protein–protein interaction. *Expert Opin. Drug Discovery* **2008**, *3*, 1123–1143.
- (182) Park, C.-M.; Bruncko, M.; Adickes, J.; Bauch, J.; Ding, H.; Kunzer, A.; Marsh, K. C.; Nimmer, P.; Shoemaker, A. R.; Song, X.; Tahir, S. K.; Tse, C.; Wang, X.; Wendt, M. D.; Yang, X.; Zhang, H.; Fesik, S. W.; Rosenberg, S. H.; Elmore, S. W. Discovery of an orally bioavailable small molecule inhibitor of pro-survival B-cell lymphoma 2 proteins. *J. Med. Chem.* **2008**, *51*, 6902–6915.
- (183) Gruttadauria, M.; Giacalone, F.; Noto, R. Supported proline and proline-derivatives as recyclable organocatalysts. *Chem. Soc. Rev.* **2008**, *37*, 1666–1688.
- (184) Berkessel, A.; Koch, B.; Lex, J. Proline-derived *N*-sulfonylcarboxamides: readily available, highly enantioselective and versatile catalysts for direct aldol reactions. *Adv. Synth. Catal.* **2004**, *346*, 1141–1146.
- (185) Qiu, J.; Stevenson, S. H.; O'Beirne, M. J.; Silverman, R. B. 2,6-Difluorophenol as a bioisostere of a carboxylic acid: bioisosteric analogues of  $\gamma$ -aminobutyric acid. *J. Med. Chem.* **1999**, *42*, 329–332.
- (186) The log *P*, cLogP, and tPSA data for **25** and **208–211** were derived using the chemical properties function of ChemDraw Ultra, version 9.
- (187) Nicolaou, I.; Zika, C.; Demopoulos, V. J. [1-(3,5-Difluoro-4-hydroxyphenyl)-1*H*-pyrrol-3-yl]phenylmethanone as a bioisostere of a carboxylic acid aldose reductase inhibitor. *J. Med. Chem.* **2004**, *47*, 2706–2709.
- (188) Soll, R. M.; Kinney, W. A.; Primeau, J.; Ganick, L.; McCaully, R. J.; Colatsky, T.; Oshii, G.; Park, C. H.; Harmpeel, D.; White, V.; McCallum, J.; Russo, A.; Dinish, J.; Wojdan, A. 3-Hydroxy-3-cyclobutene-1,2-dione: application of a novel carboxylic acid bioisostere to an in vivo active non-tetrazole angiotensin II antagonist. *Bioorg. Med. Chem. Lett.* **1993**, *3*, 757–760.
- (189) Kinney, W. A.; Lee, N. E.; Garrison, D. T.; Podlesny, E. J., Jr.; Simmonds, J. T.; Bramlett, D.; Notvest, R. R.; Kowal, D. M.; Tasse, R. P. Bioisosteric replacement of the  $\alpha$ -amino carboxylic acid functionality in 2-amino-5-phosphonopentanoic acid yields unique 3,4-diamino-3-cyclobutene-1,2-dione-containing NMDA antagonists. *J. Med. Chem.* **1992**, *35*, 4720–4726.
- (190) Catarzi, D.; Colotta, V.; Varano, F. Competitive AMPA receptor antagonists. *Med. Res. Rev.* **2007**, *27*, 239–278.
- (191) Kuduk, S. D.; Ng, C.; Feng, D.-M.; Wai, J. M.-C.; Chang, R. S. L.; Harrell, C. M.; Murphy, K. L.; Ransom, R. W.; Reiss, D.; Ivarsson, M.; Mason, G.; Boyce, S.; Tang, C.; Prueksaritanont, T.; Freidinger, R. M.; Pettibone, D. J.; Bock, M. G. 2,3-Diaminopyridine bradykinin B<sub>1</sub> receptor antagonists. *J. Med. Chem.* **2004**, *47*, 6439–6442.
- (192) Tang, C.; Subramanian, R.; Kuo, Y.; Krymgold, S.; Lu, P.; Kuduk, S. D.; Ng, C.; Feng, D.-M.; Elmore, C.; Soli, E.; Ho, J.; Bock, M. G.; Baillie, T. A.; Prueksaritanont, T. Bioactivation of 2,3-diaminopyridine-containing bradykinin B<sub>1</sub> receptor antagonists: irreversible binding to liver microsomal proteins and formation of glutathione conjugates. *Chem. Res. Toxicol.* **2005**, *18*, 934–945.
- (193) Wood, M. R.; Schirripa, K. M.; Kim, J. J.; Wan, B.-L.; Murphy, K. L.; Ransom, R. W.; Chang, R. S. L.; Tang, C.; Prueksaritanont, T.; Detwiler, T. J.; Hettrick, L. A.; Landis, E. R.; Leonard, Y. M.; Krueger, J. A.; Lewis, S. D.; Pettibone, D. J.; Freidinger, R. M.; Bock, M. G. Cyclopropylamino acid amide as a pharmacophoric replacement for 2,3-diaminopyridine. Application to the design of novel bradykinin B<sub>1</sub> receptor antagonists. *J. Med. Chem.* **2006**, *49*, 1231–1234.
- (194) Jung, M. E.; Piizzi, G. *gem*-Disubstituent effect: theoretical basis and synthetic applications. *Chem. Rev.* **2005**, *105*, 1735–1766.
- (195) Laurence, C.; Berthelot, M. Observations on the strength of hydrogen bonding. *Perspect. Drug Discovery Des.* **2000**, *18*, 39–60.
- (196) Laurence, C.; Brameld, K. A.; Graton, J.; Le Questel, J.-Y.; Renault, E. The p*K*<sub>BHX</sub> database: toward a better understanding of hydrogen-bond basicity for medicinal chemists. *J. Med. Chem.* **2009**, *52*, 4073–4086.
- (197) Abraham, M. H.; Duce, P. P.; Prior, D.V. Hydrogen bonding. Part 9. Solute proton donor and proton acceptor scales for use in drug design. *J. Chem. Soc., Perkin Trans. 2* **1989**, 1355–1375.
- (198) Nobeli, I.; Price, S. L.; Lommerse, J. P. M.; Taylor, R. Hydrogen bonding properties of oxygen and nitrogen acceptors in aromatic heterocycles. *J. Comput. Chem.* **1997**, *18*, 2060–2074.
- (199) Graton, J.; Berthelot, M.; Gal, J.-F.; Laurence, C.; Lebreton, J.; Le Questel, J.-Y.; Maria, P.-C.; Robins, R. The nicotinic pharmacophore: thermodynamics of the hydrogen-bonding complexation of nicotine, nornicotine, and models. *J. Org. Chem.* **2003**, *68*, 8208–8221.

- (200) Arnaud, V.; Le Questel, J.-Y.; Mathé-Allainmat, M.; Lebreton, J.; Berthelot, M. Multiple hydrogen-bond accepting capacities of polybasic molecules: the case of cotinine. *J. Phys. Chem. A* **2004**, *108*, 10740–10748.
- (201) Locati, A.; Berthelot, M.; Evain, M.; Lebreton, J.; Le Questel, J.-Y.; Mathé-Allainmat, M.; Planchat, A.; Renault, E.; Graton, J. The exceptional hydrogen-bond properties of neutral and protonated lobe-line. *J. Phys. Chem. A* **2007**, *111*, 6397–6405.
- (202) Arnaud, V.; Berthelot, M.; Evain, M.; Graton, J.; Le Questel, J.-Y. Hydrogen-bond interactions of nicotine and acetylcholine salts: a combined crystallographic, spectroscopic, thermodynamic and theoretical study. *Chem.—Eur. J.* **2007**, *13*, 1499–1510.
- (203) Arnaud, V.; Berthelot, M.; Le Questel, J.-Y. Hydrogen-bond accepting strength of protonated nicotine. *J. Phys. Chem. A* **2005**, *109*, 3767–3770.
- (204) Arnaud, V.; Berthelot, M.; Felpin, F.-X.; Lebreton, J.; Le Questel, J.-Y.; Graton, J. Hydrogen-bond accepting strength of five-membered N-heterocycles: the case of substituted phenylpyrrolines and myosmines. *Eur. J. Org. Chem.* **2009**, 4939–4948.
- (205) Graton, J.; Berthelot, M.; Gal, J.-F.; Girard, S.; Laurence, C.; Lebreton, J.; Le Questel, J.-Y.; Maria, P.-C.; Naus, P. Site of protonation of nicotine and nornicotine in the gas phase: pyridine or pyrrolidine nitrogen? *J. Am. Chem. Soc.* **2002**, *124*, 10552–10562.
- (206) Taft, R. W.; Anvia, F.; Taagpera, M.; Catalán, J.; Elguero, J. Electrostatic proximity effects in the relative basicities and acidities of pyrazole, imidazole, pyridazine, and pyrimidine. *J. Am. Chem. Soc.* **1986**, *108*, 3237–3239.
- (207) Johnson, D. S.; Stiff, C.; Lazerwith, S. E.; Kesten, S. R.; Fay, L. K.; Morris, M.; Beidler, D.; Liimatta, M. B.; Smith, S. E.; Dudley, D. T.; Sadagopan, N.; Bhattachar, S. N.; Kesten, S. J.; Nomanbhoy, T. K.; Cravatt, B. F.; Ahn, K. Discovery of PF-04457845: a highly potent, orally bioavailable, and selective urea FAAH inhibitor. *ACS Med. Chem. Lett.* **2011**, *2*, 91–96.
- (208) Herberich, B.; Cao, G.-Q.; Chakrabarti, P. P.; Falsey, J. R.; Pettus, L.; Rza, R. M.; Reed, A. B.; Reichelt, A.; Sham, K.; Thaman, M.; Wurz, R. P.; Xu, S.; Zhang, D.; Hsieh, F.; Lee, M. R.; Syed, R.; Li, V.; Grosfeld, D.; Plant, M. H.; Henkle, B.; Sherman, L.; Middleton, S.; Wong, L. M.; Tasker, A. S. Discovery of highly selective and potent p38 inhibitors based on a phthalazine scaffold. *J. Med. Chem.* **2008**, *51*, 6271–6279.
- (209) Pettus, L. H.; Xu, S.; Cao, G.-Q.; Chakrabarti, P. P.; Rza, R. M.; Sham, K.; Wurz, R. P.; Zhang, D.; Middleton, S.; Henkle, B.; Plant, M. H.; Saris, C. J. M.; Sherman, L.; Wong, L. M.; Powers, D. A.; Tudor, Y.; Yu, V.; Lee, M. R.; Syed, R.; Hsieh, F.; Tasker, A. S. 3-Amino-7-phthalazinylbenzoxazoles as a novel class of potent, selective, and orally available inhibitors of p38 $\alpha$  mitogen-activated protein kinase. *J. Med. Chem.* **2008**, *51*, 6280–6292.
- (210) Wu, B.; Wang, H.-L.; Pettus, L.; Wurz, R. P.; Doherty, E. M.; Henkle, B.; McBride, H. J.; Saris, C. J. M.; Wong, L. M.; Plant, M. H.; Sherman, L.; Lee, M. R.; Hsieh, F.; Tasker, A. S. Discovery of pyridazinopyridinones as potent and selective p38 mitogen-activated protein kinase inhibitors. *J. Med. Chem.* **2010**, *53*, 6398–6411.
- (211) Berthelot, M.; Laurence, C.; Safar, M.; Besseau, F. Hydrogen-bond basicity pK<sub>HB</sub> scale of six-membered aromatic N-heterocycles. *J. Chem. Soc., Perkin Trans. 2* **1998**, 283–290.
- (212) Dombroski, M. A.; Letavic, M. A.; McClure, K. F.; Barberia, J. T.; Carty, T. J.; Cortina, S. R.; Csiki, C.; Dipesa, A. J.; Elliott, N. C.; Gabel, C. A.; Jordan, C. K.; Labasi, J. M.; Martin, W. H.; Peese, K. M.; Stock, I. A.; Svensson, L.; Sweeney, F. J.; Yu, C. H. Benzimidazolone p38 inhibitors. *Bioorg. Med. Chem. Lett.* **2004**, *14*, 919–923.
- (213) McClure, K. F.; Abramov, Y. A.; Laird, E. R.; Barberia, J. T.; Cai, W.; Carty, T. J.; Cortina, S. R.; Danley, D. E.; Dipesa, A. J.; Donahue, K. M.; Dombroski, M. A.; Elliott, N. C.; Gabel, C. A.; Han, S.; Hynes, T. R.; LeMotte, P. K.; Mansour, M. N.; Marr, E. S.; Letavic, M. A.; Pandit, J.; Ripin, D. B.; Sweeney, F. J.; Tan, D.; Tao, Y. Theoretical and experimental design of atypical kinase inhibitors: application to p38 MAP kinase. *J. Med. Chem.* **2005**, *48*, 5728–5737.
- (214) Böhm, H.-J.; Klebe, G.; Brode, S.; Hesse, U. Oxygen and nitrogen in competitive situations: which is the hydrogen-bond acceptor? *Chem.—Eur. J.* **1996**, *2*, 1509–1513.
- (215) Meanwell, N. A.; Rosenfeld, M. J.; Wright, J. J. K.; Brassard, C. L.; Buchanan, J. O.; Federici, M. E.; Fleming, J. S.; Gamberdella, M.; Hartl, K. S.; Zavoico, G. B.; Seiler, S. M. Nonprostanoid prostacyclin mimetics. 4. Derivatives of 2-[3-[2-(4,5-diphenyl-2-oxazolyl)ethyl]-phenoxy]acetic acid substituted  $\alpha$  to the oxazole ring. *J. Med. Chem.* **1993**, *36*, 3871–3883.
- (216) Meanwell, N. A.; Romine, J. L.; Rosenfeld, M. J.; Martin, S. W.; Trehan, A. K.; Wright, J. J. K.; Malley, M. F.; Gougoutas, J. Z.; Brassard, C. L.; Buchanan, J. O.; Federici, M. E.; Fleming, J. S.; Gamberdella, M.; Hartl, K. S.; Zavoico, G. B.; Seiler, S. M. Nonprostanoid prostacyclin mimetics. 5. Structure–activity relationships associated with [3-[4-(4,5-diphenyl-2-oxazolyl)-5-oxazolyl]phenoxy]acetic acid. *J. Med. Chem.* **1992**, *36*, 3884–3903.
- (217) Gougoutas, J. Z.; Ojala, W. H.; Malley, M. F. 3,4-Bis-(4-chlorophenyl)sydnone. *Cryst. Struct. Commun.* **1982**, *11*, 1731–1736.
- (218) Sweet, F.; Boyd, J.; Medina, O.; Konderski, L.; Murdock, G. L. Hydrogen bonding in steroidogenesis: studies in new heterocyclic analogues of estrone that inhibit human estradiol 17 $\beta$ -dehydrogenase. *Biochem. Biophys. Res. Commun.* **1991**, *180*, 1057–1063.
- (219) Cai, J.; Fradera, X.; van Zeeland, M.; Dempster, M.; Cameron, K. S.; D. Bennett, J.; Robinson, J.; Popplestone, L.; Baugh, M.; Westwood, P. C.; Bruin, J.; Hamilton, W.; Kinghorn, E.; Long, C.; Uitdehaag, J. C. M. 4-(3-Trifluoromethylphenyl)-pyrimidine-2-carbonitrile as cathepsin S inhibitors: N3, not N1 is critically important. *Bioorg. Med. Chem. Lett.* **2010**, *20*, 4507–4510.
- (220) Jones, E. D.; Vandegraaff, N.; Le, G.; Choi, N.; Issa, W.; MacFarlane, K.; Thienthong, N.; Winfield, L. J.; Coates, J. A. V.; Lu, L.; Li, X.; Feng, X.; Yu, C.; Rhodes, D. I.; Deadman, J. J. Design of a series of bicyclic HIV-1 integrase inhibitors. Part 1: selection of the scaffold. *Bioorg. Med. Chem. Lett.* **2010**, *20*, 5913–5917.
- (221) Le, G.; Vandegraaff, N.; Rhodes, D. I.; Jones, E. D.; Coates, J. A. V.; Thienthong, N.; Winfield, L. J.; Lu, L.; Li, X.; Yu, C.; Feng, X.; Deadman, J. J. Design of a series of bicyclic HIV-1 integrase inhibitors. Part 2: Azoles: effective metal chelators. *Bioorg. Med. Chem. Lett.* **2010**, *20*, 5909–5912.
- (222) Le, G.; Vandegraaff, N.; Rhodes, D. I.; Jones, E. D.; Coates, J. A. V.; Lu, L.; Li, X.; Yu, C.; Feng, X.; Deadman, J. J. Discovery of potent HIV integrase inhibitors active against raltegravir resistant viruses. *Bioorg. Med. Chem. Lett.* **2010**, *20*, 5013–5018.
- (223) Johns, B. A.; Weatherhead, J. G.; Allen, S. H.; Thompson, J. B.; Garvey, E. P.; Foster, S. A.; Jeffrey, J. L.; Miller, W. H. The use of oxadiazole and triazole substituted naphthyridines as HIV-1 integrase inhibitors. Part 1: Establishing the pharmacophore. *Bioorg. Med. Chem. Lett.* **2009**, *19*, 1802–1806.
- (224) Johns, B. A.; Weatherhead, J. G.; Allen, S. H.; Thompson, J. B.; Garvey, E. P.; Foster, S. A.; Jeffrey, J. L.; Miller, W. H. 1,3,4-Oxadiazole substituted naphthyridines as HIV-1 integrase inhibitors. Part 2: SAR of the C5 position. *Bioorg. Med. Chem. Lett.* **2009**, *19*, 1807–1810.
- (225) Desiraju, G. R.; Steinter, T. *The Weak Hydrogen Bond in Structural Chemistry and Biology*; Oxford University Press: Oxford, U. K., 1999.
- (226) Pierce, A. C.; Sandretto, K. L.; Bemis, G. W. Kinase inhibitors and the case for CH $\cdots$ O hydrogen bonds in protein–ligand binding. *Proteins* **2002**, *49*, 567–576.
- (227) Pierce, A. C.; ter Haar, E.; Binch, H. M.; Kay, D. P.; Patel, S. R.; Li, P. CH $\cdots$ O and CH $\cdots$ N hydrogen bonds in ligand design: a novel quinazolin-4-ylthiazol-2-ylamine protein kinase inhibitor. *J. Med. Chem.* **2005**, *48*, 1278–1281.
- (228) Ioannidis, S.; Lamb, M. L.; Davies, A. M.; Almeida, L.; Su, M.; Bebernit, G.; Ye, M.; Bell, K.; Alimzhanov, M.; Zinda, M. Discovery of pyrazol-3-ylamino pyrazines as novel JAK2 inhibitors. *Bioorg. Med. Chem. Lett.* **2009**, *19*, 6524–6528.
- (229) Ioannidis, S.; Lamb, M. L.; Almeida, L.; Guan, H.; Peng, B.; Bebernit, G.; Bell, K.; Alimzhanov, M.; Zinda, M. Replacement of pyrazol-3-yl amine hinge binder with thiazol-2-yl amine: discovery of potent and selective JAK2 inhibitors. *Bioorg. Med. Chem. Lett.* **2010**, *20*, 1669–1673.

- (230) Lin, S.; Wroblewski, S. T.; Hynes, J., Jr.; Pitt, S.; Zhang, R.; Fan, Y.; Doweyko, A. M.; Kish, K. F.; Sack, J. S.; Malley, M. F.; Kiefer, S. E.; Newitt, J. A.; McKinnon, M.; Trzaskos, J.; Barrish, J. C.; Dodd, J. H.; Schieven, G. L.; Leftheris, K. Utilization of a heteroatom-sulfur non-bonding interaction in the design of new 2-aminothiazol-5-yl-pyrimidines as p38 $\alpha$  MAP kinase inhibitors. *Bioorg. Med. Chem. Lett.* **2010**, *20*, 5864–5868.
- (231) Hynes, J., Jr.; Wu, H.; Pitt, S.; Shen, D.-R.; Zhang, R.; Schieven, G. L.; Gillooly, K. M.; Shuster, D. J.; Taylor, T. L.; Yang, X.; McIntyre, K. W.; McKinnon, M.; Zhang, H.; Marathe, P. H.; Doweyko, A. M.; Kish, K.; Kiefer, S. E.; Sack, J. S.; Newitt, J. A.; Barrish, J. C.; Dodd, J.; Leftheris, K. The discovery of (R)-2-(sec-butylamino)-N-(2-methyl-5-(methylcarbamoyl)phenyl)thiazole-5-carboxamide (BMS-640994), a potent and efficacious p38 $\alpha$  MAP kinase inhibitor. *Bioorg. Med. Chem. Lett.* **2008**, *18*, 1762–1767.
- (232) Iwaoka, M.; Takemoto, S.; Tomoda, S. Statistical and theoretical investigations on the directionality of nonbonded S $\cdots$ O interactions. Implications for molecular design and protein engineering. *J. Am. Chem. Soc.* **2002**, *124*, 10613–10620.
- (233) Haginoya, N.; Kobayashi, S.; Komoriya, S.; Yoshino, T.; Suzuki, M.; Shimada, T.; Watanabe, K.; Hirokawa, Y.; Furugori, T.; Nagahara, T. Synthesis and conformational analysis of a non-amidine factor Xa inhibitor that incorporates 5-methyl-4,5,6,7-tetrahydrothiazolo[5,4,c]pyridine as S4 binding element. *J. Med. Chem.* **2004**, *47*, 5167–5182.
- (234) Jung, F. H.; Pasquet, G.; Lambert-van der Brempt, C.; Lohmann, J.-J. M.; Warin, N.; Renaud, F.; Germain, H.; De Savi, C.; Roberts, N.; Johnson, T.; Dousson, C.; Hill, G. B.; Mortlock, A. A.; Heron, N.; Wilkinson, R. W.; Wedge, S. R.; Heaton, S. P.; Odedra, R.; Keen, N. J.; Green, S.; Brown, E.; Thompson, K.; Brightwell, S. Discovery of novel and potent thiazoloquinazolines as selective aurora A and B kinase inhibitors. *J. Med. Chem.* **2006**, *49*, 955–970.
- (235) Goldstein, B. M.; Takusagawa, F.; Berman, H. M.; Srivastava, P. C.; Robins, R. K. Structural studies of a new antitumor agent: tiazofurin and its inactive analogs. *J. Am. Chem. Soc.* **1983**, *105*, 7416–7422.
- (236) Li, H.; Hallows, W. A.; Punzi, J. S.; Marquez, V. E.; Carrell, H. L.; Pankiewicz, K. W.; Watanabe, K. A.; Goldstein, B. M. Crystallographic studies of two alcohol dehydrogenase-bound analogs of thiazole-4-carboxamide adenine dinucleotide (TAD), the active anabolite of the antitumor agent tiazofurin. *Biochemistry* **1994**, *33*, 23–32.
- (237) Goldstein, B. M.; Li, H.; Hallows, W. H.; Lings, D. A.; Franchetti, P.; Cappellacci, L.; Grifantini, M. C-Glycosyl bond conformation in oxazofurin: crystallographic and computational studies of the oxazole analog of tiazofurin. *J. Med. Chem.* **1994**, *37*, 1684–1688.
- (238) Franchetti, P.; Cappellacci, L.; Grifantini, M.; Barzi, A.; Nocentini, G.; Yang, H.; O'Connor, A.; Jayaram, H. N.; Carrell, C.; Goldstein, B. M. Furanfuran and thiophenfurin: two novel tiazofurin analogs. Synthesis, structure, antitumor activity, and interactions with inosine monophosphate dehydrogenase. *J. Med. Chem.* **1995**, *38*, 3829–3837.
- (239) Nagao, Y.; Hirata, T.; Goto, S.; Sano, S.; Kakehi, A.; Iizuka, K.; Shiro, M. Intramolecular nonbonded S $\cdots$ O interaction recognized in (acylimino)thiadiazoline derivatives as angiotensin II receptor antagonists and related compounds. *J. Am. Chem. Soc.* **1998**, *120*, 3104–3110.
- (240) Hayashi, K.; Ogawa, S.; Sano, S.; Shiro, M.; Yamaguchi, K.; Sei, Y.; Nagao, Y. Intramolecular nonbonded S $\cdots$ O interaction in rabepazole. *Chem. Pharm. Bull.* **2008**, *56*, 802–806.
- (241) Bradamante, S.; Pagani, G. A. Benzyl and heteroaryl methyl carbanions: structure and substituent effects. *Adv. Carbanion Chem.* **1996**, *2*, 189–263.
- (242) Abbotto, A.; Bradamante, S.; Pagani, G. A. Charge mapping in carbanions. Weak charge demand of the cyano group as assessed from a  $^{13}\text{C}$ -NMR study of carbanions of  $\alpha$ -activated acetonitriles and phenylacetonitriles: breakdown of a myth. *J. Org. Chem.* **1993**, *58*, 449–455.
- (243) Abbotto, A.; Bradamante, S.; Pagani, G. A. Diheteroaryl-methanes. 5. E-Z isomerism of carbanions substituted by 1,3-azoles:  $^{13}\text{C}$  and  $^{15}\text{N}$ -charge/shift relationships as source for mapping charge and ranking the electron-withdrawing power of heterocycles. *J. Org. Chem.* **1996**, *61*, 1761–1769.
- (244) Abbotto, A.; Bradamante, S.; Facchetti, A.; Pagani, G. A. Diheteroaryl-methanes. 8. Mapping charge and electron-withdrawing power of the 1,2,4-triazol-5-yl substituent. *J. Org. Chem.* **1999**, *64*, 6756–6763.
- (245) Hedstrom, L. Serine protease mechanism and specificity. *Chem. Rev.* **2002**, *102*, 4501–4523.
- (246) Edwards, P. D.; Meyer, E. F., Jr.; Vijayalakshmi, J.; Tuthill, P. A.; Andisik, D. A.; Gomes, B.; Strimplerg, A. Elastase inhibitors, the peptidyl  $\alpha$ -ketobenzoxazoles, and the X-ray crystal structure of the covalent complex between porcine pancreatic elastase and Ac-Ala-Pro-Val-2-benzoxazole. *J. Am. Chem. Soc.* **1992**, *114*, 1854–1863.
- (247) Edwards, P. D.; Wolanin, D. J.; Andisik, D. A.; David, M. W. Peptidyl  $\alpha$ -keto-heterocyclic inhibitors of human neutrophil elastase. 2. Effect of varying the heterocyclic ring on in vitro potency. *J. Med. Chem.* **1995**, *38*, 76–85.
- (248) Edwards, P. D.; Zottola, M. A.; Davis, M.; Williams, J.; Tuthill, P. A. Peptidyl  $\alpha$ -keto-heterocyclic inhibitors of human neutrophil elastase. 3. In vitro and in vivo potency of a series of peptidyl  $\alpha$ -ketobenzoxazoles. *J. Med. Chem.* **1995**, *38*, 3972–3982.
- (249) Ohmoto, K.; Yamamoto, T.; Horiuchi, T.; Imanishi, H.; Odagaki, Y.; Kawabata, K.; Sekioka, T.; Hirota, Y.; Matsuoka, S.; Nakai, H.; Toda, M.; Cheronis, J. C.; Spruce, L. W.; Gyorkos, A.; Wieczorek, M. Design and synthesis of new orally active nonpeptidic inhibitors of human neutrophil elastase. *J. Med. Chem.* **2000**, *43*, 4927–4929.
- (250) Ohmoto, K.; Yamamoto, T.; Okuma, M.; Horiuchi, T.; Imanishi, H.; Odagaki, Y.; Kawabata, K.; Sekioka, T.; Hirota, Y.; Matsuoka, S.; Nakai, H.; Toda, M.; Cheronis, J. C.; Spruce, L. W.; Gyorkos, A.; Wieczorek, M. Development of orally active nonpeptidic inhibitors of human neutrophil elastase. *J. Med. Chem.* **2001**, *44*, 1268–1285.
- (251) Costanzo, M. J.; Almond, H. R., Jr.; Hecker, L. R.; Schott, M. R.; Yabut, S. C.; Zhang, H.-C.; Andrade-Gordon, P.; Corcoran, T. W.; Giardino, E. C.; Kauffman, J. A.; Lewis, J. M.; de Garavilla, L.; Haertlein, B. J.; Maryanoff, B. E. In-depth study of tripeptide-based  $\alpha$ -keto-heterocycles as inhibitors of thrombin. Effective utilization of the S1' subsite and its implications to structure-based drug design. *J. Med. Chem.* **2005**, *48*, 1984–2008.
- (252) Maryanoff, B. E.; Costanzo, M. J. Inhibitors of proteases and amide hydrolases that employ  $\alpha$ -keto-heterocycles as a key enabling functionality. *Bioorg. Med. Chem.* **2008**, *16*, 1562–1595.
- (253) Romero, F. A.; Hwang, I.; Boger, D. L. Delineation of a fundamental  $\alpha$ -keto-heterocycle substituent effect for use in the design of enzyme inhibitors. *J. Am. Chem. Soc.* **2006**, *128*, 14004–14005.
- (254) Mileni, M.; Garfunkle, J.; DeMartino, J. K.; Cravatt, B. F.; Boger, D. L.; Stevens, R. C. Binding and inactivation mechanism of a humanized fatty acid amide hydrolase by  $\alpha$ -keto-heterocycle inhibitors revealed from cocrystal structures. *J. Am. Chem. Soc.* **2009**, *131*, 10497–10506.
- (255) Hansch, C.; Leo, A.; Unger, S. H.; Kim, K. H.; Nikaitani, D.; Lien, E. J. Aromatic substituent constants for structure–activity correlations. *J. Med. Chem.* **1973**, *16*, 1207–1216.
- (256) Taylor, R.; Mullaley, A.; Mullier, G. W. Use of crystallographic data in searching for isosteric replacements: composite crystal-field environments of nitro and carbonyl groups. *Pestic. Sci.* **1990**, *29*, 197–213.
- (257) Firestine, S. M.; Davisson, V. J. A tight binding inhibitor of 5-aminoimidazole ribonucleotide carboxylase. *J. Med. Chem.* **1993**, *36*, 3484–3486.
- (258) Gnewuch, C. T.; Friedman, H. L. Pyridine isosteres of the  $\beta$ -adrenergic antagonists, 2-(p-nitrophenyl)-1-isopropylamino-2-ethanol and 3-(p-nitrophenoxy)-1-isopropylamino-2-propanol. *J. Med. Chem.* **1972**, *15*, 1321–1324.
- (259) Sang, X.; Du, K.; Kadow, J. F.; Langley, D. R.; Vite, G. D.; Vyas, D. M.; Wittman, M. D.; Wong, T. W. Synthesis and SAR of Dithiazole HER Kinase Inhibitors. Presented at the 227th National Meeting of the American Chemical Society, Anaheim, CA, United States, March 28–April 1, 2004; MEDI-44.

- (260) Li, F.; Chordia, M. D.; Huang, T.; Macdonald, T. L. In vitro nimesulide studies toward understanding idiosyncratic hepatotoxicity: diiminoquinone formation and conjugation. *Chem. Res. Toxicol.* **2009**, *22*, 72–80.
- (261) Julémont, F.; de Leval, X.; Michaux, C.; Damas, J.; Charlier, C.; Durant, F.; Pirotte, B.; Dogné, J.-M. Spectral and crystallographic study of pyridinic analogues of nimesulide: determination of the active form of methanesulfonamides as COX-2 selective inhibitors. *J. Med. Chem.* **2002**, *45*, 5182–5185.
- (262) Renard, J.-F.; Arslan, D.; Garbacki, N.; Pirotte, B.; de Leval, X. Pyridine analogues of nimesulide: design, synthesis, and in vitro and in vivo pharmacological evaluation as promising cyclooxygenase 1 and 2 inhibitors. *J. Med. Chem.* **2009**, *52*, 5864–5871.
- (263) Dhar, T. G. M.; Nagarathnam, D.; Marzabadi, M. R.; Lagu, B.; Wong, W. C.; Chiu, G.; Tyagarajan, S.; Miao, S. W.; Zhang, F.; Sun, W.; Tian, D.; Shen, Q.; Zhang, J.; Wetzel, J. M.; Forray, C.; Chang, R. S. L.; Broten, T. P.; Schorn, T. W.; Chen, T. B.; O'Malley, S.; Ransom, R.; Schneck, K.; Bendsky, R.; Harrell, C. M.; Vyas, K. P.; Zhang, K.; Gilbert, J.; Pettibone, D. J.; Patane, M. A.; Bock, M. G.; Freidinger, R. M.; Gluchowski, C. Design and synthesis of Novel  $\alpha_{1a}$  adrenoceptor-selective antagonists. 2. Approaches to eliminate opioid agonist metabolites via modification of linker and 4-methoxycarbonyl-4-phenylpiperidine moiety. *J. Med. Chem.* **1999**, *42*, 4778–4793.
- (264) Lagu, B.; Tian, D.; Nagarathnam, D.; Marzabadi, M. R.; Wong, W. C.; Miao, S. W.; Zhang, F.; Sun, W.; Chiu, G.; Fang, J.; Forray, C.; Chang, R. S. L.; Ransom, R. W.; Chen, T. B.; O'Malley, S.; Zhang, K.; Vyas, K. P.; Gluchowski, C. Design and synthesis of novel  $\alpha_{1a}$  adrenoceptor-selective antagonists. 3. Approaches to eliminate opioid agonist metabolites by using substituted phenylpiperazine side chains. *J. Med. Chem.* **1999**, *42*, 4794–4803.
- (265) Leriche, C.; He, X.; Chang, C.-w.T.; Liu, H.-w. Reversal of the apparent regioselectivity of NAD(P)H-dependent hydride transfer: the properties of the difluoromethylene group, a carbonyl mimic. *J. Am. Chem. Soc.* **2003**, *125*, 6348–6349.
- (266) Vandyck, K.; Cummings, M. D.; Nyanguile, O.; Boutton, C. W.; Vendeville, S.; McGowan, D.; Devogelaere, B.; Amssoms, K.; Last, S.; Rombauts, K.; Tahri, A.; Lory, P.; Hu, L.; Beauchamp, D. A.; Simmen, K.; Raboisson, P. Structure-based design of a benzodiazepine scaffold yields a potent allosteric inhibitor of hepatitis C NSSB RNA polymerase. *J. Med. Chem.* **2009**, *52*, 4099–4102.
- (267) Wuitschik, G.; Rogers-Evans, M.; Buckl, A.; Bernasconi, M.; Marki, M.; Godel, T.; Fischer, H.; Wagner, B.; Parrilla, I.; Schuler, F.; Schneider, J.; Alker, A.; Schweizer, W. B.; Müller, K.; Carreira, E. M. Spirocyclic oxetanes: synthesis and properties. *Angew Chem., Int. Ed.* **2008**, *47*, 4512–4515.
- (268) Berthelot, M.; Besseau, F.; Laurence, C. The hydrogen-bond basicity  $pK_{HB}$  scale of peroxides and ethers. *Eur. J. Org. Chem.* **1998**, 925–931.
- (269) Besseau, F.; Lucon, M.; Laurence, C.; Berthelot, M. Hydrogen-bond basicity  $pK_{HB}$  scale of aldehydes and ketones. *J. Chem. Soc., Perkin Trans. 2* **1998**, 101–108.
- (270) Parlow, J. J.; Kurumbail, R. G.; Stegeman, R. A.; Stevens, A. M.; Stallings, W. C.; South, M. S. Design, synthesis, and crystal structure of selective 2-pyridone tissue factor VIIa inhibitors. *J. Med. Chem.* **2003**, *46*, 4696–4701.
- (271) Parlow, J. J.; Kurumbail, R. G.; Stegeman, R. A.; Stevens, A. M.; Stallings, W. C.; South, M. S. Synthesis and X-ray crystal structures of substituted fluorobenzene and benzoquinone inhibitors of the tissue factor VIIa complex. *Bioorg. Med. Chem. Lett.* **2003**, *13*, 3721–3725.
- (272) Lee, L.; Kreutter, K. D.; Pan, W.; Crysler, C.; Spurlino, J.; Player, M. R.; Tomczuk, B.; Lu, T. 2-(2-Chloro-6-fluorophenyl)-acetamides as potent thrombin inhibitors. *Bioorg. Med. Chem. Lett.* **2007**, *17*, 6266–6269.
- (273) Kreutter, K. D.; Lu, T.; Lee, L.; Giardino, E. C.; Patel, S.; Huang, H.; Xu, G.; Fitzgerald, M.; Haertlein, B. J.; Mohan, V.; Crysler, C.; Eisenagel, S.; Dasgupta, M.; McMillan, M.; Spurlino, J. C.; Huebert, N. D.; Maryanoff, B. E.; Tomczuk, B. E.; Damiano, B. P.; Player, M. R. Orally efficacious thrombin inhibitors with cyanofluorophenylacetamide as the P2 motif. *Bioorg. Med. Chem. Lett.* **2008**, *18*, 2865–2870.
- (274) Dubowchik, G. M.; Vruthula, V. M.; Dasgupta, B.; Ditta, J.; Chen, T.; Sheriff, S.; Sipman, K.; Witmer, M.; Tredup, J.; Vyas, D. M.; Verdoorn, T. A.; Bollini, S.; Vinitzky, A. 2-Aryl-2,2-difluoroacetamide FKBP12 ligands: synthesis and X-ray structural studies. *Org. Lett.* **2001**, *3*, 3987–3990.
- (275) Watjen, F.; Baker, R.; Engelstoff, M.; Herbert, R.; MacLeod, A.; Knight, A.; Merchant, K.; Moseley, J.; Saunders, J.; Swain, C. J.; Wong, E.; Springer, J. P. Novel benzodiazepine receptor partial agonists: oxadiazolylimidazobenzodiazepines. *J. Med. Chem.* **1989**, *32*, 2282–2291.
- (276) Saunders, J.; Cassidy, M.; Freedman, S. B.; Harley, E. A.; Iversen, L. L.; Kneen, C.; MacLeod, A. M.; Merchant, K. J.; Snow, R. J.; Baker, R. Novel quinuclidine-based ligands for the muscarinic cholinergic receptor. *J. Med. Chem.* **1990**, *33*, 1128–1138.
- (277) Sani, M.; Volonterio, A.; Zanda, M. The trifluoroethylamine function as peptide bond replacement. *ChemMedChem* **2007**, *2*, 1693–1700.
- (278) Volonterio, A.; Bellosta, S.; Bravin, F.; Bellucci, M. C.; Bruche, L.; Colombo, G.; Malpezzi, L.; Mazzini, S.; Meille, S. V.; Meli, M.; Ramirez de Arellano, C.; Zanda, M. Synthesis, structure and conformation of partially-modified retro- and retro-inverso  $\Psi$ [NHCH(CF<sub>3</sub>)]Gly peptides. *Chem.–Eur. J.* **2003**, *9*, 4510–4522.
- (279) Zanda, M. Trifluoromethyl group: an effective xenobiotic function for peptide backbone modification. *New J. Chem.* **2004**, *28*, 1401–1411.
- (280) Molteni, M.; Pesenti, C.; Sani, M.; Volonterio, A.; Zanda, M. Fluorinated peptidomimetics: synthesis, conformational and biological features. *J. Fluorine Chem.* **2004**, *125*, 1735–1743.
- (281) Binkert, C.; Frigerio, M.; Jones, A.; Meyer, S.; Pesenti, C.; Prade, L.; Viani, F.; Zanda, M. Replacement of isobutyl by trifluoromethyl in pepstatin A selectively affects inhibition of aspartic proteinases. *ChemBioChem* **2006**, *7*, 181–186.
- (282) Molteni, M.; Bellucci, M. C.; Bigotti, S.; Mazzini, S.; Volonterio, A.; Zanda, M.  $\Psi$ [CH(CF<sub>3</sub>)NH]Gly-peptides: synthesis and conformation analysis. *Org. Biomol. Chem.* **2009**, *7*, 2286–2296.
- (283) Sinisi, R.; Ghilardi, A.; Ruii, S.; Lazzari, P.; Malpezzi, L.; Sani, M.; Pani, L.; Zanda, M. Synthesis and in vitro evaluation of trifluoroethylamine analogues of enkephalins. *ChemMedChem* **2009**, *4*, 1416–1420.
- (284) Black, W. C.; Bayly, C. I.; Davis, D. E.; Desmarais, S.; Falguyret, J.-P.; Leger, S.; Li, C. S.; Masse, F.; McKay, D. J.; Palmer, J. T.; Percival, M. D.; Robichaud, J.; Tsou, N.; Zamboni, R. Trifluoroethylamines as amide isosteres in inhibitors of cathepsin K. *Bioorg. Med. Chem. Lett.* **2005**, *15*, 4741–4744.
- (285) Gauthier, J. Y.; Chauret, N.; Cromlish, W.; Desmarais, S.; Duong, L. T.; Falguyret, J.-P.; Kimmel, D. B.; Lamontagne, S.; Leger, S.; LeRiche, T.; Li, C. S.; Masse, F.; McKay, D. J.; Nicoll-Griffith, D. A.; Oballa, R. M.; Palmer, J. T.; Percival, M. D.; Riendeau, D.; Robichaud, J.; Rodan, G. A.; Rodan, S. B.; Seto, C.; Therien, M.; Truong, V.-L.; Venuti, M. C.; Wesolowski, G.; Young, R. N.; Zamboni, R.; Black, W. C. The discovery of odanacatib (MK-0822), a selective inhibitor of cathepsin K. *Bioorg. Med. Chem. Lett.* **2008**, *18*, 923–928.
- (286) Holsinger, L. J.; Elrod, K.; Link, J. O.; Graupe, M.; Kim, I. J. Preparation of Peptides That Inhibit Protease Cathepsin S and HCV Replication. World Patent Application WO-2009/055467 A2, 2009.
- (287) Eastwood, P.; Gonzalez, J.; Paredes, S.; Fonquerna, S.; Cardús, A.; Alonso, J. A.; Nueda, A.; Domenech, T.; Reinoso, R. F.; Vidal, B. Discovery of potent and selective bicyclic A<sub>2B</sub> adenosine receptor antagonists via bioisosteric amide replacement. *Bioorg. Med. Chem. Lett.* **2010**, *20*, 1634–1637.
- (288) Ulrich, R. G.; Bacon, J. A.; Brass, E. P.; Cramer, C. T.; Petrella, D. K.; Sun, E. L. Metabolic, idiosyncratic toxicity of drugs: overview of the hepatic toxicity induced by the anxiolytic, panadiplon. *Chem.-Biol. Interact.* **2001**, *134*, 251–270.
- (289) Ghosh, A. K. Harnessing nature's insight: design of aspartyl protease inhibitors from treatment of drug-resistant HIV to Alzheimer's disease. *J. Med. Chem.* **2008**, *52*, 2163–2176.

(290) Ghosh, A. K.; Chapsal, B. D.; Weber, I. T.; Mitsuya, H. Inhibitors targeting protein backbone: an effective strategy for combating drug resistance. *Acc. Chem. Res.* **2008**, *41*, 78–86.

(291) Wang, T.; Zhang, Z.; Wallace, O. B.; Deshpande, M.; Fang, H.; Yang, Z.; Zadjura, L. M.; Tweedie, D. L.; Huang, S.; Zhao, F.; Ranadive, S.; Robinson, B. S.; Gong, Y.-F.; Ricarri, K.; Spicer, T. P.; Deminie, C.; Rose, R.; Wang, H.-G. H.; Blair, W. S.; Shi, P.-Y.; Lin, P.-f.; Colonna, R. J.; Meanwell, N. A. Discovery of 4-benzoyl-1-[(4-methoxy-1H-pyrrolo[2,3-b]pyridin-3-yl)oxoacetyl]-2-(R)-methylpiperazine (BMS-378806): a novel HIV-1 attachment inhibitor that interferes with CD4-gp120 interactions. *J. Med. Chem.* **2003**, *46*, 4236–4239.

(292) Lu, R.-J.; Tucker, J. A.; Zinevitch, T.; Kirichenko, O.; Konoplev, V.; Kuznetsova, S.; Sviridov, S.; Pickens, J.; Tandel, S.; Brahmachary, E.; Yang, Y.; Wang, J.; Freil, S.; Fisher, S.; Sullivan, A.; Zhou, J.; Stanfield-Oakley, S.; Greenberg, M.; Bolognesi, D.; Bray, B.; Koszalka, B.; Jeffs, P.; Khasanov, A.; Ma, Y.-A.; Jeffries, C.; Liu, C.; Proskurina, T.; Zhu, T.; Chucholowski, A.; Li, R.; Sexton, C. Design and synthesis of human immunodeficiency virus entry inhibitors: sulfonamide as an isostere for the  $\alpha$ -ketoamide group. *J. Med. Chem.* **2007**, *50*, 6535–6544.

(293) Lu, R.-J.; Tucker, J. A.; Pickens, J.; Ma, Y.-A.; Zinevitch, T.; Kirichenko, O.; Konoplev, V.; Kuznetsova, S.; Sviridov, S.; Brahmachary, E.; Khasanov, A.; Mikel, C.; Yang, Y.; Liu, C.; Wang, J.; Freil, S.; Fisher, S.; Sullivan, A.; Zhou, J.; Stanfield-Oakley, S.; Baker, B.; Sailstad, J.; Greenberg, M.; Bolognesi, D.; Bray, B.; Koszalka, B.; Jeffs, P.; Jeffries, C.; Chucholowski, A.; Sexton, C. Heterobiaryl human immunodeficiency virus entry inhibitors. *J. Med. Chem.* **2009**, *52*, 4481–4487.

(294) Durant, G. J.; Emmett, J. C.; Ganellin, C. R.; Miles, P. D.; Parsons, M. E.; Prain, H. D.; White, G. R. Cyanoguanidine-thiourea equivalence in the development of the histamine H<sub>2</sub>-receptor antagonist, cimetidine. *J. Med. Chem.* **1977**, *20*, 901–906.

(295) Lumma, W. C., Jr.; Anderson, P. S.; Baldwin, J. J.; Bolhofer, W. A.; Habecker, C. N.; Hirshfield, J. M.; Pietruszkiewicz, A. M.; Randall, W. C.; Torchiana, M. L.; Britcher, S. F.; Clineschmidt, B. V.; Denny, G. H.; Hirschmann, R.; Hoffman, J. M.; Phillips, B. T.; Streeter, K. B. Inhibitors of gastric acid secretion: 3,4-diamino-1,2,5-thiadiazole 1-oxides and 1,1-dioxides as urea equivalents in a series of histamine H<sub>2</sub>-receptor antagonists. *J. Med. Chem.* **1982**, *25*, 207–210.

(296) Algeri, A. A.; Luke, G. M.; Standridge, R. T.; Brown, M.; Partyka, R. A.; Crenshaw, R. R. 1,2,5-Thiadiazole 1-oxide and 1,1-dioxide derivatives. A new class of potent histamine H<sub>2</sub>-receptor antagonists. *J. Med. Chem.* **1982**, *25*, 210–212.

(297) Gilbert, A. M.; Antane, M. M.; Argentieri, T. M.; Butera, J. A.; Francisco, G. D.; Freeden, C.; Gundersen, E. G.; Graceffa, R. F.; Herbst, D.; Hirth, B. H.; Lennox, J. R.; McFarlane, G.; Norton, N. W.; Quagliato, D.; Sheldon, J. H.; Warga, D.; Wojdan, A.; Woods, M. Design and SAR of novel potassium channel openers targeted for urge urinary incontinence. 2. Selective and potent benzylamino cyclobutenediones. *J. Med. Chem.* **2000**, *43*, 1203–1214.

(298) Ohnmacht, C. J.; Russell, K.; Empfield, J. R.; Frank, C. A.; Gibson, K. H.; Mayhugh, D. R.; McLaren, F. M.; Shapiro, H. S.; Brown, F. J.; Trainor, D. A.; Ceccarelli, C.; Lin, M. M.; Masek, B. B.; Forst, J. M.; Harris, R. J.; Hulsizer, J. M.; Lewis, J. J.; Silverman, S. M.; Smith, R. W.; Warwick, P. J.; Kau, S. T.; Chun, A. L.; Grant, T. L.; Howe, B. B.; Li, J. H.; Trivedi, S.; Halterman, T. J.; Yochim, C.; Dyroff, M. C.; Kirkland, M.; Neilson, K. L. N-Aryl-3,3,3-trifluoro-2-hydroxy-2-methylpropanamides: K<sub>ATP</sub> potassium channel openers. Modifications on the western region. *J. Med. Chem.* **1996**, *39*, 4592–4601.

(299) Merritt, J. R.; Rokosz, L. L.; Nelson, K. H.; Kaiser, B.; Wang, W.; Stauffer, T. M.; Ozgur, L. E.; Schilling, A.; Li, G.; Baldwin, J. J.; Taveras, A. G.; Dwyer, M. P.; Chao, J. Synthesis and structure–activity relationships of 3,4-diaminocyclobut-3-ene-1,2-dione CXCR2 antagonists. *Bioorg. Med. Chem. Lett.* **2006**, *16*, 4107–4110.

(300) Dwyer, M. P.; Yu, Y.; Chao, J.; Aki, C.; Chao, J.; Biju, P.; Girijavallabhan, V.; Rindgen, D.; Bond, R.; Mayer-Ezel, R.; Jakway, J.; Hipkin, R. W.; Fossetta, J.; Gonsiorek, W.; Bian, H.; Fan, X.; Terminelli, C.; Fine, J.; Lundell, D.; Merritt, J. R.; Rokosz, L. L.; Kaiser, B.; Li, G.; Wang, W.; Stauffer, T.; Ozgur, L.; Baldwin, J.; Taveras, A. G.

Discovery of 2-hydroxy-N,N-dimethyl-3-{2-[[*(R)*-1-(5-methylfuran-2-yl)propyl]amino]-3,4-dioxocyclobut-1-enylamino}benzamide (SCH 527-123): a potent, orally bioavailable CXCR2/CXCR1 receptor antagonist. *J. Med. Chem.* **2006**, *49*, 7603–7606.

(301) Lovering, F.; Kirincich, S.; Wanga, W.; Combs, K.; Resnick, L.; Sabalski, J. E.; Butera, J.; Liu, J.; Parris, K.; Telliez, J. B. Identification and SAR of squarate inhibitors of mitogen-activated protein kinase-activated protein kinase 2 (MK-2). *Bioorg. Med. Chem.* **2009**, *17*, 3342–3351.

(302) Porter, J. R.; Archibald, S. C.; Childs, K.; Critchley, D.; Head, J. C.; Linsley, J. M.; Parton, T. A. H.; Robinson, M. K.; Shock, A.; Taylor, R. J.; Warrelow, G. J.; Alexander, R. P.; Langham, B. Squaric acid derivatives as VLA-4 integrin antagonists. *Bioorg. Med. Chem. Lett.* **2002**, *12*, 1051–1054.

(303) Malerich, J. P.; Hagihara, K.; Rawal, V. H. Chiral squaramide derivatives are excellent hydrogen bond donor catalysts. *J. Am. Chem. Soc.* **2008**, *130*, 14416–14417.

(304) Shi, Y.; Zhang, J.; Stein, P. D.; Shi, M.; O'Connor, S. P.; Bisaha, S. N.; Li, C.; Atwal, K. S.; Bisacchi, G. S.; Sitkoff, D.; Pudzianowski, A. T.; Liu, E. C.; Hartl, K. S.; Seiler, S. M.; Youssef, S.; Steinbacher, T. E.; Schumacher, W. A.; Rendina, A. R.; Bozarth, J. M.; Peterson, T. L.; Zhang, G.; Zahler, R. Ketene amination-based lactam derivatives as a novel class of orally active FXa inhibitors. *Bioorg. Med. Chem. Lett.* **2004**, *15*, 5453–5458.

(305) Peterlin-Mašič, L.; Kikelj, D. Arginine mimetics. *Tetrahedron* **2001**, *57*, 7073–7105.

(306) Peterlin-Mašič, L. Arginine mimetic structure in biologically active antagonists and inhibitors. *Curr. Med. Chem.* **2006**, *13*, 3627–3648.

(307) Ghorai, P.; Kraus, A.; Keller, M.; Gotte, C.; Igel, P.; Schneider, E.; Schnell, D.; Bernhardt, G.; Dove, S.; Zabel, M.; Elz, S.; Seifert, R.; Buschauer, A. Acylguanidines as bioisosteres of guanidines: N<sup>G</sup>-acylated imidazolylpropylguanidines, a new class of histamine H<sub>2</sub> receptor agonists. *J. Med. Chem.* **2008**, *51*, 7193–7204.

(308) Kraus, A.; Ghorai, P.; Birnkammer, T.; Schnell, D.; Elz, S.; Seifert, R.; Dove, S.; Bernhardt, G.; Buschauer, A. N<sup>G</sup>-Acylated aminothiazolylpropylguanidines as potent and selective histamine H<sub>2</sub> receptor agonists. *ChemMedChem* **2009**, *4*, 232–240.

(309) Tomczuk, B.; Lu, T.; Soll, R. M.; Fedde, C.; Wang, A.; Murphy, L.; Crysler, C.; Dasgupta, M.; Eisennagel, S.; Spurlino, J.; Bone, R. Oxyguanidines: application to non-peptidic phenyl-based thrombin inhibitors. *Bioorg. Med. Chem. Lett.* **2003**, *13*, 1495–1498.

(310) Lu, T.; Markotan, T.; Coppo, F.; Tomczuk, B.; Crysler, C.; Eisennagel, S.; Spurlino, J.; Gremminger, L.; Soll, R. M.; Giardino, E. C.; Bone, R. Oxyguanidines. Part 2: Discovery of a novel orally active thrombin inhibitor through structure-based drug design and parallel synthesis. *Bioorg. Med. Chem. Lett.* **2004**, *14*, 3727–3731.

(311) Lu, T.; Markotan, T.; Ballentine, S. K.; Giardino, E. C.; Spurlino, J.; Brown, K.; Maryanoff, B. E.; Tomczuk, B. E.; Damiano, B. P.; Shukla, U.; End, D.; Andrade-Gordon, P.; Bone, R. F.; Player, M. R. Discovery and clinical evaluation of 1-{N-[2-(amidinoaminoxy)ethyl]-amino}carbonylmethyl-6-methyl-3-[2,2-difluoro-2-phenylethylamino]pyrazinone (RWJ-671818), a thrombin inhibitor with an oxyguanidine P1 motif. *J. Med. Chem.* **2010**, *53*, 1843–1856.

(312) Pinto, D. J. P.; Smallheer, J. M.; Cheney, D. L.; Knabb, R. M.; Wexler, R. R. Factor Xa inhibitors: next-generation antithrombotic agents. *J. Med. Chem.* **2010**, *53*, 6243–6274.

(313) Lam, P. Y. S.; Clark, C. G.; Li, R.; Pinto, D. J. P.; Orwat, M. J.; Galemno, R. A.; Fevig, J. M.; Teleha, C. A.; Alexander, R. S.; Smallwood, A. M.; Rossi, K. A.; Wright, M. R.; Bai, S. A.; He, K.; Luettgen, J. M.; Wong, P. C.; Knabb, R. M.; Wexler, R. R. Structure-based design of novel guanidine/benzimidazole mimics: potent and orally bioavailable factor Xa inhibitors as novel anticoagulants. *J. Med. Chem.* **2003**, *46*, 4405–4418.

(314) Mederski, W. W. K. R.; Dorsch, D.; Anzali, S.; Gleitz, J.; Cezanne, B.; Tsaklakidis, C. Halothiophene benzimidazoles as P1 surrogates of inhibitors of blood coagulation factor Xa. *Bioorg. Med. Chem. Lett.* **2004**, *14*, 3763–3769.

- (315) Tucker, T. J.; Brady, S. F.; Lumma, W. C.; Lewis, S. D.; Gardell, S. J.; Naylor-Olsen, A. M.; Yan, Y.; Sisko, J. T.; Stauffer, K. J.; Lucas, B. J.; Lynch, J. J.; Cook, J. J.; Stranieri, M. T.; Holahan, M. A.; Lyle, E. A.; Baskin, E. P.; Chen, I.-W.; Dancheck, K. B.; Krueger, J. A.; Cooper, C. M.; Vacca, J. P. Design and synthesis of a series of potent and orally bioavailable noncovalent thrombin inhibitors that utilize nonbasic groups in the P1 position. *J. Med. Chem.* **1998**, *41*, 3210–3219.
- (316) Lee, C.-W.; Cao, H.; Ichiyama, K.; Rana, T. M. Design and synthesis of a novel peptidomimetic inhibitor of HIV-1 Tat-TAR interactions: squaryldiamide as a new potential bioisostere of unsubstituted guanidine. *Bioorg. Med. Chem. Lett.* **2005**, *15*, 4243–4246.
- (317) Rye, C. S.; Baell, J. B. Phosphate isosteres in medicinal chemistry. *Curr Med. Chem.* **2005**, *12*, 3127–3141.
- (318) Romanenko, V. D.; Kukhar, V. P. Fluorinated phosphonates: synthesis and biomedical application. *Chem. Rev.* **2006**, *106*, 3868–3935.
- (319) Blackburn, G. M.; Kent, D. E. A novel synthesis of  $\alpha$ - and  $\gamma$ -fluoroalkylphosphonates. *Chem. Commun.* **1981**, 511–513.
- (320) Blackburn, G. M.; England, D. A.; Kolkman, F. Monofluoro- and difluoro-methylenebisphosphonic acids: isopolar analogues of pyrophosphoric acid. *Chem. Commun.* **1981**, 930–932.
- (321) Smyth, M. S.; Ford, H., Jr.; Burke, T. R., Jr. A general method for the preparation of benzylic  $\alpha,\alpha$ -difluorophosphonic acids; non-hydrolyzable mimetics of phosphotyrosine. *Tetrahedron Lett.* **1992**, *33*, 4137–4140.
- (322) Combs, A. P. Structure-based drug design of new leads for phosphatase research. *IDrugs* **2007**, *10*, 112–115.
- (323) Combs, A. P. Recent advances in the discovery of competitive protein tyrosine phosphatase 1B inhibitors for the treatment of diabetes, obesity, and cancer. *J. Med. Chem.* **2010**, *53*, 2333–2344.
- (324) Combs, A. P.; Yue, E. W.; Bower, M.; Ala, P. J.; Wayland, B.; Douty, B.; Takvorian, A.; Polam, P.; Wasserman, Z.; Zhu, W.; Crawley, M. L.; Pruitt, J.; Sparks, R.; Glass, B.; Modi, D.; McLaughlin, E.; Bostrom, L.; Li, M.; Galya, L.; Blom, K.; Hillman, M.; Gonville, L.; Reid, B. G.; Wei, M.; Becker-Pasha, M.; Klabe, R.; Huber, R.; Li, Y.; Hollis, G.; Burn, T. C.; Wynn, R.; Liu, P.; Metcalf, B. Structure-based design and discovery of protein tyrosine phosphatase inhibitors incorporating novel isothiazolidinone heterocyclic phosphotyrosine mimetics. *J. Med. Chem.* **2005**, *48*, 6544–6548.
- (325) Combs, A. P.; Zhu, W.; Crawley, M. L.; Glass, B.; Polam, P.; Sparks, R. B.; Modi, D.; Takvorian, A.; McLaughlin, E.; Yue, E. W.; Wasserman, Z.; Bower, M.; Wei, M.; Rupar, M.; Ala, P. J.; Reid, B. M.; Ellis, D.; Gonville, L.; Emm, T.; Taylor, N.; Yeleswaram, S.; Li, Y.; Wynn, R.; Burn, T. C.; Hollis, G.; Liu, P. C. C.; Metcalf, B. Potent benzimidazole sulfonamide protein tyrosine phosphatase 1B inhibitors containing the heterocyclic (S)-isothiazolidinone phosphotyrosine mimetic. *J. Med. Chem.* **2006**, *49*, 3774–3789.
- (326) Black, E.; Breed, J.; Breeze, A. L.; Embrey, K.; Garcia, R.; Gero, T. W.; Godfrey, L.; Kenny, P. W.; Morley, A. D.; Minshall, C. A.; Pannifer, A. D.; Read, J.; Rees, A.; Russell, D. J.; Toader, D.; Tucker, J. Structure-based design of protein tyrosine phosphatase-1B inhibitors. *Bioorg. Med. Chem. Lett.* **2005**, *15*, 2503–2507.
- (327) Muthyala, R. S.; Subramaniam, G.; Todaro, L. The use of squaric acid as a scaffold for cofacial phenyl rings. *Org. Lett.* **2004**, *6*, 4663–4665.
- (328) Sato, K.; Seio, K.; Sekine, M. Squaryl group as a new mimic of phosphate group in modified oligodeoxynucleotides: synthesis and properties of new oligodeoxynucleotide analogues containing an internucleotidic squaryldiamide linkage. *J. Am. Chem. Soc.* **2002**, *124*, 12715–12724.
- (329) Seio, K.; Miyashita, T.; Sato, K.; Sekine, M. Synthesis and properties of new nucleotide analogues possessing squaramide moieties as new phosphate isosteres. *Eur. J. Org. Chem.* **2005**, 5163–5170.
- (330) Niewiadomski, S.; Beebejaun, Z.; Denton, H.; Smith, T. K.; Morris, R. J.; Wagner, G. K. Rationally designed squaryldiamides: a novel class of sugar-nucleotide mimics? *Org. Biomol. Chem.* **2010**, *8*, 3488–3499.
- (331) Savarino, A. A historical sketch of the discovery and development of HIV-1 integrase inhibitors. *Expert Opin. Invest. Drugs* **2006**, *15*, 1507–1522.
- (332) Johns, B. A.; Svolto, A. C. Advances in two-metal chelation inhibitors of HIV integrase. *Expert Opin. Ther. Pat.* **2008**, *18*, 1225–1237.
- (333) Kirschberg, T. A.; Balakrishnan, M.; Squires, N. H.; Barnes, T.; Brendza, K. M.; Chen, X.; Eisenberg, E. J.; Jin, W.; Kutty, N.; Leavitt, S.; Liclican, A.; Liu, Q.; Liu, X.; Mak, J.; Perry, J. K.; Wang, M.; Watkins, W. J.; Lansdon, E. B. RNase H active site inhibitors of human immunodeficiency virus type 1 reverse transcriptase: design, biochemical activity, and structural information. *J. Med. Chem.* **2009**, *52*, 5781–5784.
- (334) Powdrill, M. H.; Deval, J.; Narjes, F.; De Francesco, R.; Götte, M. Mechanism of hepatitis C virus RNA polymerase inhibition with dihydroxypyrimidines. *Antimicrob. Agents Chemother.* **2010**, *54*, 977–983.
- (335) Leonard, D. M. Ras farnesyltransferase: a new therapeutic target. *J. Med. Chem.* **1997**, *40*, 2971–2990.
- (336) Singh, S. B.; Zink, D. L.; Liesch, J. M.; Goetz, M. A.; Jenkins, R. G.; Nallin-Omstead, M.; Silverman, K. C.; Bills, G. F.; Misley, R. T. Isolation and structure of chaetomelic acids A and B from *Chaetomella acutiseta*: farnesyl pyrophosphate mimic inhibitors of Ras farnesyl-protein transferase. *Tetrahedron* **1993**, *49*, 5917–5926.
- (337) Weaver, R.; Gilbert, I. H.; Mahmood, N.; Balzarini, J. Isosteres of nucleoside triphosphates. *Bioorg. Med. Chem. Lett.* **1996**, *6*, 2405–2410.
- (338) Weaver, R.; Gilbert, I. H. The design and synthesis of nucleoside triphosphate isosteres as potential inhibitors of HIV reverse transcriptase. *Tetrahedron* **1997**, *53*, 5537–5562.
- (339) Herdewijn, P.; Marliere, P. Toward safe genetically modified organisms through the chemical diversification of nucleic acids. *Chem. Biodiversity* **2009**, *6*, 791–808.
- (340) Adelfinskaya, O.; Herdewijn, P. Amino acid phosphoramidate nucleotides as alternative substrates for HIV-1 reverse transcriptase. *Angew. Chem., Int. Ed.* **2007**, *46*, 4356–4358.
- (341) Adelfinskaya, O.; Terrazas, M.; Froeyen, M.; Marliere, P.; Nauwelaerts, K.; Herdewijn, P. Polymerase-catalyzed synthesis of DNA from phosphoramidate conjugates of deoxynucleotides and amino acids. *Nucleic Acids Res.* **2007**, *35*, 5060–5072.
- (342) Terrazas, M.; Marliere, P.; Herdewijn, P. Enzymatically catalyzed DNA synthesis using L-Asp-dGMP, L-Asp-dCMP, and L-Asp-dTMP. *Chem. Biodiversity* **2008**, *5*, 31–39.
- (343) Zlatev, I.; Giraut, A.; Morvan, F.; Herdewijn, P.; Vasseur, J.-J.  $\delta$ -Di-carboxybutyl phosphoramidate of 2'-deoxycytidine-5'-monophosphate as substrate for DNA polymerization by HIV-1 reverse transcriptase. *Bioorg. Med. Chem.* **2009**, *17*, 7008–7014.
- (344) Giraut, A.; Herdewijn, P. Influence of the linkage between leaving group and nucleoside on substrate efficiency for incorporation in DNA catalyzed by reverse transcriptase. *ChemBioChem* **2010**, *11*, 1399–1403.
- (345) Giraut, A.; Song, X.-P.; Froeyen, M.; Marliere, P.; Herdewijn, P. Iminodiacetic-phosphoramidates as metabolic prototypes for diversifying nucleic acid polymerization in vivo. *Nucleic Acids Res.* **2010**, *38*, 2541–2550.
- (346) Yang, S.; Froeyen, M.; Lescrier, E.; Marliere, P.; Herdewijn, P. 3-Phosphono-L-alanine as pyrophosphate mimic for DNA synthesis using HIV-1 reverse transcriptase. *Org. Biomol. Chem.* **2011**, *9*, 111–119.
- (347) Giraut, A.; Dyubankova, N.; Song, X.-P.; Herdewijn, P. Phosphodiester substrates for incorporation of nucleotides in DNA using HIV-1 reverse transcriptase. *ChemBioChem* **2009**, *10*, 2246–2252.
- (348) Koide, K.; Bunnage, M. E.; Gomez Paloma, L.; Kanter, J. R.; Taylor, S. S.; Brunton, L. L.; Nicolaou, K. C. Molecular design and biological activity of potent and selective protein kinase inhibitors related to balanol. *Chem. Biol.* **1995**, *2*, 601–608.
- (349) Narayana, N.; Diller, T. C.; Koide, K.; Bunnage, M. E.; Nicolaou, K. C.; Brunton, L. L.; Xuong, N.-H.; Ten Eyck, L. F.; Taylor, S. S. Crystal structure of the potent natural product inhibitor balanol in complex with the catalytic subunit of cAMP-dependent protein kinase. *Biochemistry* **1999**, *38*, 2367–2376.
- (350) Tesmer, J. J. G.; Tesmer, V. M.; Lodowski, D. T.; Steinhagen, H.; Huber, J. Structure of human G protein-coupled receptor kinase 2 in complex with the kinase inhibitor balanol. *J. Med. Chem.* **2010**, *53*, 1867–1870.

- (351) Pudlo, J. S.; Cao, X.; Swaminathan, S.; Matteucci, M. D. Oligodeoxyribonucleotides containing 2',5' acetal linkages: synthesis and hybridization properties. *Tetrahedron Lett.* **1994**, *35*, 9315–9318.
- (352) Lin, K.-Y.; Matteucci, M. D. The synthesis and hybridization properties of an oligonucleotide containing hexafluoroacetone ketal internucleotide linkages. *Tetrahedron Lett.* **1996**, *37*, 8667–8670.
- (353) Zou, R.; Matteucci, M. D. Synthesis and hybridization properties of an oligonucleotide analog containing a glucose-derived conformation-restricted ribose moiety and 2',5' formacetal linkages. *Tetrahedron Lett.* **1996**, *37*, 941–944.
- (354) Goldring, A. O.; Gilbert, I. H.; Mahmood, N.; Balzarini, J. Lipophilic bio-isosteres of nucleoside triphosphates. *Bioorg. Med. Chem. Lett.* **1996**, *6*, 2411–2416.
- (355) Goldring, A. O.; Balzarini, J.; Gilbert, I. H. Design and synthesis of bio-isosteres of thymidine triphosphate. *Bioorg. Med. Chem. Lett.* **1998**, *8*, 1211–1214.
- (356) Otoski, R. M.; Wilcox, C. S. An approach to lipophilic nucleotide phosphate analogs. Synthesis of a lipophilic isostere of ATP. *Tetrahedron Lett.* **1988**, *29*, 2615–2618.
- (357) Ladbury, J. E.; Klebe, G.; Freire, E. Adding calorimetric data to decision making in lead discovery: a hot tip. *Nat. Rev. Drug Discovery* **2010**, *9*, 23–27.
- (358) Michel, J.; Tirado-Rives, J.; Jorgensen, W. L. Energetics of displacing water molecules from protein binding sites: consequences for ligand optimization. *J. Am. Chem. Soc.* **2009**, *131*, 15403–15411.
- (359) Lam, P. Y. S.; Jadhav, P. K.; Eyermann, C. J.; Hodge, C. N.; Ru, Y.; Bachelier, L. T.; Meek, J. L.; Otto, M. J.; Rayner, M. M.; Wong, Y. N.; Chang, C.-H.; Weber, P. C.; Jackson, D. A.; Sharpe, T. R.; Erikson-Viitanen, S. Rational design of potent, bioavailable, nonpeptide cyclic ureas as HIV protease inhibitors. *Science* **1994**, *263*, 380–384.
- (360) Lam, P. Y. S.; Ru, Y.; Jadhav, P. K.; Aldrich, P. E.; DeLucca, G. V.; Eyermann, C. J.; Chang, C.-H.; Emmett, G.; Holler, E. R.; Daneker, W. F.; Li, L.; Confalone, P. N.; McHugh, R. J.; Han, Q.; Li, R.; Markwalder, J. A.; Seitz, S. P.; Sharpe, T. R.; Bachelier, L. T.; Rayner, M. M.; Klabe, R. M.; Shum, L.; Winslow, D. L.; Kornhauser, D. M.; Jackson, D. A.; Erickson-Viitanen, S.; Hodge, C. N. Cyclic HIV protease inhibitors: synthesis, conformational analysis, P2/P2' structure–activity relationship, and molecular recognition of cyclic ureas. *J. Med. Chem.* **1996**, *39*, 3514–3525.
- (361) De Lucca, G. V.; Erickson-Viitanen, S.; Lam, P. Y. S. Cyclic HIV protease inhibitors capable of displacing the active site structural water molecule. *Drug Discovery Today* **1997**, *2*, 6–18.
- (362) Nalam, M. N. L.; Peeters, A.; Jonckers, T. M. H.; Dierynck, I.; Schiffer, C. A. Crystal structure of lysine sulfonamide inhibitor reveals the displacement of the conserved flap water molecule in human immunodeficiency virus type 1 protease. *J. Virol.* **2007**, *81*, 9512–9518.
- (363) Canan Koch, S. S.; Thoresen, L. H.; Tikhe, J. G.; Maegley, K. A.; Almasy, R. J.; Li, J.; Yu, X.-H.; Zook, S. E.; Kumpf, R. A.; Zhang, C.; Boritzki, T. J.; Mansour, R. N.; Zhang, K. E.; Ekker, A.; Calabrese, C. R.; Curtin, N. J.; Kyle, S.; Thomas, H. D.; Wang, L.-Z.; Calvert, A. H.; Golding, B. T.; Griffin, R. J.; Newell, D. R.; Webber, S. E.; Hostomsky, Z. Novel tricyclic poly(ADP-ribose) polymerase-1 inhibitors with potent anticancer chemopotentiating activity: design, synthesis, and X-ray cocrystal structure. *J. Med. Chem.* **2002**, *45*, 4961–4974.
- (364) Tikhe, J. G.; Webber, S. E.; Hostomsky, Z.; Maegley, K. A.; Ekkers, A.; Li, J.; Yu, X.-H.; Almasy, R. J.; Kumpf, R. A.; Boritzki, T. J.; Zhang, C.; Calabrese, C. R.; Curtin, N. J.; Kyle, S.; Thomas, H. D.; Wang, L.-Z.; Calvert, A. H.; Golding, B. T.; Griffin, R. J.; Newell, D. R. Design, synthesis, and evaluation of 3,4-dihydro-2H-[1,4]diazepino[6,7,1-hi]-indol-1-ones as inhibitors of poly(ADP-ribose) polymerase. *J. Med. Chem.* **2004**, *47*, 5467–5481.
- (365) García-Sosa, A. T.; Firth-Clark, S.; Mancera, R. L. Including tightly-bound water molecules in de novo drug design. Exemplification through in silico generation of poly(ADP-ribose)polymerase inhibitors. *J. Chem. Inf. Model.* **2005**, *45*, 624–633.
- (366) Chen, J. M.; Xu, S. L.; Wawrzak, Z.; Basarab, G. S.; Jordan, D. B. Structure-based design of potent inhibitors of scytalone dehydratase: displacement of a water molecule from the active site. *Biochemistry* **1998**, *37*, 17735–17744.
- (367) Liu, C.; Wroblewski, S. T.; Lin, J.; Ahmed, G.; Metzger, A.; Wityak, J.; Gillooly, K. M.; Shuster, D. J.; McIntyre, K. W.; Pitt, S.; Shen, D. R.; Zhang, R. F.; Zhang, H.; Doweiko, A. M.; Diller, D.; Henderson, I.; Barrish, J. C.; Dodd, J. H.; Schieven, G. L.; Leftheris, K. 5-Cyanopyrimidine derivatives as a novel class of potent, selective, and orally active inhibitors of p38 $\alpha$  MAP kinase. *J. Med. Chem.* **2005**, *48*, 6261–6270.
- (368) Wissner, A.; Berger, D. M.; Boschelli, D. H.; Floyd, M. B., Jr.; Greenberger, L. M.; Gruber, B. C.; Johnson, B. D.; Mamuya, N.; Nilakantan, R.; Reich, M. F.; Shen, R.; Tsou, H.-R.; Upeslakis, E.; Wang, Y. F.; Wu, B.; Ye, F.; Zhang, N. 4-Anilino-6,7-dialkoxyquinoline-3-carbonitrile inhibitors of epidermal growth factor receptor kinase and their bioisosteric relationship to the 4-anilino-6,7-dialkoxyquinazoline inhibitors. *J. Med. Chem.* **2000**, *43*, 3244–3256.